USGS
science for a changing world

USGS Greater Everglades Priority Ecosystem Studies Initiative

The Hydrologic System of the South Florida Peninsula: Development and Application of the Biscayne and Southern Everglades Coastal Transport (BISECT) Model

Scientific Investigations Report 2019–5045

U.S. Department of the Interior
U.S. Geological Survey

Cover. Photograph showing the southern coastal Everglades looking westward towards Terrapin Bay, Florida. Photograph by Eric D. Swain, U.S. Geological Survey, July 24, 1997.

The Hydrologic System of the South Florida Peninsula: Development and Application of the Biscayne and Southern Everglades Coastal Transport (BISECT) Model

By Eric D. Swain, Melinda A. Lohmann, and Carl R. Goodwin

USGS Greater Everglades Priority Ecosystem Studies Initiative

Scientific Investigations Report 2019–5045

U.S. Department of the Interior
U.S. Geological Survey

U.S. Department of the Interior
DAVID BERNHARDT, Secretary

U.S. Geological Survey
James F. Reilly II, Director

U.S. Geological Survey, Reston, Virginia: 2019

For more information on the USGS—the Federal source for science about the Earth, its natural and living resources, natural hazards, and the environment—visit https://www.usgs.gov or call 1–888–ASK–USGS.

For an overview of USGS information products, including maps, imagery, and publications, visit https://store.usgs.gov.

Suggested citation:
Swain, E.D., Lohmann, M.A., and Goodwin, C.R., 2019, The hydrologic system of the south Florida peninsula—Development and application of the Biscayne and Southern Everglades Coastal Transport (BISECT) model: U.S. Geological Survey Scientific Investigations Report 2019–5045, 114 p., https://doi.org/10.3133/sir20195045.

ISSN 2328-0328 (online)

Acknowledgments

The authors would like to thank all of the personnel from Everglades National Park, South Florida Water Management District, and the U.S. Army Corps of Engineers who have provided copious support, data, review, and innovations during the development of these modeling tools.

Contents

Figures

Tables

Conversion Factors

International System of Units to U.S. customary units

Multiply	By	To obtain
	Length	
centimeter (cm)	0.3937	inch (in.)
millimeter (mm)	0.03937	inch (in.)
meter (m)	3.281	foot (ft)
kilometer (km)	0.6214	mile (mi)
	Area	
square meter (m^2)	0.0002471	acre
square kilometer (km^2)	247.1	acre
square meter (m^2)	10.76	square foot (ft^2)
square kilometer (km^2)	0.3861	square mile (mi^2)
	Flow rate	
cubic meter per second (m^3/s)	70.07	acre-foot per day (acre-ft/d)
meter per second (m/s)	3.281	foot per second (ft/s)
meter per day (m/d)	3.281	foot per day (ft/d)
cubic meter per second (m^3/s)	35.31	cubic foot per second (ft^3/s)
cubic meter per day (m^3/d)	35.31	cubic foot per day (ft^3/d)
cubic meter per day (m^3/d)	264.2	gallon per day (gal/d)
cubic meter per second (m^3/s)	22.83	million gallons per day (Mgal/d)
	Mass	
kilogram (kg)	2.205	pound avoirdupois (lb)
	Hydraulic conductivity	
meter per day (m/d)	3.281	foot per day (ft/d)

Temperature in degrees Celsius (°C) may be converted to degrees Fahrenheit (°F) as $°F = (1.8 \times °C) + 32$.

Datum

Vertical coordinate information is referenced to the North American Vertical Datum of 1988 (NAVD 88).

Horizontal coordinate information is referenced to the North American Datum of 1983 (NAD 83).

Elevation, as used in this report, refers to distance above the vertical datum.

Abbreviations

BISECT	Biscayne and Southern Everglades Coastal Transport
CERP	Comprehensive Everglades Restoration Plan
ENP	Everglades National Park
ET	evapotranspiration
FTLOADDS	Flow and Transport in a Linked Overland/Aquifer Density-Dependent System
MD	mean difference
ME	mean error
NS	Nash-Sutcliffe coefficient
NWIS	National Water Information System
PEV	percent explained variance
PSU	practical salinity unit
RMSD	root-mean square difference
RMSE	root-mean square error
SFWMD	South Florida Water Management District
SFWMM	South Florida Water Management Model
SICS	Southern Inland and Coastal Systems
SOFIA	South Florida Information Access
SWIFT2D	Simulation of Surface-Water Integrated Flow and Transport in Two Dimensions
TIME	Tides and Inflows to the Mangrove Everglades
USACE	U.S. Army Corps of Engineers
USGS	U.S. Geological Survey

The Hydrologic System of the South Florida Peninsula: Development and Application of the Biscayne and Southern Everglades Coastal Transport (BISECT) Model

By Eric D. Swain, Melinda A. Lohmann, and Carl R. Goodwin

Abstract

The Biscayne and Southern Everglades Coastal Transport (BISECT) model was developed by the U.S. Geological Survey under the Greater Everglades Priority Ecosystem Studies Initiative to evaluate, both separately and in conjunction, the likely effects on surface-water stages and flows, hydroperiod, and groundwater levels and salinity in south Florida of (1) a vertical Biscayne aquifer barrier to maintain higher wetland levels, (2) possible future changes to current water-management practices, and (3) sea-level rise. The BISECT model is a combination of the Tides and Inflows to the Mangrove Everglades (TIME) and Biscayne models of the western and eastern parts of south Florida including Everglades National Park, the southern Miami-Dade urban area, and the Biscayne Bay coast and simulates hydrodynamic surface-water flow and three-dimensional groundwater conditions dynamically for the period 1996–2004 by using the Flow and Transport in a Linked Overland/Aquifer Density-Dependent System (FTLOADDS) simulator. BISECT includes a number of parameter and algorithmic refinements that improve simulation results relative to the TIME and Biscayne models and represents the hydrologic system more explicitly, including (1) improved topographic representations, (2) refined Manning's friction coefficients, (3) improved evapotranspiration computation through spatially variable albedo, (4) increased vertical aquifer discretization, and (5) extension of the western boundary farther offshore.

Sensitivity analyses demonstrate that simulated flows into Long Sound have a different pattern of response to tidal amplitude, wind, and frictional resistance changes than do other coastal streams in the model; flows at Broad River and Lostmans River are most sensitive to tidal amplitude, wind, and frictional resistance changes; and flow to the Everglades coastal streams is substantially affected by surface-water/groundwater interactions in the eastern urban areas. Insight into the hydrologic system came from scenario simulations that represent proposed management actions, such as grouting of the aquifer to prevent seepage from the wetlands and changes to water deliveries proposed by the Comprehensive Everglades Restoration Plan (CERP), and projected sea-level rise. These scenario management changes are considered separately to isolate their specific effects and also in conjunction with sea-level rise. Scenario simulations show that (1) attempts to prevent seepage from the wetlands by grouting the aquifer along the L 31N levee produce minimal effects on surface-water levels; (2) the increased water deliveries proposed in the CERP redistribute flow to the northwestern coastal part of the study area with a minimal reduction to the southeast and a more substantial reduction in flows in the intervening coastal zones, mitigating some sea-level rise effects; (3) sea-level rise has a larger effect on the hydrology (water levels, flow, and salinity) than does CERP restoration; and (4) support for ecological models and hydrologic studies can be provided by applying BISECT to scenarios influenced by climatic and anthropogenic changes or by meteorological variability, such as extreme wet or dry periods.

Introduction

The hydrologic system of the south Florida peninsula is dynamic and complex, influenced by canals and water-control structures, subsurface stratigraphy, meteorological processes, and proximity to surrounding saline tidal water bodies. The nearly flat topography overlies a broad platform of porous and permeable carbonate rocks. The surface-water and groundwater flow gradients are low, and the surface-water and groundwater systems naturally interact readily. The area is surrounded in three directions by a limitless supply of seawater that can intrude both tidal creeks and canals and shallow aquifers. An extensive structure-regulated canal network is used to drain the hydrologic system to prevent inundation during wet periods and retain freshwater levels to control saltwater intrusion during dry periods. In urban areas, groundwater is the primary water supply and is pumped to meet the demands of a large population primarily on the southeast coast. The proximity of a major metropolitan area along the southeast coast to the largely undeveloped Everglades means that changes in hydrologic stresses in the urban areas can affect the hydrology in the Everglades and vice versa. These characteristics make the entire hydrologic

system of south Florida sensitive to natural and anthropogenic processes and changes that may occur on the surface, within the subsurface, and at the marine boundaries. To address future management of the system in response to both climatic and anthropogenic changes, the properties, processes, and interconnections of the different parts of the hydrologic system must be evaluated.

Anthropogenic changes to the hydrologic system, particularly those imposed since the late 19th century, have had a substantial effect on modifying the natural surface-water and groundwater flow fields in south Florida. Prior to the 1800s, both local rainfall and water from periodic overflows of Lake Okeechobee (fig. 1), located farther north on the peninsula, flowed generally southward in this region through shallow, wide, and slow-moving sloughs and freshwater marshlands that eventually discharged into coastal areas through numerous small- and medium-sized streams. Since that time, population growth has spurred land-use changes that have resulted in conversion of large parts of the freshwater marshes into dry ground for urban, suburban, and agricultural development. Drainage canals were initially dug to drain areas for development and route the surface water to the coast. The canal systems were progressively extended, and associated structures were constructed to control flooding, control groundwater recharge, distribute water for maintenance of ecosystems, and limit the extent of landward saltwater intrusion at many coastal streams. Groundwater pumping from the surficial Biscayne aquifer system, already strongly controlled by recharge from the canal system, has provided the primary water supply in the urban southeastern part of

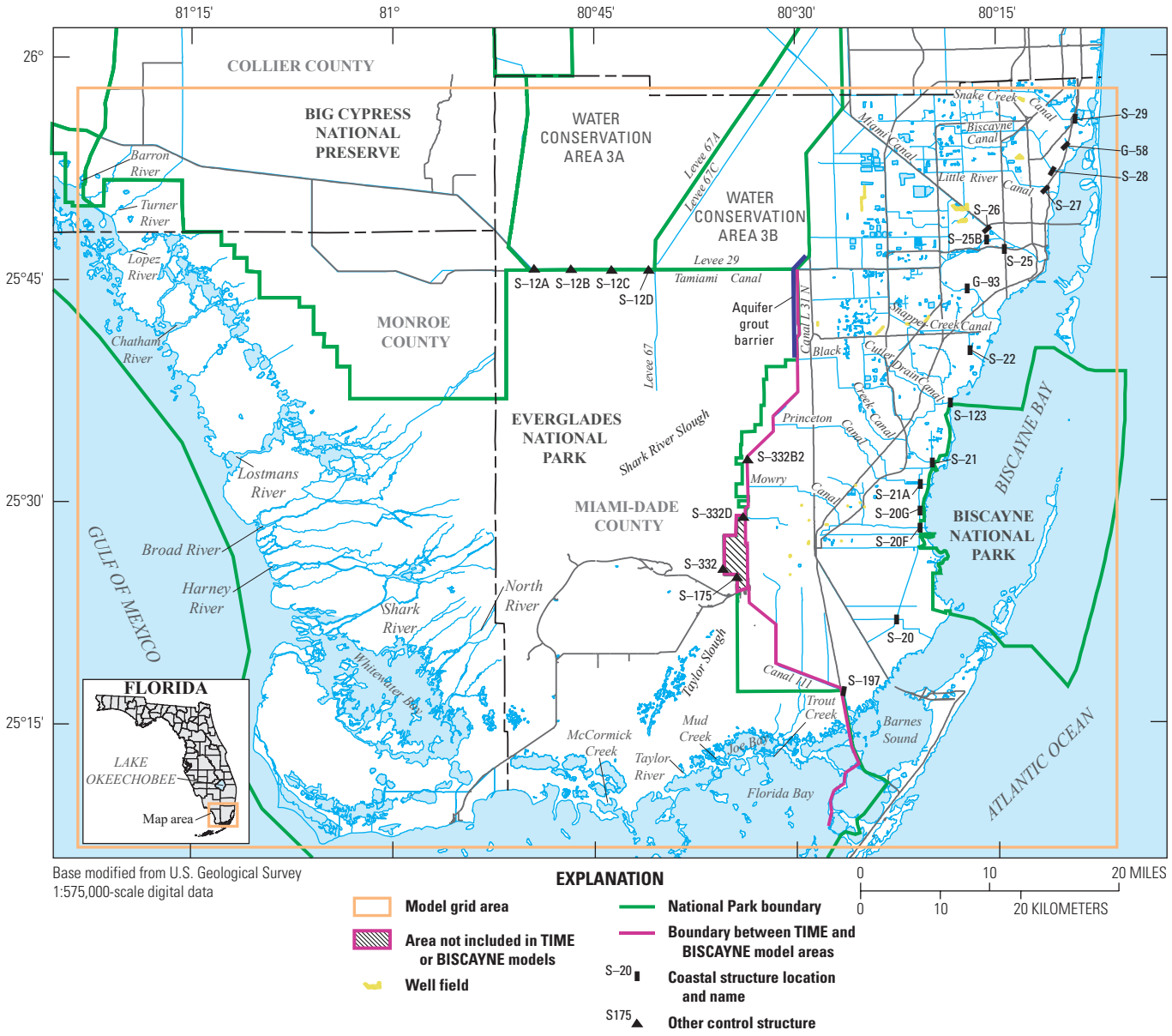

Figure 1. Study area and boundaries of the Biscayne and Southern Everglades Coastal Transport (BISECT) model and the precursor Tides and Inflows to the Mangrove Everglades (TIME) and Biscayne models, south Florida.

the peninsula and has resulted in groundwater-level declines, potentiometric depressions around pumping centers, and coastal salinity intrusion in the aquifer.

A variety of factors will likely affect the south Florida hydrologic system in the foreseeable future, and their potential impacts should be evaluated to provide reliable information with which to guide future water, ecosystem, and land-use management decisions. The maintenance of higher wetland levels in the Everglades, needed for restoring historical conditions, is challenging to achieve with substantial groundwater flowing downgradient to the eastern urban area through the highly conductive aquifer. Construction of a subsurface vertical barrier—a grout wall in the aquifer to block flow—has been proposed to help maintain wetland water levels and limit groundwater transport from Everglades National Park (ENP) to the east. Increases in freshwater deliveries to ENP, as proposed in the Comprehensive Everglades Restoration Plan (CERP) (U.S. Army Corps of Engineers, 1999), are also conceived to restore water levels to historical conditions, with the additional purpose of moderating the expected salinity increases in low-lying wetlands as a result of sea-level rise. The observed and predicted rise in sea level (Intergovernmental Panel on Climate Change, 2013), which affects the eastern, southern, and western parts of the south Florida hydrologic system, must be considered both separately and in conjunction with these proposed management changes. Water managers and others need predictive information on the likely effects of anthropogenic and sea-level changes on the hydrologic system to most effectively manage the water resources of south Florida.

To address these questions, the U.S. Geological Survey (USGS), through the Greater Everglades Priority Ecosystem Studies (GEPES) Initiative, evaluated the effects of implementation of a vertical barrier in the surficial aquifer system to prevent seepage from the wetlands, increased water deliveries to the undeveloped part of the Everglades, and a range of predicted sea-level rise rates on the hydroperiods, groundwater levels, and surface-water and groundwater salinity in the south Florida peninsula. To make these evaluations, the USGS developed the Biscayne and Southern Everglades Coastal Transport (BISECT) model (Swain and Lohmann, 2018), which simulates hydrodynamic surface-water flow and three-dimensional groundwater conditions and accounts for leakage between surface-water and groundwater parts of the system, water levels, streamflows, groundwater salinity, and surface-water salinity and temperature. This model was constructed by combining two existing models, Tides and Inflows to the Mangrove Everglades (TIME) (Wang and others, 2007) and Biscayne (Lohmann and others, 2012), and modifying the Flow and Transport in a Linked Overland/Aquifer Density-Dependent System (FTLOADDS) simulator (Langevin and others, 2005) to include spatial variations in the solar radiation reflected back into the atmosphere from the Earth's surface (albedo) to improve model results. The BISECT model was developed by using extensive field data and builds on previous studies and models to provide improved insight and understanding of the hydrologic system.

Purpose and Scope

The purpose of this report is to evaluate the possible effects of (1) a vertical barrier to lateral flow in a limited area of the Biscayne aquifer, (2) planned future changes to current water-management practices in the Everglades, and (3) sea-level rise on the integrated surface-water and groundwater hydrologic system of south Florida. Analyses were made using the BISECT model, which simulates hydrodynamic surface-water and groundwater flow in the surficial aquifer system and exchanges between surface-water and groundwater parts of the hydrologic system.

This report documents the BISECT model construction, calibration, and sensitivity analyses. Calibrated model results are discussed as a base case and compared with scenario simulation results, which include (1) two scenarios representing a vertical barrier in place for one half of and the total thickness of the Biscayne aquifer adjacent to the northern Canal L 31N, (2) a scenario representing increased upstream water deliveries into the Everglades, (3) two scenarios representing rising sea levels of 30 and 60 centimeters (cm), and (4) a scenario representing a combination of a vertical barrier for the total thickness of the Biscayne aquifer, increased upstream water deliveries, and a sea-level rise of 60 cm. Model limitations are presented to help guide interpretation of model results.

Description of the Hydrologic System

The southern 7,300 square kilometers (km^2) of the Florida peninsula (the land area within the orange boundary line shown in fig. 1) includes all of Miami-Dade County not in Water Conservation Areas 3A and 3B; all of Monroe County on mainland Florida; and a small part of southern Collier County south of the western half of Tamiami Trail (fig. 1). Home to about 2.5 million people, mostly in Miami-Dade County (the seventh most populous county in the Nation) (Rabin, 2016), the area contains urban and suburban Miami; Everglades and Biscayne National Parks; Big Cypress National Preserve; a large agricultural region; and productive and extensive mangrove, marsh, and upland ecosystems supporting a diverse population of mammals, birds, fish, reptiles, and invertebrates. The nearly flat land is mostly less than 3 meters (m) above sea level, and the study area also includes about 2,700 km^2 of surrounding marine waters including parts of the Gulf of Mexico, Florida Bay, and the Atlantic Ocean, as well as all of Biscayne Bay and Barnes Sound (fig. 1). The climate is humid subtropical, subject to a wet season with high seasonal precipitation rates and episodic storm events and a dry season with comparatively low precipitation rates.

This study area can be divided into two subareas based on development. The subarea east of the generally north-south Canal L 31 N/Canal 111 system (fig. 1) is largely urbanized, containing the vast majority of the population, whereas the subarea west of the Canal L 31 N/Canal 111 system is a vast expanse of mostly undeveloped wetlands containing ENP and

part of Big Cypress National Preserve. Both subareas share a subtropical climate; the impacts of floods, droughts, and hurricanes; and a highly modified and controlled freshwater delivery system with complex and closely connected surface-water and groundwater components that can be contaminated by nearby seawater. Both subareas will likely undergo some effects of a rising sea level, modified water deliveries, and a proposed vertical aquifer barrier.

The large, mostly undeveloped western subarea consists of several types of landscape, each dominated by distinctive vegetation assemblages whose distribution is controlled largely by small topographic differences and proximity to marine waters. The pine uplands, cypress swamps, hardwood hammocks, freshwater marshes, and wet prairies provide surface-water storage, water seepage to and from groundwater, and water vapor transfer to the atmosphere by evapotranspiration (ET). Lakes, sloughs, and streams, which occupy the lowest topographic positions, provide more direct hydraulic connection with the subsurface and with other surface features and may extend beyond the boundaries of the study area. These hydraulically connected features are considered important indicators of change for water levels and flows in the western subarea. As such, efforts continue to measure the discharge, stage, salinity, and temperature of many of these features, which supports the development of numerical models to simulate south Florida hydrology.

The largest of these hydraulically connected features is Shark River Slough, which extends southwestward from the north-central part of the study area to Shark River and other streams discharging to Whitewater Bay (fig. 1) and also directly or indirectly to the Gulf of Mexico. Taylor Slough (fig. 1) is a similar but smaller drainage feature in the south-central part of the study area and, together with several other coastal streams, provides the main source of freshwater runoff to northeastern Florida Bay.

The subarea east of the Canal L 31 N/Canal 111 system encompasses most of the urban areas of Miami-Dade County, as far north as the Snake Creek Canal near the northern Miami-Dade County line (fig. 1), and also encompasses Biscayne Bay, part of the upper Florida Keys barrier islands, Biscayne National Park, Barnes Sound, and small sections of Florida Bay and of the adjacent Atlantic Ocean. The surface-water hydrology of much of the eastern subarea is largely controlled by a network of canals and structures that are designed to manage floods, provide groundwater recharge, and mitigate saltwater intrusion. Though mostly urban, the eastern subarea also contains some agricultural and wetland areas.

The surficial aquifer system in the BISECT model area is shallow and unconfined to semiconfined and composed primarily of the Biscayne aquifer in the eastern part of the study area and the gray limestone aquifer in the western part of the study area, both of which overlie the confined Floridan aquifer system. The surficial and Floridan aquifer systems are separated by alternating beds of sand, silt, and clay that collectively restrict the movement of groundwater between the two aquifer systems. The BISECT model simulates flow primarily in the Biscayne and gray limestone aquifers because they can be represented as hydraulically disconnected from the Floridan aquifer below, they interact strongly with the surface-water system, and they provide the primary source of groundwater discharge to the offshore areas. The highly transmissive aquifer system beneath this entire land area typically varies in total thickness from about 50 to 75 feet and, also, extends offshore under Biscayne Bay and the Atlantic Ocean to the east, Florida Bay to the south, and the Gulf of Mexico to the west. Fish and Stewart (1991) and Reese and Cunningham (2000) provide detailed descriptions of the hydrogeology and aquifer properties of the Biscayne aquifer and surficial aquifer system and the formations that compose them.

Approach

A numerical model, BISECT, was developed to simulate the hydrology of about 7,300 km^2 of the south Florida peninsula and about 2,700 km^2 of the surrounding tidal water bodies (Atlantic Ocean, Gulf of Mexico, and Florida Bay) for the 1996–2004 period. This model simulates the driving hydrologic processes within the study area and is constructed and calibrated using extensive data that include streamflow, ocean tides, surface-water stage, groundwater levels, precipitation, evaporation, water salinity, water temperature, groundwater pumpage, and the location of freshwater/saltwater mixing zones in coastal streams and aquifers. The model development also benefited from long-term data collection and interpretation that refined the understanding of (1) the elevation of land surface in the Everglades and other south Florida wetlands; (2) the hydrologic framework of the subsurface underlying south Florida; (3) the rates of water flow in streams, marshes, and aquifers; (4) the nature of freshwater and saltwater mixing in streams and aquifers; and (5) the rates of freshwater and saltwater exchange between surface water and groundwater that occurs in both onshore and offshore areas. Recent efforts to quantify heat transfer processes within the BISECT model area (Swain and Decker, 2009, 2010) allow simulation of water temperature and improved representation of ET rates from several land-use types that occur in south Florida.

Some of the attributes and processes included in this model are

- accurate topographic and shallow water definition in marsh areas determined by aerial methods,
- density-dependent surface-water flow in defined channels and overland sheet flow in marshes,
- density-dependent groundwater flow in a highly transmissive aquifer system,
- precipitation on land and water surfaces,
- evaporation from open and protected water surfaces,
- ET from various vegetative and other land covers,

- downward and upward leakage of freshwater and saltwater between aquifer layers,
- downward and upward leakage of fresh and saline water between the surface and the aquifer,
- pumpage from groundwater at well fields, and
- tidal forcing in neighboring marine waters.

The simulator FTLOADDS (Langevin and others, 2005; Wang and others, 2007; Swain and Decker, 2009; Lohmann and others, 2012) was developed specifically for the highly interactive surface-water and groundwater hydrologic system components in south Florida that discharge freshwater to mix with saline ocean waters or to mix with saline waters within aquifers. This simulator accounts for mass-balanced flow and solute transport within and between the surface-water and groundwater systems by coupling two unrelated model codes: Simulation of Surface-Water Integrated Flow and Transport in Two Dimensions (SWIFT2D) (Leendertse, 1987; Schaffranek, 2004; Swain, 2005) and Simulation of Three-Dimensional Variable-Density Ground-Water Flow (SEAWAT) (Guo and Langevin, 2002). As SWIFT2D has a full hydrodynamic formulation, transient surface-water flows that are associated with tidal areas can be simulated. FTLOADDS includes a two-dimensional, spatially variable representation of albedo in the study area for use in refinement of heat transport and ET calculations (Lohmann and others, 2012).

BISECT Model Construction and Calibration

Details regarding BISECT model construction and calibration are provided in appendix 1. The BISECT model was formed by combining at their common spatial boundaries two existing south Florida hydrologic models that use the FTLOADDS simulator (see fig. 1). One is the TIME model (Wang and others, 2007), and the other is the Biscayne model (Lohmann and others, 2012). The combination was enabled by the same grid-cell size, geographic grid alignment, and the common boundary. Additional revisions to the precursor models include modification of ocean boundary conditions, modifications of groundwater-model layering scheme to improve delineation of fresh/saline water mixing zones, and removal of previously existing boundary conditions along their common boundary.

The BISECT model was calibrated to (1) measured flow, stage, and salinity for free-flowing streams discharging to coastal waters; (2) daily groundwater levels in the Biscayne aquifer; (3) wetland water levels; and (4) the general location of the saltwater-freshwater mixing zone in the Biscayne aquifer. Calibration data were primarily obtained from the South Florida Water Management District (SFWMD) corporate environmental database (DBHYDRO) (South Florida Water Management District, 2017), the USGS National Water Information System (NWIS) database (U.S. Geological Survey, 2017a), and South Florida Information Access (SOFIA) website (U.S. Geological Survey, 2017b).

Model Scenarios

A total of six scenarios were simulated as part of this study to evaluate effects of sea-level rise, construction of a proposed vertical barrier wall in part of the Biscayne aquifer, and increased freshwater deliveries to south Florida marshlands proposed by the CERP (South Florida Water Management District, 2005). Specifically, the scenario simulations incorporate (1) adding an 11-kilometer (km)-long vertical aquifer barrier that penetrates half the depth of the Biscayne aquifer; (2) adding an 11-km-long vertical aquifer barrier that fully penetrates the depth of the Biscayne aquifer; (3) adding increased freshwater deliveries specified by CERP, as derived from the SFWMD South Florida Water Management Model (SFWMM) (South Florida Water Management District, 2005); (4) adding 30 cm to the mean tide level at all ocean boundaries; (5) adding 60 cm to the mean tide level at all ocean boundaries; and (6) adding an 11-km-long vertical aquifer barrier that penetrates the full depth of the Biscayne aquifer, adding increased CERP freshwater flow deliveries, and adding 60 cm to the mean tide level at all ocean boundaries. While not all combinations of scenarios are simulated, the sixth scenario incorporates a combination of the most extensive of the hydrologic changes tested by the other scenarios.

Previous Studies

A series of studies were implemented under the Greater Everglades Priority Ecosystem Studies Initiative of the USGS that provide data important to simulating flow in the ENP area. Many of these data were used to design the original USGS Everglades-related Southern Inland and Coastal Systems (SICS) model (Swain and others, 2004) and the more extensive TIME model (Wang and others, 2007). Topographic data for the ENP wetlands were collected by using a helicopter-mounted Global Positioning System (GPS) unit and weighted line to measure land-surface elevations (Desmond and others, 2000). Land-surface elevations were measured on a grid with about 400-m spacing (Henkle, 1996). In addition, bathymetries of Joe Bay and Florida Bay were measured by the USGS (Hansen and DeWitt, 1999) by using a boat with a depth finder and a GPS unit.

Everglades ET has been studied extensively (German, 1999; Shoemaker and Sumner, 2006; Shoemaker and others, 2011). Although the original TIME model used a Penman-Monteith formulation to compute ET (Wang and others, 2007), the model was modified to represent heat transport and latent heat in addition to ET (Swain and Decker, 2010). This formulation is used in BISECT along with environmental values from field measurement sites (Shoemaker and Sumner, 2006) and albedo and stomatal resistance values further refined from those derived in Swain and Decker (2010).

The frictional resistance of the surface-water flow regime is difficult to quantify, particularly in dense wetland flow. Field and laboratory research was performed to determine the

effective frictional resistance to water flow through several Everglades vegetation types (Lee and Carter, 1999). Extensive hydraulic measurements of velocity, depth, and gradient were made in a laboratory flume containing transplanted marsh vegetation. Field measurements of velocity, depth, and vegetation type and density were also made in conjunction with point measurements of the hydraulic gradient by using a portable pipe manometer at many locations in the study area (Lee and others, 2000).

Field measurements of surface-water stage can be made accurately with relatively simple techniques, but measurements of discharge are more difficult. Consequently, stage measurements are more abundant than discharge measurements. But a discharge measurement directly defines mass transport and therefore constrains a numerical surface-water solution much better than does stage. Coastal discharge measurement stations using ultrasonic methods are provided by Hittle and others (2001). These and other coastal discharge measurements (Woods, 2010) are useful for model comparison and calibration.

The SICS model was developed to evaluate quantities and distribution of freshwater flows and water quality in the southern Everglades for the purpose of preservation and restoration of the Everglades ecosystems (Swain and others, 2004). The SICS model was used to calculate sources and magnitudes of freshwater flow to Joe Bay under high- and low-flow conditions and surface-water ponding and salinity distribution as a function of surface-water inflow and wind conditions. In addition, effects of changing nearby pumping operations on upstream flows into Taylor Slough were evaluated. The SICS model was constructed by using a modified version of the SWIFT2D program (Schaffranek, 2004), which accounts for overland flow, effects of wind on surface-water flows, drying and rewetting of flow surfaces, variable density flow and dissolved solute transport, and one-dimensional flow through streams at a local scale. For the SICS model, the SWIFT2D simulator was modified to include influx from precipitation and efflux from ET, to account for reduction in wind stress in vegetated areas, and to consider areas of restricted flow such as coastal embankments.

Freshwater flows to the coast and the changes in freshwater flows as a result of proposed CERP activities, used for calculating salinities in Florida Bay, were simulated by using the TIME model (Wang and others, 2007). Using surface-water flows simulated by the SFWMM as input, the TIME model calculated freshwater flow and nutrient inputs into Florida Bay from the Everglades for use by another model to simulate water movement and water quality in Florida Bay. The TIME model also was used to simulate surface-water levels, flow rates, and salinities in the Everglades during 1999 through 2000. The TIME model was constructed by using the FTLOADDS program, which combines the hydrodynamic, variable-density surface-water flow and solute-transport program SWIFT2D with the variable-density groundwater flow and solute-transport program SEAWAT (Guo and Langevin, 2002). The surface-water component of the FTLOADDS program differs from the version of the SWIFT2D program used for the SICS model by modifying precipitation discretization and how it affects wetting and drying of flow surfaces, by how frictional resistance is incorporated and applied, and by the computation of ET. The TIME model has also been used for a number of applications to supply hydrologic information through various hydrologic scenarios (Green and others, 2010).

To simulate effects of the Picayune Strand Restoration Project on salinity and temperature in critical manatee habitat areas, the Ten Thousand Islands (TTI) model was constructed for the western part of the Everglades (Swain and Decker, 2009). Simulation results indicated that the planned restoration project would result in increased periods of inundation and lowered salinities in most of the coastal wetlands but that flows would be lowered to a known primary dry season habitat for the manatees. The TTI model was constructed with the FTLOADDS version that was modified to incorporate heat transport and to represent flow over hydraulic barrier structures.

Causes of hypersalinity episodes in Biscayne Bay were examined with the Biscayne model (Lohmann and others, 2012), which simulated coastal canal discharges and groundwater exchange beneath the bay. Results indicated that bay salinities are controlled by the seasonal balance of precipitation and ET. Hypersaline conditions are likely a cumulative effect of prolonged reduced precipitation at the end of the dry season, which results in reduced discharge by canals into the bay, and increased ET rates that typically occur at the onset of the dry season. Results also indicated spatial variability in response to changes in canal flows and precipitation. The Biscayne model was constructed by using the FTLOADDS program modified from the version used in the TTI model by incorporating a leakage term that allows flux between the surface of the model and any specified layer of the groundwater component of the system and incorporating albedo into the calculation of ET. Albedo has been found to be an important factor in the surface-water heat budget and its effect on ET (Swain and others, 2012). The western boundary of the Biscayne model coincided with the eastern boundary of the TIME model, along the Canal L 31 N/Canal 111 system (fig. 1).

Most recently, documentation of an extensive and detailed evaluation of two south Florida hydrologic models along with their boundary interactions with the SFWMM (MacVicar and others, 1984) and the Environmental Fluid Dynamics Code (EFDC) tidal hydrodynamics model (Hamrick, 2006) has been published by the National Park Service (NPS) South Florida Natural Resources Center (SFNRC) at ENP (Bahm and Fennema, 2013). This ENP report culminates a joint project between the SFNRC and the USGS that began in 2007 and has provided a nearly continuous supply of information to substantially improve hydrologic modeling of south Florida (Bahm and others, 2010). The two models evaluated in this joint project were (1) the version of TIME (TIME version 1.0) as applied and reported by Wang and others (2007) and (2) an updated

version of TIME (TIME version 2.0) with some coding changes including the heat transport calculations, some modified boundary input from both the SFWMM and EFDC models, several Manning's *n* friction factor changes, and other input refinements intended to improve model calibration to measured data and thereby increase model reliability when used to evaluate likely future hydrologic responses to sea-level rise and Everglades restoration plans.

The TIME version 2.0 report (Bahm and Fennema, 2013) provided recommended improvements to TIME version 1.0 and also described results of TIME version 2.0 calibration and model application to predict future conditions in ENP under several sea-level rise and water-management alternatives. Many of the recommendations were incorporated into BISECT model development and are noted herein.

Simulation of Hydrologic Conditions During 1996–2004

The BISECT model represents and is calibrated to conditions during the 9-year period from January 1, 1996, through December 31, 2004. Throughout this report, the 1996–2004 calibration period is referred to as the "base-case simulation" for the purpose of comparing to scenario simulations and testing input parameter variations.

Conceptual Model

Hydrologic processes that affect the hydrologic budget in south Florida involve the interaction of the atmospheric, surface-water, and groundwater systems, influenced by features such as inland and coastal streams, inundated freshwater marshes and sloughs, and constructed canals (fig. 2). The system is ultimately recharged with freshwater by precipitation throughout the entire area and freshwater inflows along the western part of the northern model boundary. Along the coastline, coastal streams discharge fresh surface water into marine areas, and brackish water is brought into and taken out of the coastal streams by tidal and wind processes. Evaporation removes water directly from the surface-water system to the atmosphere (fig. 2).

Additionally, groundwater and surface water are exchanged (fig. 2) both by surface-water recharge, which occurs where there is a downward hydraulic pressure gradient established between surface-water stage and groundwater head such that surface water becomes a source of water to the underlying groundwater system, and by groundwater discharge, which occurs where there is an upward hydraulic pressure gradient between groundwater head and surface-water stage resulting in groundwater becoming a source of water to surface-water bodies. Such groundwater and surface-water exchange may occur in streams, canals, and inundated marshes, as well as on marine floor surfaces.

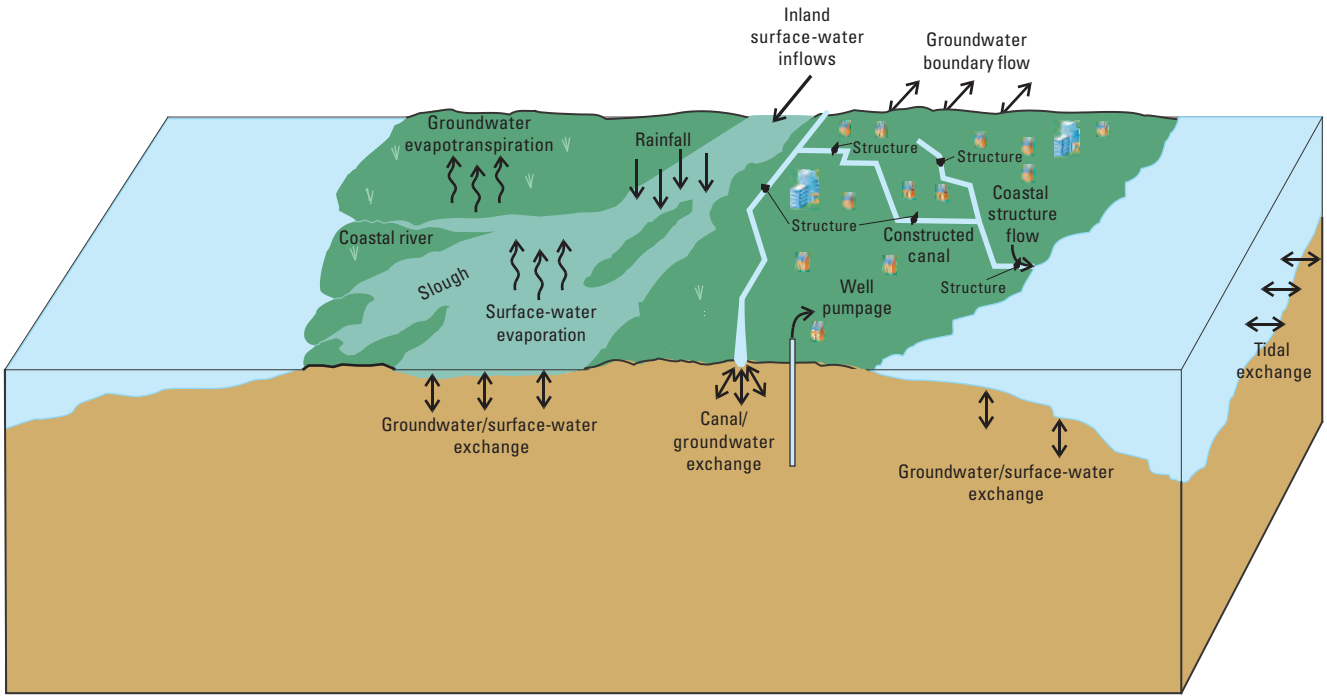

Figure 2. Conceptual model of the hydrologic system of the Biscayne and Southern Everglades Coastal Transport (BISECT) model area, south Florida.

Groundwater pumping and near-land-surface ET processes also remove water directly from the groundwater system (fig. 2). Groundwater may enter or leave the system in the coastal areas of the south Florida hydrologic system and along the inland edges of the domain. Precipitation and upstream inflows deliver freshwater to the system, while tidal processes and groundwater exchange in bays and other marine areas bring saltwater into the system (fig. 2).

Numerical Model

Simulation of the hydrologic system requires an accurate representation of the hydraulic connectivity between the extensive surface-water system of lakes, streams, canals, sloughs, marshes, and other wetlands and the highly transmissive, multilayered, shallow groundwater system underlying the entire area. Also, the density difference between freshwater and saltwater must be accounted for in order to properly simulate their movements and mixing throughout the model area because all coastal streams, as well as many coastal lakes, ponds, and marsh areas, are exposed periodically to saltwater and because the groundwater system extends under and interacts with saltwater bodies that surround the study area. Representing density differences is a critical capability for the evaluation of the anticipated increase in saltwater encroachment from sea-level rise and for an evaluation of whether vertical aquifer barriers, increased freshwater deliveries, or both can help avert or reduce such encroachment.

The BISECT model was calibrated to field data from networks of surface-water stage, groundwater levels, coastal discharge, water salinity, and water temperature stations stored on the SFWMD DBHYDRO database (South Florida Water Management District, 2017), the USGS NWIS database (U.S. Geological Survey, 2017a), and the SOFIA website (U.S. Geological Survey, 2017b).

To better understand the level of confidence that can be placed in such measured-to-simulated comparisons, several statistical parameters that quantify the degree of fit are applied. Statistics can express the total deviation of the simulation from measured values or the percentage of the measured variance expressed by the simulation. Areas with low-confidence results indicate the need for more field data or a revised conceptual model of hydrologic processes in those regions. A detailed description of the model development and calibration is presented in appendix 1.

Computed Hydrologic Budget, 1996–2004

Results from the base-case simulation were used to compute a simulated global hydrologic budget and internal fluxes between different parts of the hydrologic system. The simulated global and surface-water budgets each have less than 1-percent error in mass conservation, and the groundwater budget has only a -0.01-percent error (table 1). A common contributor to small mass-conservation error is the convergence criterion of the numerical scheme, and the groundwater simulator in BISECT has an inherently stricter iterative criterion than the alternating-direction implicit scheme of the surface-water simulator (Guo and Langevin, 2002; Schaffranek, 2004).

For the global hydrologic budget, rainfall, which brings water into the system, and surface-water evaporation, which takes water out of the system, are the largest components (table 1). When dividing by the BISECT domain area and the number of years, the mass fluxes in table 1 are 1,426 millimeters per year (mm/yr) rainfall, 1,230 mm/yr surface-water ET, and 19 mm/yr groundwater ET. However, these values are averaged over the entire domain, and groundwater ET is only simulated as a separate quantity in noninundated cells. So, the groundwater ET at dry areas with high groundwater, such as coastal zones, can be much higher than average, reaching 300–400 mm/yr.

Canal/groundwater exchange is the next largest component of the global budget. Computed separately from the groundwater/surface-water interactions, the canal leakage acts as an external boundary (fig. 2) and, combined with rainfall and ET, accounts for approximately 84 percent and 86 percent of the global inputs and outputs, respectively. Groundwater storage input and output are equivalent in magnitude and are the next largest component of the global budget.

Water coming into the system through the groundwater and inland surface-water boundary flows and leaving the system through the groundwater boundary flows, including well pumpage, are minor components of the overall budget (table 1, fig. 2). The net exchange of water through the tidal boundaries is five orders of magnitude smaller than the overall budget.

The computed exchange between the groundwater and surface-water systems (which excludes the canal leakage discussed above) labeled as “groundwater/surface-water exchange” in the surface-water budget can be compared to the magnitudes of the “canal/groundwater exchange” in the global budget to gain insight into the hydrologic system (table 1).The groundwater loses about 2.4 times more water to the canals than to the other surface-water systems and gains about 4.5 times more water from the other surface-water systems than it does from canals. This indicates that the canals can be considered predominantly drains and the wetlands predominantly groundwater recharge sources.

Model Sensitivity

As part of the BISECT model development, a sensitivity analysis was performed (app. 1). Selected input parameters are perturbed to a higher and lower value, and the responses of model outputs are evaluated. The parameters were chosen for their role in the governing equations and their physical significance and include Manning’s *n,* wind friction coefficient, tidal amplitude, thickness of the transition layer between the surface water and groundwater, canal conductance, the aquifer vertical and horizontal hydraulic conductivities, and the albedo. Model sensitivity is evaluated

Table 1. Computed water budgets for the Biscayne and Southern Everglades Coastal Transport (BISECT) model (global budget), for the groundwater part of the hydrologic system (groundwater budget), and for the surface-water part of the hydrologic system (surface-water budget) during 1996–2004.

[ET, evapotranspiration]

Input		Output	
Global budget			
Inland surface-water inflows	3.61×10^{10}	Surface-water evaporation	1.13×10^{14}
Tidal exchange	2.45×10^{09}	Tidal exchange	3.32×10^{09}
Canal/groundwater exchange	7.42×10^{12}	Canal/groundwater exchange	2.50×10^{13}
Surface-water storage	2.88×10^{12}	Groundwater ET	1.71×10^{12}
Rainfall	1.31×10^{14}	Well pumpage	4.76×10^{12}
Groundwater boundary flow	2.74×10^{12}	Groundwater boundary flow	1.70×10^{12}
Groundwater storage	1.44×10^{13}	Groundwater storage	1.44×10^{13}
Total	1.58×10^{14}	**Total**	1.61×10^{14}
		Percent error	-0.66
Groundwater budget			
Groundwater storage	1.44×10^{13}	Groundwater storage	1.44×10^{13}
Groundwater/surface-water exchange	3.34×10^{13}	Groundwater/surface-water exchange	1.04×10^{13}
Canal/groundwater exchange	7.42×10^{12}	Canal/groundwater exchange	2.50×10^{13}
Groundwater boundary flow	2.74×10^{12}	Groundwater boundary flow	1.70×10^{12}
		Well pumpage	4.76×10^{12}
		Groundwater ET	1.71×10^{12}
Total	5.80×10^{13}	**Total**	5.80×10^{13}
		Percent error	-0.01
Surface-water budget			
Rainfall	1.31×10^{14}	Surface-water evaporation	1.13×10^{14}
Groundwater/surface-water exchange	1.04×10^{13}	Groundwater/surface-water exchange	3.34×10^{13}
Tidal exchange	2.45×10^{09}	Tidal exchange	3.32×10^{09}
Inland surface-water inflows	3.61×10^{10}		
Surface-water storage	2.88×10^{12}		
Total	1.44×10^{14}	**Total**	1.46×10^{14}
		Percent error	-0.72

by comparing the base-case simulation results to the perturbed simulation results at stage measurement stations (fig. 3), discharge measurement stations (fig. 4), as well as salinity and temperature stations (figs. 3 and 4). Details on the sensitivity analysis can be found in appendix 1.

The responses of BISECT-simulated water level, discharge, and salinity to each of the perturbed input parameters in the sensitivity analyses provide insight on how model input parameterization affects model-simulated hydrology (app. 1):

1. Higher simulated tidal amplitude results in larger cumulative flows, and smaller amplitude results in lower cumulative flows in the representation of most Everglades coastal streams.
2. The simulated response of cumulative flows into Long Sound (fig. 4) to modeled variations in tidal amplitude, wind, and frictional resistance does not follow the patterns of other coastal streams.
3. Simulated cumulative coastal streamflows along the Whitewater Bay and Florida Bay coast (fig. 1) exhibit more substantial effects from increased winds than do simulated coastal streamflows along the Gulf of Mexico coast where a larger lunar tide component overwhelms the wind effects.
4. Simulated variations in flow to the Everglades coastal streams are substantially affected by groundwater/surface-water interactions in the eastern urban areas.

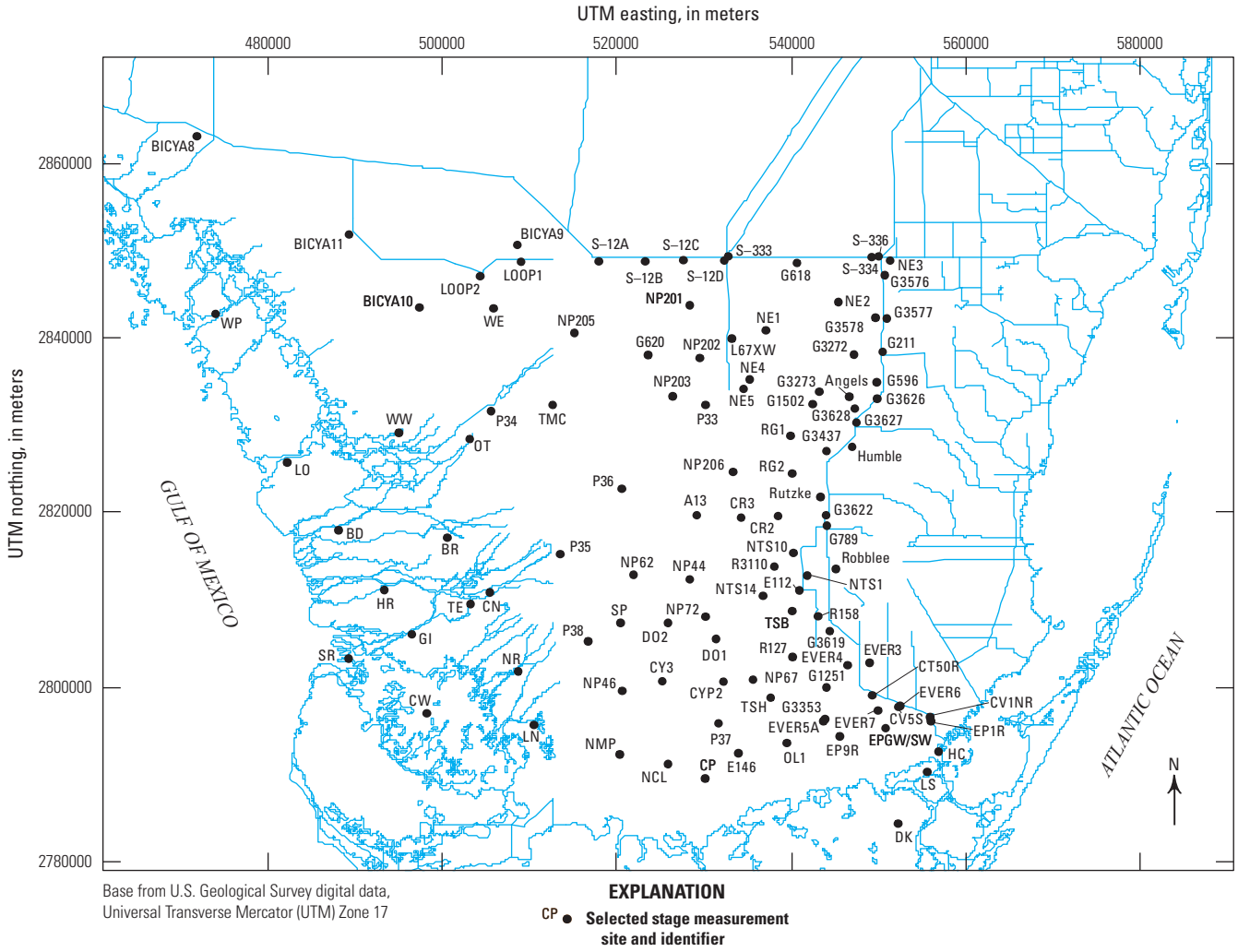

Figure 3. Locations of stage measurement stations (temperature also measured at P33; see app. 3 for station details) for the Biscayne and Southern Everglades Coastal Transport (BISECT) model application for south Florida.

5. Cumulative flows at McCormick Creek (fig. 4) are sensitive to variations in the model input tide and aquifer leakage.

6. Simulated Harney River (fig. 4) flow variations are most strongly affected by upstream model parameters such as frictional resistance, but Harney River salinity variations are most strongly affected by downstream parameters such as tidal fluctuations.

7. Simulated levels at the headwater of Taylor Slough (fig. 4) are substantially affected by aquifer leakage parameters and water exchanges with the urban canals.

8. Variations in simulated flow at Broad River and Lostmans River (fig. 4) are more sensitive to variations in the parameterization of the hydrologic system than are any of the other rivers.

Water-Management and Sea-Level Rise Scenario Results

BISECT was used to evaluate the effects of sea-level rise and anthropogenic changes on the hydrologic system of south Florida. Six scenarios were designed to represent proposed or potential changes to the system, involving three principal changes to the system and a combination of these changes, as described below. Differences between each of the six scenario simulations and the base-case simulation were quantified at field stations that measure surface-water stage, discharge, salinity, and temperature (figs. 3 and 4). These differences are quantified with the root-mean square difference (*RMSD*) and mean difference (*MD*) statistics, which are the same mathematical form as the root-mean square error (*RMSE*) and mean error (*ME*) statistics used to analyze model errors

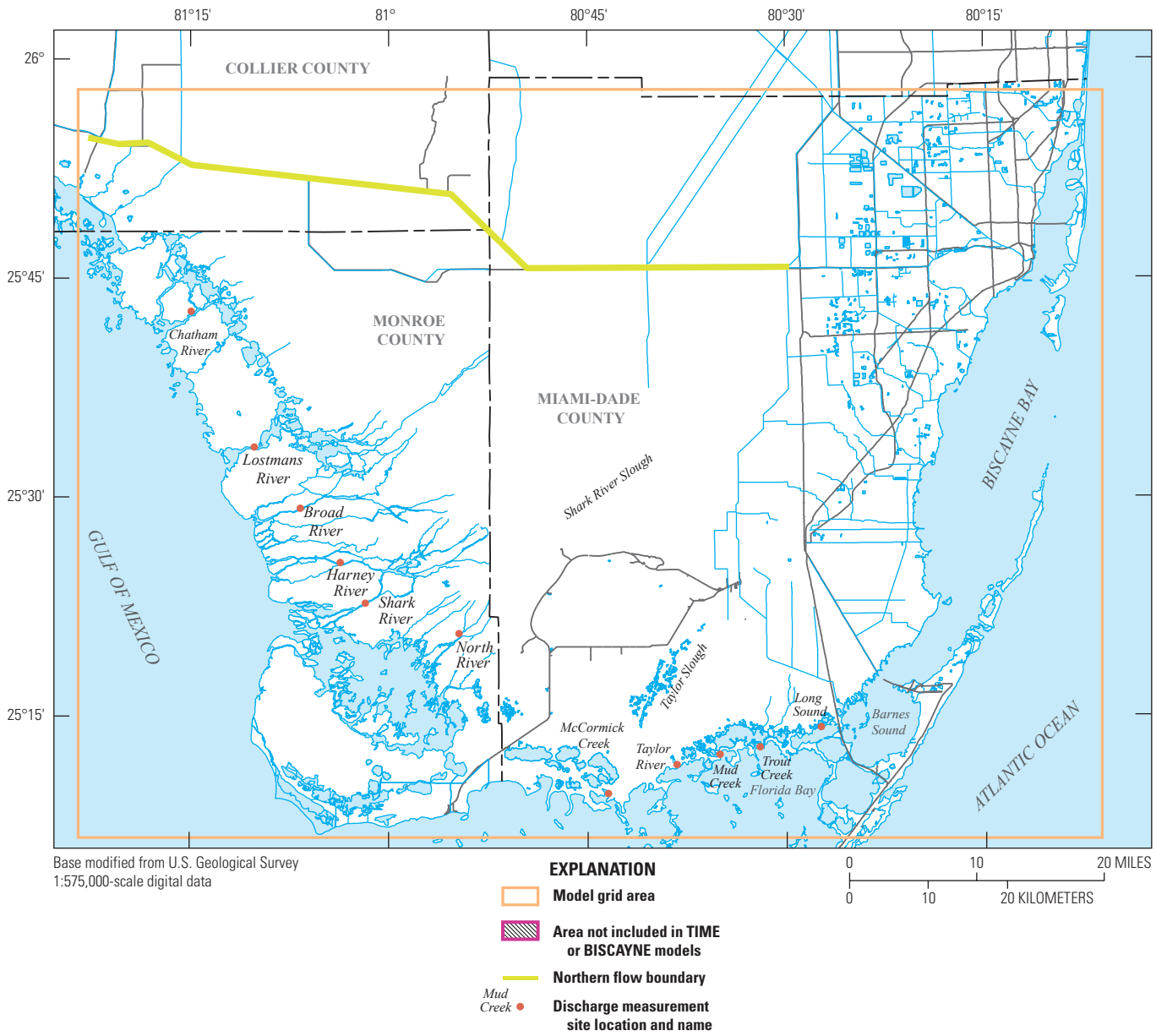

Figure 4. Locations of discharge measurement stations (salinity also measured at Harney River and Shark River sites; temperature measured at Shark River site; see app. 3 for station details) for the Biscayne and Southern Everglades Coastal Transport (BISECT) model application for the south Florida peninsula.

(see app. 1), except that a difference between simulations is expressed rather than a difference between simulation and field data. The stage time series are also used to calculate the percentage of time that each model cell is inundated, which gives insight into wetland hydroperiods and urban flooding under scenario conditions.

The two types of hydrologic management methods examined in these model scenarios are the use of aquifer barriers and modified water deliveries. Simulating these management methods assists in planning and determining what effects can be attained through modifications to the system.

Implementation of Aquifer Barriers—Scenarios 1 and 2

A proposed aquifer grout barrier along the northern part of Canal L 31N (fig. 1) is represented in scenarios 1 and 2. This barrier was originally conceived to reduce groundwater exchanges between the western wetlands and the eastern urban areas. These scenarios test how different configurations of the barrier perform and any other effects of implementing such barriers. In scenario 1 the grout barrier penetrates the Biscayne aquifer to half of its depth (10 m); in scenario 2 the barrier penetrates the Biscayne aquifer to

its full depth. Both scenarios use the 1996–2004 base-case simulation period data for all other model input. The effect on groundwater flow direction can be seen by examining simulation-period-averaged groundwater flux per unit width, averaged vertically, for the two aquifer barrier simulations with the base case (fig. 5). The easterly groundwater flux vectors in the vicinity of the barrier are reduced, most noticeably in the full-depth barrier scenario, although changes do not seem to propagate more than a kilometer or so from the barrier. The aquifer grout barrier seems to have a quite localized effect on groundwater flows.

Comparisons indicate that the aquifer barriers have relatively minor effects on the coastal stream cumulative flows, and it is difficult to define any trends in these effects (table 2). A positive percentage change indicates that the simulated cumulative volume for the scenario was larger than for the base case, and a negative change indicates that the cumulative volume for the scenario was less than for the base case. It is difficult to place any significance in these percentages; for example, the largest magnitude effect is -1.7 percent indicated at Broad River, a very small cumulative change in flows with much larger tidal fluctuations. The aquifer barriers minimally affect stage at the measurement stations, with negligible effects on mean stage (indicated by *MD*) and stage-fluctuation responses (fig. 6). Once again, it is difficult to place any significance in these small values. However, the closest measurement station (G3272) is more than 3 km from the aquifer barrier location, so localized changes near the barrier are not examined.

Computed *MD* and *RMSD* values for coastal streamflows (fig. 7) reflect the same patterns as the cumulative coastal streamflows above (table 2). The effects of the aquifer barrier on coastal discharge are negligible (fig. 7), and the highest *RMSD* values at Broad River are still considered too small to be conclusive (figs. 4 and 7). Most simulated salinity and temperature statistics for the aquifer barrier scenarios do not show any marked effects (fig. 8) as might be expected; however, the *RMSD* for temperature at P33 indicates that detectable changes in temperature fluctuations may occur, possibly with differing groundwater exchange.

The effect of varying hydrologic conditions on surface-water inundation is an important factor in habitat ecology and urban flooding. A graphical representation of the spatial distribution of the computed percent of time that modeled area is inundated during the entire base-case simulation shows the differences between hydroperiods of the Everglades and the urban eastern area (fig. 9). The percent of time inundated in the Everglades is heavily influenced by the topography and the sloughs, the southern and western coastal zones tend to be somewhat drier than the inland wetlands, and the urban area is more uniformly zero inundation. The demarcation between the natural areas to the west and the developed areas to the east is strongly reflected by wetter and drier inundation patterns (fig. 9)

The simulated hydroperiods for each scenario were compared with the base-case simulation by mapping the difference in percent of time inundated (fig. 10). Areas that are inundated nearly all of the time may show no difference in percentage of time inundated between the scenarios and the base case, although the water depths may be changing. Scenario 1 (with the aquifer barrier at one-half the aquifer depth) did not yield a change of more than 2.5 percent in hydroperiod at any location, but scenario 2 (the full-depth aquifer barrier) indicated a slight increase in hydroperiod of about 5 percent in a small area adjacent to the barrier (fig. 10*A* and *B*). The specific location of this hydroperiod increase is adjacent to the southern part of the barrier, corresponding to an area where the percent of time inundated was originally lower than 50 percent (fig. 9). The area adjacent to the northern part of the barrier (within Shark River Slough) originally had a percent of time inundated above 95 percent and did not show a substantial increase (fig. 10*B*).

Implementation of CERP—Scenario 3

The effects of CERP on the BISECT model area were investigated in scenario 3. CERP is a long-term plan with a main goal of capturing water that is normally routed to the Atlantic Ocean and the Gulf of Mexico and redirecting flows to natural areas where needed (Perry, 2004). The flow modification is largely achieved through the operation of the water-control structures south of Lake Okeechobee. The SFWMM (South Florida Water Management District, 2005) is a hydrologic management model that simulates the Florida region south of Lake Okeechobee. For this scenario, the relevant BISECT boundary conditions are derived from an SFWMM simulation representing the CERP water-management scheme. The surface-water flows generated by the SFWMM at the location of the BISECT domain's northern flow boundary (fig. 4) were extracted and formatted for input to the BISECT model (Wolfert and others, 2004; Swain and Lohmann, 2018). The output from the SFWMM does not extend beyond the year 2000; therefore, this scenario is for only the 1996–2000 period.

Substantial changes in cumulative coastal flows are indicated in scenario 3 (table 2). Increased flows are simulated at Chatham River and substantially decreased flows at Broad River, Harney River, Shark River, North River, McCormick Creek, Taylor River, and Mud Creek. The CERP inflows along the northern flow boundary (fig. 4) are similar in cumulative magnitude to the surface-water inflows in the base-case simulation but redistributed more to the western part of the model so that, when entering the model domain, coastal outflows are higher in the northwest (Chatham River) and nearly the same in the southeast (Long Sound) with a reduction in flows in the intervening coastal zones (table 2, fig. 4). One CERP objective is to move more water to the west, increasing hydroperiod and depth of inundation in the northwestern area of ENP.

Scenario 3 results indicate that the CERP has a strong effect on stage at Taylor Slough Bridge, with a drop in mean water levels (*MD*) of more than 0.3 m, and a lesser effect in the Shark River Slough area, with slightly higher stage at G3272 and lower stage at NP-201 and P-33 (fig. 6). The highest *MD*

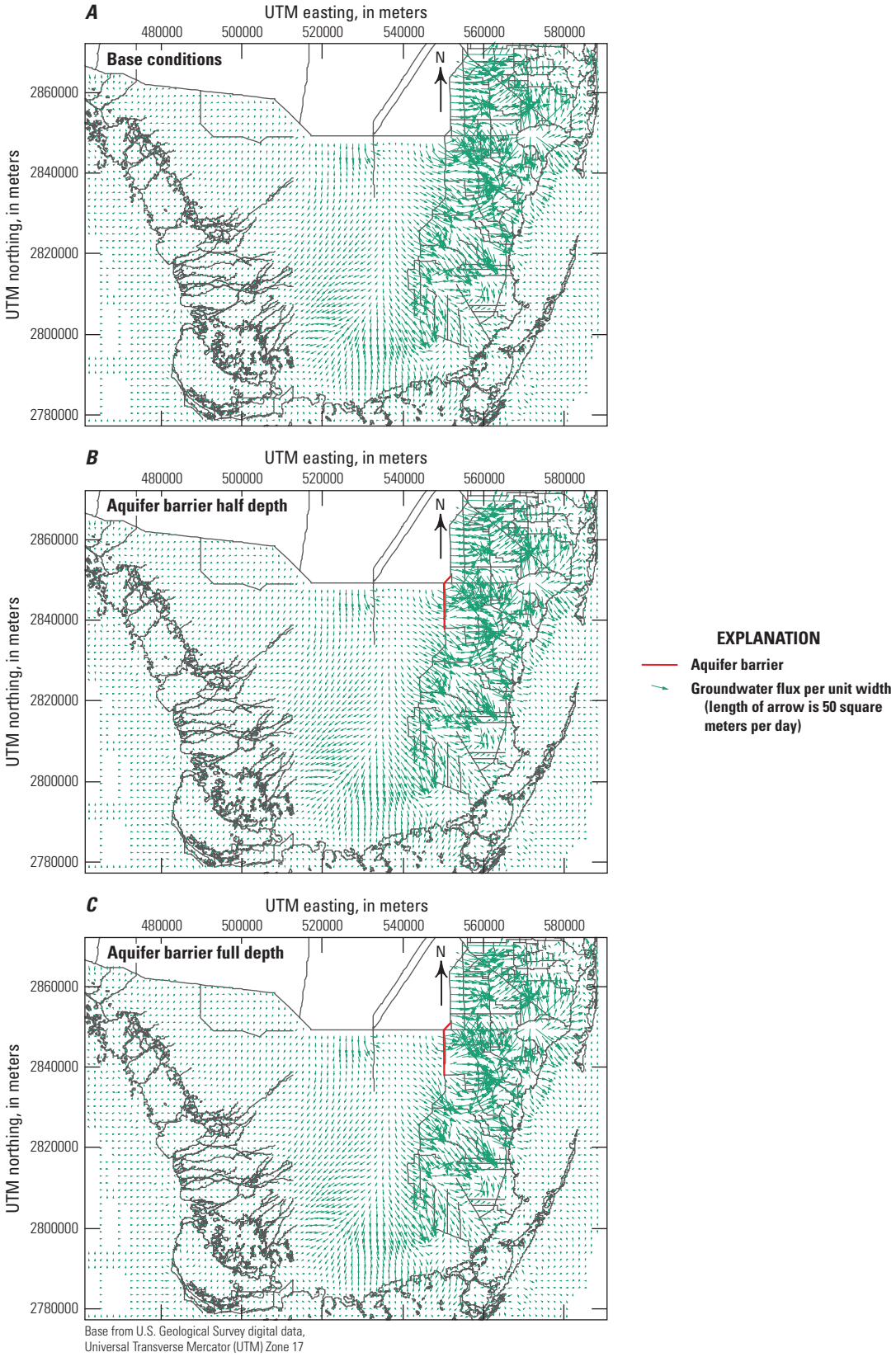

Figure 5. Simulated vertically averaged groundwater flux per unit width, averaged for the 1996–2004 period, with and without different aquifer grout barriers for the Biscayne aquifer, south Florida peninsula, by the Biscayne and Southern Everglades Coastal Transport (BISECT) model. *A*, Without aquifer barrier. *B*, With aquifer barrier half depth. *C*, With aquifer barrier full depth.

Table 2. Percentage difference in cumulative flow volume over the 1996–2004 period between model scenarios and base-case simulation by the Biscayne and Southern Everglades Coastal Transport (BISECT) model for streams in south Florida.

[m^3/s, cubic meter per second; CERP, Comprehensive Everglades Restoration Plan; cm, centimeter]

Stream	Mean flow (m^3/s)	Aquifer partial barrier	Aquifer full barrier	CERP inflows	30-cm sea-level rise	60-cm sea-level rise	Aquifer barrier, CERP inflows, 60-cm sea-level rise
Broad River	13.65	-1.66	-0.06	-4.84	24.9	14.5	9.59
Chatham River	13.45	-0.01	-0.06	18.36	70.4	73.9	80.1
Harney River	8.65	0.02	0.15	-7.31	-72.3	-41.9	-43.9
Long Sound	0.73	-0.13	-0.35	-0.55	-57.3	-27.9	27.9
Lostmans River	34.99	-0.01	0.04	-1.43	40.8	72.9	72.1
McCormick Creek	0.51	0.25	0.58	-6.09	1,085.7	2,414.4	2,184.4
Mud Creek	1.25	-0.05	-0.04	-4.64	-9.06	43.5	54.3
North River	2.19	0.00	0.31	-10.98	11.7	12.1	5.93
Shark River	11.77	0.07	0.18	-4.91	7.18	0.82	-1.17
Taylor River	2.66	-0.05	0.01	-7.79	11.3	56.9	56.5
Trout Creek	6.89	-0.04	-0.02	-2.27	-5.73	35.6	52.1

for discharge is at Chatham River (fig. 7), reflecting the overall higher flow indicated in the cumulative discharge (table 2), but Lostmans River has a slightly higher *RMSD* than does Chatham River, indicating that CERP management affects flow variability there. Mean salinity increases (*MD*) at Harney and Shark Rivers of more than 1 practical salinity unit (PSU) are simulated, as well as changes in the salinity fluctuations (*RMSD*), a likely result of the lower freshwater flows at these two sites (fig. 8). Temperature statistics do not indicate mean changes in temperature, but a small change in temperature variability is indicated inland at P33 (fig. 8), which might be expected when the time series of flows change. Longer inundation times are most prominent in the northwest and southeast parts of ENP (fig. 10*C*), the locations where CERP is designed to route flow. Slightly shorter inundation times (less than 5 percent decrease) are indicated in some areas adjacent to Shark River Slough (fig. 10*C*), which correspond to areas with less base-case inundation (fig. 9). It appears that these higher elevation areas are not inundated quite as often with CERP, but the lower areas of Shark River Slough are the same or inundated more (fig. 10*C*). This inundation pattern is due to lower peak water levels in the central part of ENP under CERP. Overall, few CERP-induced changes are seen in Shark River Slough compared to the considerable increases in hydroperiods to the northwest and southeast.

Effects of Sea-Level Rise on the Hydrologic System—Scenarios 4 and 5

To simulate effects of sea-level rise on hydrologic conditions in the study area, two scenarios, representing a 30-cm rise and a 60-cm rise, were simulated (U.S. Army Corps of Engineers, 2013). As the base-case simulation period of only 9 years is used, no attempt was made to simulate a gradual sea-level increase over a multidecadal period. Rather, the mean sea level represented in the model is raised for the entire simulation period by 30 cm and 60 cm in scenarios 4 and 5, respectively, which may underestimate effects of sea-level rise that manifest over periods longer than a decade, such as groundwater salinity intrusion. The tidal fluctuations from the conditions of the base-case simulation period were superimposed on the simulated increases in mean sea levels. The atmospheric conditions from the base-case simulation period were used for both increased sea-level-position scenarios. The simulated flows through structures were reduced from the base-case simulation flows to account for the loss of flow capacity resulting from the decrease in hydraulic gradient with an increased sea level. The design stages and flows from USACE (U.S. Army Corps of Engineers, 2005) were used to develop the flow coefficients and determine the reduction of flows. The percentage of reduction in flow at the coastal structures S-20, S-20F, S-20G, S-21, S-21A, S-22, S-25B, S-26, S-27, S-28, S-29, S-123, and G-93 (fig. 1) is computed by adding the potential increase in sea-level elevation to the current sea-level elevation at the downstream side of the structure (fig. 11). Small and manually operated coastal structures (S-25, S-197 in fig. 1) are considered closed with no flow for these simulations. Inland pump stations (S-331, S-332, S-332B2, S-332D in fig. 1) are maintained at the same flows as the base-case simulation. For inland gated structures (S-175, S-12A, S-12B, S-12C, and S-12D in fig. 1), the reduced flow is determined by multiplying the existing conditions flow by

$$\left(Z_u - SLR\right) / Z_u \tag{1}$$

where

Z_u is the design upstream stage referenced to sea level, and

SLR is the amount of sea-level rise above current sea level.

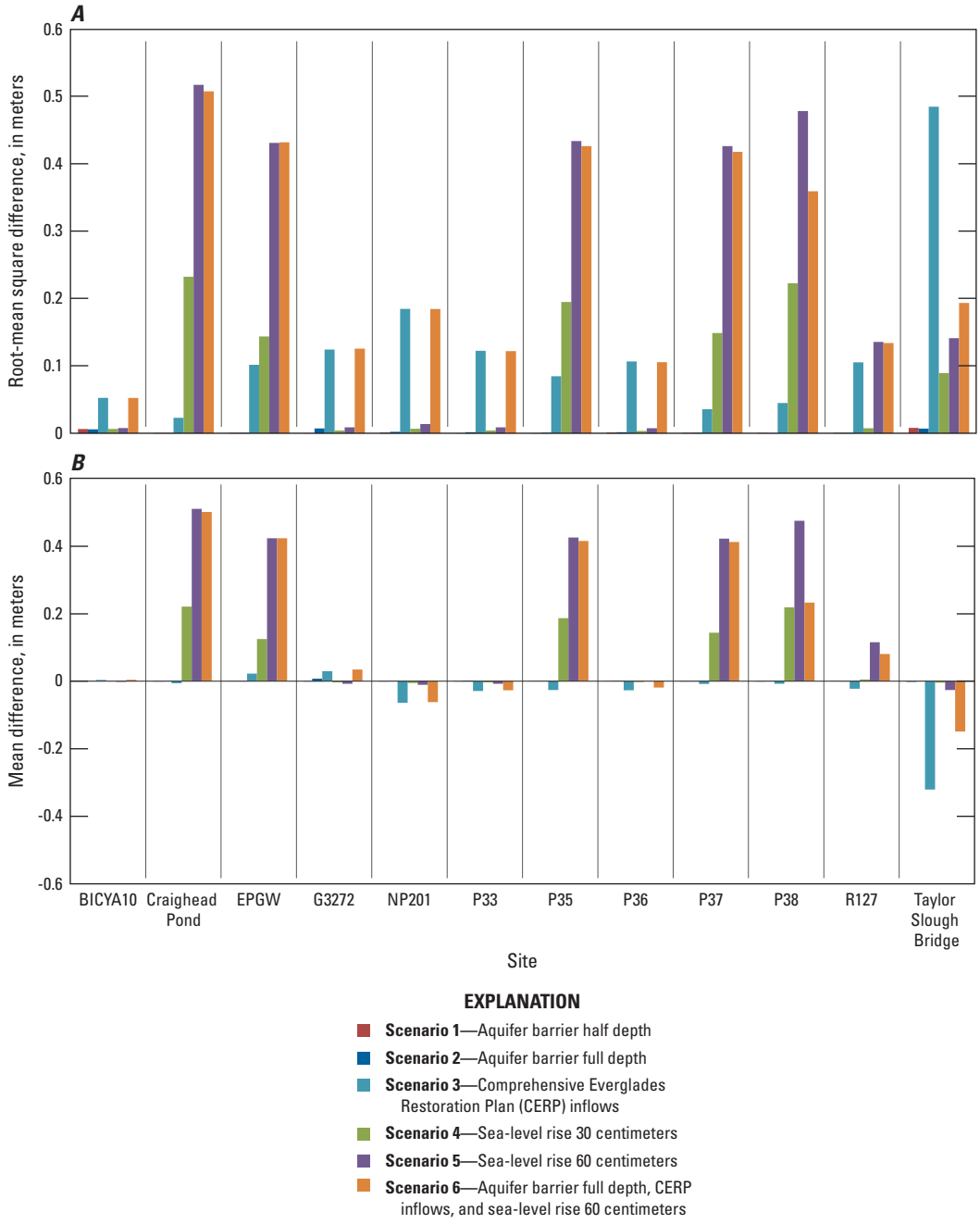

Figure 6. Scenario statistics simulated by the Biscayne and Southern Everglades Coastal Transport (BISECT) model for stage measurement stations in south Florida, 1996–2004 (see app. 3 for station details). *A*, Root-mean square difference. *B*, Mean difference.

Other flows such as bridges and culverts under Tamiami Trail from Tamiami Canal (fig. 1) are reduced by the same percentage as the S-12 structures. Separate time series of these modified flow data are produced for the 30-cm and 60-cm sea-level rise simulations.

The differences in coastal stream cumulative flow between the sea-level rise scenarios and the base-case simulation are counterintuitive, as the expected lower coastal flow seaward in the sea-level rise scenario may not be reflected in the cumulative streamflows. As the sea level rises, the increased coastal inundation at high tide allows more overland flow inland, outside of the stream channels where measurements are made, whereas at low tide, seaward flows are contained in stream channels. This results in an apparent higher cumulative streamflow to tide. So, the difference in cumulative streamflow between the sea-level rise scenarios and the base-case simulation should not be interpreted as a measure of total coastal exchange but instead reflects how much the inland overland flow component increases with sea-level rise. The cumulative outflow as a percentage of total

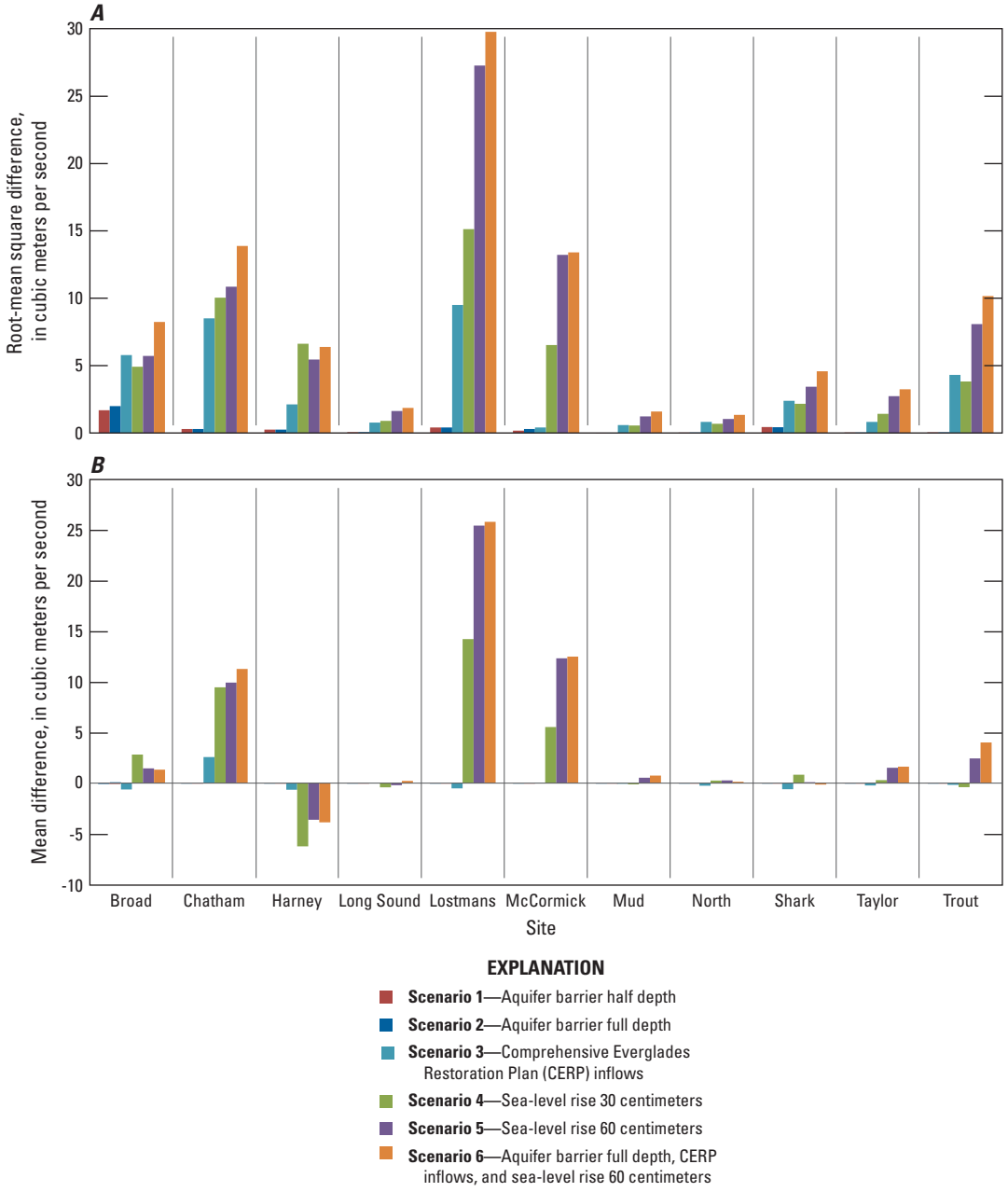

Figure 7. Scenario statistics simulated by the Biscayne and Southern Everglades Coastal Transport (BISECT) model for discharge measurement stations at streams in south Florida, 1996–2004 (see app. 3 for station details). *A*, Root-mean square difference. *B*, Mean difference.

outflow at McCormick Creek increases more than at other coastal streams for both sea-level rise scenarios (table 2), which would indicate that the surrounding area inundates and allows substantial inland flow during higher tides, which then flows outward mostly through the stream at lower tides. Conversely, Harney River has the largest percentage inflow change (negative) in the 30-cm sea-level rise scenario, indicating that flow is confined mostly to the stream during both inflow and outflow.

Marked increases in mean stages (*MD*) between both sea-level rise scenarios and the base-case simulation were simulated at the coastal and slough sites, especially Craighead Pond, EPGW, P35, P37, and P38 (fig. 6). The same sites show the greatest variation in stage temporal patterns relative to the base case (*RMSD*). Site R127 (fig. 3), farther inland in Taylor Slough (fig. 4), shows a stage increase for the 60-cm sea-level rise but not for the 30-cm rise (fig. 6). Generally, the strongest effects on stage of all of the scenarios are in the sea-level rise scenarios.

Statistical analysis of the discharge measurement sites (fig. 7) reflects the findings of the cumulative discharge comparisons (table 2), and it is difficult to define any trends in these effects. However, the cumulative discharge changes

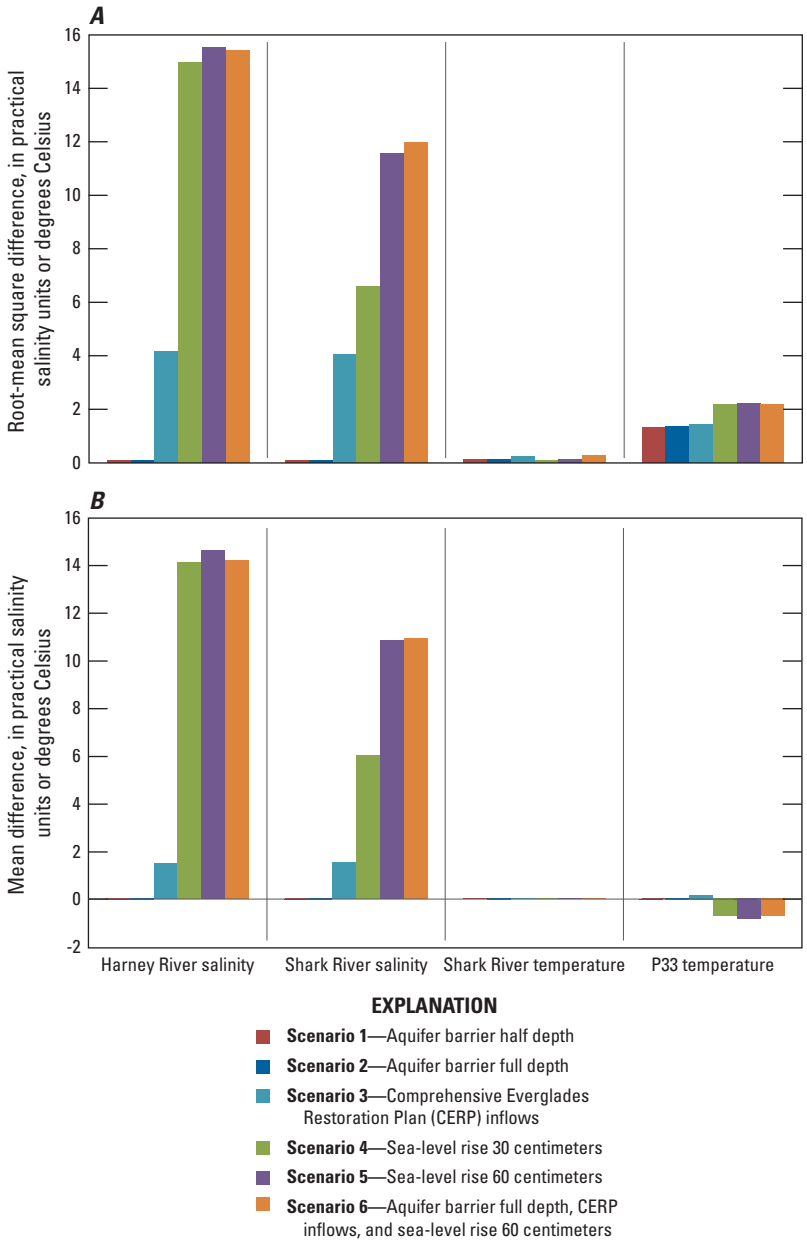

Figure 8. Scenario statistics simulated by the Biscayne and Southern Everglades Coastal Transport (BISECT) model for salinity and temperature measurement stations at streams in south Florida, 1996–2004 (see app. 3 for station details). *A*, Root-mean square difference. *B*, Mean difference.

are reported as a percentage of average discharge (table 2), whereas the mean discharge is not normalized. For both sea-level rise scenarios, the largest mean outflow change (*MD*) is at Lostmans River (fig. 7), which also has the biggest change in temporal fluctuations (*RMSD*). As described above for the case of McCormick Creek, these Lostmans River statistics indicate that the surrounding area inundates substantially with higher sea level and overland inflows. However, total flows at Lostmans River are approximately 70 times that at McCormick Creek, so this change at Lostmans River is not as large in proportion to the total discharge as in the case of McCormick Creek.

Of all the scenarios, sea-level rise has the largest effect on coastal salinity (fig. 8). The mean salinity (*MD*) increases as much as 14 PSU at Harney River for the 30-cm rise scenario and slightly more than that in the 60-cm scenario. Shark River has less of a salinity increase, and it differs more between the 30-cm and 60-cm sea-level rise scenarios. The locations of these two streams affect their response to sea-level rise; Shark River is somewhat more enclosed in Whitewater Bay than is Harney River (fig. 4) and responds less to salinity intrusion induced by sea-level rise.

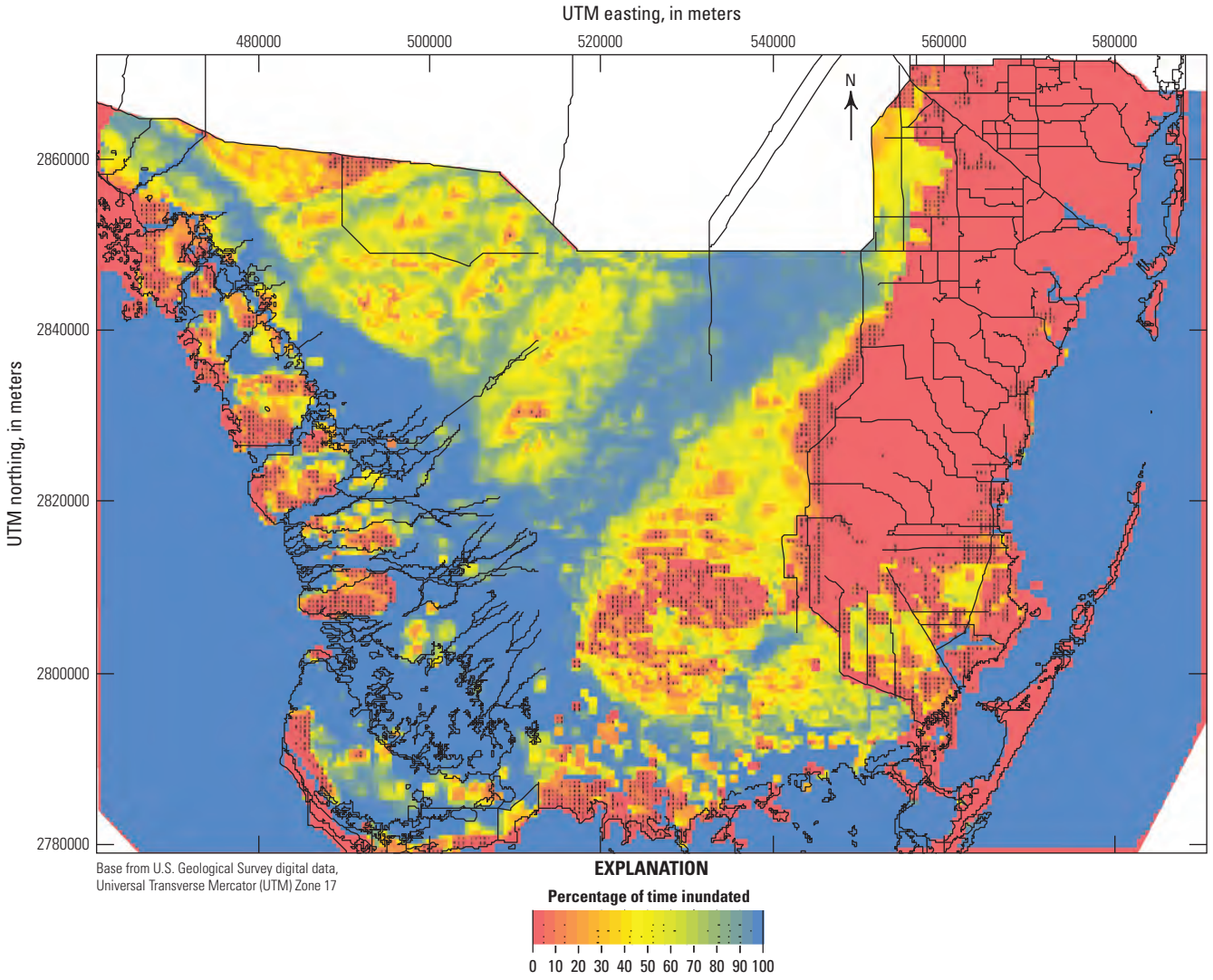

Figure 9. Simulated percentage of time inundated for the base-case simulation of the 1996–2004 period in the Biscayne and Southern Everglades Coastal Transport (BISECT) model for south Florida.

Temperature responses to sea-level rise at Shark River are negligible (fig. 8), but there is a detectable drop in average temperature at the inland site P33 (*MD*) in both the 30-cm and 60-cm scenarios, which could be the difference in temperature as offshore waters are pushed inland. P33 also has differences in the temperature pattern (*RMSD*), which would be expected if sea-level rise was changing flow patterns.

Areas showing a larger percentage of time inundated with sea-level rise follow the coastline, particularly along the western and southern coastline represented in the model (fig. 10). This vulnerability to sea-level rise is strongly a function of the topography in these areas, which is high enough to be infrequently inundated at base-case simulation sea levels but low enough for the sea levels in the scenarios to affect inundation. The topographies of the coastal areas with smaller increases in inundation are either so high as to be less affected by the sea-level increase, as in the eastern and northeastern coastal areas, or low enough to be already inundated in the base-case simulation, as in the southwestern coastal area (fig. 9).

Effects of Proposed Aquifer Management Plans in Response to Sea-Level Rise—Scenario 6

Scenario 6 is used to evaluate combined effects of some of the system changes that were individually examined in the previous scenarios. As the possible extents of the management and climate effects are of most interest, the more extreme changes in aquifer barrier and sea level were chosen, incorporating changes used in scenario 2 (the aquifer barrier extending to the full aquifer depth), scenario 3 (CERP water deliveries implemented), and scenario 5 (a 60-cm sea-level rise). As the CERP dataset represents only the period 1996–2000, this scenario is restricted to this period. The differences in computed coastal stream cumulative flows between scenario 6 and the base case are similar to those differences between scenario 5 and the base case, indicating that the effects of sea-level rise are greater than effects of CERP or the aquifer barrier on coastal flows. This combined

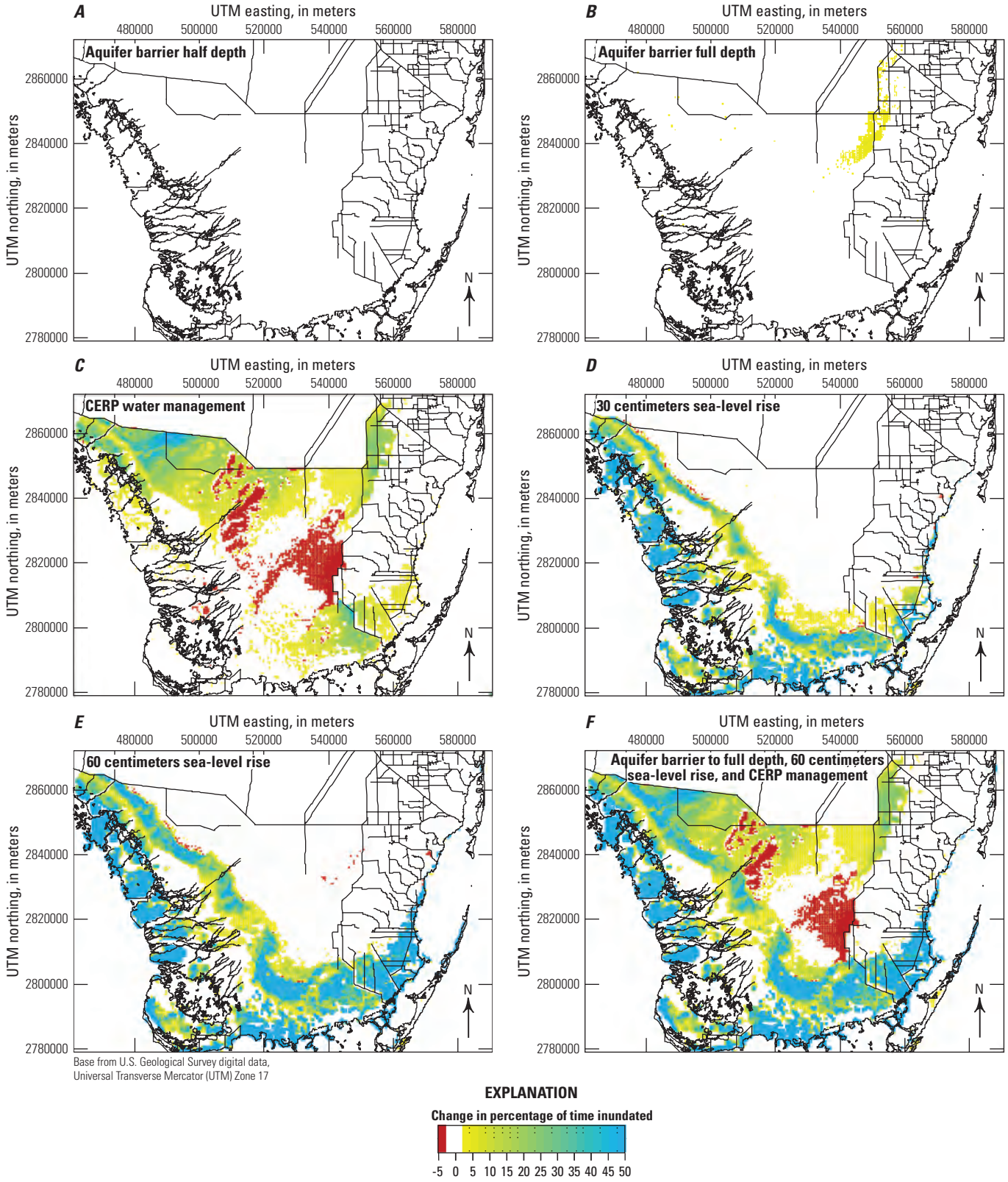

Figure 10. Changes in simulated percentage of time inundated during the 1996–2004 period for various scenarios in the Biscayne and Southern Everglades Coastal Transport (BISECT) model for the south Florida peninsula. *A*, Aquifer barrier half depth. *B*, Aquifer barrier full depth. *C*, Water management proposed by the Comprehensive Everglades Restoration Plan (CERP). *D*, Sea-level rise of 30 centimeters. *E*, Sea-level rise of 60 centimeters. *F*, Aquifer barrier full depth, sea-level rise of 60 centimeters, and water management proposed by the CERP.

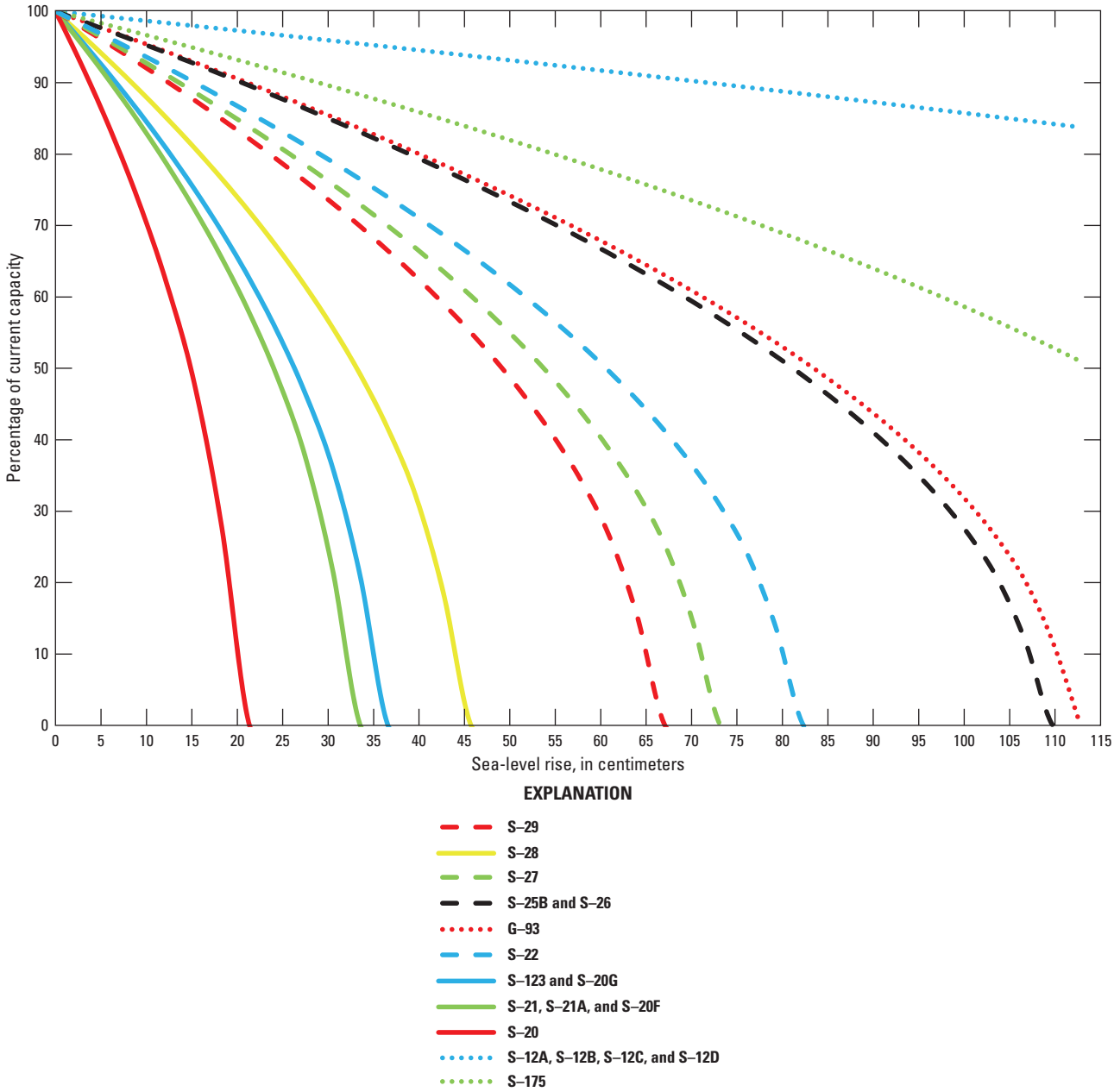

Figure 11. Percentage of current capacity of flow at hydraulic structures in the south Florida peninsula in response to increased sea levels.

scenario of the aquifer barrier, CERP inflows, and sea-level rise produces water-level changes similar to the 60-cm sea-level rise scenario at Craighead Pond, EPGW, P35, and P37 (fig. 6), whereas the water-level changes are more similar to the CERP scenario at G3272, NP201, P33, and P36 and somewhat at Taylor Slough Bridge (fig. 6). The similarity of water-level changes between scenarios delineates the coastal locations that are dominated by sea-level rise and the inland locations that are dominated by CERP water-management changes. The salinity statistics at coastal locations for scenario 6 are also similar to those for scenario 5, 60-cm sea-level rise (fig. 8), indicating that CERP restoration and the aquifer barrier have lesser effects on salinity compared to sea-level rise. To separately compare the aquifer barrier and CERP water-management effects with sea-level rise, further simulations would be necessary, but scenario 6 does demonstrate how a typical implementation of these features might perform.

Patterns of inundation duration for scenario 6 are similar in inland areas to the CERP water-management scenario 3 and almost the same as the 60-cm sea-level rise scenario 5 near the coast (fig. 10). Slight differences in inundation near and south from the location of the aquifer barrier for scenario 6 (fig. 10) indicate that the full-depth barrier can have a greater effect on hydrologic conditions compared to the other forcing functions. These results indicate that the CERP water-management

scenario does not appreciably affect inundation in coastal areas where sea-level effects dominate. Conversely, the pattern of inundation changes in the inland areas in the northwest and central areas of ENP indicates that the area is dominated by the response to the CERP-associated changes, not by sea-level rise. These coastal and inland zones are divided by a relatively well demarcated line (fig. 10), indicative of topographic constraints on the extent of tidal effects. The inundation in the southeastern area of ENP is affected by both CERP inflows and sea-level rise in the separate scenarios 3 and 5, but in the combined scenario 6 the inundation resembles the sea-level rise pattern, indicating that CERP has a lesser effect.

Effects of Environmental and Management Changes

The simulations yield the following insights into possible effects of the proposed scenarios and the behavior of the hydrologic system of the BISECT model area.

1. Aquifer barriers along the L 31N levee produce minimal surface-water changes with the full-depth aquifer barrier demonstrating some localized increase in hydroperiod (percent of time inundated).

2. CERP restoration redistributes cumulative flows markedly to the northwest (substantially higher outflow at Chatham River), and the hydroperiods are increased to the northwest and southeast of Shark River Slough. Most of Shark River Slough sees little change in hydroperiod except for some increase in the north. The redistribution of flows supports the wetland needs of northwestern ENP and the area south of Canal 111, but central ENP does not gain benefits from additional flows.

3. Sea-level change has a more pronounced effect on coastal hydrology than does CERP restoration and generally has a greater effect in areas where both are factors, but inland from a line demarcated by topography, CERP effects on inundation are largely unaffected by sea-level rise.

4. Coastal salinities are substantially affected by sea-level rise, and CERP restoration does not mitigate coastal salinities in the Shark River Slough outlet area to historical values. The differences in coastal flows induced by CERP are small relative to the flow differences induced by sea-level change.

Model Limitations

The BISECT model was constructed by using the FTLOADDS simulator and is subject to the limitations inherent to this computational tool. Both input and output quantities such as water level, salinity concentration, and model-input parameters are averaged across each model cell with a resulting limit in the spatial resolution of simulation results. The spatial averaging induces a temporal smoothing of simulation results because phenomena of small temporal scale commonly occur on a small spatial scale. Consequently, the peaks and troughs in simulated time series are often not as extreme as they are in measured data, and the model is more appropriate to examine longer term regional rather than local hydrologic conditions.

The network of canals that predominate in the eastern part of the modeled area is represented using head-dependent flux boundaries with user-defined water levels; therefore, the response of canal stages to hydrologic changes cannot be simulated, and the canals behave as an infinite water source and sink (app. 1). This limitation can be a concern when simulating hydrologic conditions that differ from those under which the user-defined canal levels were created. For example, if coastal canal discharges are reduced because of sea-level rise, the canal stages would tend to be higher than the user-defined stages. However, regulators may attempt to maintain design stages in canals through structure operations if possible, so simulating canals with the specified stage may be realistic under many conditions when limited hydrologic changes occur.

The surface-water and groundwater boundaries are subject to limitations similar to those for user-defined canal levels. Groundwater heads, tidal levels, surface-water flows, salinity, and conditions at the model boundaries are specified. Thus, simulated hydrologic conditions near the boundaries cannot vary beyond a narrow range because of the constraining effect of the boundaries. Along the offshore boundaries, it is reasonable to assume predefined hydrologic conditions because the offshore waters are a large source and sink. Compared to conditions near the coast, the groundwater heads and surface-water inflows at the northern boundary would realistically vary more with regional hydrologic changes than is represented in the model but are restricted in the simulation to user-defined values. Caution should therefore be used in interpreting results in this part of the modeled area. The surface-water flows at the northern boundary were changed for the sea-level rise simulations (fig. 11) in an attempt to account for interactions beyond the boundary.

The topography and bathymetry in the BISECT model area were derived from several sources and averaged for the 500-m cells. Because the area is largely inaccessible and the terrain is rough, the land-surface elevations in the Everglades wetlands were obtained from an airborne helicopter method (Desmond, 2003) where points were taken at 400-m spacing in the field. This method could result in elevation data that deviate from the mean elevation in the cell depending on where the measurement was taken. Regardless of the source of the topography data, the 500-m spatial averaging omits a considerable amount of spatial variation in elevation within a cell. This lack of simulated variation particularly affects the simulation of the drying and rewetting process. A cell that is simulated as dry may actually contain inundated areas smaller than the grid scale and even have sufficient inundation to have flow to adjoining cells. With stream channel widths smaller than the grid scale, modifications to certain cell elevations at the locations of streams were necessary to allow simulation of their flow (app. 1). The cell elevations were lowered sufficiently for the cells to remain wet but not as low as the

actual streambeds because that would make the simulated stream volumes much larger than the actual stream volumes. This approximation allows the model to achieve the proper connectivity of flow, although the entire modified cell should not be considered truly wet.

All BISECT simulations are initiated with water-level, salinity distribution, and temperature values that are considered reasonable for the starting date. The surface-water component of FTLOADDS defines a level-pool stage for initial conditions. A "warm-up" period occurs at the beginning of the simulation, during which errors in initial conditions dissipate and the hydrologic controlling factors begin to dominate the simulated processes. The warm-up period for water levels is less than a few months, and the distribution of surface-water salinity cannot be considered reasonable until after the first wet season. Groundwater salinity responds considerably more slowly, and initial salinity conditions were developed through a separate warm-up period of hundreds of years of simulation time (app. 1).

The large and diverse set of input data is based on field information with variable spatial and temporal distribution (app. 1). If a parameter is specified in model input at a certain spatial and temporal resolution, effects on smaller scales are not simulated. Atmospheric data such as solar radiation, humidity, air temperature, and wind are input uniformly across the entire model domain. Most of these parameters can be considered to be spatially homogeneous across large areas, but wind is known to vary widely across the model area. The surface-water flow computations occur every 10 minutes, but none of the boundary conditions are specified at this short a timescale. Wind is specified as a 4-hour average; although there are certainly wind variations on a smaller temporal scale that are ignored by the model, it would not be realistic to apply 15-minute wind data measured at a point over an entire region as smaller temporal scale variations occur on small spatial scales. Surface-water inflows are specified on a daily interval, so the effects of rapid changes in the hydraulic structure discharges north of the study area cannot be represented on a subdaily basis. Daily volumes are correct, but the timing of inundation from structure releases can be inaccurate on this time scale, and rapid structure operations are not represented. Rainfall is represented as a 6-hour average, so the surface-water response is likewise temporally smoothed to this time scale. Although total rainfall values are correct, sudden heavy rainfall could cause higher short-term inundation than represented by the model. Tidal levels are specified on a 30-minute basis, and the tidal cycle is well represented; therefore, the hydrodynamic effects at the coast, which are important to salinity mixing, are properly represented.

Some input data require extensive estimation because adequate measured data are not available (app. 1). The temperatures of surface-water inflows and groundwater leakage are estimated on the basis of a daily average air temperature. This estimate results in highly uncertain surface-water temperatures at the northern boundary. Quantities such as the wind friction coefficient and the offshore Manning's *n* are set to nominal values and are not based on any local measured data, resulting in high uncertainty in their effects. Errors in wind friction coefficient can affect simulated coastal discharges because wind drives reversals in the flows of coastal rivers. Manning's *n* values affect surface-water flows throughout the model; values that are too high cause excessive ponding, whereas low values allow too much discharge loss at the coast.

The groundwater boundary heads are defined daily, as is the groundwater time step, which is considered adequate for the rate of groundwater response (app. 1). The exchange between the surface-water and groundwater regimes is also calculated on a daily basis, and therefore rapid groundwater responses to rainfall events appear to be temporally damped.

The spatial variability of aquifer hydraulic conductivity occurs on much smaller scales than those represented in BISECT, and the amount of data available to define hydraulic conductivity is much less in the western portion of the BISECT domain than in the urbanized east. With such limited information, hydraulic conductivities for large portions of the western model domain are set uniformly to a lower value (500 m per day) and do not show the spatial variability as do those for the eastern model domain. The hydraulic conductivity field is a combination of the data developed for the precursor TIME and Biscayne models, so there is an artificial north-south demarcation at the border of these model areas (app. 2). Although this border is artificial, the hydraulic conductivity variation across it is within the uncertainty to which it is known. Consequently, the simulated groundwater conditions represent a spatial average and may be more variable in reality than as represented by the model.

The ET representation is linked to the simulation heat transport computations, and potential errors in the latent heat value in the heat transport directly affect ET (app. 1). The model's tendency to underestimate temperature in the coastal surface water could indicate that the simulated latent heat value is too high for a given set of environmental parameters; the higher latent heat (and therefore ET) cools the water and yields a lower simulated temperature to achieve heat balance. A possibly related problem was evidenced by the need to reduce groundwater ET values because the model was computing very high salinity values in the coastal groundwater (app. 1). This solution assumes that the groundwater ET originally calculated by the heat transport algorithm is too high over the entire model domain. However, if this lower groundwater ET is strictly a coastal feature, as certain research in mangrove properties indicates (Passioura and others, 1992), then this model adjustment may cause inland groundwater ET to be underestimated. The rate at which ET is reduced as the water level drops below land is a spatially uniform value in the model input, so differences between coastal and inland parameters that control groundwater ET cannot be specified without further modifications of model structure.

Although the BISECT model has these limitations, it is a useful and effective tool for understanding the regional hydrologic system of south Florida. A number of parameters,

processes, and physics that are not included in other representations of this domain are simulated in the BISECT model. The best uses of BISECT are in (1) comparing regional differences in hydrology due to proposed or anticipated changes in the system; (2) developing insight into hydrologic system characteristics not well defined by field data; (3) providing hydrologic properties and boundary conditions for other analyses and models in the study area; (4) determining the relative importance of specific controlling parameters on the hydrology; and (5) determining where in the model domain additional field data are most needed. As long as the user considers the inherent assumptions and limitations in the BISECT simulation, it is an appropriate tool to address a wide variety of hypothetical predicted and water-management changes to the hydrologic system.

Potential Applications of BISECT

The BISECT model is well suited to the following applications:

1. Developing a hindcast simulation of the years 1926–1940, a period that includes major storm events and historical aerial photography of Everglades vegetation.
2. Simulating future conditions including sea-level rise with future rainfall and temperature data downscaled from global climate models.
3. Providing hydrologic conditions to ecological applications and models of habitat dynamics and species behavior.
4. Determining the effects of water-management changes, increased wellfield pumping, and other changes to the surface-water and groundwater systems.
5. Balancing the different hydrologic requirements between the natural areas to the west of the Canal L 31N system and the developed areas to the east.

BISECT simulates water level, flow, salinity with density effects, and leakage in both the surface-water and groundwater systems, as well as temperature in the surface water, which makes it suitable for diverse applications. The capabilities of the FTLOADDS code to represent hydrodynamic flow, surface-water/groundwater interactions, and salinity and heat transport allow BISECT to simulate all of the important physical processes of the hydrologic system. The numerical model can be used to separate factors and their effects on the hydrology, yielding useful insight into the system that measured data cannot provide. Model-simulated water level, flow, salinity, and temperature can provide needed input to ecologic models and studies of hydrology under climatic and anthropogenic changes. Some applications can be satisfied with a simpler technique that provides sufficient information without the extended complexity incorporated into BISECT. The dynamics of the system to be simulated should be considered when determining the suitability of the BISECT model for a particular purpose.

Summary

The hydrologic system of the south Florida peninsula is characterized by a dominant canal and water-control-structure network in proximity to surrounding saline tidal water bodies, nearly flat topography overlying porous and permeable carbonate rocks, low surface-water and groundwater flow gradients, and highly connected surface water and groundwater. These characteristics make the entire hydrologic system of south Florida sensitive to processes and changes that may occur on the surface, within the subsurface, and at the marine boundaries. Higher wetland levels in the Everglades, needed for restoring historical conditions, are challenging to meet because of groundwater losses downgradient through the highly conductive Biscayne aquifer to the eastern urban area. Construction of a subsurface vertical barrier, a grout wall in the aquifer to block flow, has been proposed to help maintain these wetland water levels and limit groundwater transport from Everglades National Park (ENP) to the east. Increases in freshwater deliveries to ENP, as proposed in the Comprehensive Everglades Restoration Plan (CERP), are also proposed to restore water levels to historical conditions, with the additional purpose of moderating the expected salinity increases in low-lying wetlands as sea level rises. The question of how these environmental and water-management changes will affect the system and to what degree the management interacts with the environmental factors is complex and essential to the future plans of the South Florida Water Management District, ENP, and the U.S. Army Corps of Engineers.

To address these questions, the U.S. Geological Survey studied the implementation of a vertical barrier in the surficial aquifer system to prevent seepage from the wetlands, the effects of increased water deliveries, and a range of predicted sea-level rise rates on the hydroperiods, groundwater levels, and surface-water and groundwater salinity in the south Florida peninsula by using a numerical modeling approach. The Biscayne and Southern Everglades Coastal Transport (BISECT) numerical model, developed with the Flow and Transport in a Linked Overland/Aquifer Density-Dependent System (FTLOADDS) simulator, represents hydrodynamic surface-water flow and three-dimensional groundwater conditions and accounts for leakage between surface-water and groundwater parts of the system, water levels, streamflows, groundwater salinity, and surface-water salinity and temperature.

The FTLOADDS simulator was previously used to construct separate models of areas in the south Florida peninsula (the Tides and Inflows to the Mangrove Everglades [TIME] model and Biscayne model), which were combined to create BISECT. Refinements and improvements made during

this process include (1) improved topographic representations, (2) refined Manning's friction coefficients, (3) improved evapotranspiration (ET) computation through spatially variable albedo, (4) increased vertical aquifer discretization, and (5) extension of the western boundary farther offshore. The combination of models to produce BISECT allows a more comprehensive representation of how the wetland areas of ENP interact hydrologically with the eastern urban areas of Miami-Dade County.

Scenarios that simulate climatic and anthropogenic changes yielded substantial insight into the hydrology in the BISECT model area, which includes about 7,300 square kilometers of the south Florida peninsula and about 2,700 square kilometers of the surrounding tidal water bodies (Atlantic Ocean, Gulf of Mexico, and Florida Bay). These analyses indicate the following.

1. Aquifer barriers along the L 31N levee produce minimal surface-water changes with effects most visible when the barrier extends the full depth of the aquifer.

2. CERP restoration redistributes cumulative flows markedly to the northwest and also to the southeast, with minimal effect in Shark River Slough.

3. Sea-level change has a more pronounced effect on hydrology than does CERP restoration.

4. Coastal salinities are substantially affected by sea-level rise, and CERP restoration does not return coastal salinities to historical values.

Analyses of the sensitivity of model results to input parameters yielded insight into how the numerical model responds to input parameter change and the uncertainty in the prediction of output values by locations. Insights include the following.

1. Higher tidal amplitude results in the simulation of larger cumulative flows, and smaller tidal amplitude results in lower cumulative flows for most Everglades coastal rivers. Bias in input tidal amplitude components, therefore, can produce equivalent bias in coastal flows.

2. The response of cumulative flows into Long Sound to modeled variations in tidal amplitude, wind, and frictional resistance does not follow the patterns of other coastal streams, so the simulated hydrology of the Long Sound area appears disconnected from coastal areas farther west.

3. Simulated cumulative coastal stream flows along the Whitewater Bay and Florida Bay coasts tend to exhibit more apparent effects from increased winds than do coastal stream flows along the Gulf of Mexico coast, where a larger lunar tide component overwhelms the wind effects.

4. Variations in flow to the Everglades coastal streams are substantially affected by groundwater/surface-water interactions in the eastern urban areas, so uncertainty in the simulation of urban infiltration has implications to Everglades coastal flow.

5. Simulated cumulative flows at McCormick Creek are sensitive to tidal fluctuations and aquifer leakage, so uncertainty is high at this location.

6. Harney River flow variations are most strongly affected by upstream conditions such as frictional resistance, but Harney River salinity variations are most strongly affected by downstream conditions such as tidal fluctuations. The simulation of mixing, which involves the tidal fluctuations, is more important to predicting the coastal salinity than are flows from inland areas.

7. The headwater of Taylor Slough is substantially affected by aquifer leakage and water exchanges with the urban canals, as are the coastal streams, indicating the degree of interconnectivity of the hydrologic system.

8. Flows at Broad River and Lostmans River are more sensitive to variations in the hydrologic system than are flows at any of the other streams and should be considered to have the highest uncertainty.

The BISECT model is limited by the assumptions and approximations in the FTLOADDS simulator and the input data. Users of model results must consider the inherent limitations in the scheme, which for BISECT can be summarized as follows.

1. The numerical discretization results in spatial and temporal smoothing of simulated output so that transient extreme values are affected.

2. The canal network in the study area is represented with user-defined time-varying stage values and as an infinite source and sink of water for the aquifer, which works well for conditions that remain similar to existing conditions but could prove unrealistic for more extreme changes in hydrology.

3. Both groundwater and surface-water boundary conditions restrict computed values in proximity to the boundaries, so model results can be unrealistically fixed in these areas.

4. The resolution of surface-water wetting and drying is limited by the cell dimensions of 500 meters, as smaller variations in topography and inundation cannot be represented.

5. Initial conditions are defined for all parameters, and the simulation must proceed for a sufficient amount of time for results to reflect the system dynamics rather than residual initial effects.

6. The time series of the different types of input data are at various time-step resolutions, based on the data type, which limits the small temporal-scale effects of each parameter on the simulated hydrology.

7. The spatial variability of the aquifer properties is difficult to determine with limited field information, especially in the western portions of the model area, so only larger scale groundwater flow patterns are represented.

8. The ET computations rely on heat transport computations and have several potential error sources. As ET undoubtedly must vary between the coast and inland, calibration of the spatially uniform groundwater ET parameters required balancing the effects of ET on coastal salinities versus inland groundwater levels. During calibration, ET from groundwater was reduced to get a better match to coastal groundwater salinities, likely resulting in too low an ET rate inland. However, offshore and coastal temperatures indicate that surface-water evaporation, much larger in magnitude than groundwater ET, may still be overestimated.

Considering the model's capabilities and limitations, we offer that BISECT is a useful hydrologic tool that can be used to simulate regional past and future hydrologic conditions in the south Florida peninsula. Model-simulated water level, flow, salinity, and temperature can provide needed input to ecologic models and studies of hydrology under climatic and anthropogenic changes.

References Cited

Bahm, K.E., and Fennema, R.J., 2013, Evaluation and application of the TIME model v2.0—Restoration alternatives and sea level rise in Everglades National Park: Hydrologic Model Report SFNRC Technical Series 2013.1, 92 p.

Bahm, K.E., Swain, E., Fennema, R.J., and Kotun, K., 2010, Everglades National Park and sea-level rise—Using the TIME model to predict salinity and hydroperiods, *in* Greater Everglades Ecosystem Restoration (GEER) Science Conference, Naples, Fla., July 12–16, 2010, p. 12.

Desmond, G.B., 2003, Measuring and mapping the topography of the Florida Everglades for ecosystem restoration: U.S. Geological Survey Greater Everglades Science Program: 2002 Biennial Report: U.S. Geological Survey Open-File Report 03-54, p. 31–32.

Desmond, G.B., Cyran, Edward, Caruso, Vince, Schupe, Gordon, Glover, Robert, and Henkle, Charles, 2000, Topography of the Florida Everglades, *in* Greater Everglades Ecosystem Restoration (GEER) Science Conference, December 11–15, 2000, Naples, Fla., p. 284–285.

Fish, J.E., and Stewart, M.T., 1991, Hydrogeology of the surficial aquifer system, Dade County, Florida: U.S. Geological Survey Water-Resources Investigations Report 90–4108, 56 p.

Fitterman, D.V., and Deszcz-Pan, M., 2001, Saltwater intrusion in Everglades National Park, Florida measured by airborne electromagnetic surveys, *in* First International Conference on Saltwater Intrusion and Coastal Aquifers-Monitoring, Modeling, and Management (SWICA-M3), Essaouira, Morocco: Rabat, Morocco, Laboratoire d'Analyse des Systémes Hydrauliques (LASH), 11 p.

German, E.R., 1999, Regional evaluation of evapotranspiration in the Everglades: Proceedings of the 3rd International Symposium on Ecohydraulics, Salt Lake City, Utah, July 13–16, 1999.

Green, T.W., Slone, D.H., Swain, E.D., Cherkiss, M.S., Lohmann, Melinda, Mazzotti, F.J., and Rice, K.G., 2010, Spatial and stage-structured population model of the American crocodile for comparison of Comprehensive Everglades Restoration Plan (CERP) alternatives: U.S. Geological Survey Open-File Report 2010–1284, 38 p.

Guo, Weixing, and Langevin, C.D., 2002, User's Guide to SEAWAT—A Computer Program for Simulation of Three-Dimensional Variable-Density Ground-Water Flow: U.S. Geological Survey Techniques of Water-Resources Investigations, book 6, chap. A7, 77 p.

Hamrick, J., 2006, The environmental fluid dynamics code—Theory and computation: Prepared for the U.S. Environmental Protection Agency, Office of Research and Development, by Tetra Tech, Inc., Fairfax, Va.

Hansen, M., and DeWitt, N.T., 1999, Modern and historical bathymetry of Florida Bay, *in* Proceedings of the 1999 Florida Bay and Adjacent Marine Systems Science Conference, November 1–5 1999, Key Largo, Fla.

Henkle, Charles, 1996, South Florida high-accuracy elevation data collection project: U.S. Geological Survey Fact Sheet FS–162–96, 3 p.

Hittle, Clinton, Patino, Eduardo, and Zucker, Mark, 2001, Freshwater flow from estuarine creeks into northeastern Florida Bay: U.S. Geological Survey Water-Resources Investigations Report 01–4164, 32 p.

Intergovernmental Panel on Climate Change, 2013, Climate change 2013—The physical science basis, *in* Stocker, T.F., Qin, D., Plattner, G.-K., Tignor, M., Allen, S.K., Boschung, J., Nauels, A., Xia, Y., Bex, V., and Midgley, P.M., eds., Contribution of Working Group I to the Fifth Assessment Report of the Intergovernmental Panel on Climate Change: Cambridge, U.K., and New York, U.S.A., Cambridge University Press, 1,535 p.Langevin, C.D., Swain, E.D., and Wolfert, M.A., 2005, Simulation of integrated surface-water/ground-water flow and salinity for a coastal wetland and adjacent estuary: Journal of Hydrology v. 314, p. 212–234.

Lee, J.K., and Carter, Virginia, 1999, Field measurement of flow resistance in the Florida Everglades, *in* Gerould, Sarah, and Higer, Aaron, comps., U.S. Geological Survey Program on the South Florida Ecosystem—Proceedings of the South Florida Restoration Science Forum, May 17–19, 1999, Boca Raton, Florida: U.S. Geological Survey Open File Report 99–181.

Lee, J.K., Visser, H.M., Jenter, H.L. and Duff, M.P., 2000. Velocity and stage data collected in a laboratory flume for water-surface slope determination using a pipe manometer: U.S. Geological Survey Open-File Report 2000-393, 28 p.

Leendertse, J.J., 1987, Aspects of SIMSYS2D, a system for two-dimensional flow computation: Santa Monica, Calif., The Rand Corporation, Report R-3572-USGS, 80 p.

Lohmann, M.A., Swain, E.D., Wang, J.D., and Dixon, Joann, 2012, Evaluation of effects of changes in canal management and precipitation patterns on salinity in Biscayne Bay, Florida, using an integrated surface-water/groundwater model: U.S. Geological Survey Scientific Investigations Report 2012–5099, 94 p.

MacVicar, T.K., VanLent, Thomas, and Castro, Alvin, 1984, South Florida Water Management Model documentation report: South Florida Water Management District Technical Publication 84–3, 123 p.

Perry, William, 2004, Elements of south Florida's Comprehensive Everglades Restoration Plan: Ecotoxicology, v. 13, p. 185–193.

Rabin, Charles, 2016. South Florida population hits 6 million for first time: Miami Herald, March 24, 2016.

Reese, R.S., and Cunningham, K.J., 2000, Hydrogeology of the gray limestone aquifer in southern Florida: U.S. Geological Survey Water-Resources Investigations Report 99–4213, 244 p.

Schaffranek, R.W., 2004, Simulation of surface-water integrated flow and transport in two dimensions—SWIFT2D user's manual: U.S. Geological Survey Techniques and Methods, 6 B–1, 115 p.

Shoemaker, W.B., Lopez, C.D., and Duever, M., 2011, Evapotranspiration over spatially extensive plant communities in the Big Cypress National Preserve, southern Florida, 2007–2010: U.S. Geological Survey Scientific Investigations Report 2011–5212, 46 p.

Shoemaker, W.B., and Sumner, D.M., 2006, Alternate corrections for estimating actual wetland evapotranspiration from potential evapotranspiration: Wetlands, v. 26, no. 2, p. 528–543.

South Florida Water Management District, 2005, Documentation of the South Florida Water Management Model: Jacksonville, Fla., Hydrologic Realities, Inc., ver. 5.5, November 2005, 305 p.

South Florida Water Management District, 2017, DBHYDRO database, accessed June 2, 2017, at https://www.sfwmd.gov/science-data/dbhydro.

Swain, E.D., 2005, A model for simulation of Surface-Water Integrated Flow and Transport in Two Dimensions—SWIFT2D user's guide for application to coastal wetlands: U.S. Geological Survey Open-File Report 2005–1033, 88 p.

Swain, E.D., and Decker, J.D., 2009, Development, testing, and application of a coupled hydrodynamic surface-water/groundwater model (FTLOADDS) with heat and salinity transport in the Ten Thousand Islands/Picayune Strand Restoration Project Area, Florida: U.S. Geological Survey Scientific Investigations Report 2009–5146, 42 p.

Swain, E.D., and Decker, J.D., 2010, A measurement-derived heat-budget approach for simulating coastal wetland temperature with a hydrodynamic model: Wetlands, v. 30, no. 3, p. 635–648.

Swain, E.D., and Lohmann, M.A., 2019, FTLOADDS (combined SWIFT2D surface-water model and SEAWAT groundwater model) simulator used to assess proposed sea-level rise response and water-resource management plans for the hydrologic system of the south Florida peninsula for the Biscayne and Southern Everglades Coastal Transport (BISECT) model: U.S. Geological Survey data release, http://dx.doi.org/10.5066/P9MDUQPK.

Swain, E.D., Wolfert, M.A., Bales, J.D., and Goodwin, C.R., 2004, Two-dimensional hydrodynamic simulation of surface-water flow and transport to Florida Bay through the Southern Inland and Coastal Systems (SICS): U.S. Geological Survey Water-Resources Investigations Report 03–4287, 56 p., 6 pls.

Swain, Michael, Swain, Matthew, Lohmann, Melinda, and Swain, E.D., 2012, Experimental determination of soil heat storage for the simulation of heat transport in a coastal wetland: Journal of Hydrology v. 422–423, p. 53–62.

U.S. Army Corps of Engineers, 1999, Central and Southern Florida Comprehensive Review Study: Jacksonville Fla., U.S. Army Corps of Engineers, April 1999.

U.S. Army Corps of Engineers, 2005, Central and Southern Florida Project for flood control and other purposes—System operating manual, v. 5, East Coast canals: Jacksonville Fla., U.S. Army Corps of Engineers, December 2005.

U.S. Army Corps of Engineers, 2013, Incorporating sea level change in civil works programs: U.S. Army Corps of Engineers Circular no. 1100–2–8162, 18 p.

U.S. Geological Survey, 2017a, National Water Information System: Web Interface, accessed 6/2/2017 at https://waterdata.usgs.gov/nwis.

U.S. Geological Survey, 2017b, South Florida Information Access (SOFIA) Data Exchange, accessed 6/2/2017 at https://sofia.usgs.gov/exchange/sfl_hydro_data/.

Wang, J.D., Swain, E.D., Wolfert, M.A., Langevin, C.D., James, D.E., and Telis, P.A., 2007, Application of FTLOADDS to simulate flow, salinity, and surface-water stage in the southern Everglades, Florida: U.S. Geological Survey Scientific Investigations Report 2007–5010, 112 p.

Wolfert, M.A., Langevin, C.D., and Swain, E.D., 2004, Assigning boundary conditions to the Southern Inland and Coastal Systems (SICS) model using results from the South Florida Water Management Model (SFWMM): U.S. Geological Survey Open-File Report 2004–1195, 30 p.

Woods, Jeff, 2010, Surface water discharge and salinity monitoring of coastal estuaries in Everglades National Park, USA, in support of the Comprehensive Everglades Restoration Plan: Proceedings of the 3rd International Perspective on Current & Future State of Water Resources & the Environment, Chennai, India, 2010.

Appendixes 1–5

Appendix 1. BISECT Model Construction

The Biscayne and Southern Everglades Coastal Transport (BISECT) model (Swain and Lohmann, 2018) was constructed using the Flow and Transport in a Linked Overland/Aquifer Density-Dependent System (FTLOADDS) simulator. FTLOADDS is a computational code that links two simulators, a two-dimensional surface-water code (Simulation of Surface-Water Integrated Flow and Transport in Two Dimensions [SWIFT2D]) and a three-dimensional groundwater code (Computer Program for Simulation of Three-Dimensional Variable-Density Ground-Water Flow [SEAWAT]), to simulate the complex hydrology of south Florida (Langevin and others, 2005) and provide likely hydrologic responses to possible future conditions. To accomplish this task, FTLOADDS exchanges leakages and salinity between SWIFT2D and SEAWAT, as well as the constituent salinity. Also, in the FTLOADDS connection, each model maintains the original grid labeling conventions, as well as all other numerical conventions and input designated by each model code.

It is important to distinguish between the simulator, FTLOADDS, which is the numerical tool used, and the model, Biscayne and Southern Everglades Coastal Transport (BISECT), which is the application of the simulator to a specific area and set of hydrologic parameters. Just as FTLOADDS is the computational combination of two preexisting simulators, BISECT is the spatial combination of two preexisting models of different regions. These models were developed as part of two previous U.S. Geological Survey (USGS) modeling efforts that have been completed in parts of the south Florida hydrologic system. The first of these, Tides and Inflows to the Mangrove Everglades (TIME; Wang and others, 2007), covers the undeveloped western part of the system, and the second, Biscayne (Lohmann and others, 2012), covers the highly developed eastern part. Both models were constructed in cooperation with the South Florida Water Management District (SFWMD) by using similar versions of the simulator code, FTLOADDS, and both also have the same map-view numerical grid orientation and spacing. In addition, these two models have a long common boundary along the north-south trending Canal L 31 N/Canal 111 system (fig. 1–1). BISECT was created by numerically placing both of these models together at their common boundary, within an appropriately expanded grid system, providing a significant numerical advantage over operation of each precursor model individually. Rather than having to supply extensive and sometimes approximate time series input for several variables along the lengthy Canal L 31 N/Canal 111 system boundary, much less input data are required in BISECT because the boundary no longer exists and most hydrologic computations along the former boundary are accommodated by FTLOADDS as cells within the BISECT computational field. Since both precursor models were subject to extensive calibration and testing, most model features, parameters, and coefficients were also initially incorporated into BISECT.

Modifications to BISECT Model After Merging of TIME and Biscayne Models

Several modifications were made to the model in consultation with the U.S. Army Corps of Engineers (USACE), Everglades National Park (ENP), and the SFWMD to improve simulation results and better answer the questions about how construction of a proposed vertical aquifer barrier and possible increases in freshwater delivery may mitigate the effects of sea-level rise on the hydrologic system of south Florida. These modifications include the following.

1. The extension of the western model boundary farther offshore (see Wang and others, 2007) into the Gulf of Mexico to more accurately simulate seawater and freshwater mixing in both coastal and estuarine areas, as well as in aquifers in the western part of the study area. This new boundary location also allows a rising sea level to encroach inland along the whole western shoreline of the study area. This boundary change is in response to a specific recommendation of the National Park Service (NPS) TIME version 2.0 report (Bahm and Fennema, 2013).

2. Additional and updated topography and offshore bathymetry were added in some places with data from the USACE, National Oceanic and Atmospheric Administration (NOAA), and the Florida Division of Emergency Management (FDEM). In an area like south Florida, with little topographic relief, small changes can sometimes have substantial impacts on local and even regional surface-water flow magnitudes and directions. Extending the western model boundary farther offshore also required additional bathymetric data.

3. The vertical aquifer discretization was changed from 10 layers in TIME (see Wang and others, 2007) and 20 layers in Biscayne (see Lohmann and others, 2012) to 15 layers in BISECT. Layer 2 in BISECT occurs 2 meters (m) below the North American Vertical Datum of 1988 (NAVD 88), and each layer has a thickness of 2 meters (m), enhancing the ability of the model to define seawater intrusion in the most critical parts of south Florida aquifers, as well as in extensive peat layers within the ENP mangrove ecotone (Bahm and Fennema, 2013). The smaller number of layers in the eastern area also helps keep numerical computation times shorter.

4. Spatially variable albedo was included in the computation of the solar radiation term (see Lohmann and others, 2012) throughout BISECT to improve the simulation of water temperature and evapotranspiration (ET) in most of the study area. ET is a large term in the hydrologic budget of the south Florida hydrologic

system and must be simulated as accurately as possible (Shoemaker and Sumner, 2006). Using computed water temperatures as a measure of heat-budget accuracy, albedo can be a useful model calibration parameter.

5. The Manning's *n* friction factor dataset used by TIME version 2.0 (Bahm and Fennema, 2013) was incorporated into BISECT because of useful modifications that improved simulated model flow computations in the vicinity of Taylor Slough Bridge. The data were smoothed at some locations to avoid the possibility of introducing numerical instability at locations with large cell-to-cell differences in Manning's *n*.

Some aspects of the TIME and Biscayne models do not transfer directly into BISECT when the models are merged. One example of lack of transferability is tidal boundary conditions. The major purpose for developing the TIME model was to provide optimal freshwater stream outflow from the Everglades to both Florida Bay and the Gulf of Mexico coasts for subsequent input to the Florida Bay model (Environmental Fluid Dynamics Code [EFDC]). The Florida Bay model was developed for the USACE and SFWMD in support of the Florida Bay/Florida Keys Feasibility Study (FBFKFS) in 2001 (Worth and others, 2002). Details on how TIME-simulated freshwater information for streams was transferred to the dissimilar Florida Bay model are presented in Wang and others (2007, section 3.4, p. 23). However, model salinity values simulated by the TIME and EFDC models sometimes diverged substantially from measured values while being similar at other times. Reasons for this discrepancy are documented in Bahm and Fennema (2013, app. F).

The western boundary of TIME (fig. 1–1) included six separate tidal boundaries, all near the mouths of coastal streams. Between the stream mouths, the boundary followed the shoreline. The six tidal boundary segments, from south to north, are located along the coastlines of (1) Whitewater Bay,

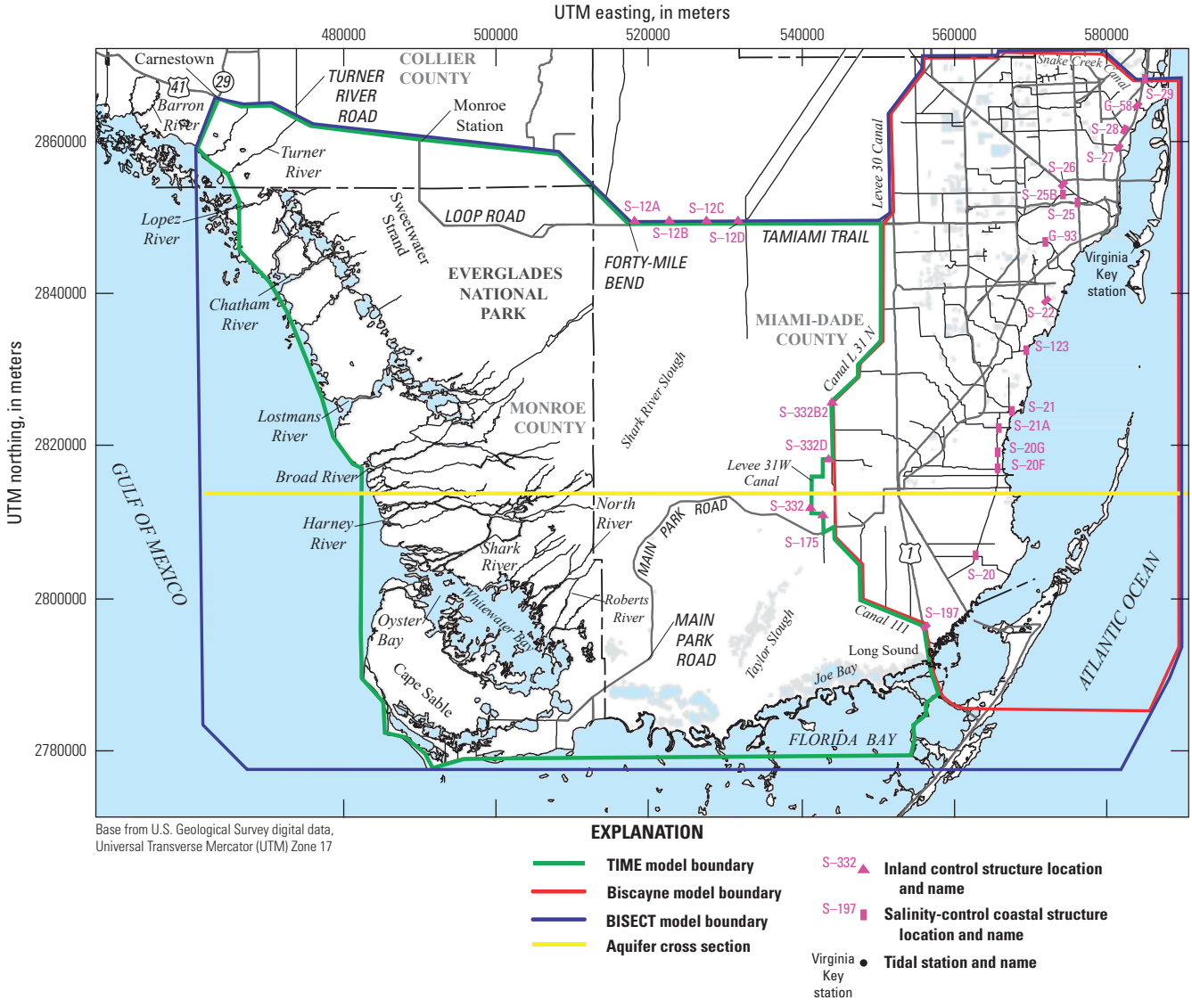

Figure 1-1. Active modeled area and location of aquifer cross sections in the Biscayne and Southern Everglades Coastal Transport (BISECT) model area, south Florida peninsula.

Shark River, Harney River, and the Broad River; (2) Lostmans River; (3) Chatham River; (4) Lopez River; (5) Turner River; and (6) Barron River. These western TIME model boundaries provided the freshwater outflows where they were needed for operation of the Florida Bay model. For the purposes of BISECT, however, the TIME western boundary has several inherent difficulties. Since much of the boundary is on the shore, with simulated ocean water only along the six tidal boundaries, land inundation due to sea-level rise could not be properly represented. Simulated nearshore mixing of freshwater and saltwater would be severely restricted or misrepresented, and offshore mixing would be absent. Without the representation of ocean water and subsurface layers offshore of the coast, the exchange of seawater and groundwater along the Gulf Coast could not be simulated. The effects of future modified water deliveries to the Everglades on the salinity of western streams, also a purpose of BISECT, could not be reliably simulated.

To rectify these difficulties, the BISECT model was modified so that a single long western model boundary was selected along the western side of the model, connecting with an east-west no-flow section on the southern boundary (fig. 1–2). This new boundary allows the simulation of nearshore and estuarine salinity reduction caused by increased freshwater flows during the wet seasons, possible increased freshwater deliveries as proposed by the Comprehensive Everglades Restoration Plan (CERP) (USACE, 1999), and other hydrologic simulation improvements made to the BISECT model. The new boundary placement also enables water and dissolved constituent exchange between the Gulf of Mexico and underlying aquifers. This change also improves the capability of BISECT to represent extreme events, such as storm surges, or any event that brings tidal water above the elevation of the shore, including sea-level rise.

In the model's spatial discretization (fig. 1–3), the western BISECT tidal boundary extends from the cell located

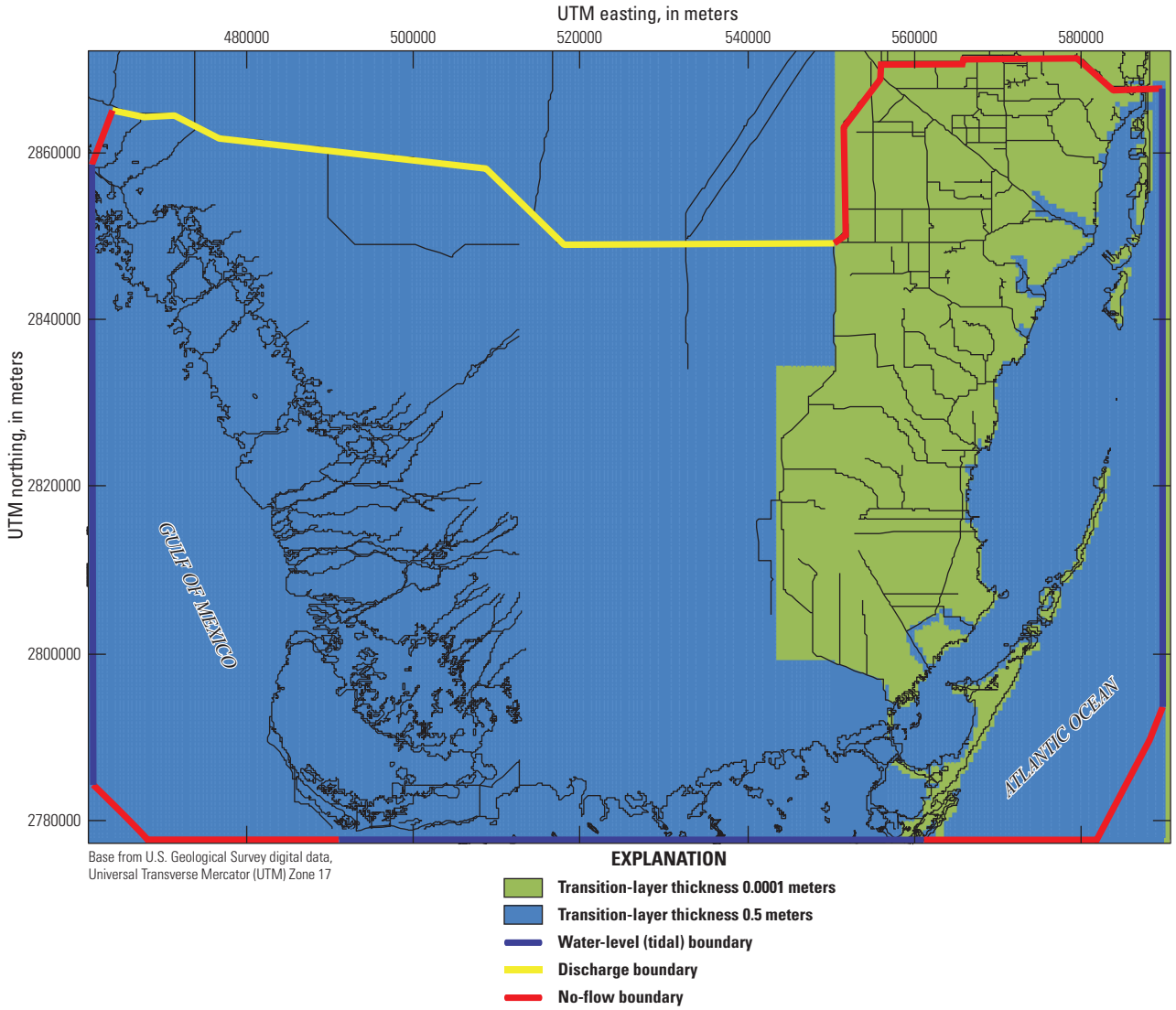

Figure 1-2. Transition-layer zones and surface-water model boundaries for the Biscayne and Southern Everglades Coastal Transport (BISECT) model for the south Florida peninsula.

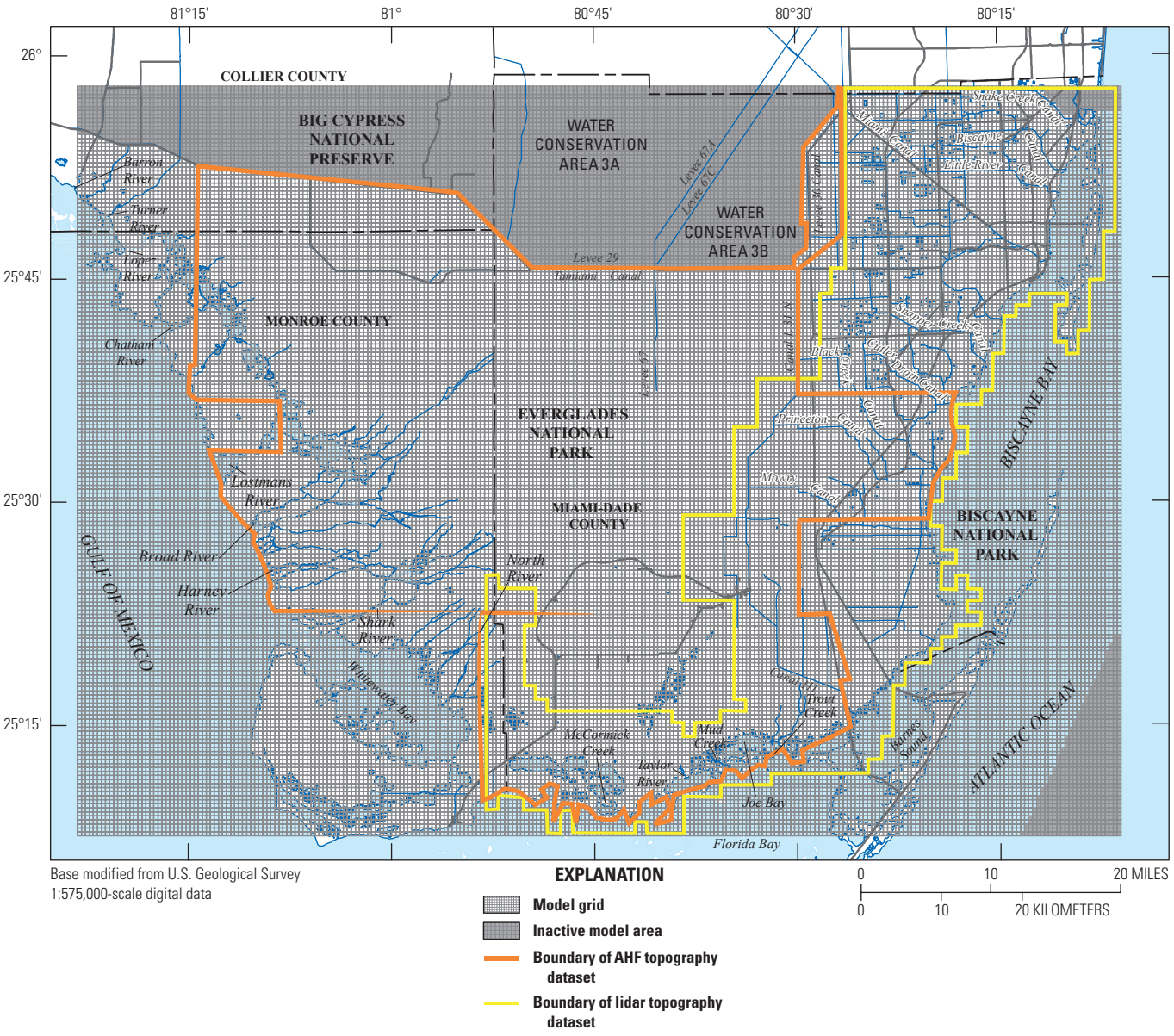

Figure 1-3. Biscayne and Southern Everglades Coastal Transport (BISECT) model grid and boundary area of the Airborne Height Finder (AHF) and light detection and ranging (lidar) topography datasets, south Florida peninsula.

at column 1, row 11 of the model grid northward to the mouth of the Barron River at the cell located at column 1, row 136. The tidal function applied along this boundary is the same function used in the TIME model for the longest western tidal boundary segment (fig. 1–2) beginning at Cape Sable and extending northward offshore of Shark, Harney, Broad, and Lostmans Rivers (fig. 1–1). The function used includes mean water level and the harmonic constants for the three principal tidal components (M2, O1, and K1) as provided by the Florida Bay model (Wang, and others, 2007; J. Hamrick, TetraTech, written commun., 2005). At the southern end of the BISECT long western tidal boundary, the no-flow boundary section includes a short 45-degree boundary, from cell locations at column 1, row 11 to column 11, row 1, to avoid unwanted numerical oscillations at the original sharp 90-degree corner at this offshore location.

The part of the southern tidal boundary of BISECT within Florida Bay (figs. 1–1 and 1–2) remains unchanged from that of the precursor TIME model, from the grid cell located at column 95 row 1 at Cape Sable to the cell at column 187 row 1 in northeastern Florida Bay (fig. 1–3). This boundary was originally chosen for the same reasons as the TIME model western tidal boundaries; therefore, it also incorporates some of the same shortcomings as previously discussed, albeit to a lesser degree. Although this TIME model boundary adequately met the freshwater inflow needs of the Florida Bay model, a more southerly boundary location could better suit the purposes of BISECT for the same reasons given in the discussion of TIME's western tidal boundary. However, the very shallow Florida Bay has no location that is more suitable for a tidal boundary, primarily because of the multitude of small islands and shoals that emerge and submerge during most tidal cycles.

The tidal functions defined at the east and west ends of the Florida Bay tidal boundary were supplied by the Florida Bay model (Wang, and others, 2007; J. Hamrick, TetraTech, written commun., 2005). Tidal amplitudes in northeastern Florida Bay are much lower than at the southern tip of Cape Sable, and there is also a significant phase lag from Cape Sable to northeastern Florida Bay. Both amplitude and phase for all cells along the Florida Bay tidal boundary are linearly interpolated from the Florida Bay model results. The Cape Sable end of the boundary does not allow exchange of water between Florida Bay and the Gulf of Mexico. The boundary section from Cape Sable to the western boundary (figs. 1–1 and 1–2) is a no-flow vertical boundary, which has no impact on tidal inundation in the study area and is remote from freshwater and saltwater mixing further north along the west coast of the study area.

A southward extension of 13 rows of 500-m grid cells of the Biscayne model was needed to reach the location of the southern boundary of the BISECT model. Starting from the grid cell located at column 188, row 1 (fig. 1–3) in northeastern Florida Bay (fig. 1–1), another no-flow boundary extends eastward into the Atlantic Ocean to the grid cell at row 243, column 1 and then north-northeastward to the grid cell at column 259, row 31 (fig. 1–2). This eastern boundary is similar to the boundary used in the Biscayne model. The angled corner, in this case, is needed to control numerical oscillations potentially caused by rapidly increasing ocean depths in this area. A tidal function based on long-term NOAA tidal observations at Virginia Key (fig. 1–1) was used in the Biscayne model (Lohmann and others, 2012), and was applied to the BISECT model boundary from the cell located at column 259, row 32 to the cell at column 259, row 178. A no-flow boundary from the cell located at column 258, row 178 to the shoreline at the cell located at column 256, row 178 (fig. 1–3) completes the BISECT tidal and related boundary conditions.

In the TIME model, the surficial aquifer was discretized by using 10 layers with the bottom of the uppermost layer at 7 m below NAVD 88, and each successive layer was 7 m thick (Wang and others, 2007). In the Biscayne model, the surficial aquifer was defined by using 20 layers with the bottom of the uppermost layer at 4 m below NAVD 88. Layer 2 was 1.5 m thick, and layers 3–20 were each 2.75 m thick (Lohmann and others, 2012). In the much larger BISECT model, a compromise was chosen between the 10 layers in TIME and the 20 layers in Biscayne, yielding 15 groundwater layers as described next in the "Spatial and Temporal Discretization" section, to allow reasonable simulation times and adequate definition of the mixing zone in the surficial aquifer.

Spatial and Temporal Discretization

The BISECT map-view model grid is, with a few minor modifications, the common 500-m grid system developed for the precursor TIME and Biscayne models (fig. 1–3). All three model grids can be referenced to a common origin in the Gulf of Mexico, in Zone 17 North of the Universal Transverse Mercator (UTM) projected coordinate system. The center of the BISECT grid cell (1,1) is located 461,000 m east of the central meridian of the UTM system and 2,779,000 m north of the equator (Wang and others, 2007). The BISECT model grid is composed of 259 cells west to east and 186 cells south to north, with each cell measuring 500 m on each side (see fig. 1–3). The total rectangular area of the grid includes an area of 12,043.5 square kilometers (km^2). Since the model boundaries do not extend to the edge of the grid in all locations, the active area of the surface-water simulation is 10,205 km^2 with 40,820 active computation cells. This map-view grid is shared by the surface-water and groundwater parts of the BISECT model.

In the vertical dimension, the BISECT grid structure has a variable discretization to capture hydrogeologic layering and vertical variations in groundwater salinity. For groundwater and especially for areas of saltwater encroachment into freshwater aquifers, it is important to have a vertical grid structure that can well define zones where fresh groundwater and saline groundwater mix. The movement of these mixing zones, within aquifers, either landward or seaward, indicates either seawater encroachment or the ability to resist and possibly reverse such encroachment. Therefore, BISECT has a different vertical grid structure from either TIME or Biscayne in order to better evaluate encroachment due to sea-level rise and the adequacy of an aquifer barrier or increased freshwater deliveries to resist or overcome such encroachment.

In the BISECT model, 15 groundwater layers (fig. 1–4), as seen at the aquifer cross-section location indicated in figure 1–1, were used to allow reasonable simulation times and adequate definition of the mixing zone in the surficial aquifer that is most vulnerable to saltwater intrusion by a rising sea level. The BISECT aquifer representation has the bottom of the uppermost layer at 2 m below NAVD 88. The next 10 layers are uniformly 2 m thick, providing high resolution, and the lower 4 layers are assigned variable thicknesses to closely approximate the geologic formations that are not a critical part of the seawater intrusion concern (fig. 1–4). Thus layers 12 through 15 correspond to the Fort Thompson Formation, Pinecrest Beds, gray limestone aquifer, and the lower clastic unit/sand aquifer, respectively. Two geologic cross sections show the features reflected in the lower four layers (fig. 1–5). Resolving the groundwater movement and mixing at this 2-m-thickness resolution in the uppermost aquifer also improves the computation of water and salt exchange between groundwater and surface water.

The model independently calculates groundwater flow and solute transport and surface-water flow and solute transport. Solutions to each set of equations require different temporal discretization. Groundwater flow is calculated by using daily time steps during the 9-year period from January 1, 1996, through December 31, 2004 (3,288 daily stress periods). Groundwater solute-transport time steps were determined dynamically on the basis of the maximum time step required for convergence of the transport equation and ranged from a few seconds to as much as 1 day. A fixed

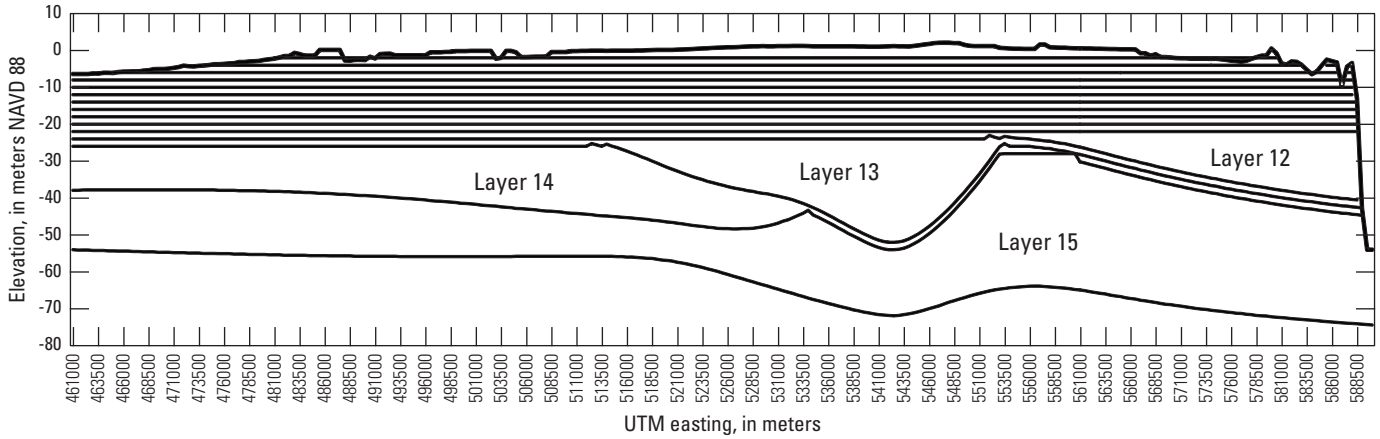

Figure 1-4. Biscayne and Southern Everglades Coastal Transport (BISECT) model aquifer layers (line of section shown in fig. 1–1). NAVD 88, North American Vertical Datum of 1988; UTM, Universal Transverse Mercator.

10-minute time step was used for the surface-water component of the model to account for rapidly changing hydrodynamic factors, such as tidal action, that affect surface-water flow and transport solutions. The simulation period (1996–2004) coincides with an intensive data collection program to measure the discharge of five coastal streams in the study area (Patino, 1996). This simulation period contains both wet and dry seasons but no extreme flood or drought events.

Topography and Bathymetry

The topography and bathymetry within the BISECT model (fig. 1–6) are largely modified and expanded from topographic and bathymetric input for the TIME and Biscayne models, using multiple data sources including Desmond (2003), Hansen and DeWitt (1999), NOAA (2010), and FDEM (2007). Topographic data for most of the onshore part of the model area, west of the L–31 levee system, and in some wetland areas east of the L–31 levee system, were taken from Desmond (2003), which used the Airborne Height Finder (AHF) system (fig. 1–3). This system was developed by the USGS specifically for application where other methods were not feasible, such as in the highly vegetated, partially inundated, and very extensive wetlands of south Florida. The AHF data were collected on a 400-m horizontal spacing and have a vertical accuracy specification of ±15 centimeters (cm) (Desmond, 2003). A complete description of the AHF data collection system and additional data were further documented by Jones and others (2012). Topographic data for the onshore area east of the L–31 levee system were taken from light detection and ranging (lidar) data (fig. 1–3) collected by the USACE with specifications of 1.16-m horizontal accuracy and 18-cm fundamental vertical accuracy (FDEM, 2007). The AHF and lidar data areas overlap considerably (fig. 1–3), and it was decided to use the Canal L 31 N/Canal 111 system (fig. 1–1) as a divide between the areas to the west where AHF data are used to define topography in BISECT and the areas to the east where lidar topographic data are used. Bathymetric data for the offshore area along the west coast of the model were taken from Hansen and DeWitt (1999) and from NOAA National Geophysical Data Center (NGDC) (2017).

Bathymetric data for the southern and eastern offshore areas were also taken from the NOAA NGDC Coastal Relief Model dataset (NOAA, 2017). Topography in inland areas that have neither AHF nor lidar data (fig. 1–3) are estimated with 1-foot contour data developed for the Florida Coastal Everglades Long Term Ecological Research Program (LTER, 1998).

Several adjustments to topographic and bathymetric input data were made to the final version of BISECT. Perhaps the most important change, mentioned earlier in the "Modifications to BISECT Model After Merging of TIME and Biscayne Models" section, is the decision to extend the western boundary of BISECT farther westward (to column 1 of the model grid) than the western boundary of the TIME model (fig. 1–1) in order to better simulate coastal mixing of freshwater and saltwater, allow exchange of surface water and groundwater in the nearshore region of the bottom of the Gulf of Mexico, and allow simulated sea-level rise to inundate the gulf shoreline as naturally as possible. The source of bathymetry for this added coastal area is the NOAA NGDC Coastal Relief Model dataset (NOAA, 2017).

The southern boundary of the precursor Biscayne model did not extend as far south as the southern boundary of the former TIME model (see fig. 1–1), so BISECT required a boundary extension, which added a small section of northeastern Florida Bay, a small additional segment of the Atlantic Ocean, and an additional 6 kilometers (km) of the Florida Keys. Data for this expansion were also taken from the NGDC Coastal Relief Model dataset (NOAA, 2017).

Hydraulic Properties

Hydraulic properties are defined herein as parameters that characterize water flow and constituent transport both in and between surface-water and groundwater systems of the BISECT model. For the surface-water component of the model, Manning's friction factor, *n*, is the only hydraulic property requiring input specification at every surficial cell

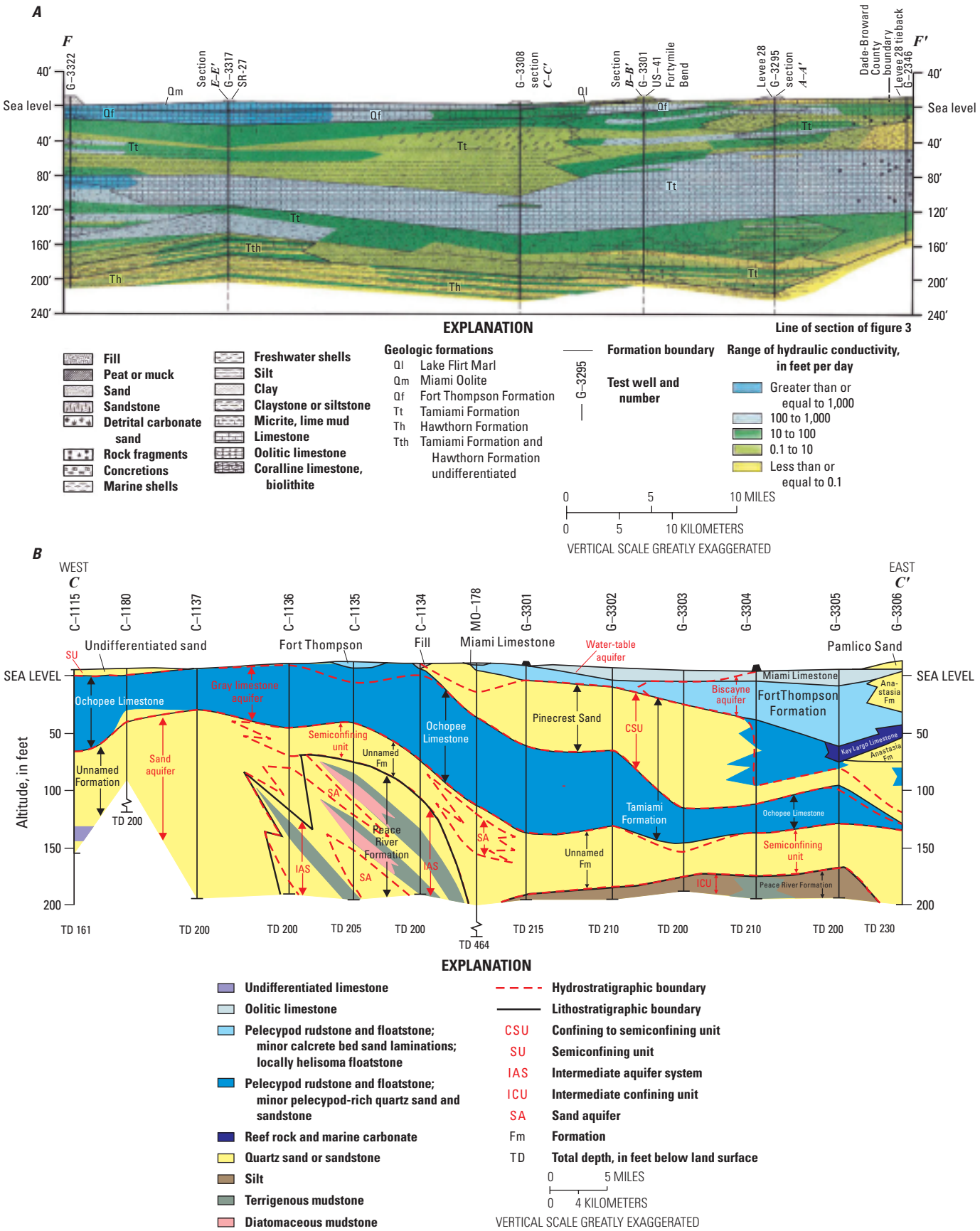

Figure 1-5. Geologic framework at *A*, cross section *F*–*F*′ (modified from Fish and Stewart, 1991, pl. 6) and *B*, cross section *C*–*C*′ (modified from Reese and Cunningham, 2000, fig. 13), south Florida peninsula.

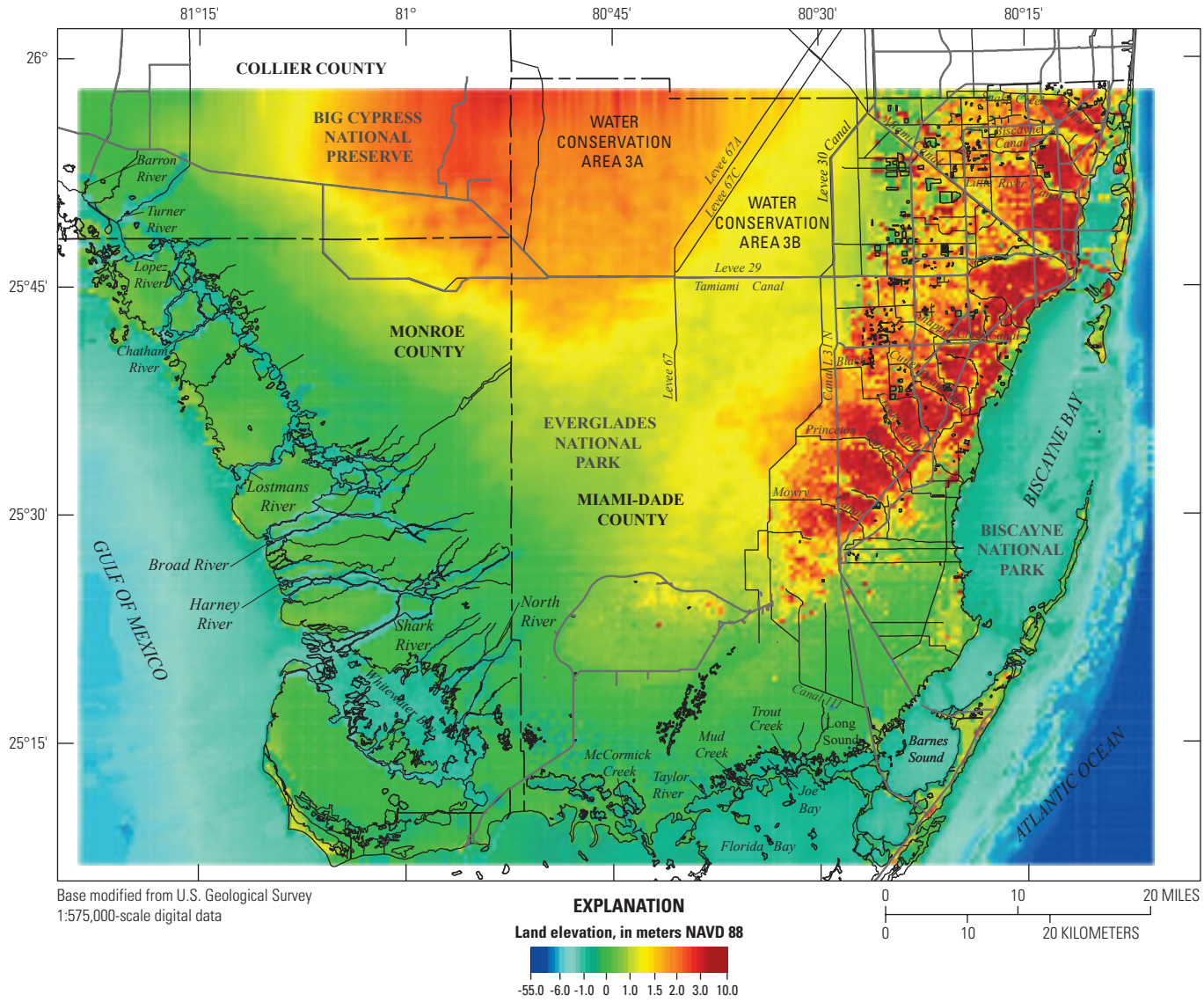

Figure 1-6. Topography and bathymetry within the Biscayne and Southern Everglades Coastal Transport (BISECT) model grid. NAVD 88, North American Vertical Datum of 1988.

in both x and y horizontal directions. Most, but not all, x and y friction factors are the same. For the groundwater component, several hydraulic properties must be specified at each subsurface cell. They are aquifer hydraulic conductivity, anisotropy, storage, and porosity. Leakage parameters are specified to characterize flow and transport at the juxtaposition of every surface-water cell that has an adjacent groundwater cell. These terms are defined in the following sections.

Surface-Water Properties

Manning's friction factor (n) for all surface-water cells in the western part of the BISECT model were initially taken directly from the TIME model (Wang and others, 2007). It should be noted that the application of Manning's equation to determine frictional resistance to flowing water, where n represents a wetted-perimeter roughness value, assumes that such flows are fully turbulent. As flow through the vegetated marshlands of south Florida are mostly in the transition zone between laminar and turbulent (Lee and Carter, 1996), Manning's n cannot be viewed as a physical roughness element dimension but rather as an effective roughness that includes friction and drag due to contact with land, as well as contact with vegetation within the water column (Wang and others, 2007). Additionally, small-scale topographic features within each surficial 500-m by 500-m grid cell may require a higher Manning's n (effective n) value to best represent the added resistance and likely longer flow paths through each cell (Wang and others, 2007). Lee and Carter (1996) determined appropriate effective n values for various marsh vegetation types and density, which were used in conjunction with remote and land-based vegetation type and vegetation density maps

(Jones, 1999) to assign appropriate effective *n* values for marshland throughout ENP. Also, for marshland areas in the eastern part of the BISECT domain, the same techniques were used to assign effective *n* friction factor values based on 1995 geographic information system (GIS) land-use distributions (SFWMD, 1995), which are suitable surrogates for vegetation maps (Lohmann and others, 2012).

No mechanism is available within the BISECT model to remove ponded water from urban areas and convey it directly to nearby canals because urban stormwater drainage systems are not coded into the FTLOADDS simulator. Instead, high effective *n* values are assigned to urban lands to represent built-up obstructions that limit large-scale lateral movement of ponded water. In addition, rapid downward leakage into the surficial aquifer mimics the actual drainage features in urban areas and provides a suitable groundwater pathway to the nearest canal (Lohmann and others, 2012).

In surficial cells encompassing defined small streams, Manning's *n* or effective *n* was decreased in the direction of flow to enhance flow in the direction of the streambed. Also, multiple *n* values were reduced to a single representative value for cells throughout the eastern part of the study area, where multiple land-use types frequently occur in the 0.25 km^2 grid cells. Simple fractional-area weighting was used to determine the effective *n* value for cells with more than one land-use type.

Aquifer Properties

The hydraulic conductivity for the Biscayne aquifer in the eastern part of the model was derived from data collected from borehole cores, aquifer tests, and from other methods described in Fish and Stewart (1991). These data were interpolated with a kriging method in the eastern part of the model and then applied to model layers 1–12 (fig. 1–4). A horizontal to vertical hydraulic conductivity anisotropy ratio of 100:1 was used to derive a corresponding vertical hydraulic conductivity in each model cell from the assigned horizontal hydraulic conductivities. The method applied is the same as that used in previous groundwater models (Lohmann and others, 2012; Langevin, 2001). The confined storage coefficient for layers 1–3 was set to 0.02 and for layers 4–15 to a value of 5.9×10^{-5}. The unconfined storage coefficient and porosity were uniformly specified as 0.2.

West of the Canal L 31 N/Canal 111 system a single averaged hydraulic conductivity value was used for each of the aquifer types because there is a lack of data in the western part of the BISECT model area and under the Biscayne aquifer in the east (figs. 1–4 and 1–5). Based on values developed for the TIME model (Wang and others, 2007), hydraulic conductivity values were set to 5,000–7,000 meters per day (m/d) for model cells in layers 1–13 where the Biscayne aquifer and Pinecrest Formation exist, set to 500 m/d in layers 1–14 where the gray limestone aquifer exists, and set to 50 m/d in layer 15, which is composed of the sand aquifer/semiconfining unit. The configuration of hydraulic conductivity in each of the layers is shown in appendix 2.

Groundwater/Surface-Water Leakage Properties

Leakage between the surface water and the uppermost layer of the aquifer is represented as flow through a surficial transition layer with a defined hydraulic conductivity and thickness. However, a well-defined transition layer does not exist for some land types. In the Everglades wetlands, a distinct peat layer is common and is the closest physical manifestation of the transition layer, but in the adjacent urban areas the aquifer can be effectively in contact with the surface, especially with an extensive drainage system.

Two transition-layer zones are defined (fig. 1–2). Zone 1 represents the wetlands and associated areas, which commonly have a peat layer, and has a hydraulic conductivity of 500 m/d and a thickness of 0.5 m. Zone 2 represents the urban and developed areas. Zone 2 transition-layer hydraulic conductivity is assigned a value of 500 m/d, and the thickness is only 0.0001 m, which provides substantially less resistance than in zone 1.

Boundary Conditions

Boundary conditions are set to be as close and similar to actual conditions as possible based on available data. These boundary conditions describe how water and transported constituents, such as dissolved solutes and heat energy, enter and exit the modeled system. As external boundaries, cells representing the top layer of BISECT must be supplied with precipitation values and sufficient information to compute ET, and surface-water and groundwater edge cells need information that will represent water and solute exchange with their nonmodeled neighboring areas. As internal boundaries, exchanges to and from the groundwater and surface water are computed and distributed appropriately (fig. 1–7). These and other boundary conditions may be specified explicitly, or they may be a function of model-simulated and (or) user-specified information.

Many of the boundary condition types and data used to define boundaries in the BISECT model were taken from the precursor TIME and Biscayne models (Wang and others, 2007; Lohmann and others, 2012). Along the L–31 levee system, which bounded the precursor models (fig. 1–1), BISECT solves the flow and transport equations explicitly. This feature allows a computation of groundwater flux between the undeveloped Everglades areas and the urbanized east, consistent with groundwater flow simulated throughout the model domain. The Canal L 31 N/Canal 111 system is retained, however, as surficial water-level boundary conditions, with extensive available data, allowing recharge to and leakage from the first layer of the groundwater part of BISECT. Some other important boundary modifications have also been made in BISECT, and they are discussed herein.

Surface-Water Inflows, Coastal Structure Flows, and Tidal Exchange

The northern surface-water boundary of BISECT is mostly defined by a line just south or east of a series of canals. From west to east, the canals are (1) the Tamiami Canal, (2) the

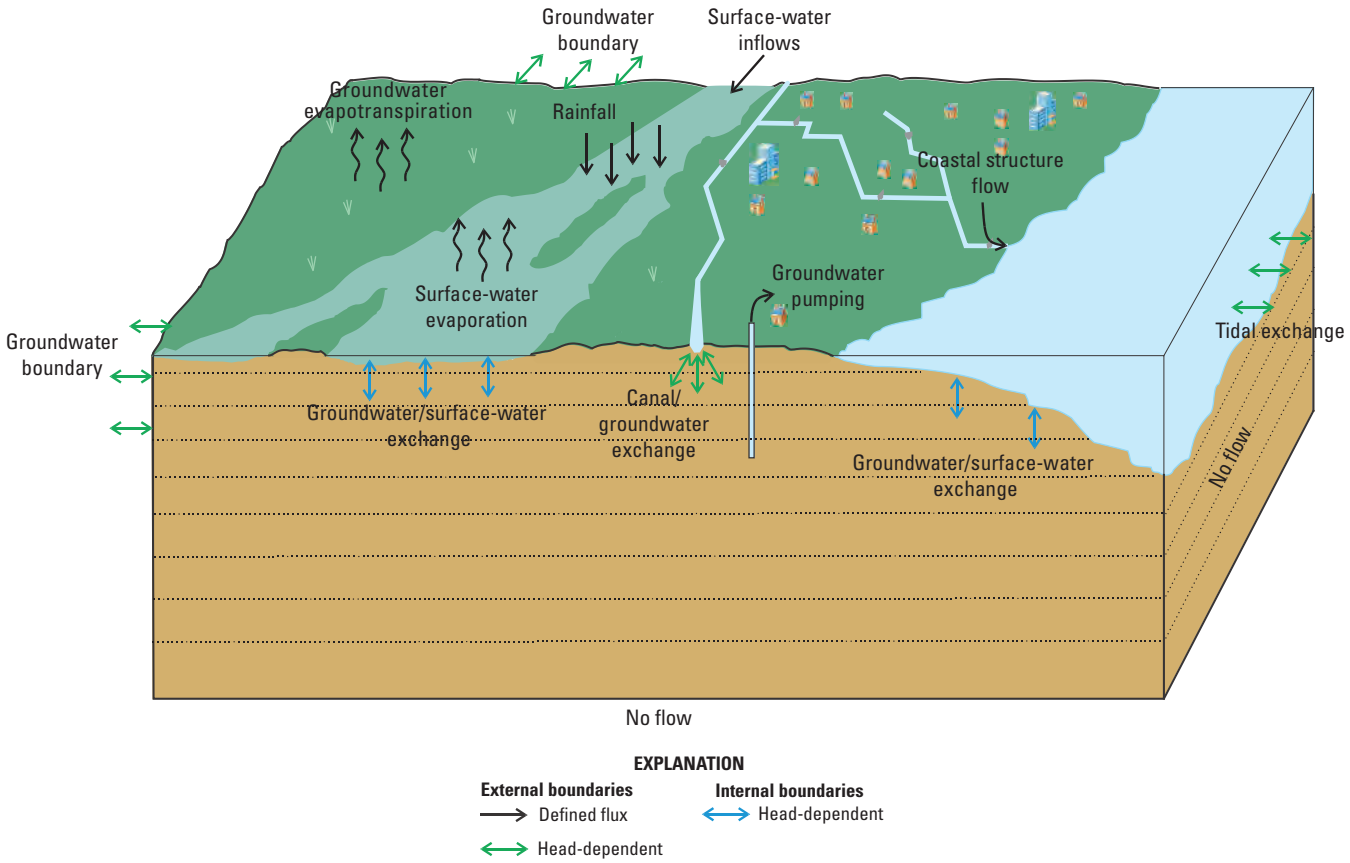

Figure 1-7. External and internal model boundary condition types of the Biscayne and Southern Everglades Coastal Transport (BISECT) model for the south Florida peninsula.

Levee 30N Canal, and (3) the C–9, or Snake Creek, Canal (fig. 1–1). Overland flow receives water and solutes from canal exchanges where the Tamiami Canal discharges directly to the modeled area across a large part of the northern boundary through four hydraulic structures (S–12A to S–12D in fig. 1–1) and also through numerous culverts, under Tamiami Trail, to the west of these structures. Likewise, discharges from canals are added to the wetlands at S–332, S–332D, S–332B2, and S–175 (fig. 1–1). These are classified as external boundaries to the model, as they represent interactions with hydrology outside what is simulated. The same boundary condition type also occurs into the surface-water cell just offshore of all 16 salinity-control coastal structures (fig. 1–1) within the BISECT modeled area. In all of these examples, water, solutes, and heat that originate outside the modeled area are applied as surface-water boundary conditions. In the case of these particular boundaries, the inflow salinity is zero, and no other solutes are simulated. Structure flow data were available from either the SFWMD DBHYDRO database (South Florida Water Management District, 2017) or the USGS South Florida Information Access (SOFIA) website (U.S. Geological Survey, 2017) for the BISECT time period, and the flows were applied as described by Wang and others (2007) and Lohmann and others (2012).

The offshore surface-water component of the system has three principal tidal boundaries: in the Atlantic Ocean along the east coast of south Florida, in the Gulf of Mexico along the west coast, and in Florida Bay along much of the southern BISECT boundary (figs. 1–1 and 1–2). Other lateral boundaries are defined as no-flow segments, such as along Barron River, from Carnestown to the Gulf of Mexico in Collier County (figs. 1–1 and 1–2).

All active tidal boundary cells in BISECT have a feature that allows the salinity of water at the boundary to equal the salinity of the mostly fresher water exiting the model domain during ebb tides. When flood flow into the model domain is restored, the salinity at the boundary returns to defined boundary values through a cosine function during a user-defined “return period” (Schaffranek, 2004). At the end of the return period in the BISECT model, the user-defined constant ocean salinity of 35 parts per million is restored as the boundary salinity value. The purpose of this capability is to more realistically approximate the fact that, under actual conditions, somewhat less saline water can and does reenter the modeled area after the onset of flood tides, particularly if the tidal boundary is near coastal sources of freshwater. The return period for all tidal boundary cells in BISECT is 60 minutes. Most BISECT tidal boundaries (fig. 1–2) are sufficiently remote from the mouths of freshwater streams to make this feature inconsequential. In Florida Bay, however, this return period ensures that the freshwater discharges into northeastern Florida Bay are not overwhelmed by repetitive influx of unrealistically higher salinity water on every flood-tide cycle.

Wind Stress

Although it is not a separately defined water flux, wind drag on the water surface can contribute to movement of both freshwater and saltwater into and out of the estuarine regions near the mouths of streams discharging to saltwater bodies, particularly in low velocity, low gradient areas. Wind drag can also contribute to the movement of water from place to place within the extensive marshlands of south Florida and across the ocean and bay regions of the study area. Data on wind velocity and direction applied to the surface-water model of BISECT were acquired from the NOAA Virginia Key weather station and from the USGS Old Ingraham Highway ET station (OIH) (fig. 1–8). The ET data collection site is described by German (2000). The data from these two sites were averaged in 4-hour periods and applied as a uniform wind field at every time step to all active surface cells of the BISECT model grid. In spite of some damping of peaks in the wind field, this averaged dataset provides a reasonable estimate of wind velocity and direction. Short-term peaks in wind velocity, which occur in localized areas, were not applied to the entire model domain.

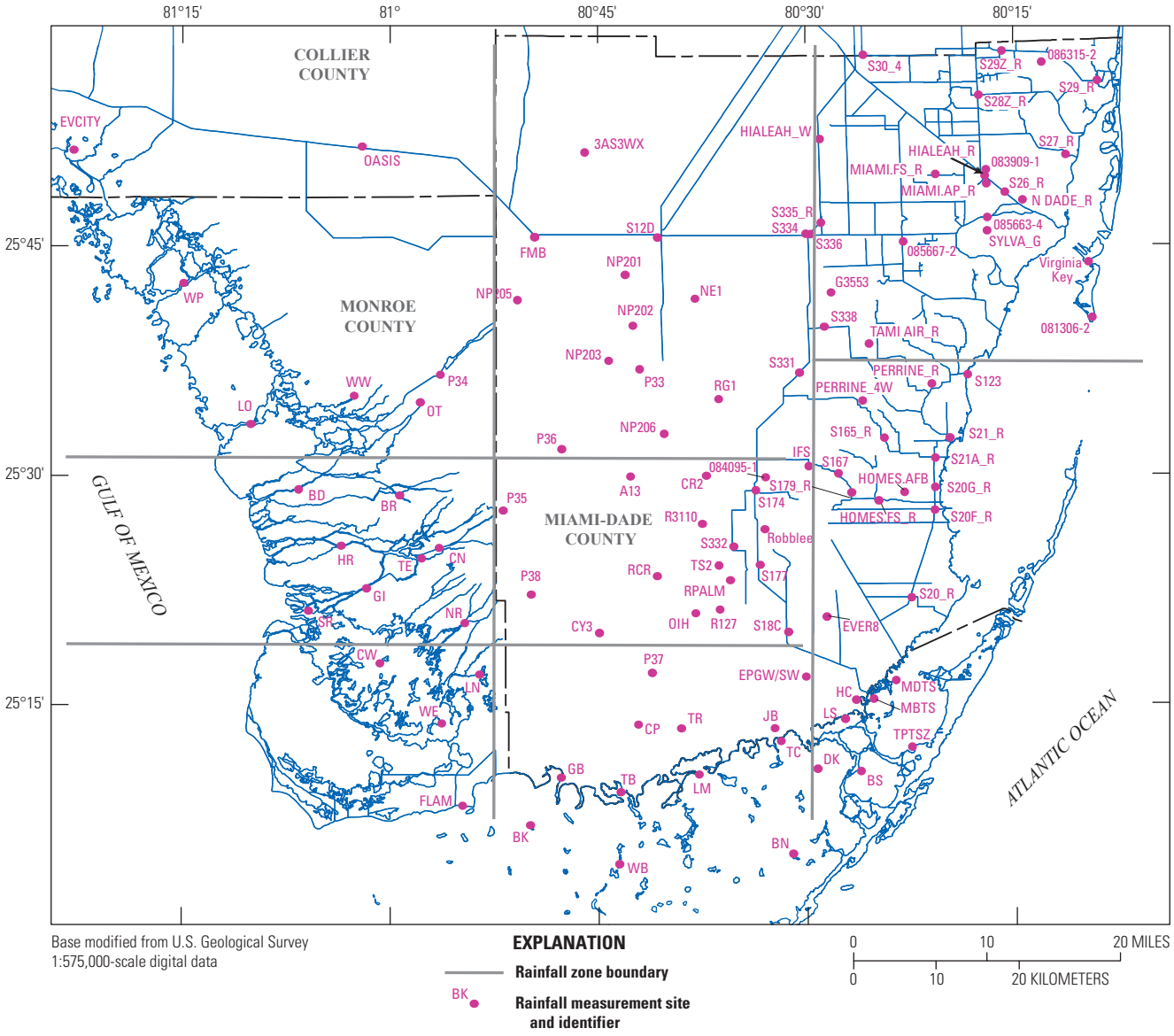

Figure 1-8. Biscayne and Southern Everglades Coastal Transport (BISECT) model rainfall zones and rainfall measurement sites, south Florida peninsula (see app. 3 for station details).

Wind stress τ is calculated by using a drag coefficient $\theta = 0.0018$ in the momentum flux formula:

$$\tau = \theta \rho_{air} v^2 \quad (1)$$

where

ρ_{air} is the air density, and

v is the wind velocity vector at 10 m above the surface.

For computational efficiency, the wind stress was precomputed and input to the BISECT model. The value chosen for the drag coefficient θ is more representative of stress over a vegetated land surface than over an open-water surface for the relatively low (well below 10 meters per second) wind speeds (Large and Pond, 1981) that typically occur across the study area.

Rainfall

The rainfall input to active surface-water cells of the BISECT model at each 10-minute time step is based on recorded daily rainfall amounts from 107 daily rain gage sites in or near the study area (fig. 1–8) (South Florida Water Management District, 2017). Rainfall is classified as an external boundary to the model, as it represents interactions with the atmosphere (fig. 1–7). Eight rainfall zones (fig. 1–8) with nearly equal average yearly rainfall were qualitatively identified on the basis of similar zones in the precursor TIME and Biscayne models. The six westernmost zones were created for the TIME model with consideration for spatial variability in rainfall volumes (Wang and others, 2007). The two eastern zones were modified from two of the zones developed for the Biscayne model (Lohmann and others, 2012). The 15-minute field data from the stations in each rainfall zone are used to compute 6-hour average rainfall rates for the zone, which are applied to each active BISECT surface cell at each time step.

Surface-Water Evaporation, Groundwater Evapotranspiration, and Heat Transport

The processes of evaporation and plant transpiration (that is, ET) convert liquid water into atmospheric water vapor from lakes, streams, ponds, marshes, and all other vegetated and shallow subsurface regions in the study area. ET is the process that removes the largest volumes of water from south Florida's annual water budget (McPherson and Halley, 1996; German, 2000). Annual ET averages about 100 cm of water and is exceeded in magnitude, on average, only by precipitation of about 125 cm, the largest term adding to the south Florida water budget (German, 1999). These quantities are somewhat higher than average in the simulation period used for BISECT, but the proportionality between ET and precipitation is similar. Since the average annual water supply for the study area is largely the difference between ET and precipitation, relatively small errors in estimating the BISECT model ET boundary condition can cause substantial differences between actual and simulated water budgets of the modeled region. This factor may limit model applicability to calibrated conditions and make model hindcasting or forecasting less reliable (Wang and others, 2007). Efforts were therefore undertaken to improve the accuracy of ET in BISECT and for related boundary conditions.

The term potential evapotranspiration (PET) is defined as the total flux of water that could potentially be converted to water vapor under existing radiation, wind, temperature, vegetative, and other conditions. Actual ET flux cannot exceed the PET value and is often less because there is insufficient available water to be vaporized. PET represents the sum of the potential fluxes from both evaporation and transpiration, even when one or the other is absent. For instance, even in open ocean or bay water, where no vegetation and, therefore, no transpiration occurs, the term PET is used; conversely, when there is no water available for evaporation, but plants still transpire water from the ground, the term PET is also used.

The process of developing the heat transport and ET formulation used in BISECT is described in appendix 4. This ET formulation includes

1. physically based sensible and latent heat exchange processes between the atmosphere and the modeled area at every time step, as well as addition of heat transport capability within the surface-water part of the FTLOADDS processor (Decker and Swain, 2008; Swain and Decker, 2009),

2. data derived from detailed physical heat budget experiments to determine the depth of soil actively storing and releasing heat diurnally to the overlying water column in the Everglades area (Swain and others, 2012), and

3. adjustments in albedo values for the surface-water heat budget, because albedo in shallow Everglades and other nearby coastal marshlands varies substantially (Sumner and others, 2011), largely controlled by variations in vegetation and inundation status.

Surface-water and groundwater ET are classified as external boundaries to the model, as they represent interactions with the atmosphere (fig. 1–7). The Penman-Monteith (PM) equation application detailed by Decker and Swain (2008) is used by the heat transport representation to compute latent heat and ET and is applied to every inundated cell in BISECT at every time step. The required input data of solar radiation, relative humidity, air temperature, and wind speed, was obtained from field stations listed in appendix 3. Cells with significant vegetation use a stomatal resistance in the PM equation of 140 seconds per meter (s/m), a value that was slightly lowered from the calibrated value in Swain and Decker (2010). All other inundated cells with no vegetation (streams, lakes, and oceans) use the same PM equation with a stomatal resistance of 0 s/m.

When the surface cells are effectively dry, the PM equation is used to compute a PET, which is applied at a reduced rate to the groundwater. The reduction in ET at deeper groundwater levels is inversely proportional to the square of the depth below land surface, which was found to work best in calibration, and is simulated with a calibrated extinction depth. BISECT model simulations indicate that groundwater ET must be substantially lower than PET or else unrealistic hypersalinity is simulated when modeling coastal groundwater. ET from the unsaturated zone or canopy storage is not explicitly modeled but neglecting additional sources of ET should cause the computed groundwater ET to be too low instead of too high. A lower ET rate can be indicated, as Barr and others (2009) noted that mangroves lower their transpiration rate in saline soils to avoid too much salinity concentration. Passioura and others (1992) discovered that mangrove transpiration rates in saline areas can be reduced to about 1 millimeter per day, only about 40 percent of the average rates in the BISECT model area. Acceptable results with BISECT are obtained with an ET rate of 0.36 PET when groundwater is at land surface, decreasing to zero at a depth of 0.4 m. As this subsurface ET reduction assumes saline groundwater and mangrove surface coverage, it is possible that higher groundwater ET values are more appropriate further inland. Representing groundwater ET rates that are highest inland and lower at the coast would require spatial variability in the subsurface ET reduction parameter, which is not currently a model capability.

The albedo used in the PM equation can be user input as spatially variable values. A value of 16.9 percent was previously defined for inland areas (Swain and Decker, 2010) and offshore areas vary between 8 percent and 28 percent. For details on the spatial distribution of albedo and the development of heat transport and ET in BISECT, see appendix 4.

Groundwater/Surface-Water Exchange

The hydrodynamic surface-water representation exchanges water with the topmost active layer of the groundwater model, which is layer 1 in the inland areas and shallow offshore areas such as Florida Bay (fig. 1–9). As this exchange occurs between the computed surface water and computed groundwater, it is considered an internal boundary in BISECT (fig. 1–7). Farther offshore, the seafloor bottom elevation drops below the bottom of layer 1, and lower layers of the groundwater model are in hydraulic contact with tidal waters. At the lateral marine margins of BISECT, a no-flow boundary condition was implemented for all layers of the groundwater component of the model, which helps prevent numerical instabilities from occurring in the surface-water component of the model. This boundary condition effectively applies the assumption that the horizontal groundwater gradient is zero at these three offshore boundaries.

Canal-Groundwater Exchange

Leakage between the canals and aquifer as a function of the head difference is accounted for in the groundwater simulation. The canals are subdivided into 1,600 individual reaches by using the MODFLOW River Package applied to the top layer of groundwater cells in SEAWAT (Guo and Langevin, 2002).

BISECT does not explicitly represent the canal flows, as it does overland flow, so canals are simply represented as source/sinks at a defined water level. As the canals are essentially outside the model simulation, canal leakage is classified as an external boundary to the model (fig. 1–7). The resulting water and solute transfer, for each time step, is either into or out of the aquifer groundwater cell that underlies the specific canal reach. All of the canals in this part of south Florida are incised into the topmost layer of the Biscayne aquifer, one of the most permeable nonartesian aquifers in the world (Parker and others, 1955). There is a continuous and substantial interchange of water and solutes between these canals and the aquifer. At each canal segment, the rate and direction of the canal-groundwater exchange are dependent on the difference between canal-segment stage, the nearby head in the aquifer, and the hydraulic conductivity between them.

Water levels assigned in 53 of the sections between canal control structures were uniform within each reach and calculated as the mean of the upstream structure tail-water and downstream structure headwater stages for the control structures that define each section. For the other seven sections between structures, the water level assigned to the cells varied along the section for one of the following reasons: (1) the distance between the upstream and downstream control structures was large enough for a substantial water-level difference to exist; (2) the section contained multiple control structures; or (3) the stage values at the upstream and downstream control structures were highly variable. For the cells in these sections, assigned water levels were calculated by using a bilinear interpolation between the upstream tail-water and the downstream structure headwater stages. Water levels at the tail water and headwater of the control structures were obtained from the SFWMD DBHYDRO database (South Florida Water Management District, 2017). The canal bottom elevations were estimated.

The vertical hydraulic conductance (streambed conductance in MODFLOW) for each cell in a canal reach was calibrated on the basis of an initial conductance calculated from the vertical hydraulic conductivity values assigned to the aquifer and the layer 1 and 2 cell thicknesses at that location. For some reaches, assigned conductance values were uniform for all cells within the reach, even if the hydraulic conductivities were variable, because a few presumptive model experiments indicated that leakage is relatively insensitive to varying the conductance values spatially.

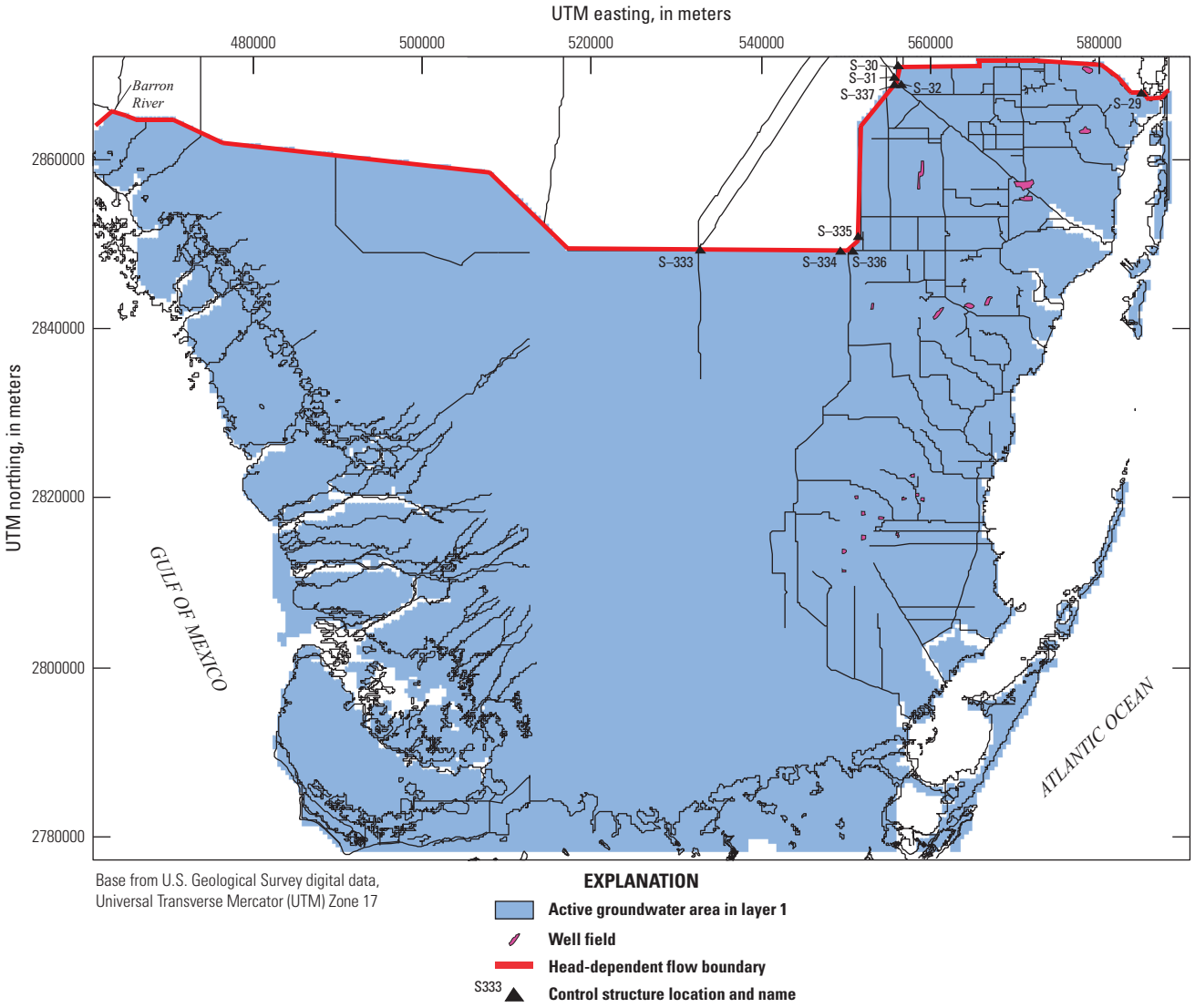

Figure 1-9. Groundwater model top layer and boundary conditions in the Biscayne and Southern Everglades Coastal Transport (BISECT) model for the south Florida peninsula.

Groundwater Boundaries and Pumping

The simulated groundwater component of BISECT is bounded from below by a confining unit with substantially lower hydraulic conductivity than the modeled aquifer layers. This boundary is very poorly connected to the groundwater model layers of interest in this investigation and a no-flow boundary is considered most appropriate (fig. 1–7). Water levels in the Tamiami Canal, the Levee 30N Canal, and the C-9, or Snake Creek, Canal (fig. 1–1) are used to define the groundwater boundary heads extending along the entire northern boundary of BISECT (fig. 1–9). The groundwater heads defined by these stations are classified as external boundaries to the model, as they represent interactions with hydrology outside the simulated area (fig. 1–7). General-head boundary (GHB) conditions are used to simulate groundwater inflows supplied to all the edge cells of all layers of this groundwater boundary. The stage values required by these GHB conditions are interpolated from recorded stages at the Barron River, S-333, S-334, S-335, S-336, S-337, S-30, S-31, S-32, and S-29 structures (fig. 1–9). Data for these sites are available in the SWFWMD DBHYDRO database (South Florida Water Management District, 2017). As vertical variations are not measured, these head values are applied hydrostatically in all aquifer layers.

Water is also removed from the BISECT groundwater component at selected subsurface cells, as a boundary condition, to represent groundwater pumping at production well fields (fig. 1–9). As all groundwater municipal pumping within the BISECT model area is confined to the urban region of the precursor Biscayne model (Lohmann and others, 2012) and the timeframe of both BISECT and Biscayne models are the same (1996 through 2004, inclusive), the groundwater pumping boundary condition for BISECT is the same as described in Lohmann and others (2012) for the Biscayne model.

Initial Conditions

Initial conditions are set to represent hydrologic conditions as closely as possible to estimated conditions at the beginning of the simulation using available data and knowledge of the rate at which hydrologic conditions change. For conditions that change rapidly (for example, surface-water stage) spatially uniform and generic values are initially assigned, and the model is assumed to achieve a reasonable distribution of values within the early part of the simulation period. For conditions that change slowly (for example, groundwater salinity) multiple simulations are used under static conditions to approach a steady-state distribution of values, which are then used as initial conditions for the simulation. Future-condition scenarios (involving sea-level rise, increased freshwater deliveries, and a vertical salinity barrier) all originate with these dynamically stable initial condition values, so differences in the resulting 9-year simulations are strictly due to differences in the tested scenario parameters.

Initial surface-water stages for all active surface-water cells are set to a spatially uniform 0.1 m referenced to NAVD 88. In this case, surface-water drainage adjusts within a few days of simulated time to realistic time-varying values in areas with ground elevations lower than 0.1 m NAVD 88. This warm-up period is on the order of days, but for areas with ground elevations higher than 0.1 m NAVD 88, it may take more than 1 month of simulated time to reach realistic time-varying levels, relying on precipitation to add water to the higher elevation cells. This warm-up period must be considered when evaluating model results.

Similarly, surface-water salinity for all active surface-water cells is initially set to values of 34 practical salinity units (PSU) for areas with an elevation less than -0.2 m NAVD 88 and is set to 0 PSU elsewhere, as an approximation of the large offshore/inshore salinity difference. In this case, reliable and dynamically stable salinity values for inland areas are not reached until after a warm-up period of about 6 months of simulated time has elapsed and the first wet season is well underway. Most of the salinity comparisons of model results are made at the coast, where simulated salinity reaches equilibrium in less than 1 month.

The surface-water temperature is initialized to 20 degrees Celsius (ºC) in all cells. The simulated temperatures tend to reach an acceptable spatial distribution after a warm-up period of 1–2 days of simulation time due to the balance of the heat budget terms used in the heat transport equations (Swain and Decker, 2009). The variability of temperature is much smaller than that of other parameters and tends to spatially equilibrate because of heat transfer.

Establishing realistic and dynamically stable initial conditions for groundwater heads and particularly groundwater salinity takes long simulated time periods relative to establishing surface-water conditions. To establish stable groundwater head and salinity configurations, multiple 9-year (1996–2004) conditions were simulated successively. Each successive 9-year sequence uses the final groundwater conditions from the previous segment to represent starting conditions (Lohmann and others, 2012). Boundary conditions, groundwater pumping, and the surface-water initial conditions are the same for each 9-year simulation. When the total salt content within the model was similar at the beginning and end of the 9-year simulation, the dynamic groundwater conditions were considered stable. After 648 years of simulated time (72 9-year sequences) the beginning and ending simulated salt content in the aquifer agreed to within 0.6 percent (fig. 1–10*A*). Two additional 9-year sequences were simulated to ensure stability of the salt content and similarity of results.

The conditions at the end of the 648-year sequence were chosen as the initial conditions for all further calibration, sensitivity, and scenario runs to determine likely impacts of sea-level rise, vertical salinity barriers, and increased freshwater deliveries on the hydrologic system in south Florida. The primary reason for this lengthy process is that the lower layers of the groundwater part of the BISECT model have very low permeability and transmissivity; water movement and the movement of the saltwater/freshwater interface toward an eventual equilibrium position are extremely slow. The net change in total salt mass over the final 9-year time series is much smaller than the variations in salt mass during those 9 years (fig. 1–10*B*), so very near steady state is achieved.

This establishment of initial groundwater salinity distributions was facilitated by prior work by Fitterman and Deszcz-Pan (2001), who measured groundwater salinity distributions in the western part of the BISECT model area, and Sonenshein (1996), who mapped the approximate location of the freshwater/saltwater mixing zone in the eastern part of the BISECT model area. These types of high-quality, field-measured groundwater data could be used as initial conditions in a groundwater model to avoid the need for a lengthy model warm-up period; however, establishing dynamic equilibrium initial conditions within the model that are demonstrably stable is the only way to ensure that the effects of simulated future changes to south Florida hydrologic conditions are due only to the future changes themselves and not to some unknown combination of future changes and incompletely resolved initial conditions. Thus, the field mapping data provided a useful starting point for the multiple 9-year simulations that developed the groundwater salinity initial conditions but were not used directly to represent initial conditions.

Model Calibration Procedure

The objectives of calibration were (1) for measured and simulated data values to be qualitatively as similar as possible and (2) for the resulting simulated hydrologic time series data (stage, discharge, head, salinity, and temperature) to represent as much of the relevant statistical characteristics of the corresponding measured data as possible. The BISECT model relies substantially on the calibrated parameters of the precursor TIME and Biscayne models (Wang and

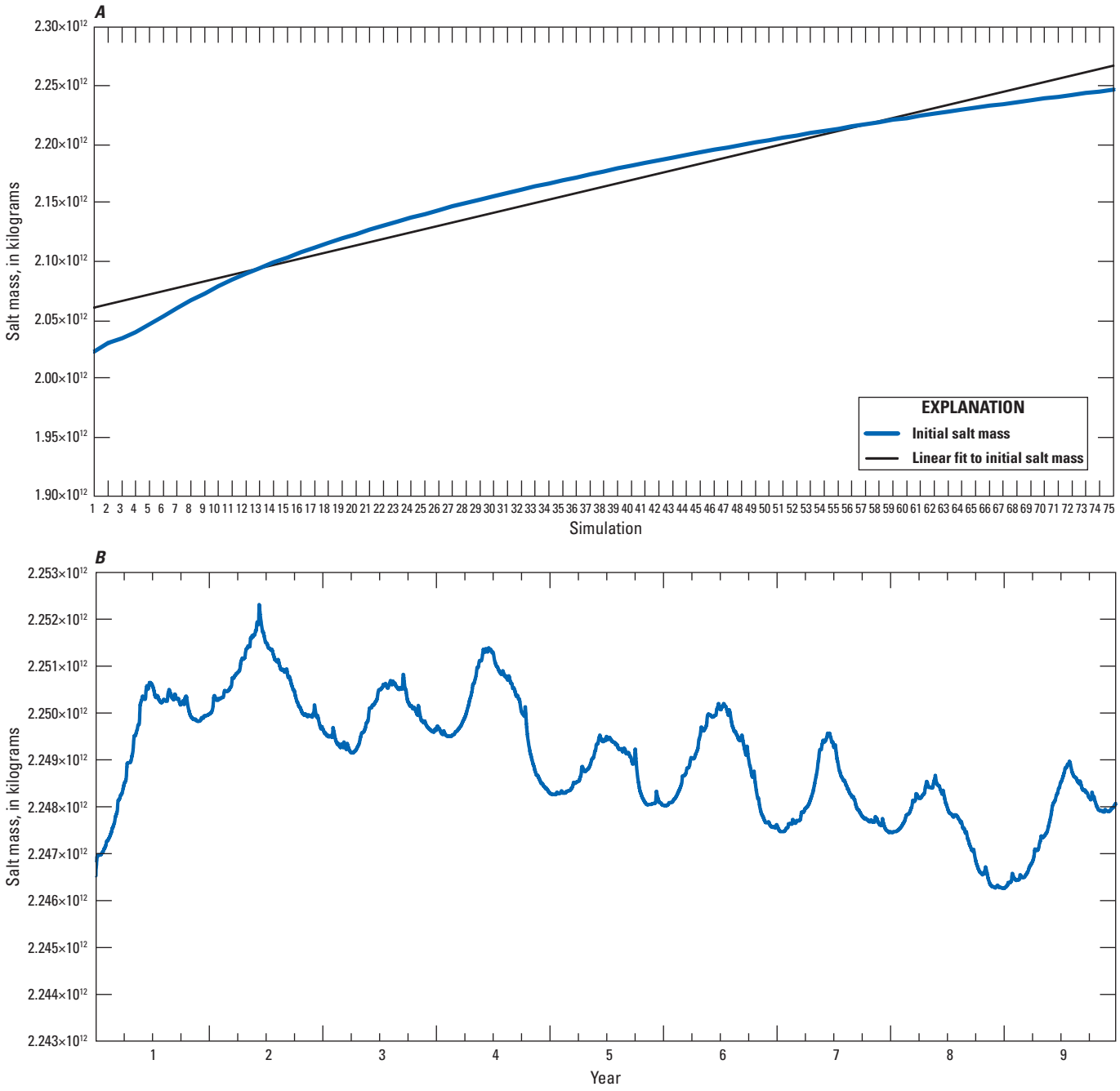

Figure 1-10. Change in salt mass in the Biscayne aquifer as simulated by the Biscayne and Southern Everglades Coastal Transport (BISECT) model for the south Florida peninsula. *A*, Change in initial salt mass during seventy-four 9-year simulations and the linear projection line. *B*, Seasonal change in salt mass during the final 9-year simulation.

others, 2007; Lohmann and others, 2012). When the TIME and Biscayne models were initially merged to create a preliminary version of BISECT, a qualitatively acceptable model fit was achieved, without recalibrating BISECT. Documented model sensitivity analyses for the TIME model, however, indicated that simulated coastal stream discharges are most sensitive to land elevation and frictional resistance parameters (Swain and others, 2004; Wang and others, 2007). So, the BISECT model was calibrated by adjusting these parameters. Elevation of land surface for selected cells and Manning's *n* for other selected cells were manually adjusted to calibrate to improve fit of simulated to observed discharge in coastal streams.

The location of the subsurface freshwater-saltwater interface is not used quantitatively as a calibration target, but it is examined qualitatively as an important aspect of the BISECT model, particularly for evaluating how the interface may move with future hydrologic changes. Simulated and measured salinity data indicate the subsurface freshwater-saltwater interface location and are visually compared to evaluate model fit.

As calibration was performed by varying the input parameters to which the model output values are most sensitive, as discussed above, other input parameters were taken directly from the precursor TIME and Biscayne models. These include aquifer horizontal and vertical conductivities, canal hydraulic conductance, the thickness and hydraulic conductivity of the transitional layer between the surface-water and groundwater parts of the system, hydraulic conductance of the head-dependent flux boundaries, and the groundwater storage parameters.

Surface-Water Flow to the Gulf of Mexico and Florida Bay

Matching the observed surface-water flow is critically important in the western and largest part of the BISECT modeled area because the flow of the 11 coastal streams in this area (fig. 1) integrates all of the hydrologic and meteorological processes in each watershed. Simulating flows at coastal streams is complex, with multiple influences from oceanic and atmospheric processes. Although primarily affected by daily tidal action and singular events such as storms and frontal passages, other influences on the flow of coastal streams include long-period oceanic water-level changes and the effects of onshore and offshore winds blowing across large fetches of the Gulf of Mexico and Florida Bay.

The simulated flow in the coastal streams is a major factor in the mass balance in the model, as the coastal streams are the primary flux connection between the inland and offshore zones. This mass balance is affected by functions and processes including precipitation, ET, other water sources such as the S-12 structures and groundwater inflow at the northern boundary of BISECT, groundwater recharge and discharge, tidal and other coastal water-level fluctuations, and the physics of water movements under the influences of topography and frictional effects. Therefore, if mean stream discharge and time histories of both daily simulated and measured stream discharge at a gaging site are similar, there is a strong likelihood that all or many of the aforementioned hydrologic and meteorological processes and transport functions in that watershed are properly accounted for in the model. Conversely, if there are large differences in mean stream discharge and time histories of simulated and measured streamflow in a watershed, then one or more of the same hydrologic and meteorological processes or transport functions may not be properly accounted for in the model, resulting in less reliable model results in such regions. Large differences between measured and simulated stream discharge are also an indication that additional effort is needed to either identify and correct the cause, or field investigations are needed to gain more knowledge of hydrologic, meteorological, and transport processes and then, with more complete understandings, improve how they are represented in BISECT.

Three adjustments were made to improve the match to observed streamflow based on the performance of previous modeling efforts: (1) adjustments in flow-way connectivity in the streams, (2) adjustments of frictional resistance in the wetlands, and (3) adjustments of frictional resistance in the streams. The first adjustment was made because measured and simulated streamflow discrepancies can be partially caused by incorrect flow-way connectivity of these streams. Small errors in the land elevation of 500-m by 500-m cells that define the streams can allow either too much or too little water flow in the streams that connect Everglades marshlands to the coast. Only the North River area required slightly increased elevations of several cells (fig. 1–11) because the original simulated flows were too high (Wang and others, 2007). In five other streams, northwest of North River (fig. 1–11), the land-surface elevation of several cells was reduced to improve the connectivity of these coastal streams.

The second adjustment made to improve the match to observed streamflow was the same as done previously by Bahm and Fennema (2013) during development of the TIME model version 2.0. They included some significant Manning's *n* adjustments designed to promote additional marsh surface-water migration to Taylor Slough (fig. 1–1) and create better agreement between simulated and measured flows. The three rectangular areas of Manning's *n* enhancements are identified by arrows in figure 1–12 (original image). Similar, but less extensive, modifications were also made to selected friction factors in the North River and Shark River areas to likewise improve model simulation of streamflow. These areas produced some large cell-to-cell Manning's *n* spatial discontinuities that could induce numerical instabilities. As a solution, simple moving-average spatial smoothing was applied to these areas (fig. 1–12, smoothed image). The range of the moving average was varied depending on the magnitude of the discontinuities.

A third adjustment of the Manning's *n* parameter was made to improve the calibration to streamflow. These frictional modifications were made in only the predominant direction of flow of each stream, north-south or east-west, and only in a 6,000-m reach along each stream channel centered at each flow-measuring site. The resulting Manning's *n* parameter changes are shown as the difference between the north-south and east-west values in figure 1–13. This effort achieved the goal of improving the comparisons to measured flows at the coastal discharge measurement sites (app. 5).

The first two adjustments described above were performed originally with the TIME model and continued to be used in BISECT. The third adjustment was made only in the BISECT model. For a discussion of the comparison of the TIME model simulated coastal discharge to that of the BISECT model, see appendix 5.

Calibration Performance Statistics

A number of statistical tools can be used to determine how close a time series of BISECT-simulated values was to the corresponding time series of measured values. Bahm and Fennema (2013) give concise descriptions of four such tools (covariance, correlation, Nash-Sutcliffe efficiency parameter, and percent explained variance) and also provide short summaries of how each can be used and interpreted.

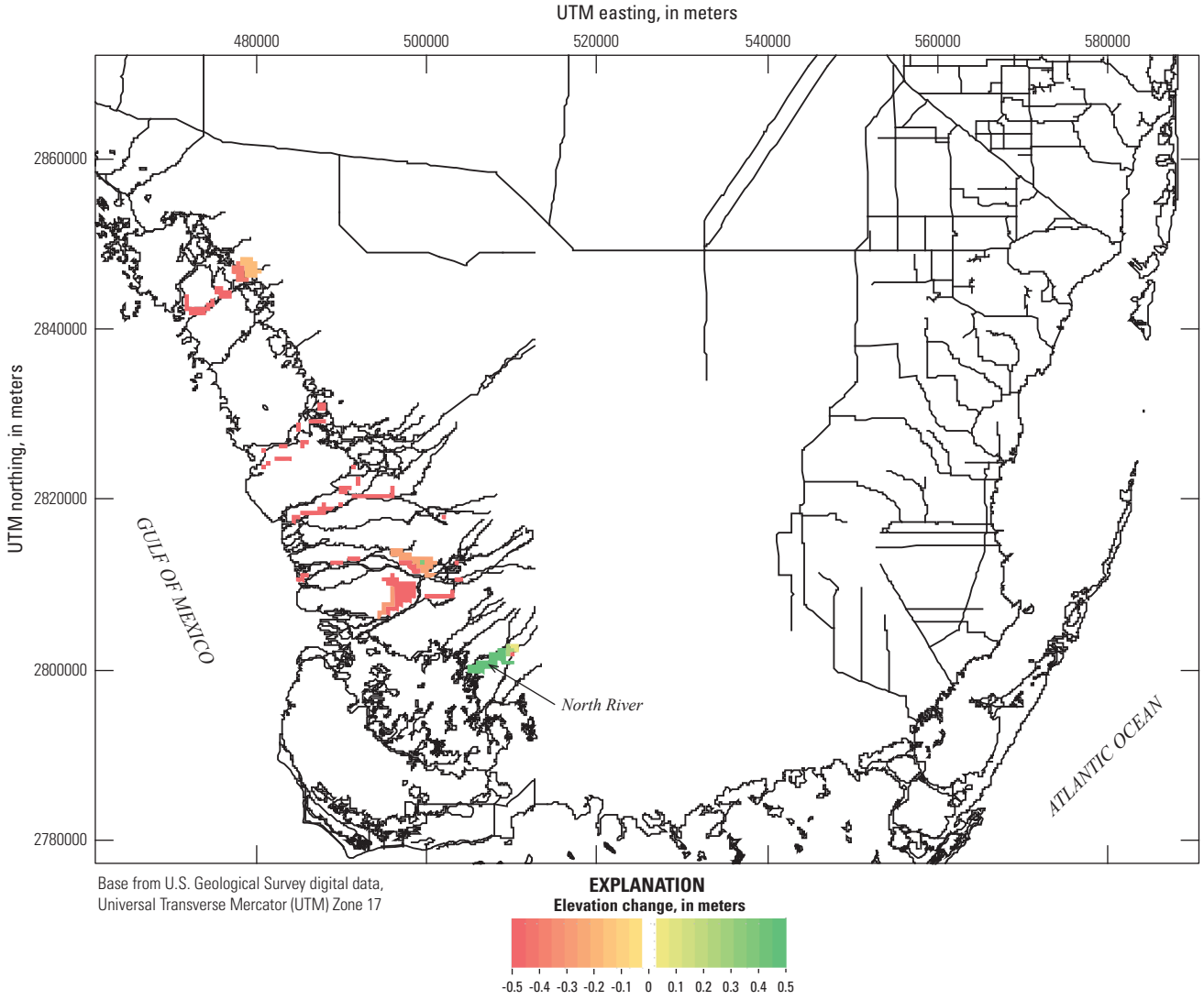

Figure 1-11. Changes in topographic elevations in coastal areas as simulated by the Biscayne and Southern Everglades Coastal Transport (BISECT) model for the south Florida peninsula.

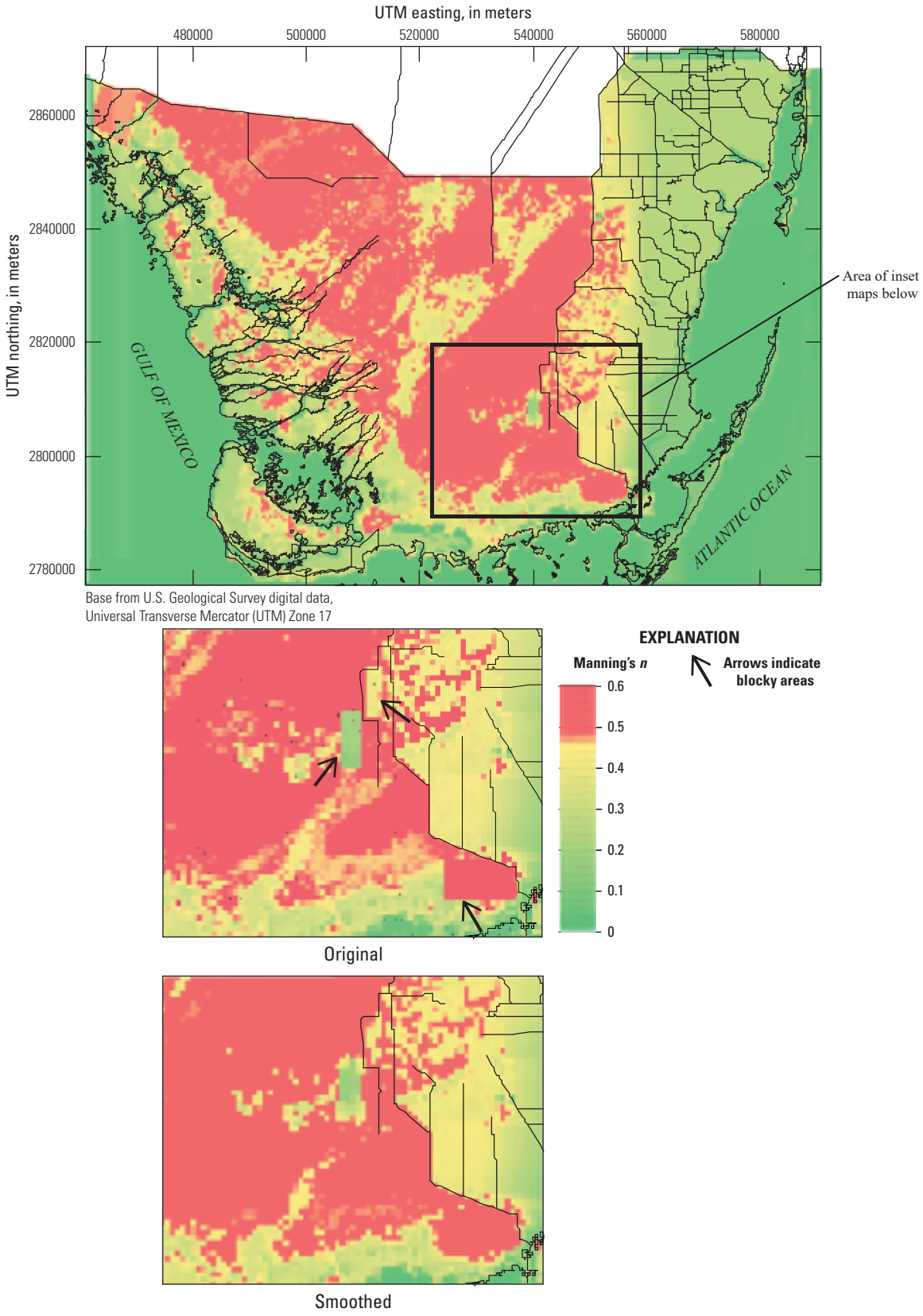

Figure 1-12. Manning's *n* values before and after spatial smoothing in the Biscayne and Southern Everglades Coastal Transport (BISECT) model for the south Florida peninsula.

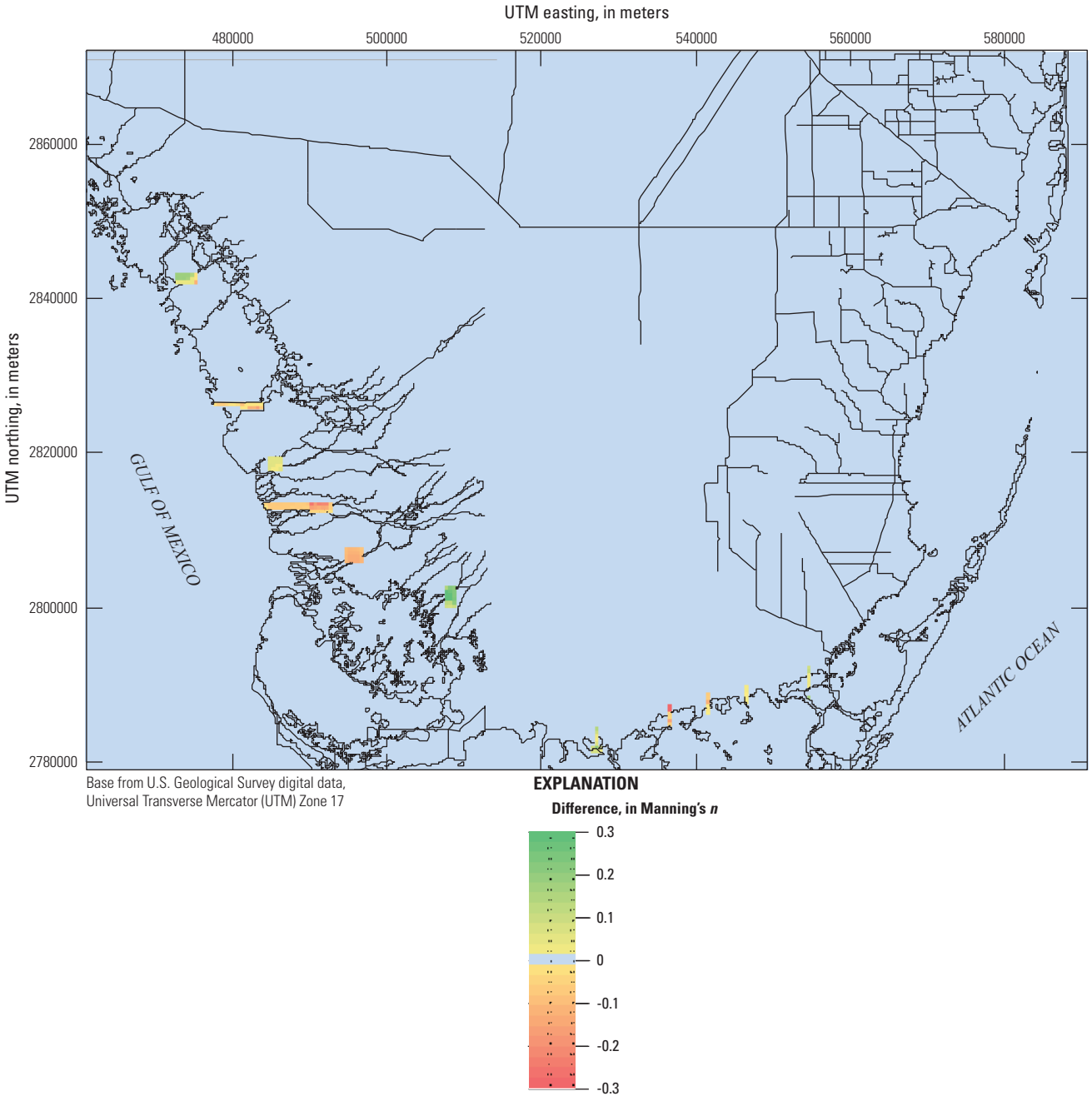

Figure 1-13. Difference in Manning's *n* between east-west and north-south directions of riverflow as simulated by the Biscayne and Southern Everglades Coastal Transport (BISECT) model for the south Florida peninsula.

Covariance (*CoVar*) is a measure of the similarity of the fluctuations of two variables. The mean values of both simulated and measured series are subtracted from each of their respective daily values, and the products of the resulting deviations are summed and averaged:

$$CoVar = \frac{\sum_{i=1}^{N}\left(X_c^i - \overline{X_c}\right)\left(X_m^i - \overline{X_m}\right)}{N-1} \quad (2)$$

where

N is the number of values in the time series,
X_c^i is the ith simulated value,
X_m^i is the ith measured value,
$\overline{X_c}$ is the average of the simulated values, and
$\overline{X_m}$ is the average of the measured values.

The covariance value indicates whether the two datasets are fluctuating around their respective means in a similar manner. Higher covariance values indicate greater fluctuation similarity. The units of covariance values are the square of the series units.

Correlation (*Corr*) is a related statistic that is defined as the covariance of the measured and simulated values divided by the square root of the product of their variances:

$$Corr = \frac{\sum_{i=1}^{N}\left(X_c^i - \overline{X_c}\right)\left(X_m^i - \overline{X_m}\right)}{\sqrt{\sum_{i=1}^{N}\left(X_c^i - \overline{X_c}\right)^2 \sum_{i=1}^{N}\left(X_m^i - \overline{X_m}\right)^2}} \quad (3)$$

Correlation is dimensionless and more precisely describes the degree to which the measured and simulated datasets vary in a similar manner. Because it is dimensionless, using this statistic for comparisons between time series having different variances is more appropriate. A correlation value of 1.0 indicates perfect correlation. Both correlation and covariance values are frequently used to describe the degree of similarity between datasets.

The Nash-Sutcliffe efficiency parameter (Nash and Sutcliffe, 1970) is another statistical tool that quantifies the fit between measured and simulated time series by how well the measured series' variance is explained by the simulated time series. The Nash-Sutcliffe (*NS*) parameter takes the following form.

$$NS = 1 - \frac{\sum_{i=1}^{N}\left(X_c^i - X_m^i\right)^2}{\sum_{i=1}^{N}\left(X_m^i - \overline{X_m}\right)^2} \quad (4)$$

The *NS* coefficient compares the residual squared (numerator) to the measured variance (denominator) and produces a proportion of the error relative to the measured variance, and it can range in value from negative infinity to 1.0, which indicates that the simulated and measured time series are identical. An *NS* value of 0 indicates that the model simulation has a squared error no better than the squared error of the mean of the measured data. An *NS* value less than 0 indicates that the mean of the measured data is a better predictor than the model. This method gives significant weight to large differences between measured and simulated values, such as when the means of the measured and simulated time series are different or when fluctuations are not synchronized. This parameter is particularly useful in the model calibration process because it focuses attention to specific areas or processes that may need model calibration adjustments that were previously unrecognized.

A useful variant of the *NS* parameter, called the mean-adjusted Nash-Sutcliffe parameter or the percent explained variance (*PEV*) parameter, specifically evaluates the simulation of temporal fluctuations by correcting for different mean values of the simulated and measured data. The *PEV* parameter is particularly useful whenever comparisons of fluctuations about the means are of particular importance as it specifically gives the fraction of the variance in the measured time series that is explained by the simulated time series.

$$PEV = 1 - \frac{\sum_{i=1}^{N}\left[\left(X_c^i - \overline{X_c}\right) - \left(X_m^i - \overline{X_m}\right)\right]^2}{\sum_{i=1}^{N}\left(X_m^i - \overline{X_m}\right)^2} \quad (5)$$

In addition to covariance, correlation, Nash-Sutcliffe efficiency, and *PEV* statistical parameters, two other common statistics used in this report are the root-mean square error (*RMSE*),

$$RMSE = \sqrt{\frac{\sum_{i=1}^{N}\left(X_c^i - X_m^i\right)^2}{N}} \quad (6)$$

and the mean error (*ME*),

$$ME = \frac{\sum_{i=1}^{N}\left(X_c^i - X_m^i\right)}{N} \quad (7)$$

RMSE is the square root of the average of the squared differences between simulated and measured time series values. *ME* is simply the average of the differences between simulated and measured time series values. Both of these statistics have the same units as the series themselves. Since computation of *ME* involves the use of both positive and negative values that offset one another, *RMSE* values are always higher than *ME* values for the same set of compared time series. Another relation between parameters is that greater magnitudes of *RMSE* and *ME* indicate greater differences between *NS* and *PEV*.

Comparison of Simulated Values and Field Measurements

Simulated coastal streamflow, water levels in surface water and groundwater, flux exchanges between canals and

the aquifer, salinity in the surface water and groundwater, and surface-water temperature all were compared to field data, and model fit was described by using the previously mentioned calibration performance statistics.

Coastal Streamflow

The BISECT-simulated values of daily average coastal streamflow (or discharge) are compared to daily average measured values from a streamflow measuring program (Hittle and others, 2001; Levesque, 2004) (fig. 1–14). Five of the 11 streams (Trout Creek, Long Sound, McCormick Creek, Mud Creek, and Taylor River) have complete sets of measured streamflow data for the 9-year, "base-case" simulation period, from 1996 to 2004, inclusive (fig. 1–6). Five other streams (Broad River, Chatham River, Shark River, Lostmans River, and North River) have field-measured streamflow data starting at various times in 2001 (fig. 1–6). Harney River has field-measured streamflow data beginning in October 2003.

Most of the measured discharge data have a moderately to substantially greater magnitude of small temporal scale (daily) variability than do the simulated discharge data. This difference is expected because measured flow data are collected at a single point or a single stream cross section, whereas the model-calculated daily streamflows are averaged across 500-m by 500-m cells, resulting in a more attenuated response to simulated rainfall, runoff, and other processes. The overall tendency for measured data to show larger daily fluctuations is also noted in surface-water salinity in ENP and daily canal/aquifer exchanges to and from the Biscayne aquifer in the eastern part of BISECT.

Model results for surface-water discharge indicate that Taylor River has the lowest *NS* and *PEV*, compared with other sites, indicating dissimilar measured and simulated values and larger errors (table 1–1). These statistics may seem at odds with the observation that *RMSE* and *ME* values for Taylor River are smaller than those for other streams, indicating smaller errors, but these parameters are proportional to average flow, which is lower at Taylor River. Harney and Lostmans Rivers have higher *PEV* values relative to their *NS* values, indicating that errors in mean values predominate. Only four of the *PEV* values for stream observations are greater than 0.4, but the majority of the *NS* values are greater than 0.3 (table 1–1).

Surface-Water Stage

Surface-water stage is measured at 149 field sites (fig. 1–15). For the purpose of comparison with model results, two criteria were considered for site selection: (1) to include only a single site from each cluster of sites with highly correlated measured data and (2) to minimize large spatial distances between observations.

To eliminate clusters of highly correlated sites, a matrix of correlations and a matrix of interstation distances were created for each pair of stations in figure 1–15. For each component in these two matrices, the correlation and distance between the stations were applied in the equation

$$(1 - correlation) \times distance \quad (8)$$

producing a value that is large when a station is poorly correlated and (or) distant from other stations and is small when the station is highly correlated and (or) close to nearby stations. These values were summed for each station (table 1–2). When ordered from smallest to largest value of (1-*correlation*) x *distance*, the stations that are most clustered with similar stations occur at the top of the list (table 1–2).

The stations for comparison of water level were then selected from groups of more highly correlated and proximal sites. To ensure that two nearby highly correlated stations are not both chosen, the selected stations were mapped to ensure that they are distributed throughout the entire study area (fig. 1–15). When spatial gaps were identified, additional stations were added, with priority given to stations with higher correlation and proximity to other stations (table 1–2). Overall, 12 stations were selected, as highlighted in table 1–2 and shown in red in figure 1–15. A poorly represented area was identified in the northwestern part of the study area. Stations are so sparse in that area that none were selected by their correlation or proximity. Of the stations in the northwest, BICYA10 is centrally located and has the lowest (1-*correlation*) x *distance* value (table 1–2).

Stage values measured at the 12 selected field stations (fig. 1–15) are compared to model-simulated results (fig. 1–16). Gaps in the measured data occur either at times when no data were collected or when the water level was below land surface. Visual inspection of figure 1–16 indicates that measured and model-simulated results are generally close; station NP201 shows the most distinct deviations. Simulated surface-water levels at Craighead Pond can be as much as 0.2 m above the measured value when the levels are at their lowest. This discrepancy may be a result of insufficient local drainage. Simulated and measured stage values at stations EPGW and P37 appear to be similar (fig. 1–16).

Simulated surface-water stage values are compared with field-measured values by using *NS*, *PEV*, *RMSE*, and *ME* (table 1–3). EPGW has the lowest *RMSE*, and NP-201 has the highest *RMSE*, indicating that these stations have the lowest and highest error magnitudes, respectively. Station P-33 has the highest *NS* and *PEV* values, indicating lowest ratio of error to variance, whereas BICYA10 has the lowest *NS* and *PEV* values. The spatial distribution of the *NS* errors is shown in figure 1–17. Error in simulated stage is greatest at sites closest to the northern border of the modeled area.

The surface-water *ME* values indicate how much the simulated stages are above or below the measured values (fig. 1–18). With the exception of NP-201, where the simulated stage is substantially lower than the measured stage, sites with either high or low *ME* values are evenly distributed across the modeled area.

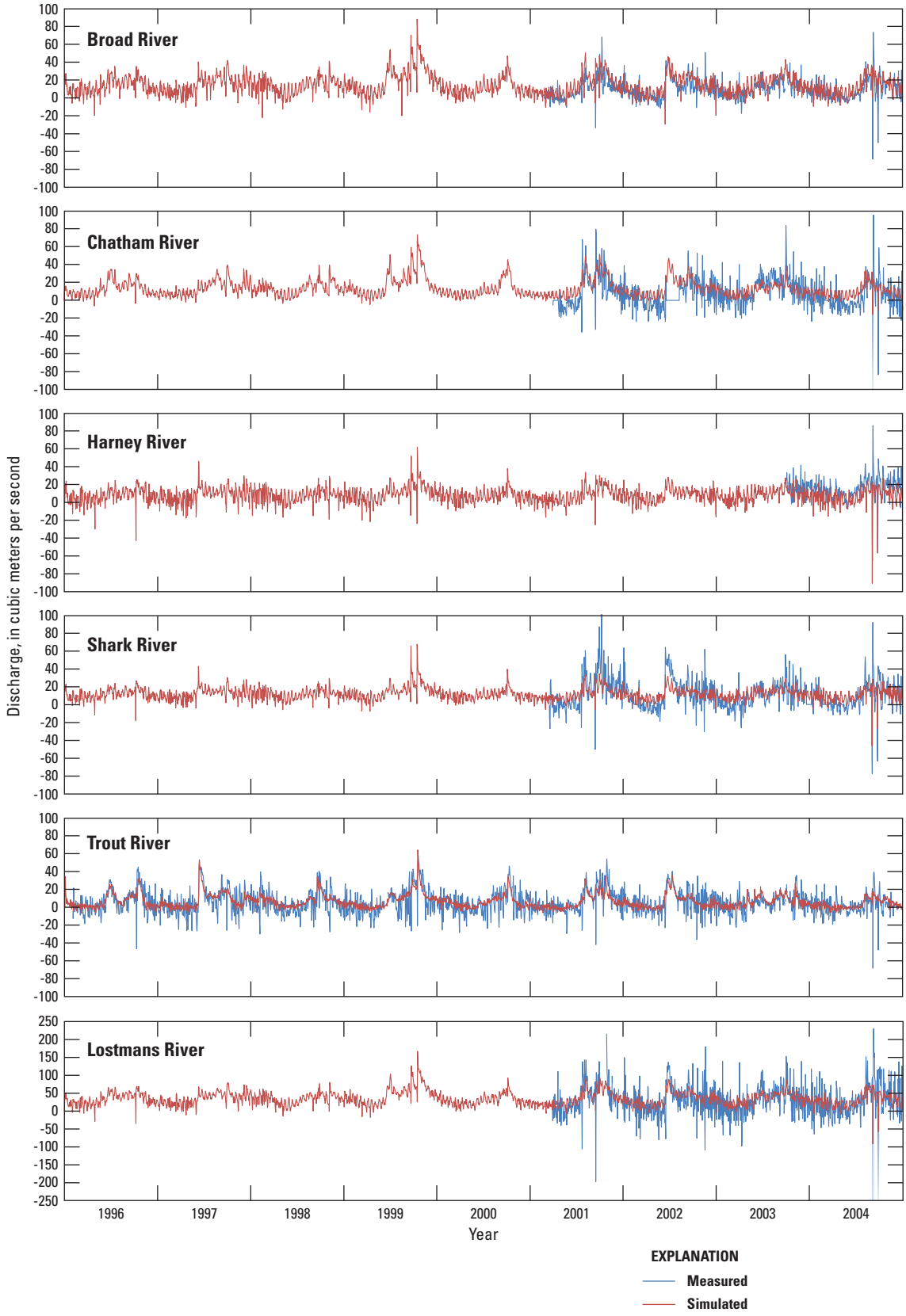

Figure 1-14. Comparisons between measured coastal discharges and coastal discharges simulated by the Biscayne and Southern Everglades Coastal Transport (BISECT) model for the south Florida peninsula, 1996–2004 (see app. 3 for station details).

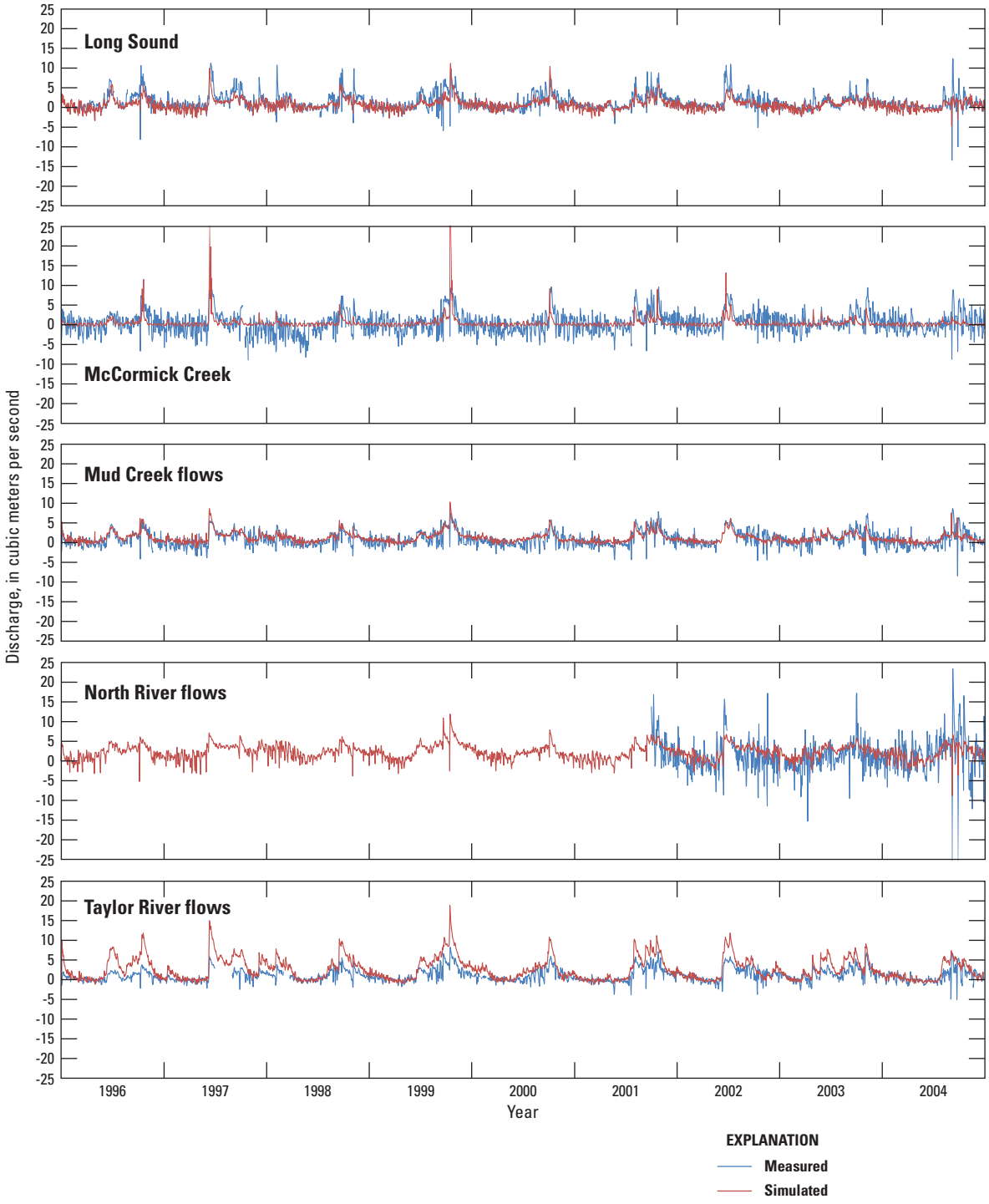

Figure 1-14. Comparisons between measured coastal discharges and coastal discharges simulated by the Biscayne and Southern Everglades Coastal Transport (BISECT) model for the south Florida peninsula, 1996–2004 (see app. 3 for station details).—Continued

Table 1–1. Surface-water discharge model-fit statistics simulated by the Biscayne and Southern Everglades Coastal Transport (BISECT) model for the south Florida peninsula, 1996–2004.

[*PEV*, percent explained variance; *NS*, Nash-Sutcliffe coefficient; *RMSE*, root-mean square error; m^3/s, cubic meter per second; *ME*, mean error. See app. 3 for station details]

Based on daily average measured and simulated discharge				
Location and parameter	***PEV***	***NS***	***RMSE*** (m^3/s)	***ME*** (m^3/s)
Broad River discharge	0.372	0.300	9.119	2.923
Chatham River discharge	0.442	0.383	13.191	4.071
Harney River discharge	0.395	-0.053	12.695	-8.282
Long Sound discharge	0.470	0.372	1.630	-0.644
Lostmans River discharge	0.307	0.292	36.563	5.245
McCormick Creek discharge	0.100	0.100	2.468	-0.018
Mud Creek discharge	0.474	0.438	1.403	0.354
North River discharge	0.301	0.264	3.781	0.853
Shark River discharge	0.396	0.396	12.795	0.155
Taylor River discharge	-0.311	-1.184	2.371	1.499
Trout Creek discharge	0.382	0.374	10.132	1.097

Groundwater Levels

Simulated groundwater heads were compared with measured heads at 49 monitoring wells (fig. 1–19), and the error statistics were determined (table 1–4). The *NS* values for groundwater head indicate that the largest errors relative to the variance in head are in the eastern urban area (fig. 1–19), likely related to the higher *ME* at these stations (fig. 1–20). The mean errors are mostly positive in the eastern urban part of the modeled area, as well as in the southern wetlands (fig. 1–20). The groundwater data in the western parts of the modeled area are sparse, but the *ME* values are generally negative in the undeveloped area, indicating that the simulated groundwater heads are generally lower than measured values in this area (fig. 1–20). To evaluate model fit regionally, the groundwater sites were separated into three groups: within ENP (fig. 1–21), along the Canal L 30 and Canal L 31 N/Canal 111 system (fig. 1–22), and along the east coast of Miami-Dade County (fig. 1–23). In ENP, simulated groundwater head does not drop as low as measured values at the lowest levels (fig. 1–21). This pattern may occur because the simulated groundwater ET rate is most likely too small. The ET computations for the groundwater simulation were chosen to produce ET values low enough to prevent excessive hypersalinity in coastal groundwater, which may be too low for inland areas. Spatially variable subsurface ET reduction parameters (see section "Surface-Water Evaporation, Groundwater Evapotranspiration, and Heat Transport") could remedy this situation, but are not currently an option in the model code.

Canal Exchanges

Although drainage basins are difficult to delineate in the BISECT domain because of the very low and variable water slopes, 10 basins have been defined on the basis of the canal system configuration (fig. 1–24). Several canal reach basins were combined for the purpose of computations; exchanges in the C-9 West, C-9 East, and C-11 East Basins are summed together, as are exchanges in the C-2, C-4, and Coral Gables Canal Basins (fig. 1–24). The differences in measured discharge between the upstream and downstream canal control structures within each basin are the measured canal/aquifer exchange, and these are compared with the simulated values (fig. 1–25). The magnitudes and directions of the canal-aquifer exchanges indicated by the measured data are reproduced in the simulated exchanges, but with fewer extremes than in the measured data. The error statistics indicate the canal/aquifer exchange at the Canal 1 and Canal 111 canals have the lowest *PEV* and *NS* values and somewhat higher *RMSE* and *ME* values (table 1–5). When evaluating these statistics, it also must be considered that the field-measured values are dependent on the rating curves at the control structures, so the inherent uncertainty in this rating computation contributes to uncertainty in the comparison of canal leakage to simulated values.

Surface-Water Salinity

Surface-water salinity data are collected at sites in both coastal and offshore areas (fig. 1–26). Sites in the Biscayne Bay area have monthly data (fig. 1–27), and those in the ENP area have 15-minute data (fig. 1–28). General observed patterns and variations in salinity are simulated at all sites. The error statistics indicate that the best match between observed and model-calculated salinity is in the Florida Bay area (stations GB and BS in table 1–6) and the worst is in far northern and far southern Biscayne Bay (stations NIB and BB51 in table 1–6). Differences between observed and simulated salinity may be greatest in the smaller subembayments in the northern and southern parts of Biscayne Bay because they are spatially isolated, and small errors in simulated volume exchanges can substantially affect salinity (fig. 1–26).

The magnitude of the spatial and temporal variations in surface-water salinity can be examined by comparing simulated wet-season salinity on June 12, 1997, to dry-season salinity on February 6, 2001 (fig. 1–29). The inland extent of simulated elevated salinity is not substantially different between the wet and dry seasons at the regional scale, but the values of salinity, both inland and offshore, are substantially higher in some areas in the dry season. The southwestern coast shows the greatest difference in simulated salinity between wet and dry seasons (fig. 1–29), a location expected to be largely affected by flow from Shark River Slough.

Groundwater Salinity

Although no continuous groundwater salinity data are available for analysis, a comparison of the spatial distribution

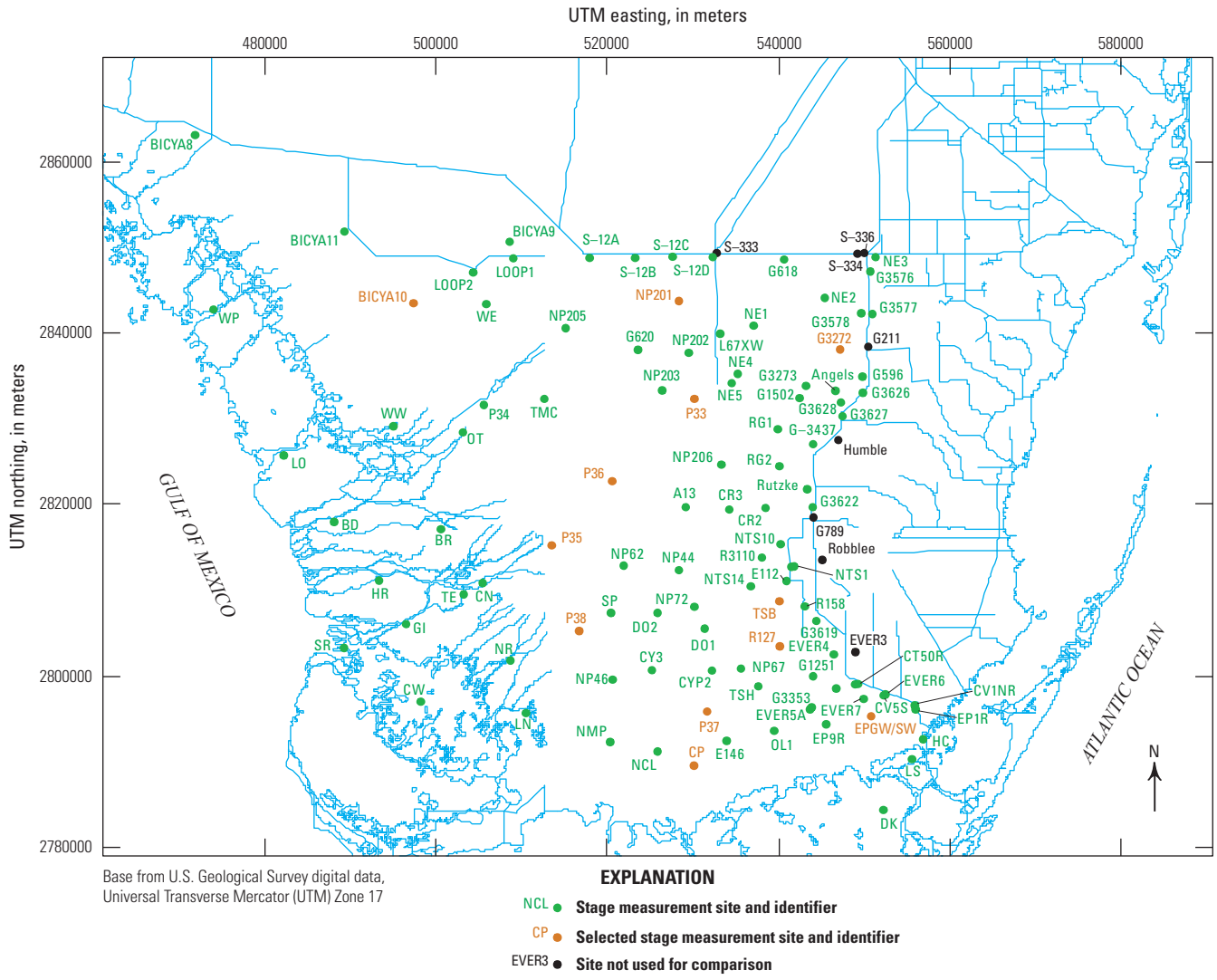

Figure 1-15. Locations of selected stage measurement stations (temperature also measured at P33; see app. 3 for station details) for the Biscayne and Southern Everglades Coastal Transport (BISECT) model application for south Florida.

of groundwater salinity at the bottom of model layer 12 can be compared to field estimates of the extent of saltwater intrusion, defined as 1,000 PSU salinity, by Sonenshein (1996) and by Prinos and others (2014) (fig. 1–30). These field estimates are limited to the eastern part of the modeled area, but the comparison with model results shows a similar inland extent of elevated aquifer salinity, except in the northeast, where the model-represented salinity extents further inland. A similar difference in the field estimates and model results in the northeastern area was seen in the Biscayne model (Lohmann and others, 2012).

To compare the extent of salinity intrusion in the western and southern parts of the modeled area, a comparison can be made with a salinity map at a depth of 15 m, derived from a helicopter-borne electromagnetic (HEM) survey (Fitterman and Deszcz-Pan, 2001) (fig. 1–31). The HEM data (Fitterman and Deszcz-Pan, 2001) were converted from resistivity to chloride concentration, and equivalent salinity values were calculated. The dashed line in figure 1–31 represents salinity of approximately 2 PSU evaluated by this method. This 2-PSU line extends farther south than the model-simulated 2-PSU contour near Taylor Slough, but farther to the west, the lines are closer together (fig. 1–30). This pattern may indicate that the leakage of freshwater flow from Taylor Slough into the aquifer may be underrepresented in the model.

Surface-Water Temperature

The model was used to simulate surface-water temperatures, which were compared with measured values. Eleven sites in the Biscayne Bay area have monthly temperature data (fig. 1–32), and 12 sites in the ENP area have 15-minute temperature data (fig. 1–33). The model simulates the trends and fluctuations in temperature patterns, but generally underestimates temperatures for all sites. Error statistics for simulated surface-water temperature are shown in table 1–7 (site locations shown in fig. 1–26). Although multiple studies have examined ET rates in various inland locations (Abtew, 1996; German, 2000; Shoemaker and others, 2011),

Table 1–2. Surface-water stage measurement stations and correlation-distance parameter.

[Highlighted stations chosen for model comparison; corr, Pearson correlation coefficient. See app. 3 for station details]

Station	Sum of (1 - corr) x distance to other stations
RG2	1077547
RG1	1094707
S175	1117211
Rutzke	1120077
CR2	1120886
R127	1126886
NP62	1134264
Angels	1153682
NTS1	1156276
NTS10	1172919
E112	1176908
EVER4	1177286
TSH	1184503
G1251	1184507
NTS14	1189319
CR3	1197974
R158	1200019
NP44	1216588
R3110	1225434
OL1	1236152
P37	1241276
L31W	1247470
EVER3	1253422
CY2	1263153
G3272	1277844
P35	1282598
NE5	1283899
DO1	1289801
EVER7	1302711
P38	1303175
E146	1307497
G3620	1307806
G3354	1311784
NP46	1315328
EVER5A	1317082
NP206	1321466
DO2	1323566
SP	1325287
TR	1331397
G3273	1348112
FROGP	1359074
CT50R	1361902
CY3	1367228
S18C	1381672
G1487	1383712
G3627	1391073
G211	1396603
G3353	1412227
NP67	1419864
P36	1422228

Station	Sum of (1 - corr) x distance to other stations
Humble	1443398
G3437	1448032
S178	1455201
S176	1462591
CV1NR	1467739
NE4	1473163
EVER6	1475060
G620	1497124
G3619	1501696
EPGW/SW	1502705
S177	1503541
TSB	1508452
P33	1524499
NCL	1527204
G613	1539976
CP	1543909
NR	1546047
CT27R	1558783
G3578	1559069
EP1R	1572219
NP203	1586586
NP202	1596060
Robblee	1634453
NP205	1644350
G596	1658541
G1074B	1667214
G3628	1672370
G3622	1676247
S331	1686744
TMC	1707124
OT	1723254
L31NMILE7	1756207
L31NMILE5	1762128
NMP	1768372
CN	1773026
S332	1800199
NP201	1806023
L31NMILE4	1819146
S197	1824422
G3576	1830686
G3577	1831027
P34	1863388
L31NMILE3	1864841
S333	1877699
EP9R	1884699
NP72	1892297
G618	1922872
HR	1943583
G69	1945925
NE3	1948970

Station	Sum of (1 - corr) x distance to other stations
L31NMILE1	1956640
CV5S	1967945
S336	1972808
G3626	2018169
NE1	2023703
S338	2043819
S334	2086359
BICYA10	2118940
S12D	2172086
S343A	2186344
S12C	2229157
S343B	2305672
G789	2321708
TE	2328458
S12B	2332145
MK	2353303
BR	2360282
LOOP1	2362182
BICYA9	2363285
NE2	2480474
S12A	2520399
LM	2546574
WW	2554167
GI	2583639
HC	2700434
LOOP2	2703631
LO	2733997
TC	2760702
LN	2786646
LB	2947738
DK	3011462
L67XW	3013952
BICYA11	3046416
GB	3141667
TB	3242510
BICYA8	3269613
LS	3310120
WE	3336732
BN	3353969
A13	3411582
WB	3541419
CW	3635455
SR	4045932
BK	4150298
G1502	4376213
BD	4486613
BARRON	4805319
WP	4858862
BS	7072901

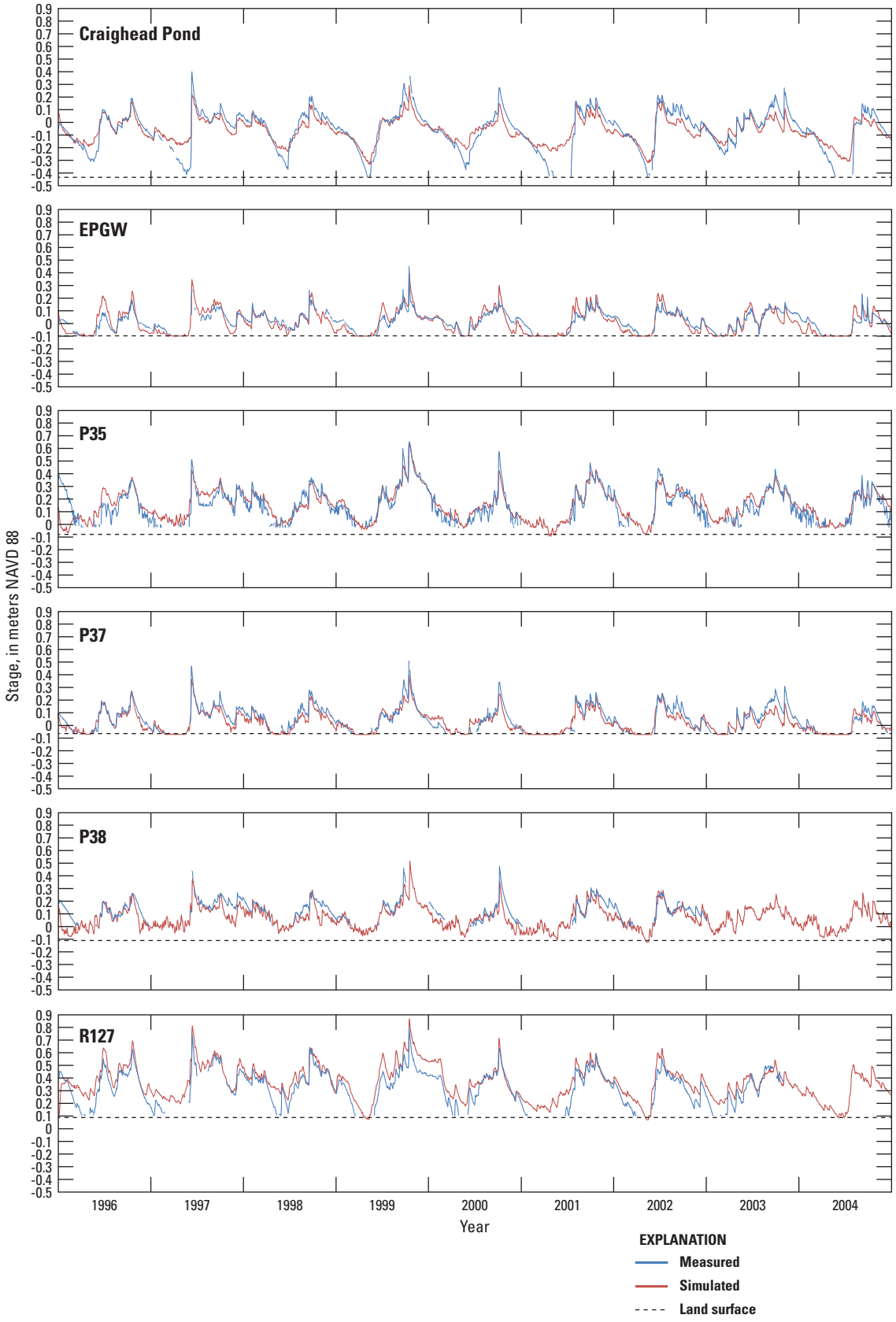

Figure 16. Comparisons between measured surface-water stage values and surface-water stage values simulated by the Biscayne and Southern Everglades Coastal Transport (BISECT) model for the south Florida peninsula, 1996–2004 (see app. 3 for station details).

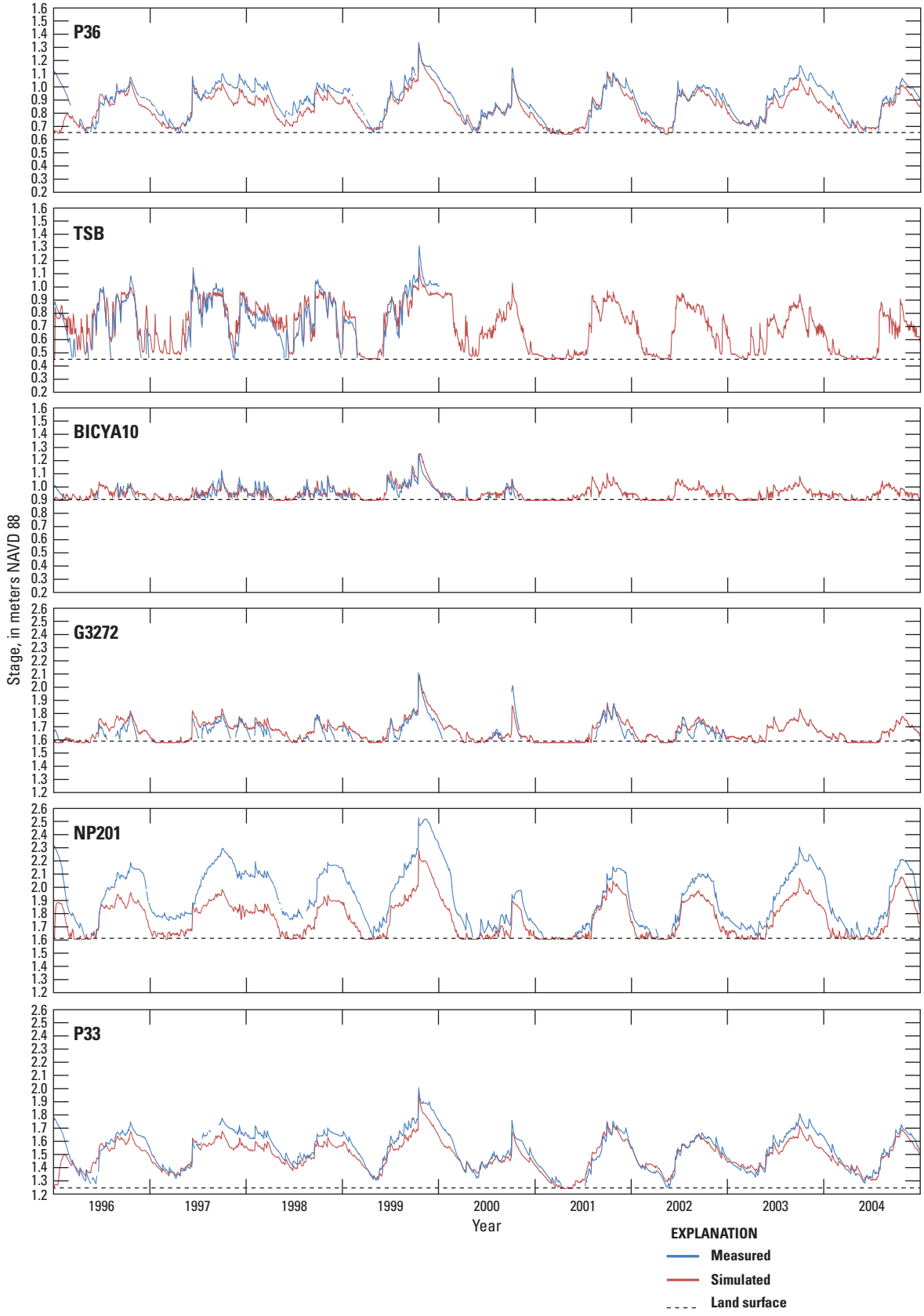

Figure 16. Comparisons between measured surface-water stage values and surface-water stage values simulated by the Biscayne and Southern Everglades Coastal Transport (BISECT) model for the south Florida peninsula, 1996–2004 (see app. 3 for station details).—Continued

Table 1–3. Surface-water stage statistics simulated by the Biscayne and Southern Everglades Coastal Transport (BISECT) model for the south Florida peninsula, 1996–2004.

[*PEV*, percent explained variance; *NS*, Nash-Sutcliffe coefficient; *RMSE*, root-mean square error; *ME*, mean error. See app. 3 for station details]

Location and parameter	*PEV*	*NS*	*RMSE* (meters)	*ME* (meters)
BICYA10 stage	0.230	0.055	0.176	0.076
Craighead Pond stage	0.674	0.673	0.101	0.006
EPGW stage	0.618	0.611	0.060	0.008
G3272 stage	0.566	0.188	0.126	0.086
NP-201 stage	0.741	0.184	0.193	-0.160
P33 stage	0.803	0.749	0.075	-0.035
P35 stage	0.757	0.689	0.093	0.043
P36 stage	0.777	0.707	0.079	-0.039
P37 stage	0.709	0.700	0.058	-0.010
P38 stage	0.579	0.562	0.071	-0.014
R127 stage	0.786	0.547	0.122	0.089
Taylor Slough Bridge stage	0.499	0.459	0.214	-0.058

the ET rates in coastal and nearshore areas are not well known, and the resulting temperatures and salinities are used as surrogate indicators of the latent heat flux and ET magnitudes. The underestimation of temperature, especially offshore, may indicate that latent heat values, and thus ET, are higher in the model than in the system. The need to reduce effective groundwater ET values based on salinity values (see section "Surface-Water Evaporation, Groundwater Evapotranspiration, and Heat Transport") further supports these conclusions.

A comparison of simulated surface-water wet-season temperatures on June 12, 1997, to dry-season temperatures on February 6, 2001, indicates that the average simulated temperature is higher in the modeled area in the wet season, but consistently for both seasons the nearshore coastal areas are cooler than farther offshore (fig. 1–34), reflecting the potential overestimation of ET discussed in the previous paragraph. High simulated temperatures near the canals in the wet season are caused by values estimated from air temperature. During summer months, air temperature is often higher than water temperature, so simulated boundary canal inflow temperatures may be too high.

Model Sensitivity

The BISECT model simulation was tested for sensitivity to eight principal input parameters. The parameters were chosen for their importance to the governing equations and their physical significance and are perturbed to a higher and lower value as described below.

1. Manning's *n*: The friction coefficient has a strong effect on surface-water flow and is varied 10 percent higher and lower to account for uncertainty in determining values. This adjustment affects the simulation of wetlands and coastal streams but not that of the canal network, which is computed separately.

2. Wind friction coefficient: The wind friction coefficient affects surface-water flow and is directly proportional to the frictional force of the wind on the water surface. The value is doubled and halved to determine the significance of wind forcing.

3. Tidal amplitude: Three amplitudes and frequencies are represented in the tidal boundaries, corresponding to the M2, K1, and O1 tidal components (Schureman, 1976). The amplitudes of these components were determined through spectral analysis of field time series data (Wang and others, 2007; Lohmann and others, 2012). The tidal fluctuations drive the hydrodynamic computation in the surface water, and uncertainty affects the semidiurnal inundation and constituent mixing. The amplitude of each tidal component is varied 10 percent higher and lower to examine the model sensitivity.

4. Transition-layer thickness: The thickness of the surface layer that provides the primary resistance to surface-water/groundwater leakage varies from 0.0001 m in drier areas to 0.05 m in wetlands with a substantial peat layer. To test the sensitivity of the model to the variations in transition-layer thickness, scenarios with spatially uniform thicknesses at the lowest and highest values (0.0001 m and 0.05 m, respectively) are simulated.

5. Canal conductance: The conductance of the canals, representing the connectivity of the canal to the aquifer, is highly uncertain because of lack of field information. These values are multiplied by 10 and 0.1 for the sensitivity analysis.

6. Aquifer horizontal conductivity: Aquifer properties in the BISECT model area have been investigated extensively in the development of the TIME and Biscayne models. Hydraulic conductivity sensitivities were previously tested for the TIME and Biscayne models, so for the purpose of the combined BISECT model, doubling and halving these values was considered sufficient for the sensitivity analysis.

7. Aquifer vertical conductivity: For reasons similar to those justifying sensitivity testing of horizontal conductivity, aquifer vertical conductivity values were doubled and halved for the sensitivity analysis.

8. Albedo: The value of albedo derived from measurements in the wetlands, 16.9 percent, was originally used for the entire TIME model area, inland and coastal (Swain and Decker, 2010). The spatial variation in the albedo of shallow and deep offshore waters used in BISECT is omitted in the sensitivity analysis, and the albedo value of 16.9 percent is applied uniformly across the model domain.

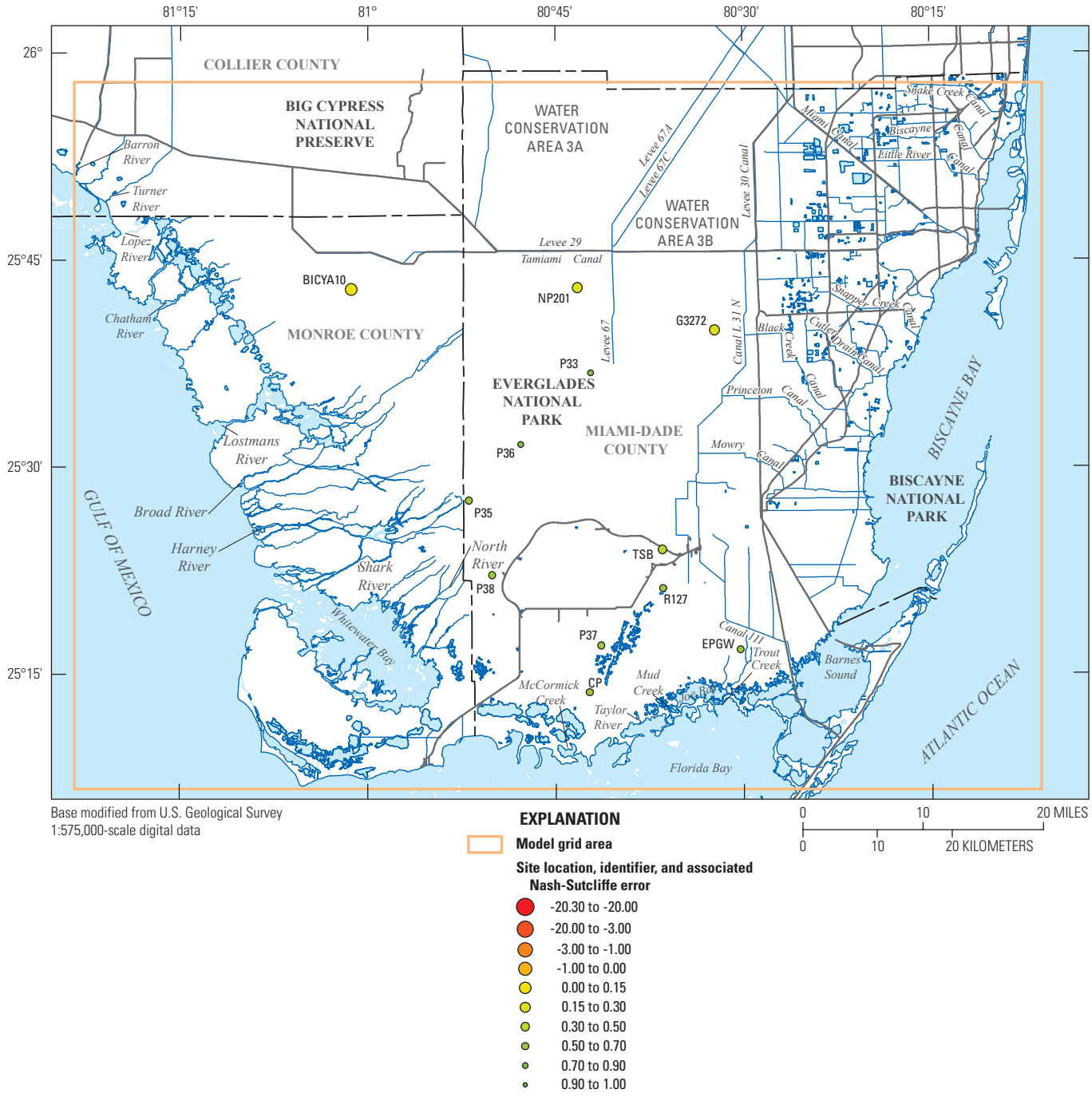

Figure 1-17. Surface-water Nash-Sutcliffe errors simulated by the Biscayne and Southern Everglades Coastal Transport (BISECT) model for stations in the south Florida peninsula, 1996–2004 (see app. 3 for station details).

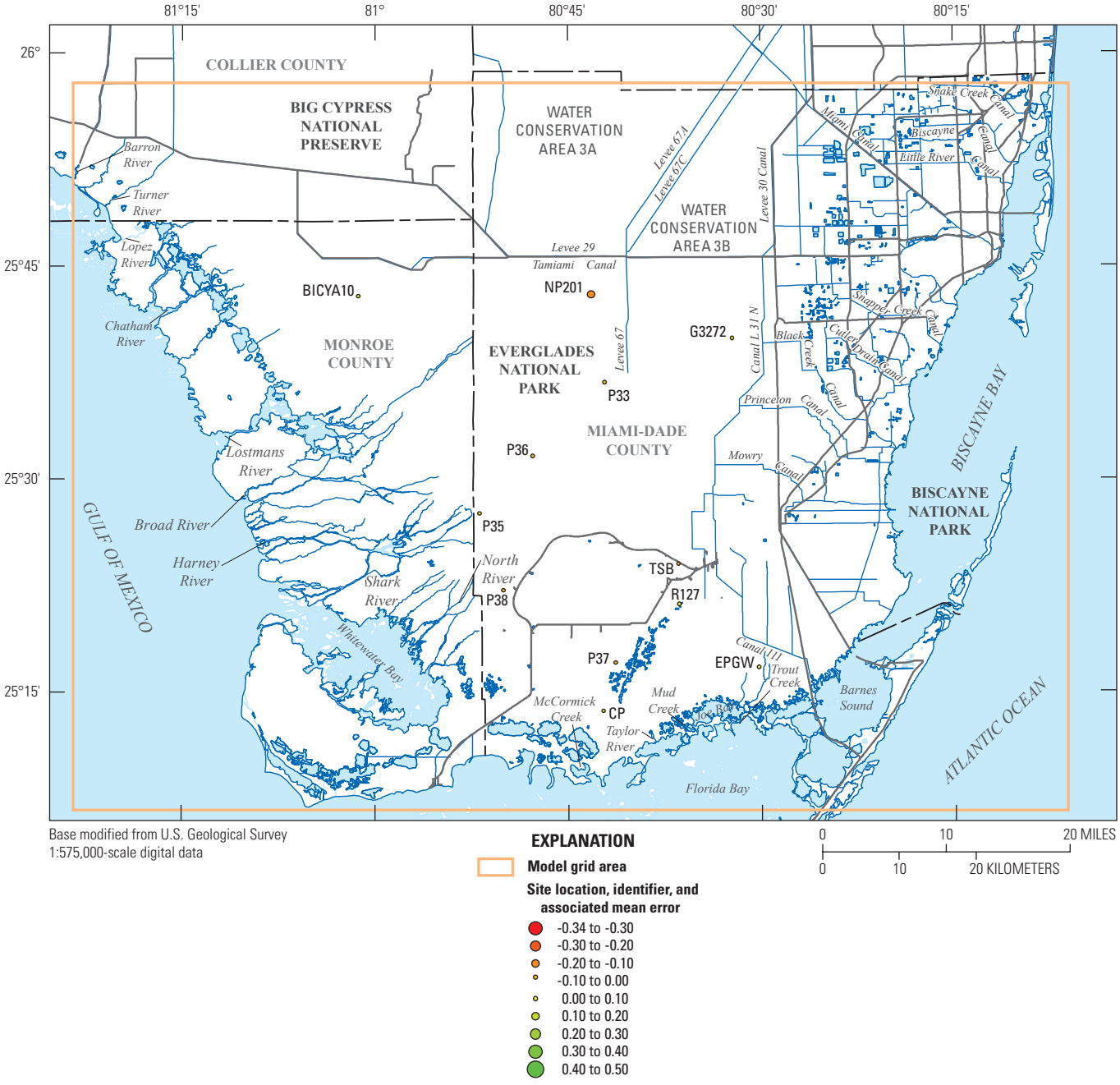

Figure 1-18. Surface-water mean errors simulated by the Biscayne and Southern Everglades Coastal Transport (BISECT) model for stations in the south Florida peninsula, 1996–2004 (see app. 3 for station details).

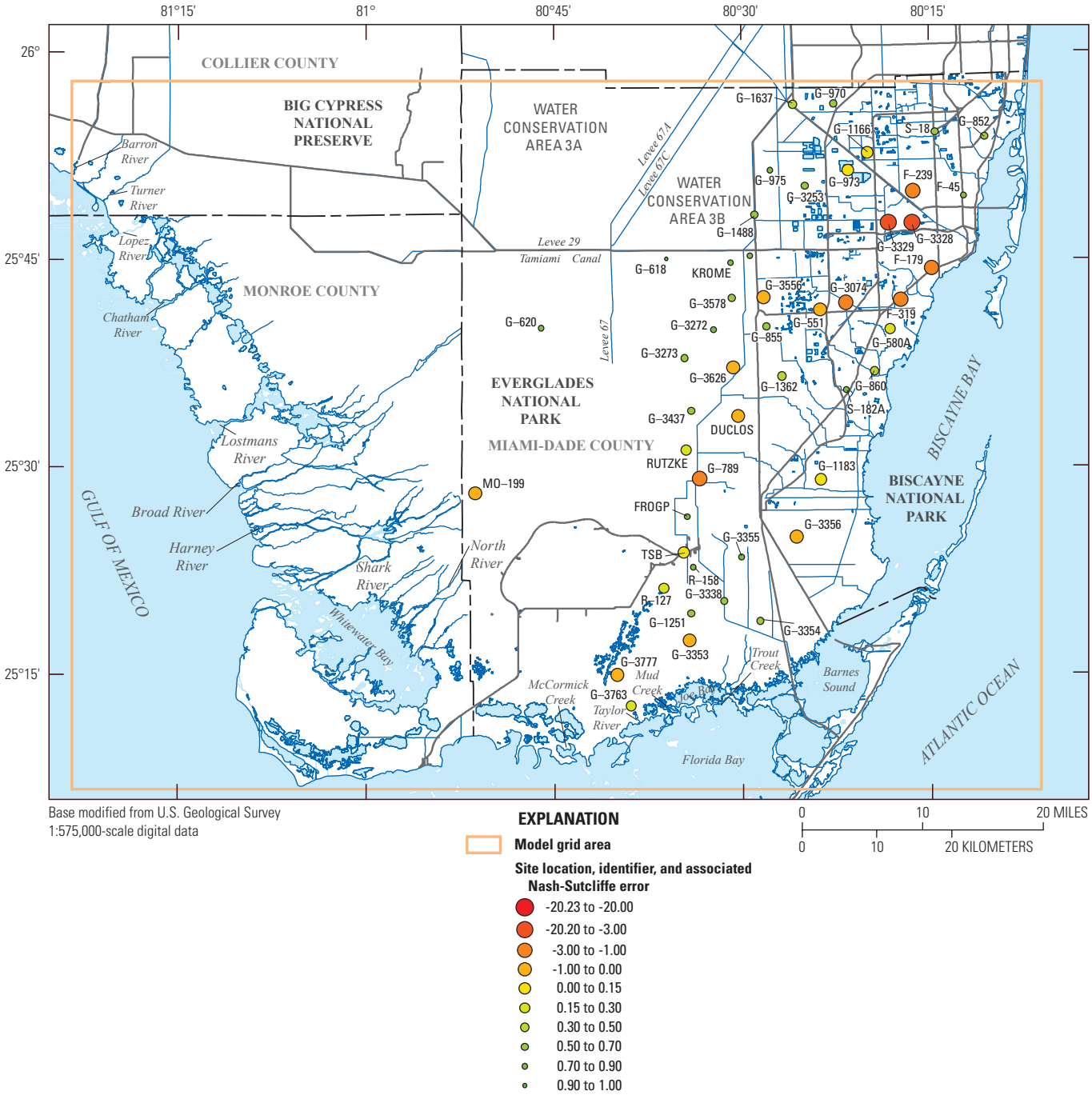

Figure 1-19. Locations of groundwater stations and associated Nash-Sutcliffe errors simulated by the Biscayne and Southern Everglades Coastal Transport (BISECT) model for the south Florida peninsula, 1996–2004 (see app. 3 for station details).

Table 1–4. Error statistics for groundwater heads simulated by the Biscayne and Southern Everglades Coastal Transport (BISECT) model for the south Florida peninsula, 1996–2004.

[*PEV*, percent explained variance; *NS*, Nash-Sutcliffe coefficient; *RMSE*, root-mean square error; *ME*, mean error. See app. 3 for station details]

Groundwater station name	*PEV*	*NS*	*RMSE* (meters)	*ME* (meters)
DUCLOS	0.890	-0.376	0.256	0.245
F-179	0.701	-1.424	0.305	0.285
F-239	0.783	-1.164	0.414	0.393
F-319	0.418	-1.981	0.224	0.201
F-45	0.730	0.703	0.122	0.037
FROGP	0.781	0.707	0.141	0.071
G-1166	0.632	0.109	0.128	0.098
G-1183	0.605	0.117	0.135	0.100
G-1251	0.790	0.624	0.098	0.065
G-1362	0.876	0.424	0.166	0.147
G-1488	0.878	0.515	0.137	-0.118
G-1637	0.870	0.332	0.164	0.147
G-3074	0.242	-1.192	0.554	0.448
G-3253	0.748	0.686	0.309	-0.137
G-3272	0.702	0.701	0.131	-0.008
G-3273	0.745	0.594	0.151	0.092
G-3328	-1.245	-18.059	0.488	0.458
G-3329	-0.333	-3.123	0.311	0.256
G-3338	0.968	0.637	0.098	-0.093
G-3353	0.780	-0.527	0.128	0.118
G-3354	0.890	0.543	0.102	0.089
G-3355	0.753	0.727	0.098	0.030
G-3356	0.718	-0.203	0.180	0.157
G-3437	0.701	0.633	0.171	0.073
G-3556	0.797	-0.116	0.231	0.209
G-3576	0.841	0.737	0.096	-0.061
G-3578	0.819	0.694	0.111	-0.071
G-3619	0.871	0.730	0.080	0.058
G-3626	0.811	-0.360	0.195	0.181
G-3763	0.177	0.174	0.354	-0.020
G-3777	0.203	-0.081	0.747	0.382
G-551	0.463	-0.898	0.587	0.497
G-580A	0.792	0.183	0.141	0.122
G-618	0.934	0.908	0.041	0.022
G-620	0.740	0.737	0.108	-0.013
G-789	0.751	-1.536	0.337	0.320
G-852	0.509	0.508	0.134	-0.003
G-855	0.839	0.632	0.136	0.102
G-860	0.411	0.386	0.109	0.022
G-970	0.733	0.678	0.080	0.033
G-973	0.226	0.143	0.161	0.050
G-975	0.891	0.891	0.075	-0.005
KROME	0.934	0.863	0.066	-0.048
MO-199	-0.003	-0.570	0.569	-0.342
R-127	0.762	0.252	0.165	0.136
R-158	0.771	0.145	0.217	0.185
RUTZKE	0.663	0.277	0.264	0.193
S-18	0.535	0.535	0.092	-0.002
S-182A	0.804	0.799	0.070	-0.011

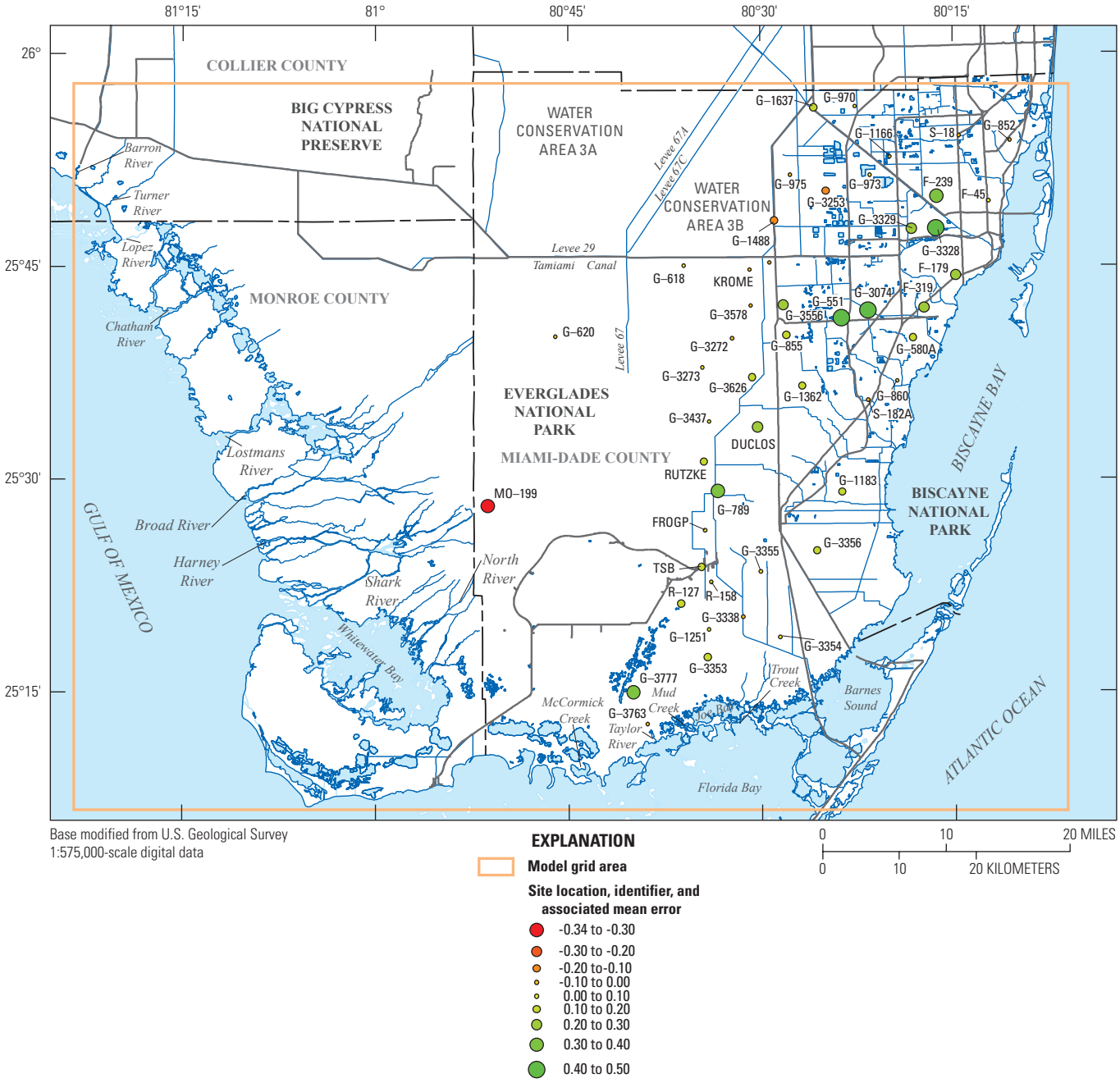

Figure 1-20. Locations of groundwater stations and associated mean errors simulated by the Biscayne and Southern Everglades Coastal Transport (BISECT) model for the south Florida peninsula, 1996–2004 (see app. 3 for station details).

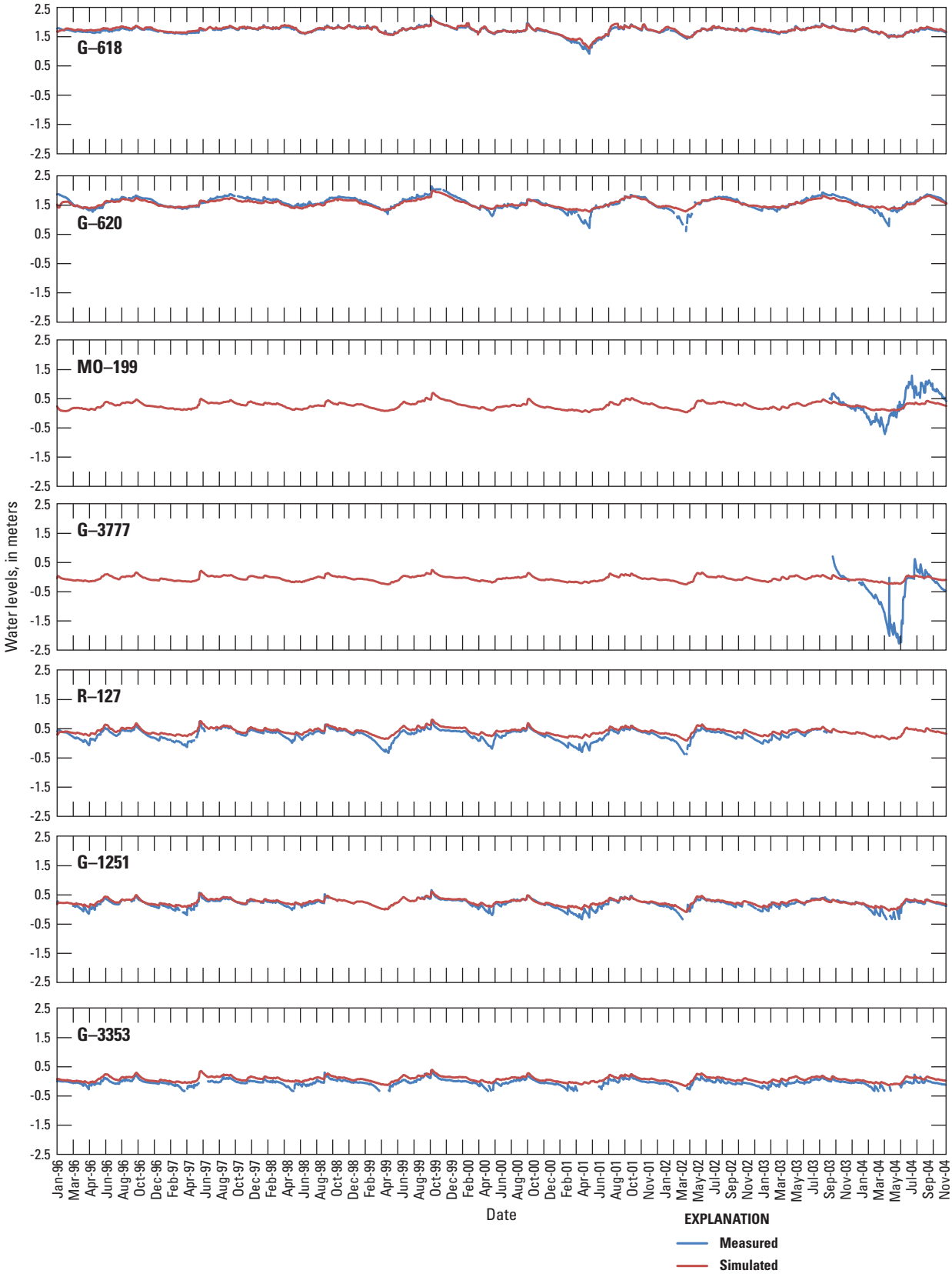

Figure 1-21. Measured and simulated groundwater levels from the Biscayne and Southern Everglades Coastal Transport (BISECT) model for selected stations in Everglades National Park, 1996–2004 (see app. 3 for station details).

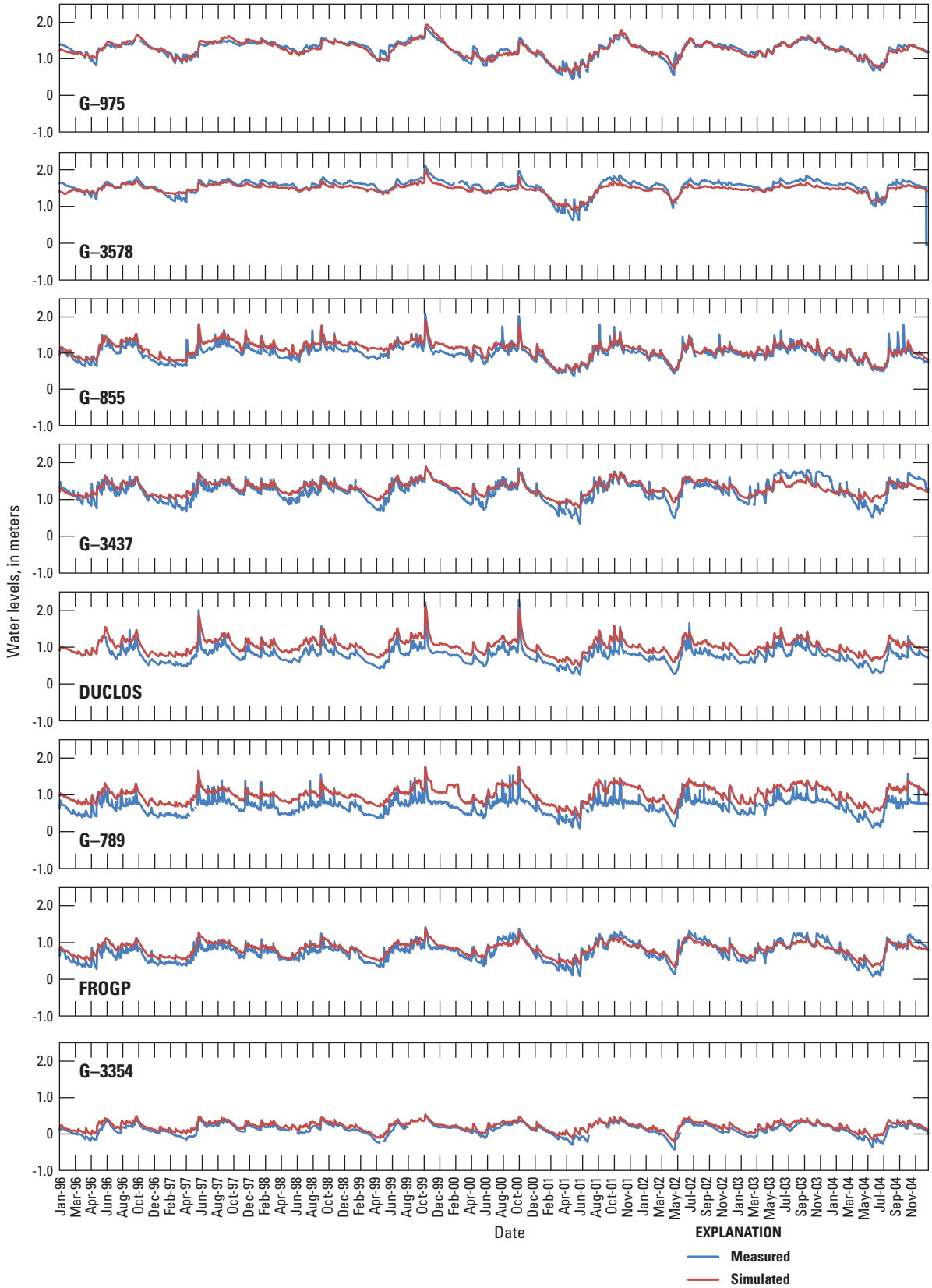

Figure 1-22. Measured and simulated groundwater levels from the Biscayne and Southern Everglades Coastal Transport (BISECT) model for selected stations along the Canal L 30 and Canal L 31 N/Canal 111 systems, 1996–2004 (see app. 3 for station details).

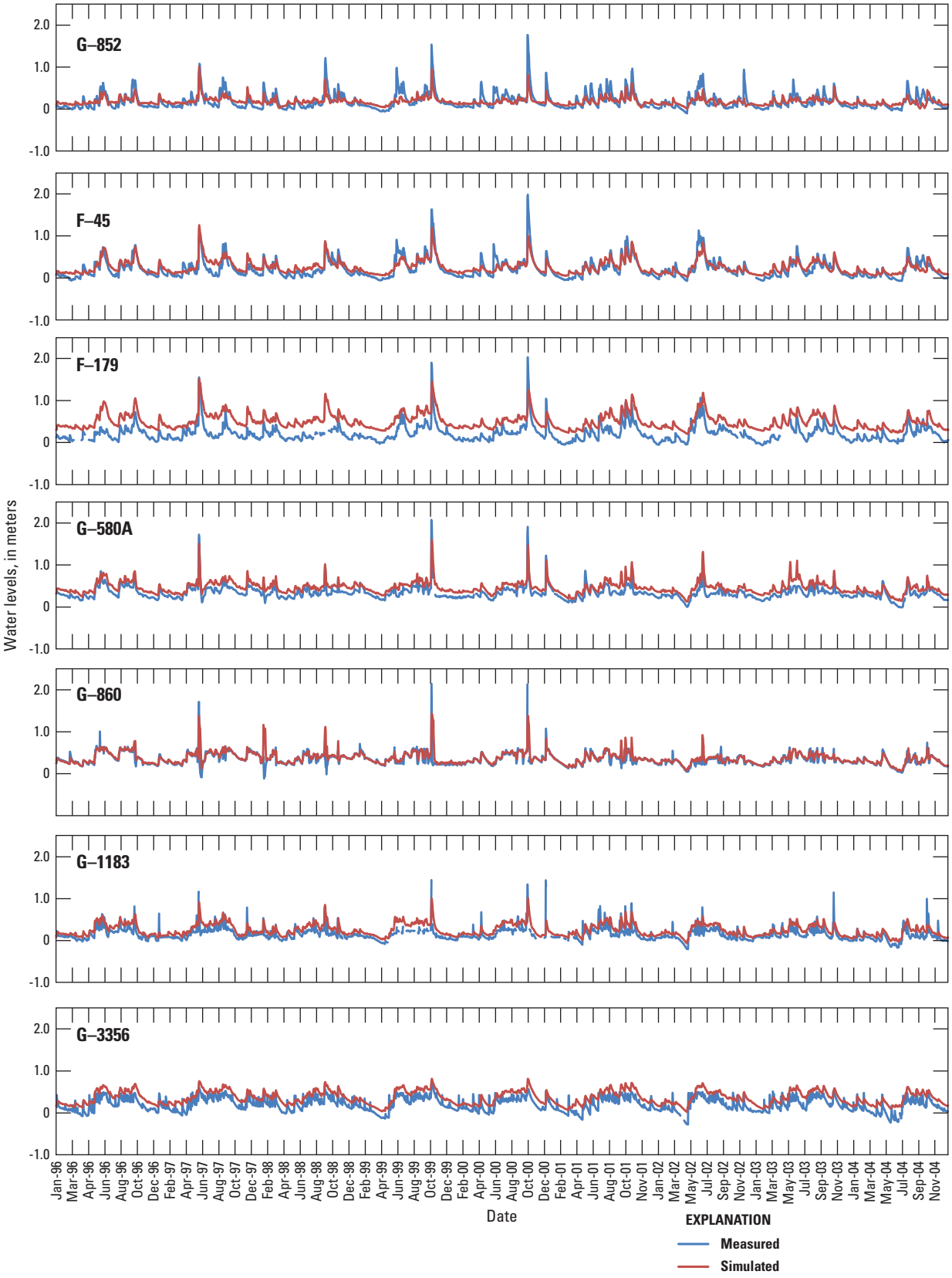

Figure 1-23. Measured and simulated groundwater levels from the Biscayne and Southern Everglades Coastal Transport (BISECT) model for selected stations along the east coast of Miami-Dade County, Florida, 1996–2004 (see app. 3 for station details).

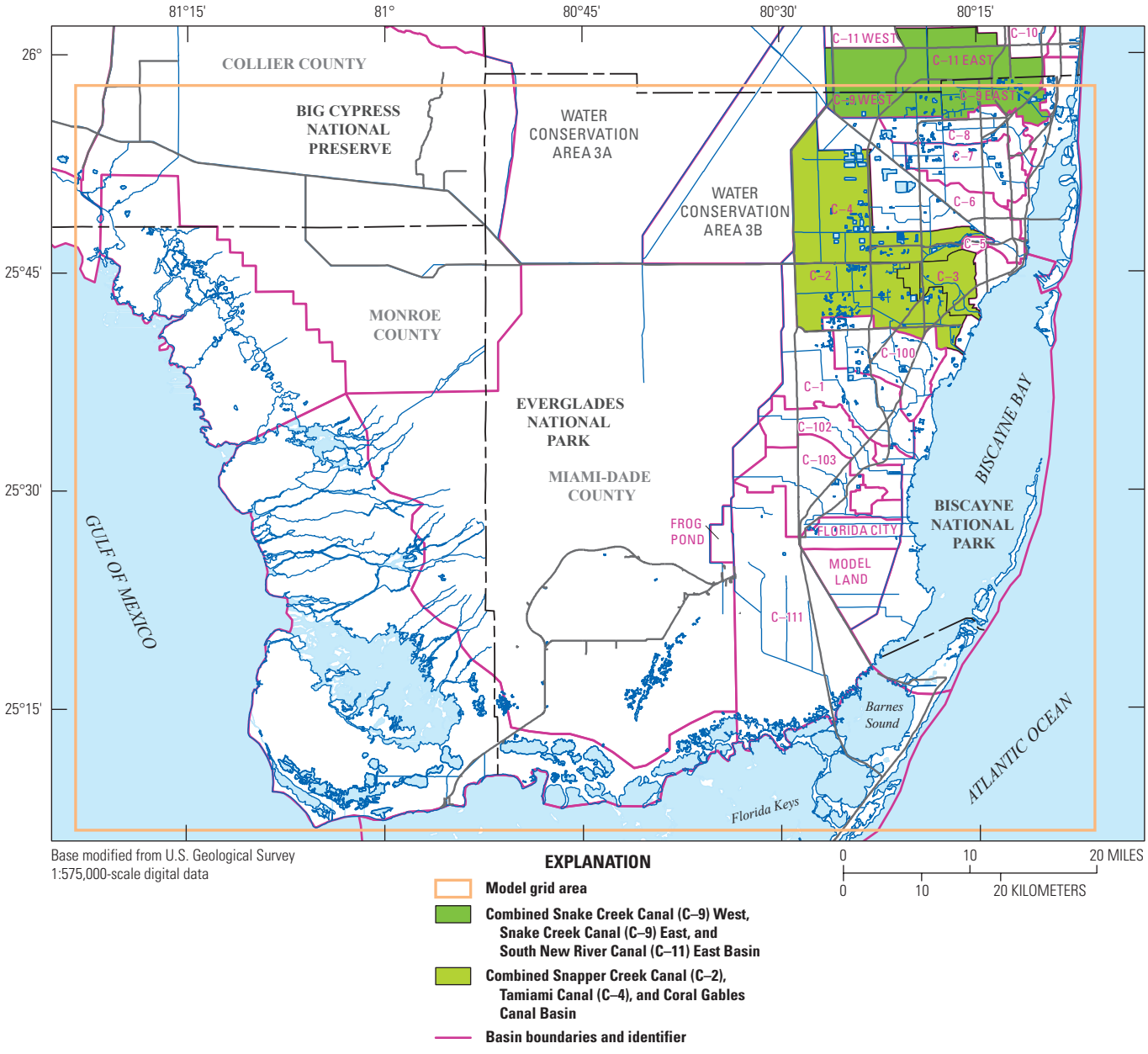

Figure 1-24. Combined canal/groundwater leakage basins in Miami-Dade County, Florida.

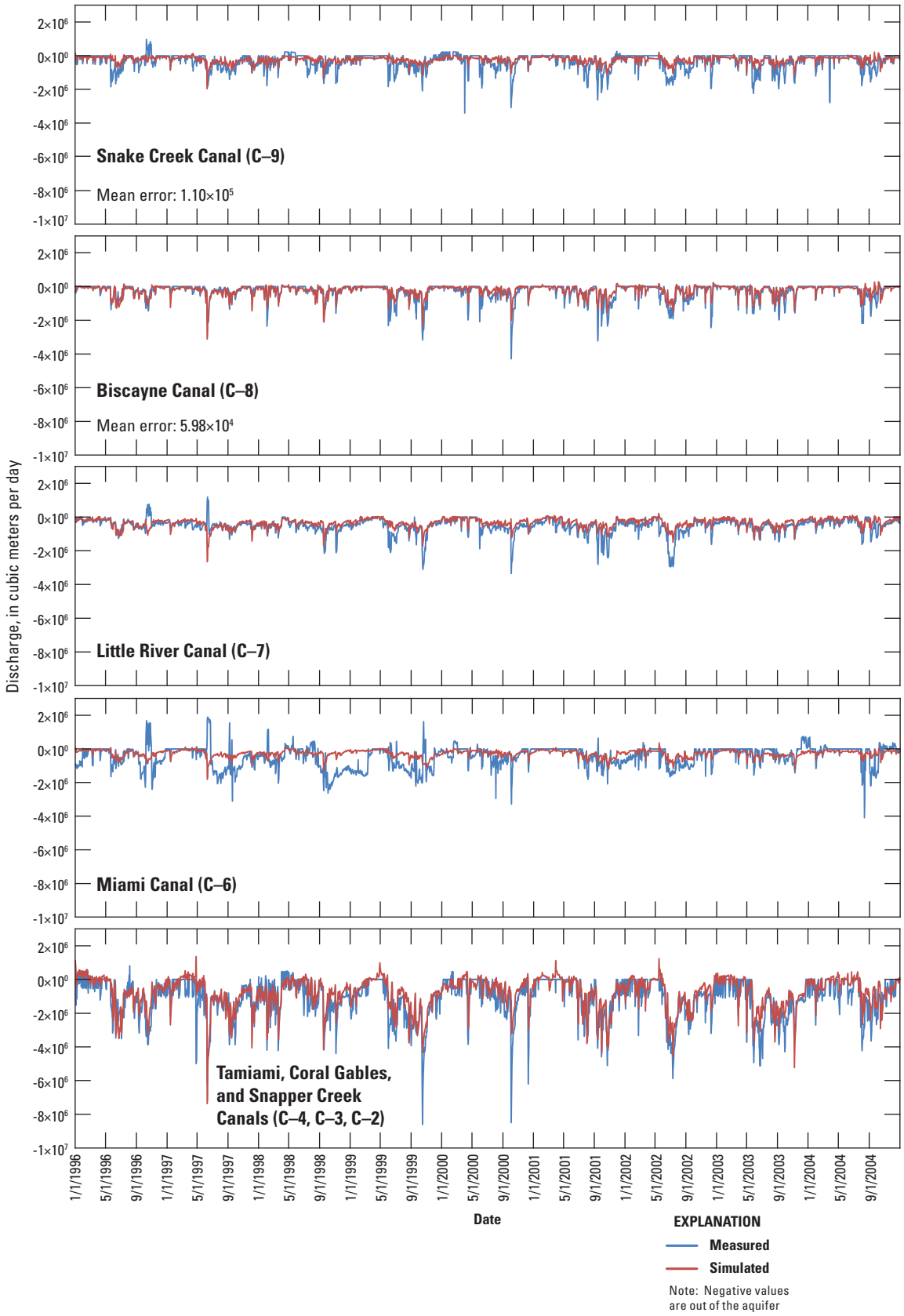

Figure 1-25. Simulated and measured daily canal/aquifer from the Biscayne and Southern Everglades Coastal Transport (BISECT) model in selected drainage basins in Miami-Dade County, Florida, 1996–2004 (see app. 3 for station details).

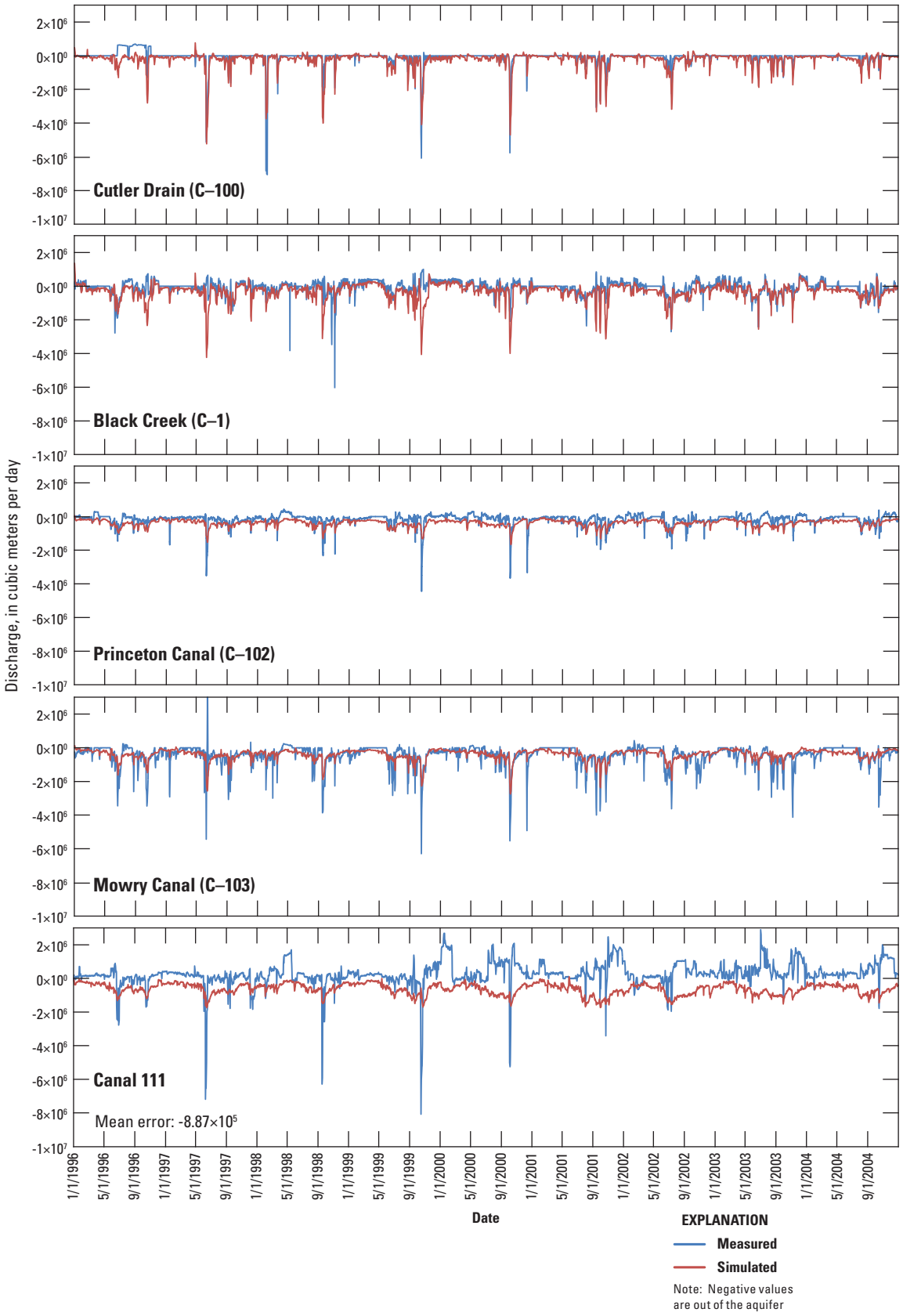

Figure 1-25. Simulated and measured daily canal/aquifer from the Biscayne and Southern Everglades Coastal Transport (BISECT) model in selected drainage basins in Miami-Dade County, Florida, 1996–2004 (see app. 3 for station details).

Table 1–5. Error statistics for simulated and estimated canal/aquifer exchanges simulated by the Biscayne and Southern Everglades Coastal Transport (BISECT) model for the south Florida peninsula, 1996–2004.

[*PEV*, percent explained variance; *NS*, Nash-Sutcliffe coefficient; *RMSE*, root-mean square error; m^3/s, cubic meter per second; *ME*, mean error]

Basin name (canal name)	*PEV*	*NS*	*RMSE* (m^3/s)	*ME* (m^3/s)
C-9 (Snake Creek Canal)	0.429	0.372	3.65×10^5	1.10×10^5
C-8 (Biscayne Canal)	0.702	0.685	2.60×10^5	5.98×10^4
C-7 (Little River Canal)	0.412	0.258	3.77×10^5	1.72×10^5
C-6 (Miami Canal)	0.126	0.025	6.15×10^5	1.98×10^5
C-4, C-3, C-2 (Tamiami, Coral Gables, and Snapper Creek Canals)	0.734	0.660	6.64×10^5	3.10×10^5
C-100 (Cutler Drain Canal)	0.558	0.467	3.62×10^5	-1.50×10^5
C-1 (Black Creek Canal)	-0.263	-0.564	5.21×10^5	-2.29×10^5
C-102 (Princeton Canal)	0.439	0.073	3.31×10^5	-2.08×10^5
C-103 (Mowry Canal)	0.409	0.400	4.80×10^5	5.74×10^4
Canal 111	-0.103	-1.485	1.19×10^6	-8.87×10^5

Model sensitivity is evaluated by comparing the base-case simulation results to the perturbed simulation results. Differences in cumulative coastal streamflows are computed as a percentage of cumulative flow at each individual stream rather than as a percentage of the total coastal flow (table 1–8).

For the parameter ranges tested, the simulated streamflows differ the most between base-case and perturbed simulation results when the Manning's *n* and tidal amplitude values are perturbed (table 1–8), indicating the highest sensitivities. At 9 of the 11 simulated streams, increasing Manning's *n* friction values reduces flow, and decreasing Manning's *n* increases flow, as might be expected. However, McCormick Creek and Long Sound exhibit the opposite behavior, indicating that the simulated flow at these locations may be controlled more by surpluses and deficits of volumes through all of the other coastal outflows rather than the local frictional resistance. This behavior is likely because McCormick Creek and Long Sound are simulated as less hydraulically connected to topographically low wetlands compared to the other nine coastal streams.

At 10 of the 11 coastal streams, a higher tidal amplitude results in larger total flows and a smaller amplitude results in lower total flows, even though the average tidal levels are similar (table 1–8). As a higher tidal amplitude results in greater tidal extremes, the lower low tide must increase water drainage offshore to a higher degree than the equivalent higher high tide pushes water inland. This behavior is consistent with the fact that the offshore area has much more storage capacity than do the inland wetlands. However, Long Sound simulated flows respond in an opposite fashion to tidal amplitude changes. Considering that Long Sound flows did not follow the same behavior as most of the coastal streams in the Manning's *n* sensitivity analysis either, it is reasonable to attribute Long Sound's uniqueness in part to its relative lack of simulated hydraulic connection to the wetland system that drives other coastal streamflows. In addition, the offshore waters at Long Sound are more shielded from the open-ocean tide than are those at the other coastal streams (fig. 1–1), which would likely reduce its simulated sensitivity to tidal amplitude perturbations.

All coastal streams in the model exhibit less cumulative flow when simulated wind friction is increased (table 1–8). When wind effects are decreased, the streams along the Whitewater Bay and Florida Bay coast (Shark River, North River, McCormick Creek, Taylor River, Mud Creek, and Trout Creek) have increased flow, and streams along the Gulf of Mexico coast (Lostmans, Broad, Chatham, and Harney Rivers) have reduced flow. Long Sound flow is the only exception to this pattern. In addition, streams along the Whitewater Bay and Florida Bay coast tend to exhibit larger magnitude simulated responses to wind effects than do streams along the Gulf of Mexico coast. These patterns indicate that (1) simulated wind forcing is less of a factor along the Gulf of Mexico coast, where diurnal tide is higher in magnitude, and (2) the most important effect of wind is to retard the net streamflow out to tide. It was shown in the earliest application of FTLOADDS (Swain and others, 2004) that reversals of flow (inland direction) at Trout Creek were completely wind driven, as appears to be the case for most of the streams along the Whitewater Bay and Florida Bay coast. Along the Gulf of Mexico coast, the lunar tide is larger than in Whitewater Bay and Florida Bay and is the dominant factor over wind in controlling streamflow.

Setting the transition-layer thickness to 0.05 m increases flow at all coastal streams, and a transition-layer thickness of 0.0001 m decreases flow at all streams. The areas that have the thinner transition-layer thickness in the base-case simulation are in the eastern urban part of the modeled area, indicating that some of the water that infiltrates and is lost in this area would flow to the Everglades coastal streams if urban infiltration was reduced, as could be the case with changes in water management and runoff volumes.

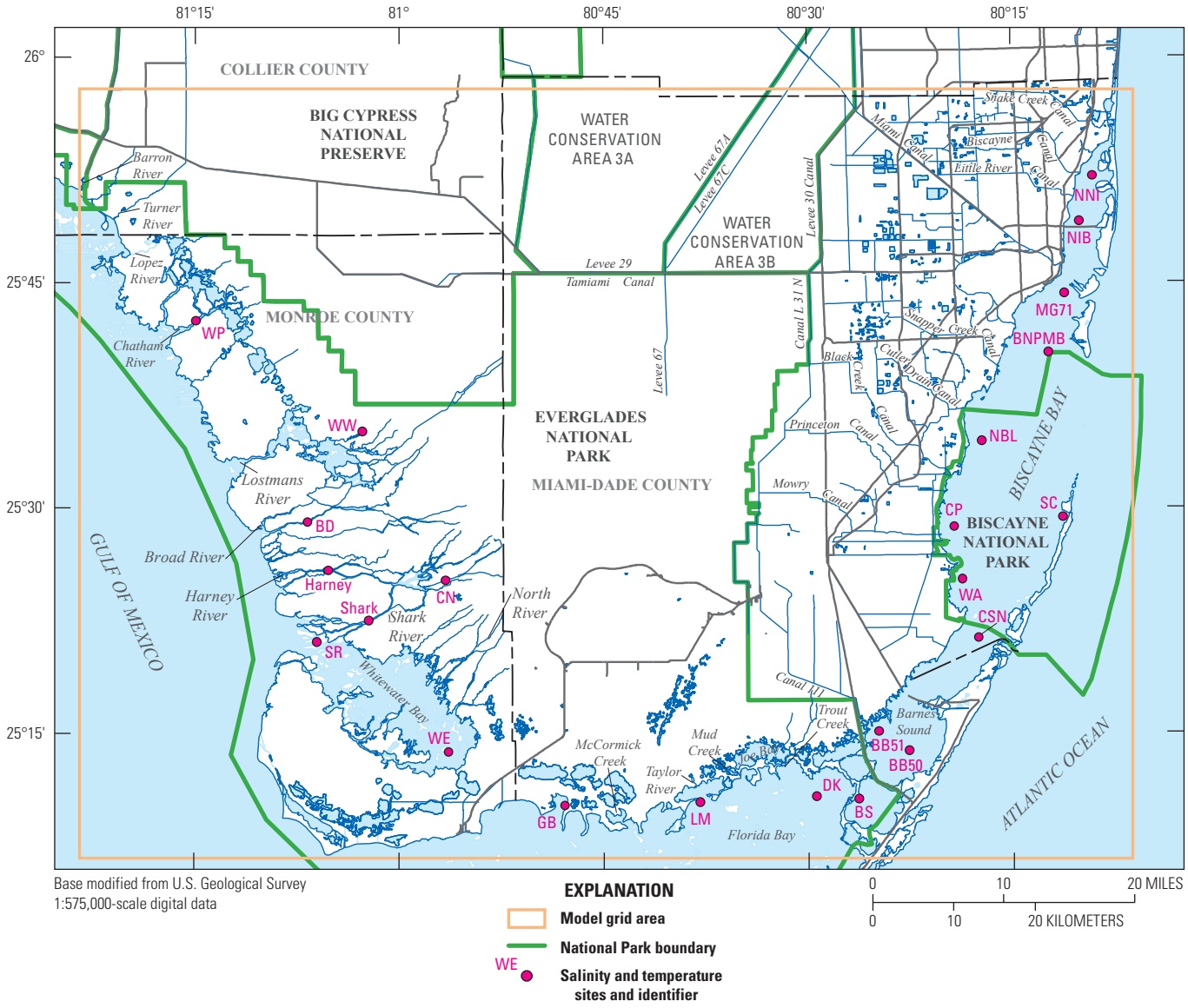

Figure 1-26. Locations of selected surface-water salinity and temperature sites in the Biscayne and Southern Everglades Coastal Transport (BISECT) model area in the south Florida peninsula (see app. 3 for station details).

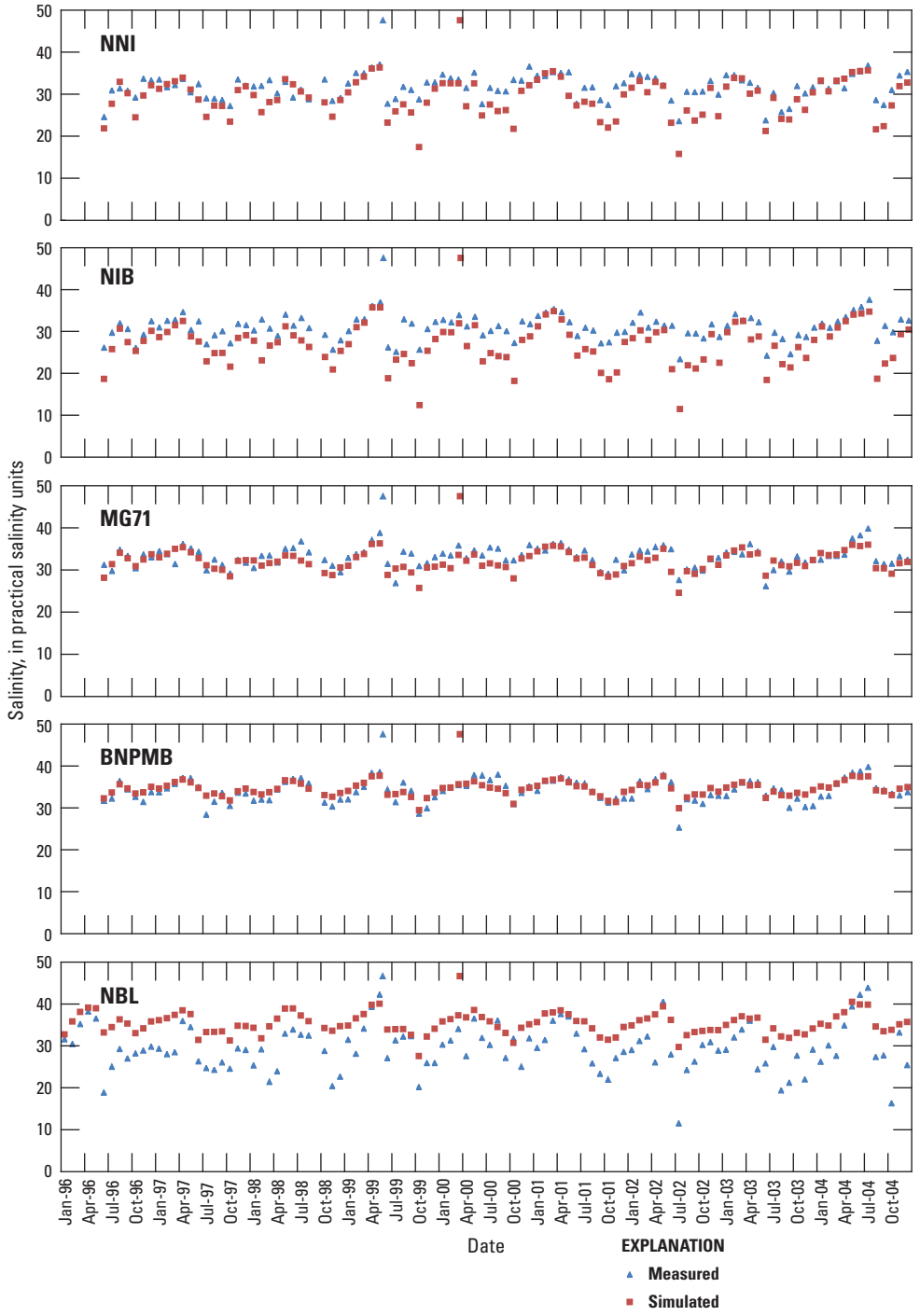

Figure 1-27. Simulated and vertically averaged surface-water salinity measured monthly in Biscayne Bay, south Florida peninsula, 1996–2004 (see app. 3 for station details).

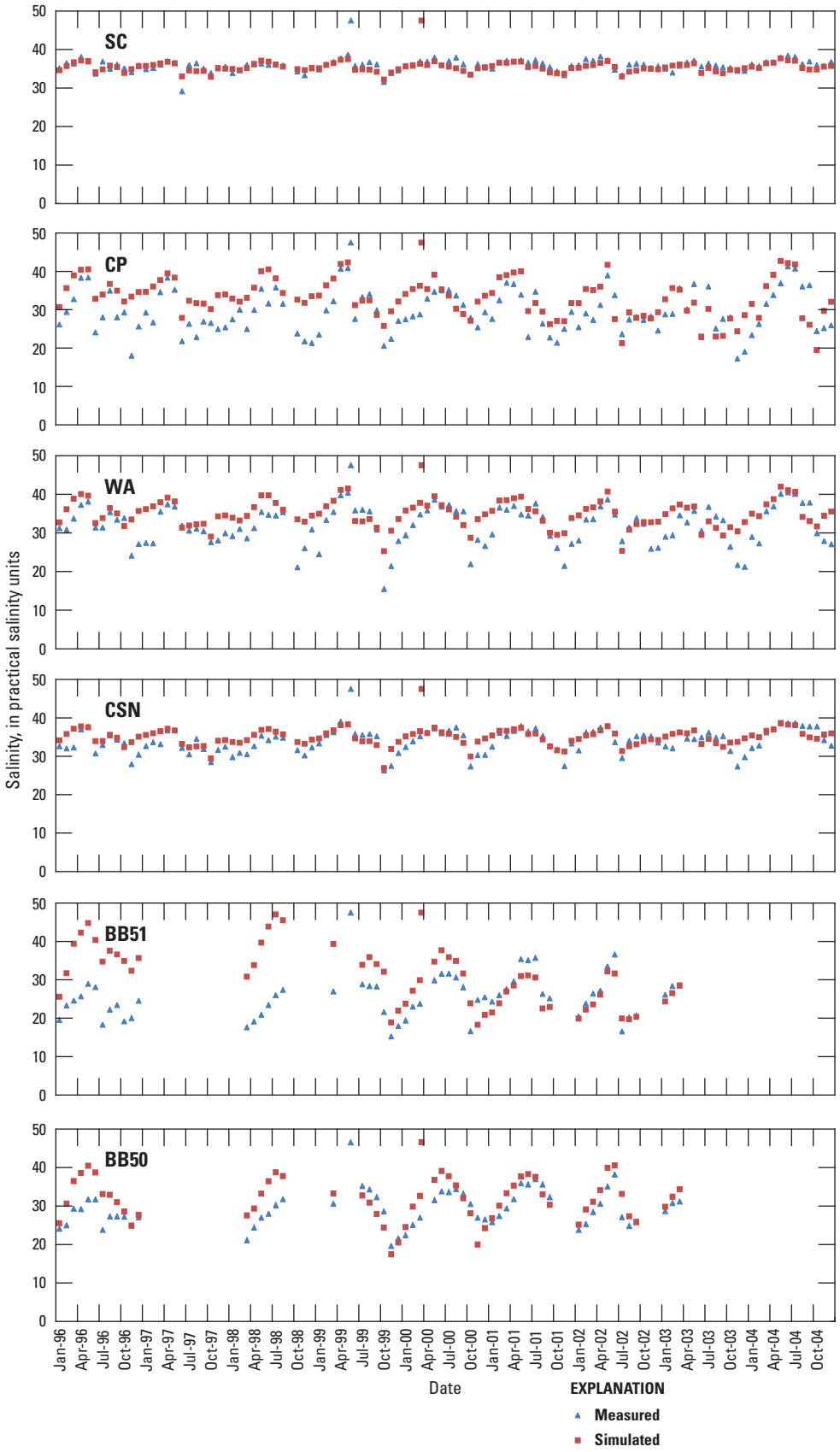

Figure 1-27. Simulated and vertically averaged surface-water salinity measured monthly in Biscayne Bay, south Florida peninsula, 1996–2004 (see app. 3 for station details).—Continued

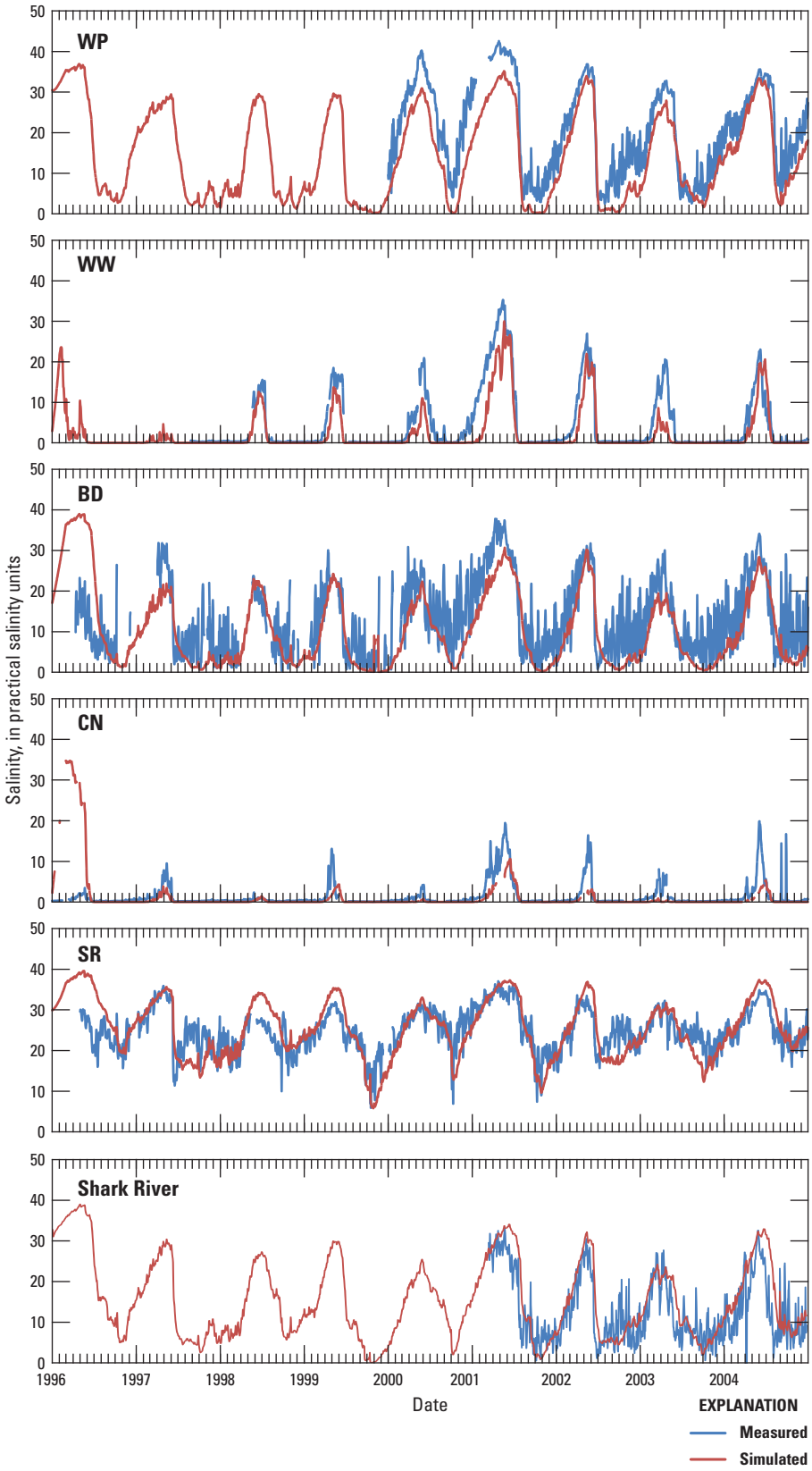

Figure 1-28. Simulated and measured daily surface-water salinity in Everglades National Park, south Florida peninsula, 1996–2004 (see app. 3 for station details).

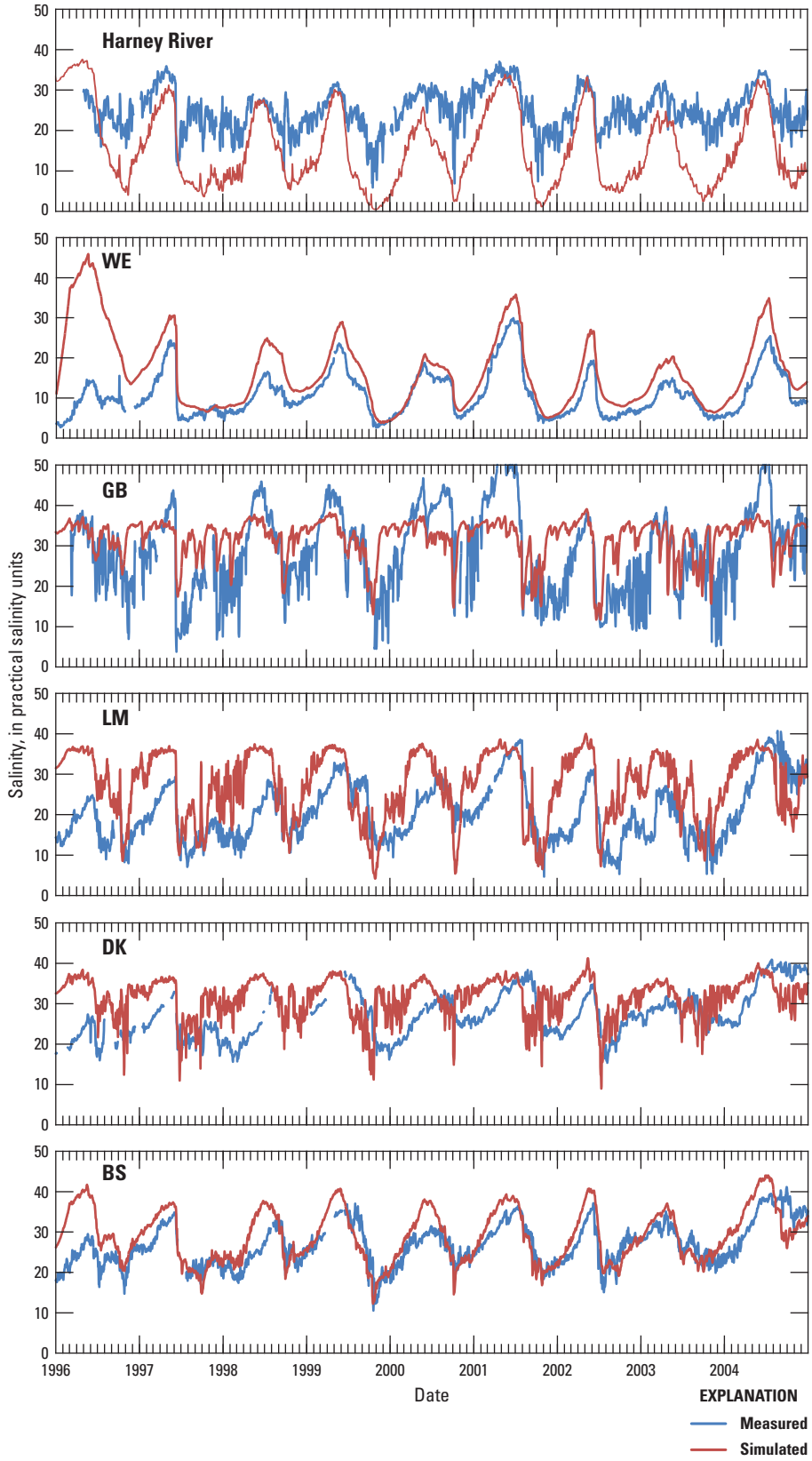

Figure 1-28. Simulated and measured daily surface-water salinity in Everglades National Park, south Florida peninsula, 1996–2004 (see app. 3 for station details).—Continued

Table 1–6. Error statistics for surface-water salinity simulated by the Biscayne and Southern Everglades Coastal Transport (BISECT) model for the south Florida peninsula, 1996–2004.

[*PEV*, percent explained variance; *NS*, Nash-Sutcliffe coefficient; *RMSE*, root-mean square error; PSU, practical salinity units; *ME*, mean error. See app. 3 for station details]

Salinity station name	*PEV*	*NS*	*RMSE* (PSU)	*ME* (PSU)
NNI	0.168	-0.700	3.682	-2.631
NIB	0.028	-2.159	4.952	-4.121
MG71	0.479	0.246	2.088	-1.161
BNPMB	0.681	0.662	1.497	0.353
NBL	0.468	-0.627	6.991	5.733
SC	0.535	0.422	1.063	-0.470
CP	0.348	-0.075	5.619	3.524
WA	0.445	0.085	4.777	2.996
CSN	0.504	0.399	2.266	0.948
BB51	-1.277	-2.401	9.356	5.378
BB50	0.245	-0.105	4.490	2.526
WP	0.893	0.622	6.829	-5.782
WW	0.777	0.704	4.081	-2.020
BD	0.374	0.252	7.763	-3.141
CN	-1.281	-1.320	4.454	-0.574
SR	0.220	0.219	4.522	0.193
WE	-0.361	-1.366	8.763	5.710
GB	0.219	0.134	9.726	3.049
LM	-0.216	-1.077	10.561	6.801
DK	-0.277	-0.858	7.752	4.334
BS	0.319	0.129	4.958	2.316
Harney River	0.308	0.277	6.108	1.257
Shark River	0.620	0.547	5.489	2.211

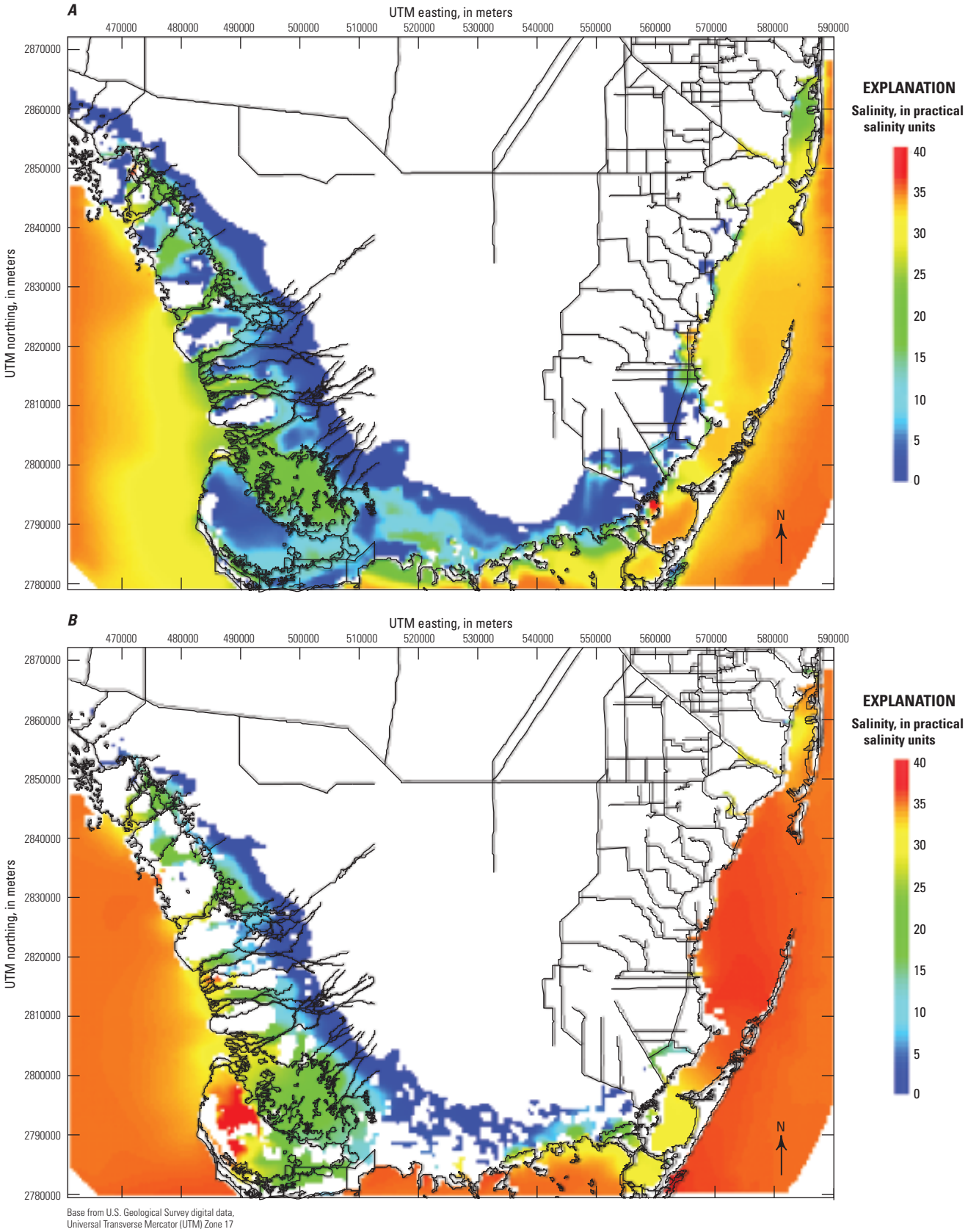

Figure 1-29. Simulated distribution of surface-water salinity for *A*, wet season (June 12, 1997) and *B*, dry season (February 6, 2001).

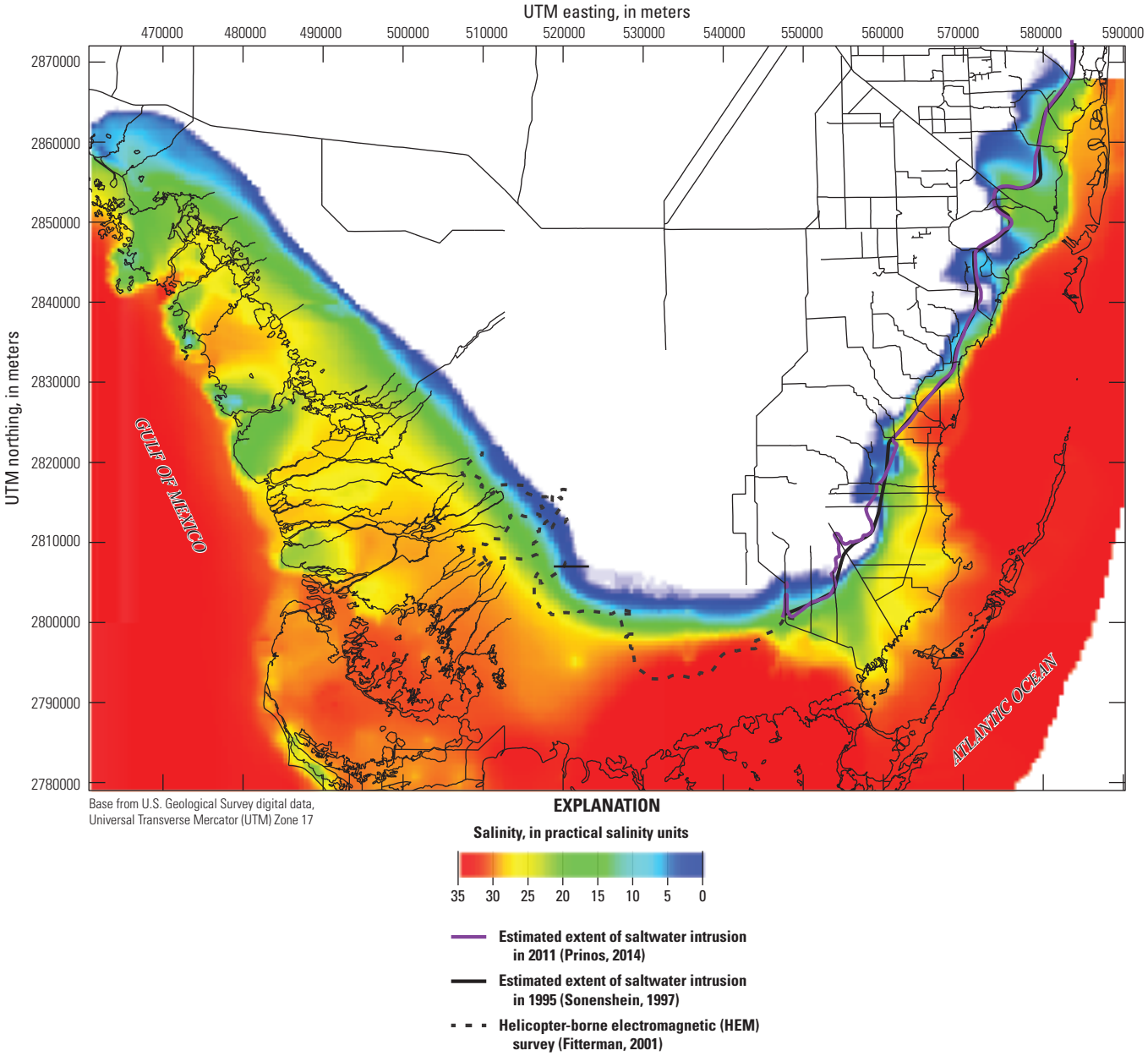

Figure 1-30. Simulated distribution of groundwater salinity at the bottom of modeled layer 12 of the Biscayne and Southern Everglades Coastal Transport (BISECT) model for the south Florida peninsula, 2004; this corresponds to the base of the Biscayne aquifer in the eastern portion of the model and to approximately 24 meters down into the gray limestone aquifer to the west.

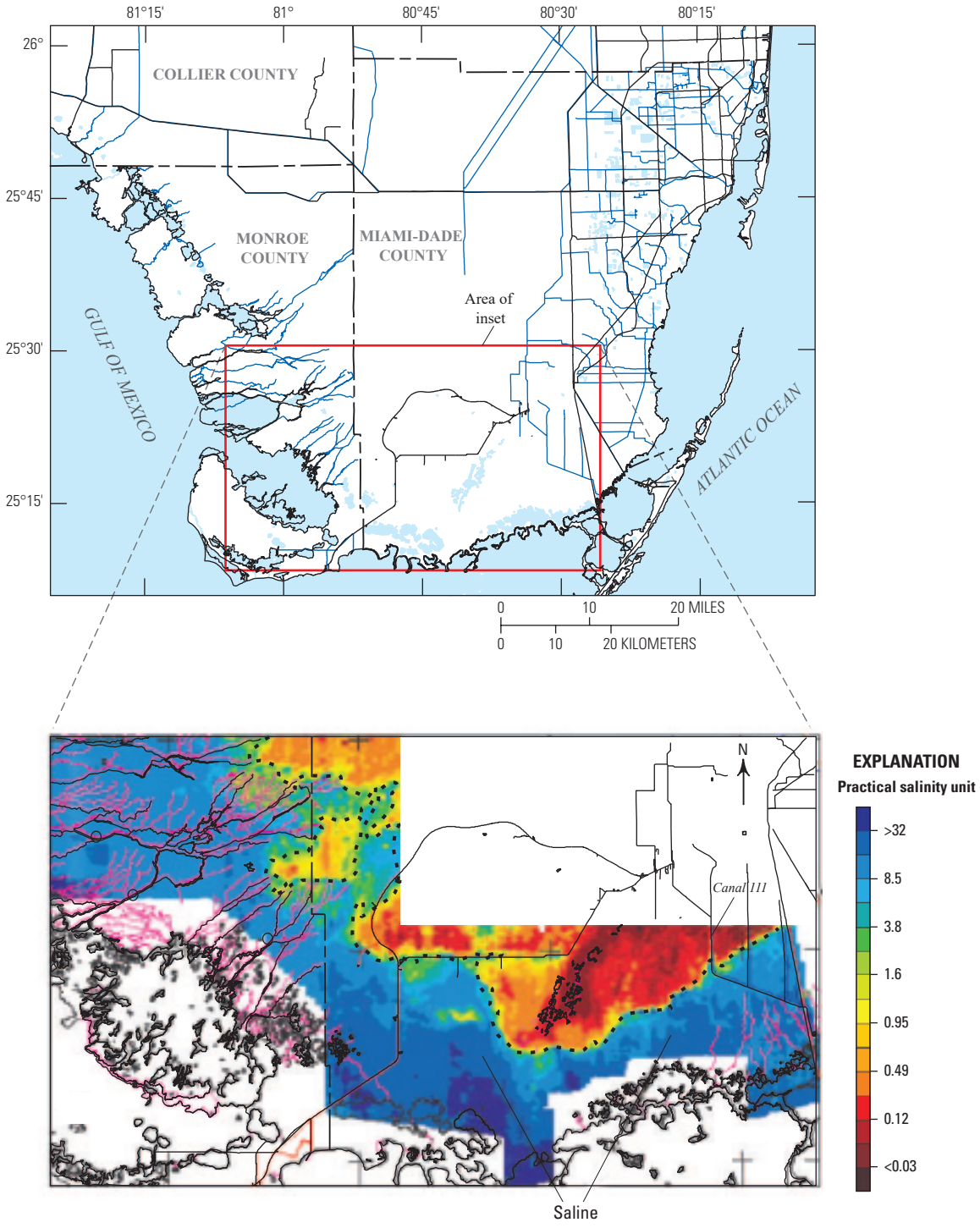

Figure 1-31. Helicopter-borne electromagnetic (HEM) salinity survey of Everglades National Park (modified from Fitterman and Deszcz-Pan, 2001). The dashed line represents salinity of approximately 2 practical salinity units.

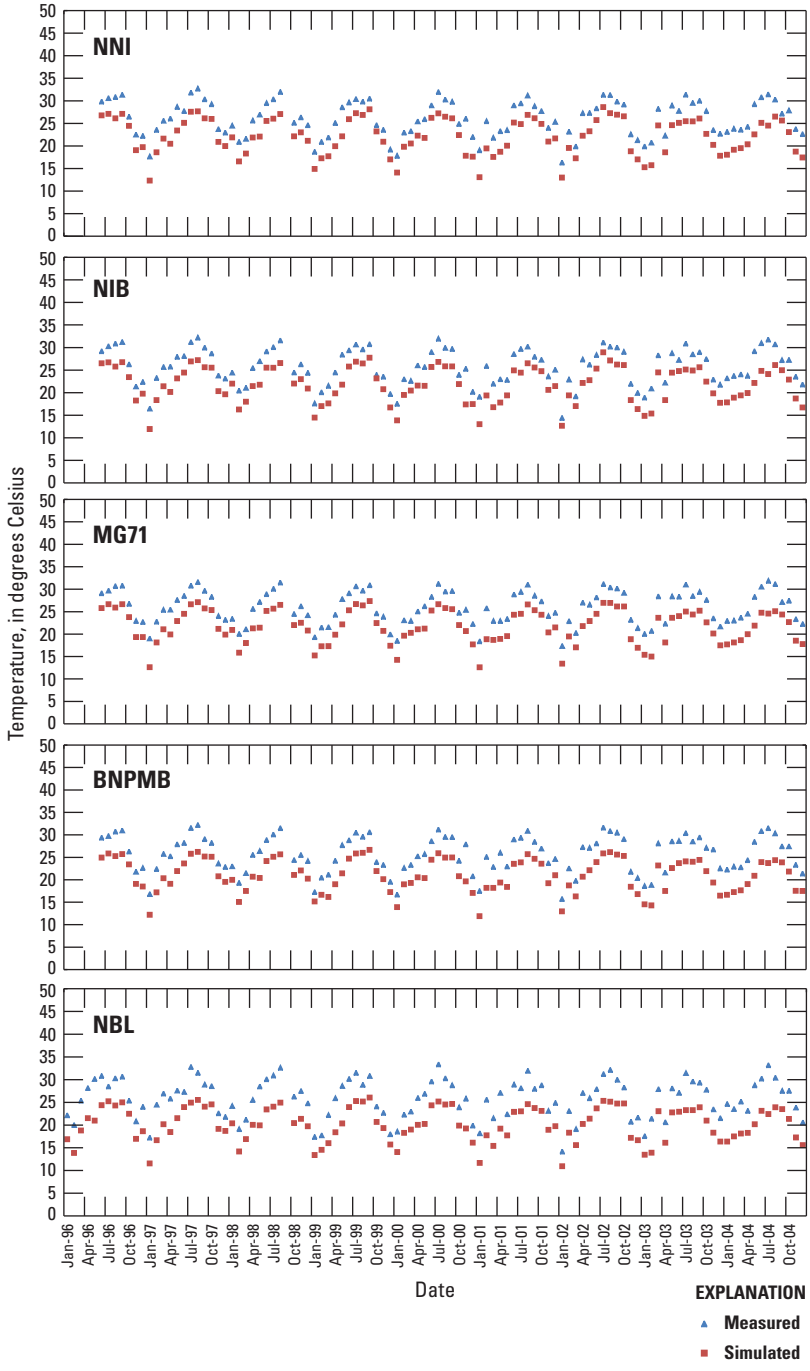

Figure 1-32. Vertically averaged surface-water temperature measured monthly and simulated by the Biscayne and Southern Everglades Coastal Transport (BISECT) model in the Biscayne Bay area, south Florida peninsula, 1996–2004 (see app. 3 for station details).

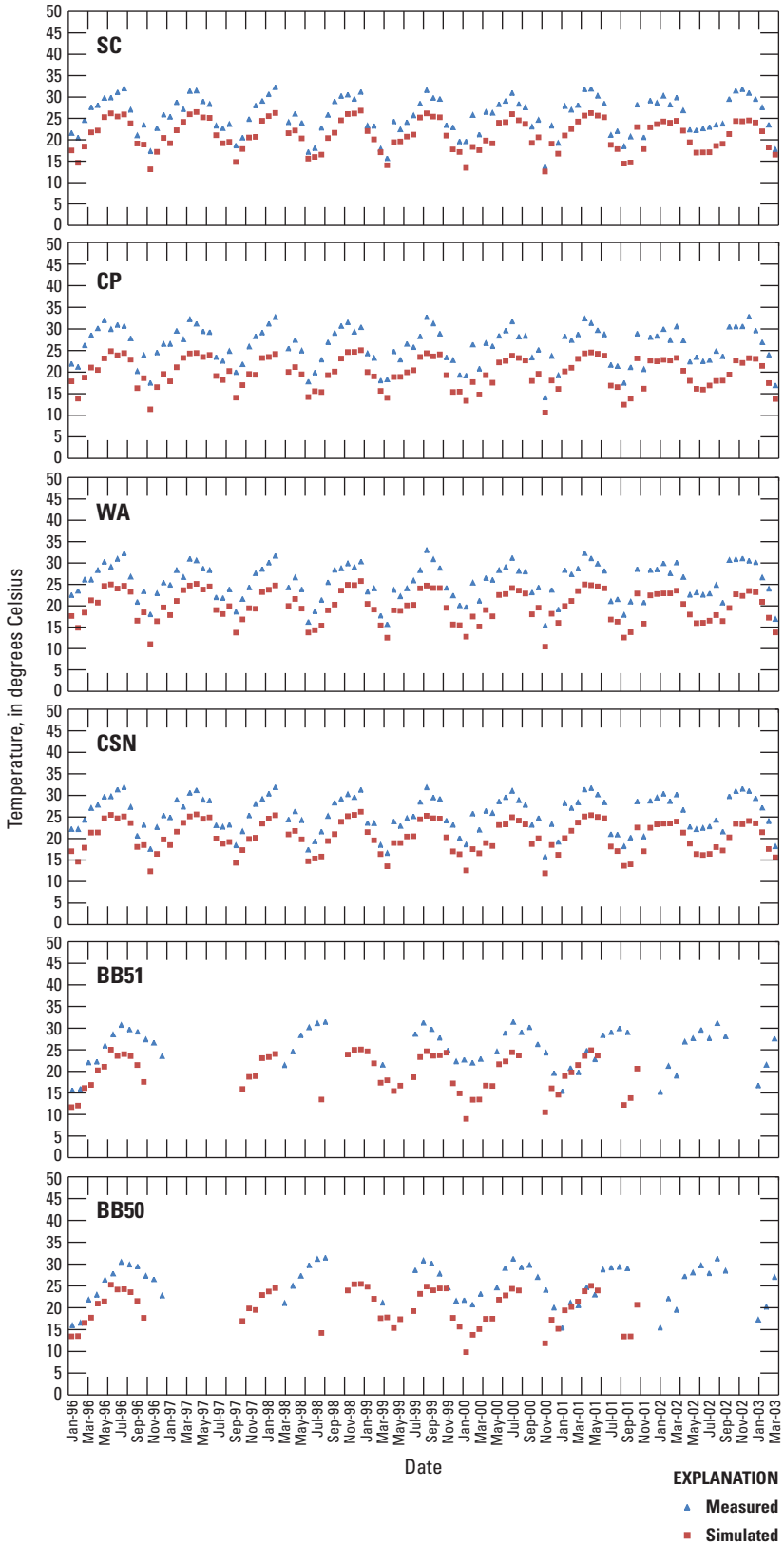

Figure 1-32. Vertically averaged surface-water temperature measured monthly and simulated by the Biscayne and Southern Everglades Coastal Transport (BISECT) model in the Biscayne Bay area, south Florida peninsula, 1996–2004 (see app. 3 for station details).

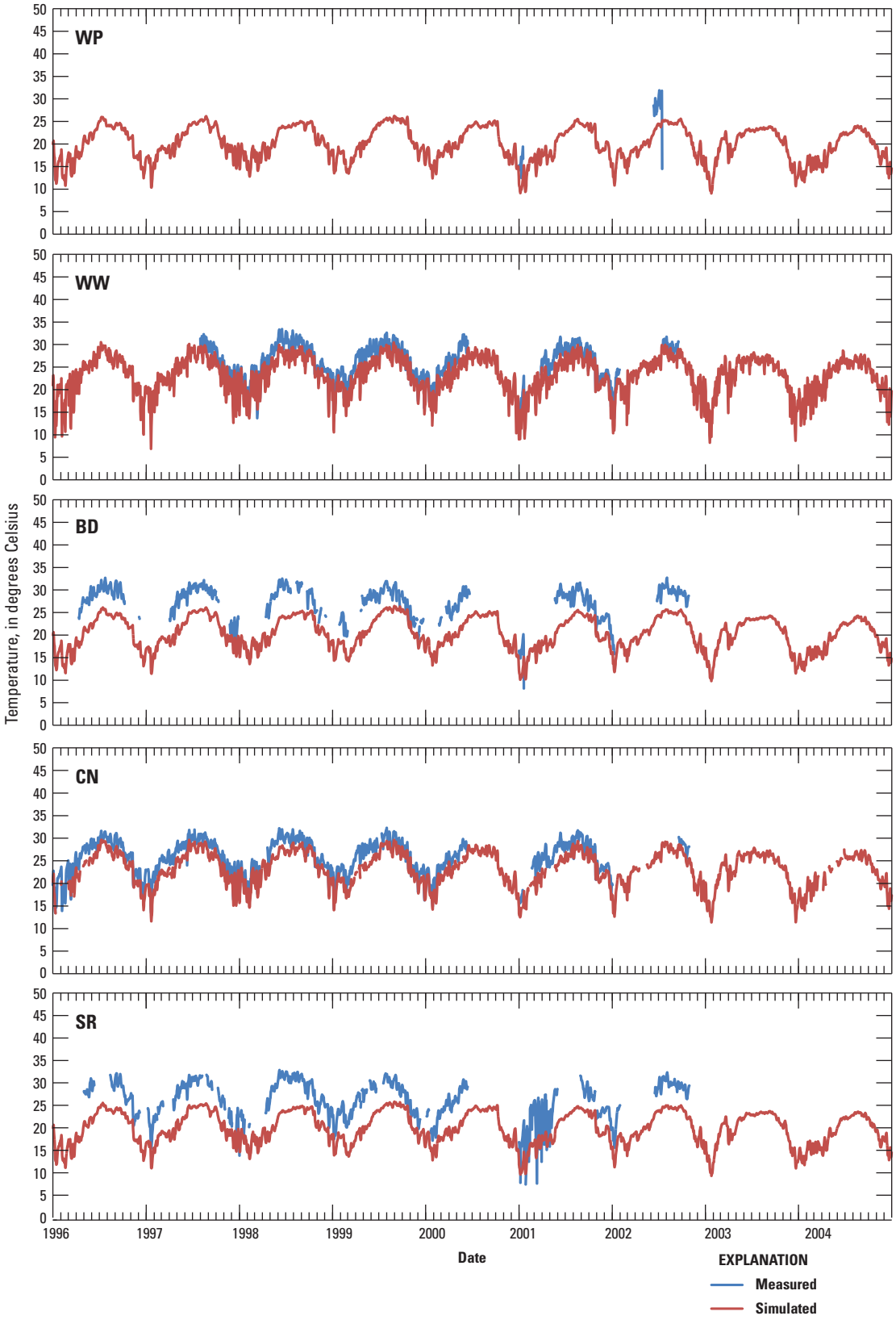

Figure 1-33. Daily surface-water temperature measured and simulated by the Biscayne and Southern Everglades Coastal Transport (BISECT) model in the Everglades National Park area, south Florida peninsula, 1996–2004 (see app. 3 for station details).

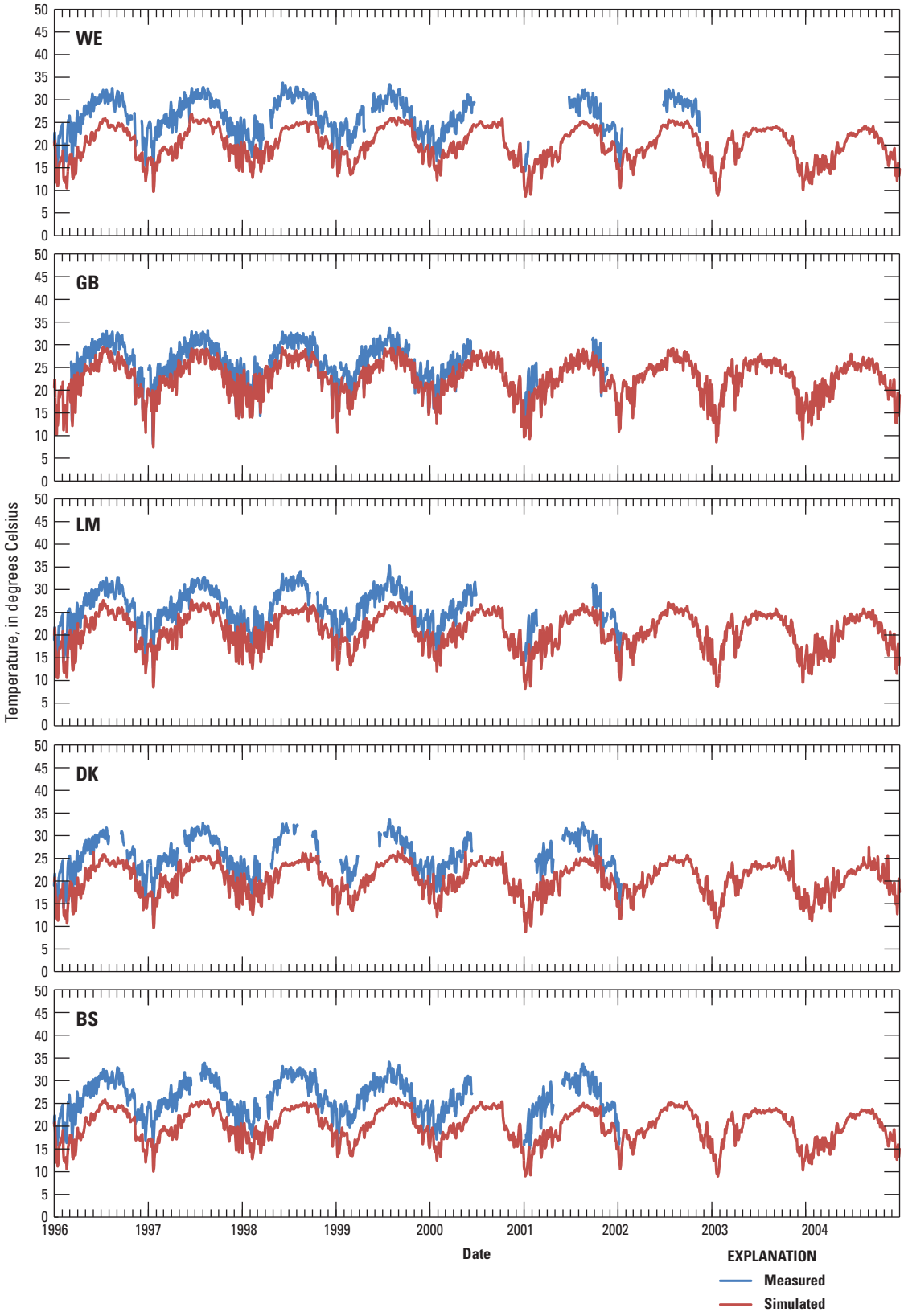

Figure 1-33. Daily surface-water temperature measured and simulated by the Biscayne and Southern Everglades Coastal Transport (BISECT) model in the Everglades National Park area, south Florida peninsula, 1996–2004 (see app. 3 for station details).—Continued

Table 1–7. Error statistics for surface-water temperature simulated by the Biscayne and Southern Everglades Coastal Transport (BISECT) model, south Florida peninsula, 1996–2004.

[*PEV*, percent explained variance; *NS*, Nash-Sutcliffe coefficient; *RMSE*, root-mean square error; °C, degree Celsius; *ME*, mean error. See app. 3 for station details]

Temperature station name	*PEV*	*NS*	*RMSE* (°C)	*ME* (°C)
NNI	0.910	-0.136	4.152	-3.984
NIB	0.904	-0.077	4.187	-3.997
MG71	0.928	-0.369	4.326	-4.211
BNPMB	0.905	-0.447	4.876	-4.713
NBL	0.859	-0.873	5.828	-5.605
SC	0.867	-0.256	4.833	-4.570
CP	0.853	-1.242	6.416	-6.203
WA	0.858	-0.968	5.913	-5.695
CSN	0.879	-0.712	5.470	-5.273
BB51	0.898	-0.772	6.079	-5.902
BB50	0.904	-0.538	5.586	-5.409
WP	0.851	0.260	5.556	-4.965
WW	0.922	0.589	2.619	-2.357
BD	0.764	-1.663	5.489	-5.241
CN	-1.945	-3.229	7.869	-4.336
SR	0.799	-1.157	6.017	-5.729
WE	0.839	-1.045	5.863	-5.627
GB	0.890	0.372	3.388	-3.079
LM	0.880	-0.485	5.135	-4.924
DK	0.768	-0.828	5.583	-5.217
BS	0.835	-1.543	6.335	-6.126
P-33	0.897	0.727	2.084	-1.625
Shark	0.716	0.275	3.129	-2.441

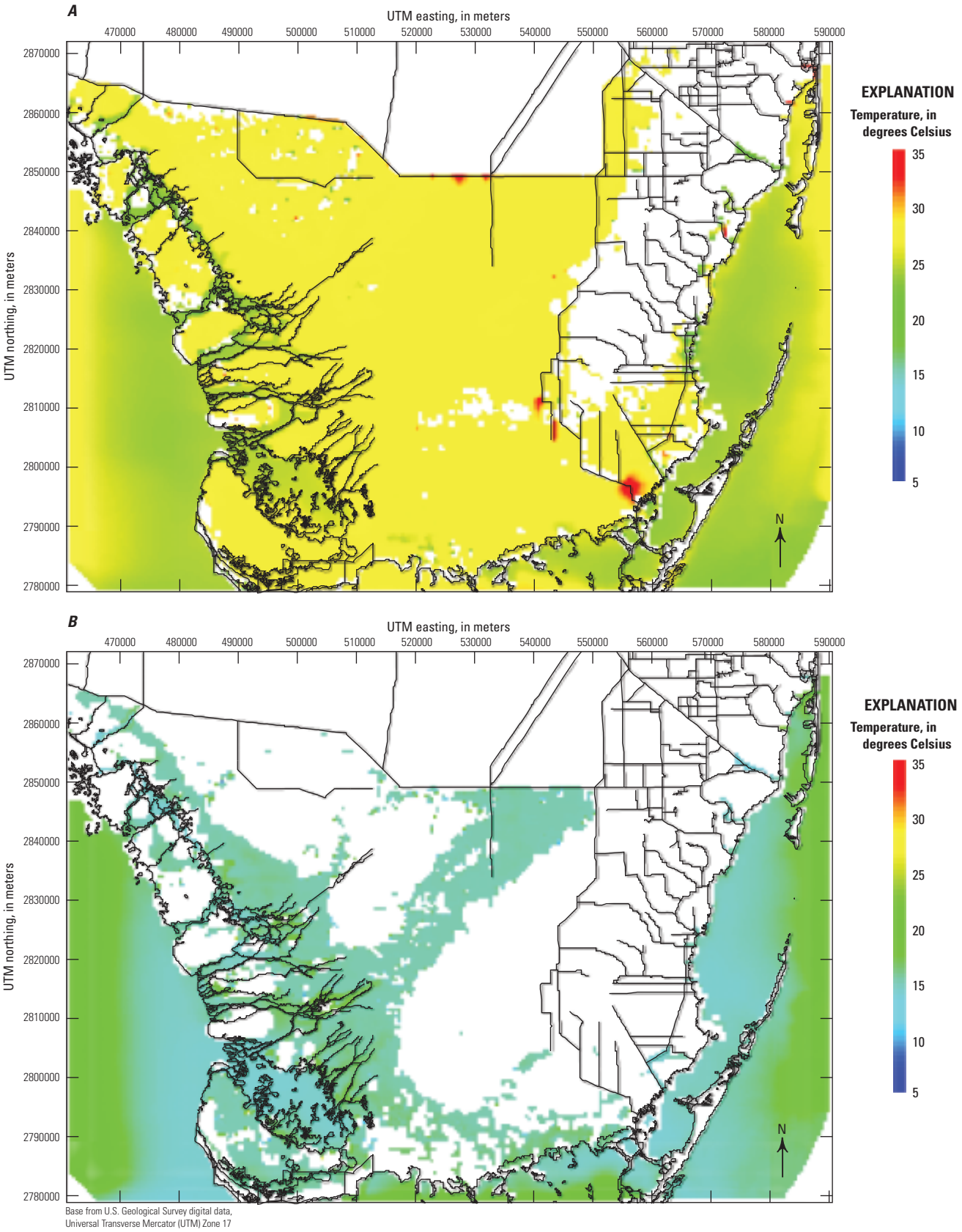

Figure 1-34. Distribution of surface-water temperature for *A*, wet season (June 12, 1997) and *B*, dry season (February 6, 2001) simulated by the Biscayne and Southern Everglades Coastal Transport (BISECT) model, south Florida peninsula, 1996–2004.

Table 1–8. Volumetric differences between cumulative flows at coastal streams for sensitivity simulation and base-case simulation of the Biscayne and Southern Everglades Coastal Transport (BISECT) model, south Florida peninsula, 1996–2004.

[%, percent; tidal amp, amplitude of all tidal components; trans layer, transition layer between groundwater and surface water; canal conduct, hydraulic conductance of canal bed layer. See app. 3 for station details]

	Broad River	Chatham River	Harney River	Long Sound	Lostmans River	McCormick Creek	Mud Creek	North River	Shark River	Taylor River	Trout Creek
Manning's *n* +10%	-6.14	-6.11	-10.42	1.11	-6.48	2.53	-3.87	-1.79	-7.44	-4.48	-2.23
Manning's *n* -10%	5.48	7.36	13.09	-2.04	7.61	-1.81	5.02	1.72	9.32	5.42	2.48
Wind × 1/2	-1.81	-0.97	-0.73	-1.12	-0.53	0.07	0.52	1.01	-0.05	0.64	0.32
Wind × 2	-0.44	0.14	-0.24	-0.46	-0.13	-1.60	-1.22	-1.72	-0.40	-1.64	-1.11
Tidal amp + 10%	5.70	6.90	0.12	-0.90	10.01	11.03	2.43	5.43	9.32	3.82	2.66
Tidal amp - 10%	-3.72	-6.65	-3.14	0.99	-9.30	-8.95	-2.01	-3.61	-8.04	-2.90	-2.23
Trans layer 0.05 m	0.34	-0.02	0.33	2.26	0.10	0.73	1.12	0.61	0.24	0.80	1.46
Trans layer 0.0001 m	-0.75	0.06	0.55	-1.95	0.30	3.22	0.43	1.00	0.42	1.75	0.05
Canal conduct × 10	-0.24	-0.08	-0.43	-2.23	-0.11	-0.60	-2.07	-0.76	-0.32	-1.83	-2.40
Canal conduct × 0.1	-0.85	0.06	1.61	6.19	0.36	3.18	7.54	2.81	1.19	6.64	8.94
Aquifer conduct × 2	-0.83	0.64	0.25	-0.11	0.19	-0.91	0.26	0.43	0.05	0.42	0.10
Aquifer conduct × 1/2	-0.63	-0.37	0.60	-1.66	0.16	2.52	1.18	0.46	0.67	1.82	1.03
Aquifer vertical conduct × 2	-1.78	0.02	0.38	-0.54	0.10	-0.02	0.36	0.29	0.31	0.82	0.16
Aquifer vertical conduct × 1/2	-2.17	-0.01	0.33	-0.45	0.13	1.12	0.45	0.29	0.34	0.86	0.31
Constant albedo	0.54	-0.26	-0.12	-0.43	-0.15	-1.96	-0.64	-0.21	-0.08	-0.77	-0.68

McCormick Creek simulated flow appears to be more sensitive to some of the parameters than flow at other streams. Wind, tidal amplitude, aquifer horizontal and vertical conductivity, and albedo all seem to affect McCormick Creek more than they affect other streams, indicating more uncertainty in predicting McCormick Creek flows compared to other streams. McCormick Creek is the primary outlet for the West Lake system, which appears to be more hydraulically isolated than the rest of the BISECT domain is. Harney River is sensitive to Manning's *n* but insensitive to tidal amplitude, indicating that upstream conditions have a more dominant effect than do downstream water levels and that the uncertainty in Manning's *n* estimates is a factor in Harney River predictions.

The root-mean square difference (*RMSD*) and mean difference (*MD*) statistics are used for analyzing model sensitivity; these parameters are the same form as the *RMSE* and *ME* statistics used to analyze model errors except that a difference between simulations is expressed rather than a difference with field data. Stage data from 12 sites (fig. 1–15) are used for comparison statistics (fig. 1–35). Statistics indicate that locations around the headwaters of Taylor Slough (Taylor Slough Bridge, R127, G3272) are sensitive to reductions in aquifer and canal conductances, whereas locations in Shark River Slough (P33, P35, P36, P37, P38) have the lowest sensitivities to all parameters. BICYA10 and NP201 are most sensitive to changes in Manning's *n.* Increasing stage as friction increases indicates that resistance to coastal drainage is a factor in these areas of the model.

RMSD and *MD* values computed for 11 coastal discharge sites (fig. 1–6) indicate that simulated flows in Broad River and Lostmans River have the highest overall sensitivities to changes in Manning's *n*, canal conductance, aquifer conductance, and albedo (fig. 1–36). The *RMSD* values demonstrate high sensitivity at Broad River, but the *MD* does not, indicating that parameter variations affect the variability of simulated flow at Broad River more than they affect the mean flow. All streams show sensitivity to both the tidal amplitude and the Manning's *n*, indicating that simulated flows at these coastal outlets are highly affected by the parametrization of the surface-water system.

RMSD and *MD* values computed for effects of changes in the five perturbed parameters on simulated salinity and temperature indicate substantial spatial differences in the simulated system response (fig. 1–37). Salinity values show somewhat similar patterns at Harney and Shark Rivers, with lower friction factors and higher tidal amplitudes yielding higher salinities. Shark River temperatures are more sensitive to changes in most of the simulated parameters than are temperatures at P33. The difference in offshore and inland temperatures (fig. 1–34) means that changes in flow patterns will cause some change in temperature statistics at coastal locations such as at the Shark River station. Adopting a spatially constant albedo, which could affect the heat budget, has only limited effects on temperature and is not shown in figure 1–37.

Harney River salinities show the greatest sensitivity to tidal amplitude compared to other parameters (fig. 1–37). In contrast, the flow at Harney River is more sensitive to Manning's *n* than is tide (fig. 1–36 and table 1–8). This difference in parameter sensitivity between flow and salinity at Harney River indicates that the tidal-driven dynamic mixing affects salinity more than it affects the volumetric outflow. The dynamics are different at Shark River, where both coastal salinities and discharge are as or more sensitive to Manning's *n* as is tide, (figs. 1–36 and 1–37, table 1–8). The Shark River outlet is more sheltered by land from the open offshore region than is Harney River (fig. 1–1), so tidal effects at Shark River are relatively smaller.

The sensitivity analyses described above provide a number of insights on how BISECT model input parameterization affects model-simulated hydrology.

1. Higher simulated tidal amplitude results in larger cumulative flows, and smaller amplitude results in lower cumulative flows in the representation of most Everglades coastal streams.

2. The simulated response of cumulative flows into Long Sound to modeled variations in tidal amplitude, wind, and frictional resistance do not follow the patterns of other coastal streams.

3. Simulated cumulative coastal streamflows along the Whitewater Bay and Florida Bay coast exhibit more substantial effects from increased winds than do simulated coastal streamflows along the Gulf of Mexico coast.

4. Simulated variations in flow to the Everglades coastal streams are substantially affected by groundwater/surface-water interactions in the eastern urban areas.

5. Cumulative flows at McCormick Creek are sensitive to variations in the model input tide and aquifer leakage.

6. Simulated Harney River flow variations are most strongly affected by upstream model parameters such as frictional resistance, but Harney River salinity variations are most strongly affected by downstream parameters such as tidal fluctuations.

7. Simulated levels at the headwater of Taylor Slough are substantially affected by aquifer leakage parameters and water exchanges with the urban canals.

8. Variations in simulated flow at Broad River and Lostmans River are more sensitive to variations in the parameterization of the hydrologic system than are any of the other rivers.

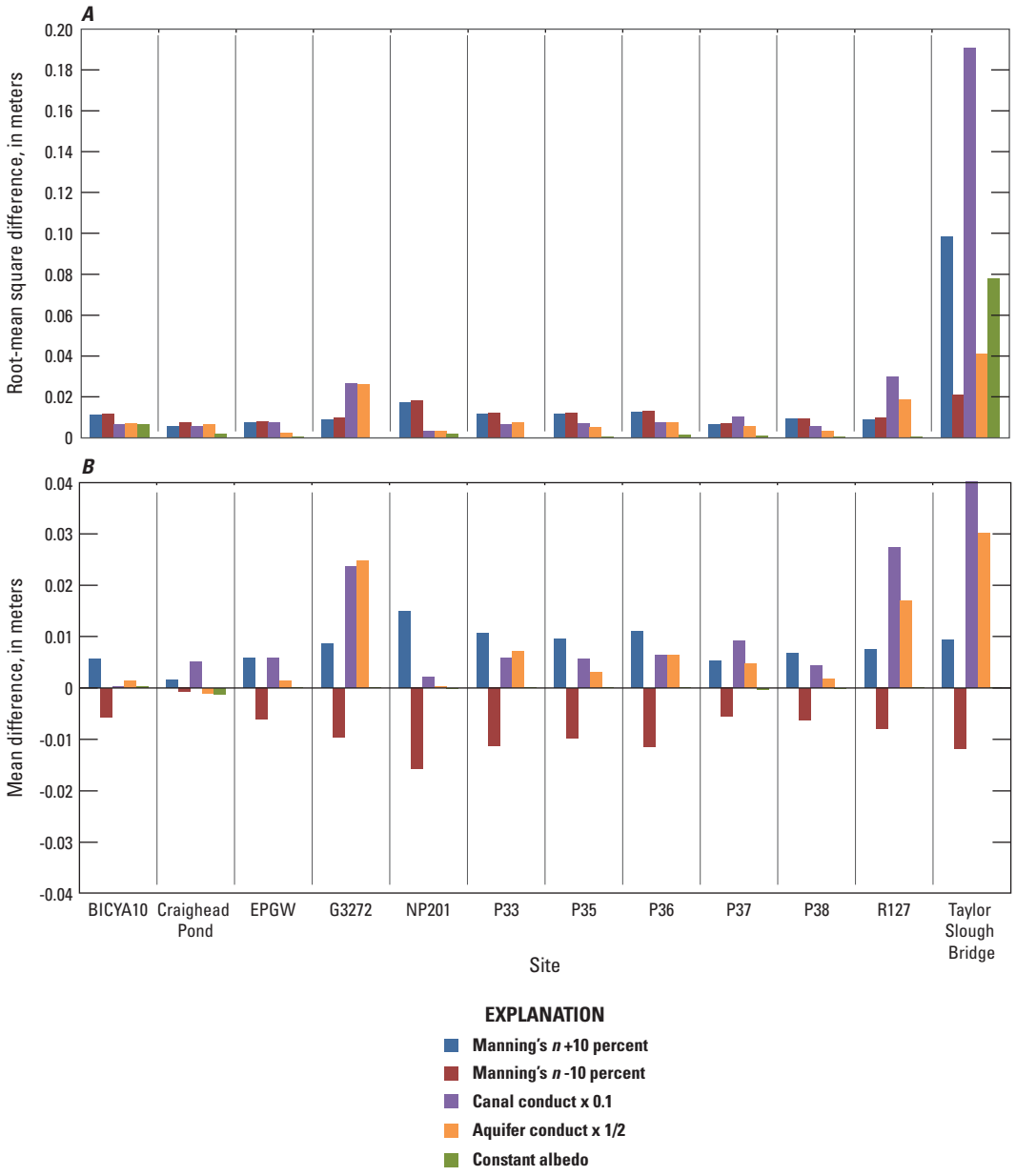

Figure 1-35. *A*, Root-mean square difference and *B*, mean difference between sensitivity simulation and base-case simulation surface-water stages for the five most sensitive parameter perturbations: Manning's *n* increased 10 percent, Manning's *n* decreased 10 percent, canal conductance divided by 10, aquifer conductance divided by 2, and albedo set to constant (see app. 3 for station details).

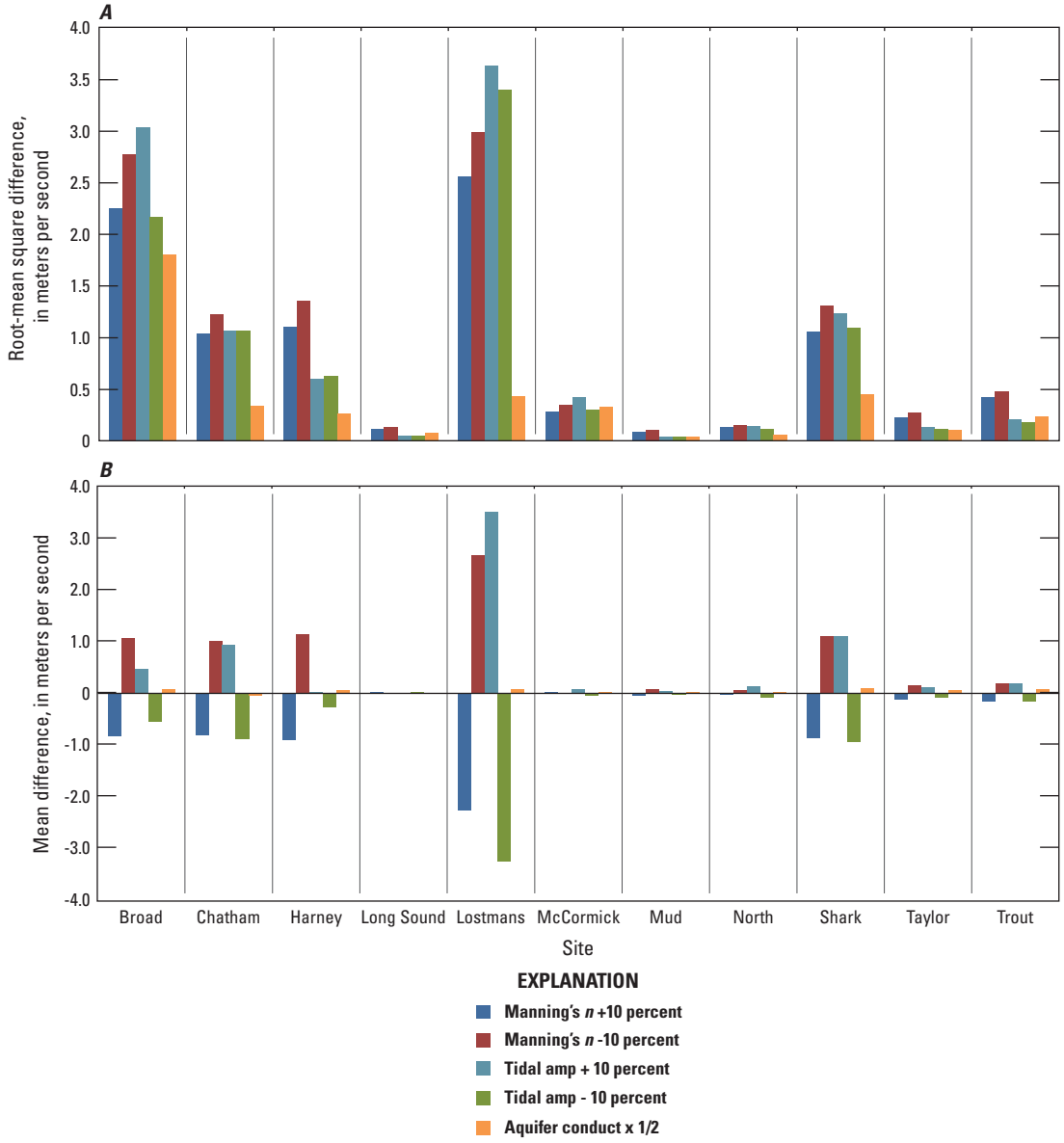

Figure 1-36. *A*, Root-mean square difference and *B*, mean difference between sensitivity simulation and base-case simulation coastal discharges for the five most sensitive parameters: Manning's *n* increased 10 percent, Manning's *n* decreased 10 percent, tidal amplitude increased 10 percent, tidal amplitude decreased 10 percent, and aquifer conductance divided by 2 (see app. 3 for station details).

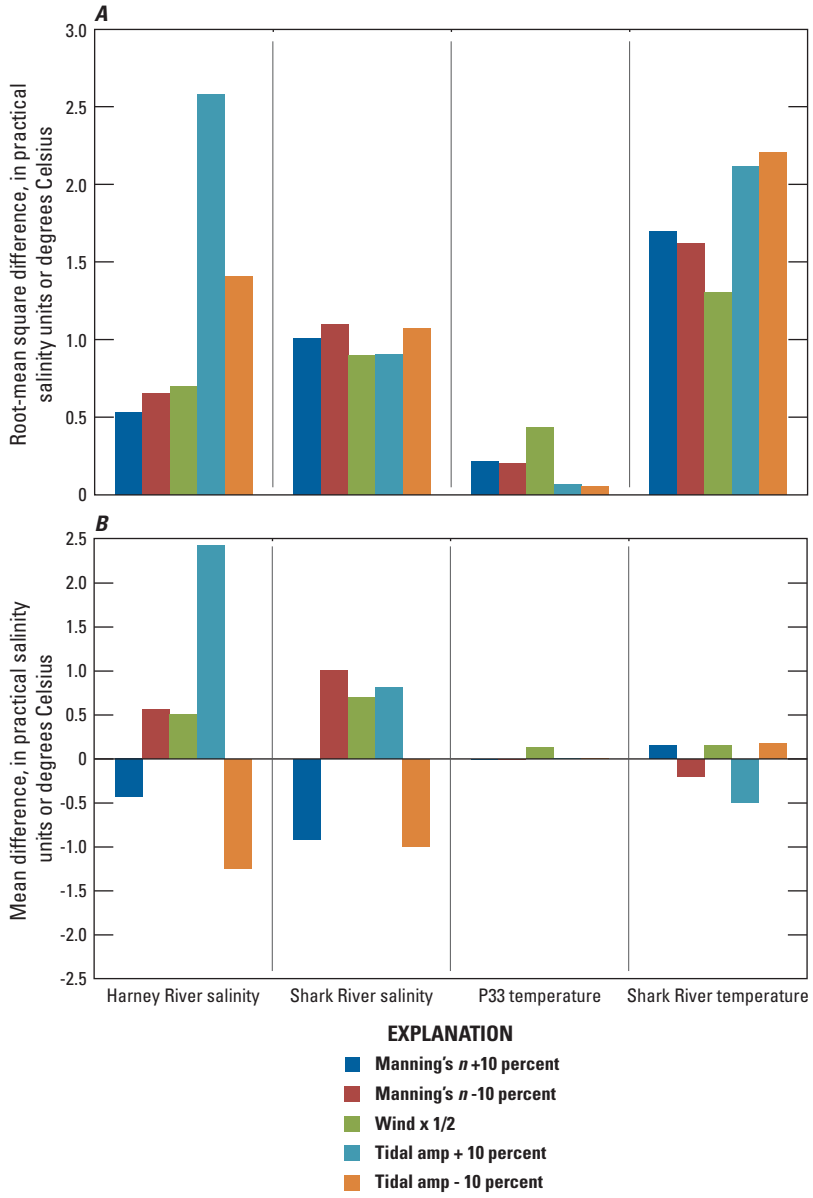

Figure 1-37. *A*, Root-mean square difference and *B*, mean difference between sensitivity simulation and base-case simulation salinities and temperatures for the five most sensitive parameters: Manning's *n* increased 10 percent, Manning's *n* decreased 10 percent, wind friction divided by 2, tidal amplitude increased 10 percent, and tidal amplitude decreased 10 percent (see app. 3 for station details).

References Cited

Abtew, W., 1996, Evapotranspiration measurements and modeling for three wetland systems in South Florida: JAWRA Journal of the American Water Resources Association, v. 32, p. 465–473.

Bahm, K.E., and Fennema, R.J., 2013, Evaluation and application of the TIME model v2.0—Restoration alternatives and sea level rise in Everglades National Park: Hydrologic Model Report SFNRC Technical Series 2013.1, 92 p.

Barr, J.G., Fuentes, J.D., Engel, V., and Zieman, J.C., 2009, Physiological responses of red mangroves to the climate in the Florida Everglades: Journal of Geophysical Research, v. 114, G02008, doi:10.1029/2008JG000843.

Decker, Jeremy, and Swain, Eric, 2008, Hydrologic modeling of south Florida environmental parameters and application to ecology, salinity, and heat transport: 2008 Greater Everglades Ecosystem Restoration Conference, Naples, Fla., July 28–August 1, 2008, p. 81.

Desmond, G.B., 2003, Measuring and mapping the topography of the Florida Everglades for ecosystem restoration, *in* Torres, A.E., Higer, A.L., Henkel, H.S., Mixson, P.R., Eggleston, J.R., Embry, T.L., and Clement, Gail, comps., U.S. Geological Survey Greater Everglades Science Program, 2002 biennial report: U.S. Geological Survey Open-File Report 03–54, p. 31–32.

Fish, J.E., and Stewart, M.T., 1991, Hydrogeology of the surficial aquifer system, Dade County, Florida: U.S. Geological Survey Water-Resources Investigations Report 90–4108, 56 p.

Fitterman, D.V., and Deszcz-Pan, M., 2001, Saltwater intrusion in Everglades National Park, Florida measured by airborne electromagnetic surveys, *in* First International Conference on Saltwater Intrusion and Coastal Aquifers-Monitoring, Modeling, and Management (SWICA-M3), Essaouira, Morocco: Rabat, Morocco, Laboratoire d'Analyse des Systémes Hydrauliques (LASH), 11 p.

Florida Department of Emergency Management (FDEM), 2007, Florida GIS—Baseline specifications for orthophotography and lidar v 1.2.: FDEM, accessed 4/30/2018, at https://kipdf.com/baseline-specifications-for-orthophotography-and-lidar-florida-gis_5aae110c1723dd98fc4816c4.html.

German, E.R., 1999, Regional evaluation of evapotranspiration in the Everglades: Proceedings of the 3rd International Symposium on Ecohydraulics, Salt Lake City, Utah, July 13–16, 1999.

German, E.R., 2000, Regional evaluation of evapotranspiration in the Everglades: U.S. Geological Survey Water-Resources Investigations Report 00–4217, 48 p.

Guo, Weixing, and Langevin, C.D., 2002, User's guide to SEAWAT—A computer program for simulation of three-dimensional variable-density ground-water flow: Techniques of Water-Resources Investigations, book 6, chap. A7, 77 p.

Hansen, M., and DeWitt, N.T., 1999, Modern and historical bathymetry of Florida Bay, *in* Proceedings of the 1999 Florida Bay and Adjacent Marine Systems Science Conference, November 1–5, 1999, Key Largo, Fla.

Hittle, Clinton, Patino, Eduardo, and Zucker, Mark, 2001, Freshwater flow from estuarine creeks into northeastern Florida Bay: U.S. Geological Survey Water-Resources Investigations Report 01–4164, 32 p.

Jones, J.W., 1999, Land characterization for hydrologic modeling in the Everglades: Proceedings of the 3rd International Symposium on Ecohydraulics, Salt Lake City, Utah, July 13–16 1999.

Jones, J.W., Desmond, G.B., Henkle, Charles, and Glover, Robert, 2012, An approach to regional wetland digital elevation model development using a differential Global Positioning System and a custom-built helicopter-based surveying system: International Journal of Remote Sensing, v. 33, no. 2, p. 450–465.

Langevin, C.D. 2001. Simulation of ground-water discharge to Biscayne Bay, southeastern Florida. U.S. Geological Survey Water-Resources Investigations Report 00–4251.

Langevin, C.D., Swain, E.D., and Wolfert, M.A., 2005, Simulation of integrated surface-water/ ground-water flow and salinity for a coastal wetland and adjacent estuary: Journal of Hydrology, v. 314, p. 212–234.

Large, W.G., and Pond, S., 1981, Open ocean momentum flux measurements in moderate to strong winds: Journal of Physical Oceanography, v. 11, p. 324–336.

Lee, J.K., and Carter, Virginia, 1999, Field measurement of flow resistance in the Florida Everglades, *in* Gerould, Sarah, and Higer, Aaron, comps., U.S. Geological Survey Program on the South Florida Ecosystem—Proceedings of the South Florida Restoration Science Forum, May 17–19, 1999, Boca Raton, Florida: U.S. Geological Survey Open File Report 99–181.

Levesque, V.A., 2004, Water flow and nutrient flux from five estuarine rivers along the southwest coast of the Everglades National Park, Florida, 1997–2001: U.S. Geological Survey Scientific Investigations Report 2004–5142, 24 p.

Lohmann, M.A., Swain, E.D., Wang, J.D., and Dixon, Joann, 2012, Evaluation of effects of changes in canal management and precipitation patterns on salinity in Biscayne Bay, Florida, using an integrated surface-water/groundwater model: U.S. Geological Survey Scientific Investigations Report 2012–5099, 94 p.

Long Term Ecological Research LTER, 1998, USGS Digital Raster Graphics - South Florida Mosaic: accessed April 5, 2018 at http://fcelter.fiu.edu/data/GIS/interactive_map/layer_info.epl?layer=drg250k.

McPherson, B.F., and Halley, Robert, 1996, The south Florida environment—A region under stress: U.S. Geological Survey Circular 1134, 61 p.

Nash, J.E., and Sutcliffe, J.V., 1970, River flow forecasting through conceptual models part I—A discussion of principles: Journal of Hydrology, v. 10, no. 3, p. 282–290.

National Oceanic and Atmospheric Administration (NOAA) Coastal Services Center, 2010, Lidar data collected in marshes—Its error and application for sea level rise modeling: Accessed June 8, 2017 at https://coast.noaa.gov/data/digitalcoast/pdf/lidar-marshes-slamm.pdf.

National Oceanic and Atmospheric Administration (NOAA) National Geophysical Data Center, 2017. Coastal Relief Model: Accessed June 8, 2017 at http://www.ngdc.noaa.gov/mgg/coastal/crm.html.

Parker, G.G., Ferguson, G.E., and Love, S.K., 1955, Water resources of southeastern Florida, with special reference to geology and ground water of the Miami area: U.S. Geological Survey Water Supply Paper 1255, 965 p.

Passioura, J.B., Ball, M.C., and Knight, J.H., 1992, Mangroves may salinize the soil and in so doing limit their transpiration rate: Functional Ecology, v. 6, no. 4, p. 476–481.

Patino, E., 1996, Gaging flows in northeastern Florida Bay: U.S. Geological Survey Fact Sheet 130–96, 1 p.

Prinos, Scott T.; Wacker, Michael A.; Cunningham, Kevin J.; Fitterman, David V., 2014. Origins and delineation of saltwater intrusion in the Biscayne aquifer and changes in the distribution of saltwater in Miami-Dade County, Florida. U.S. Geological Survey Scientific Investigations Report 2014-5025, Report: xi, 101 p.

Reese, R.S., and Cunningham, K.J., 2000, Hydrogeology of the gray limestone aquifer in southern Florida: U.S. Geological Survey Water-Resources Investigations Report 99–4213, 244 p.

Schaffranek, R.W., 2004, Simulation of surface-water integrated flow and transport in two dimensions—SWIFT2D user's manual: U.S. Geological Survey Techniques and Methods, 6 B–1, 115 p.

Schureman, P., 1976, Manual of harmonic analysis and prediction of tides: Washington D.C., U.S. Government Printing Office, U.S. Department of Commerce, Coast and Geodetic Survey, Special Publication No. 98.

Shoemaker, W.B., Lopez, C.D., and Duever, M., 2011, Evapotranspiration over spatially extensive plant communities in the Big Cypress National Preserve, southern Florida, 2007–2010: U.S. Geological Survey Scientific Investigations Report 2011–5212, 46 p.

Shoemaker, W.B., and Sumner, D.M., 2006, Alternate corrections for estimating actual wetland evapotranspiration from potential evapotranspiration: Wetlands, v. 26, no. 2, p. 528–543.

Sonenshein, R.S., 1996, Delineation of saltwater intrusion in the Biscayne aquifer, eastern Dade County, Florida, 1995: U.S. Geological Survey Water-Resources Investigations Report 96–4285, 1 sheet.

South Florida Water Management District, 1995, Land cover land use 1995: South Florida Water Management District, West Palm Beach, Fla., accessed June 8, 2017, at http://my.sfwmd.gov/gisapps/sfwmdxwebdc/dataview.asp?query=unq_id=297.

South Florida Water Management District (SFWMD), 2017, DBHYDRO database, accessed June 2, 2017, at https://www.sfwmd.gov/science-data/dbhydro.

Sumner, David M., Wu, Qinglong, and Pathak, Chandra S., 2011, Variability of Albedo and Utility of the MODIS Albedo Product in Forested Wetlands: Wetlands, v. 31, no. 2, p. 229–237.

Swain, E.D., and Decker, J.D., 2009, Development, testing, and application of a coupled hydrodynamic surface-water/groundwater model (FTLOADDS) with heat and salinity transport in the Ten Thousand Islands/Picayune Strand Restoration Project area, Florida: U.S. Geological Survey Scientific Investigations Report 2009–5146, 42 p.

Swain, E.D., and Decker, J.D., 2010, A measurement-derived heat-budget approach for simulating coastal wetland temperature with a hydrodynamic model: Wetlands, v. 30, no. 3, p. 635–648.

Swain, E.D., and Lohmann, M.A., 2019, FTLOADDS (combined SWIFT2D surface-water model and SEAWAT groundwater model) simulator used to assess proposed sea-level rise response and water-resource management plans for the hydrologic system of the south Florida peninsula for the Biscayne and Southern Everglades Coastal Transport (BISECT) model: U.S. Geological Survey data release, http://dx.doi.org/10.5066/P9MDUQPK.

Swain, E.D., Wolfert, M.A., Bales, J.D., and Goodwin, C.R., 2004, Two-dimensional hydrodynamic simulation of surface-water flow and transport to Florida Bay through the Southern Inland and Coastal Systems (SICS): U.S. Geological Survey Water-Resources Investigations Report 03–4287, 56 p., 6 pls.

Swain, Michael, Swain, Matthew, Lohmann, Melinda, and Swain, E.D., 2012, Experimental determination of soil heat storage for the simulation of heat transport in a coastal wetland: Journal of Hydrology, v. 422–423, p. 53–62.

U.S. Army Corps of Engineers (USACE), 1999, Central and Southern Florida Comprehensive Review Study: Jacksonville Fla., U.S. Army Corps of Engineers, April 1999.

U.S. Geological Survey, 2017, South Florida Information Access (SOFIA) data exchange: Accessed June 2, 2017, at https://sofia.usgs.gov/exchange/sfl_hydro_data/.

Wang, J.D., Swain, E.D., Wolfert, M.A., Langevin, C.D., James, D.E., and Telis, P.A., 2007, Applications of Flow and Transport in a Linked Overland/Aquifer Density Dependent System (FTLOADDS) to simulate flow, salinity, and surface-water stage in the southern Everglades, Florida: U.S. Geological Survey Scientific Investigations Report 2007–5010, 112 p.

Worth, Dewey, Weaver, Cecella, and Trulock, Shelly, 2002, Florida Bay and Florida Keys feasibility study overview: Accessed October 1, 2015, at http://www.evergladesplan.org/docs/fs_fl_bay_feas_hires.pdf.

Appendix 2. Aquifer Hydraulic Conductivities by Model Layers

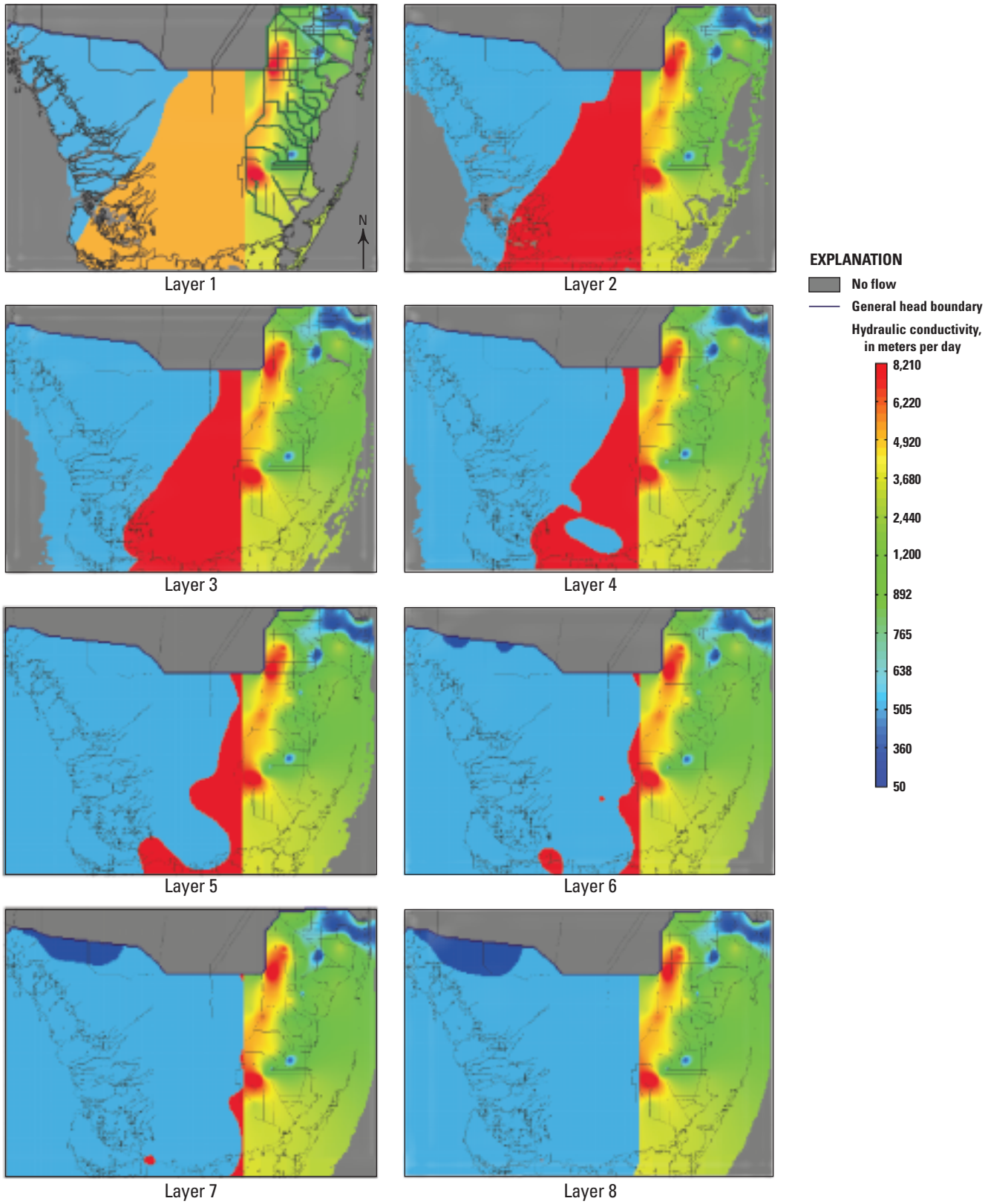

Figure 2-1. Aquifer layer hydraulic conductivities for the Biscayne and Southern Everglades Coastal Transport (BISECT) model application for south Florida.

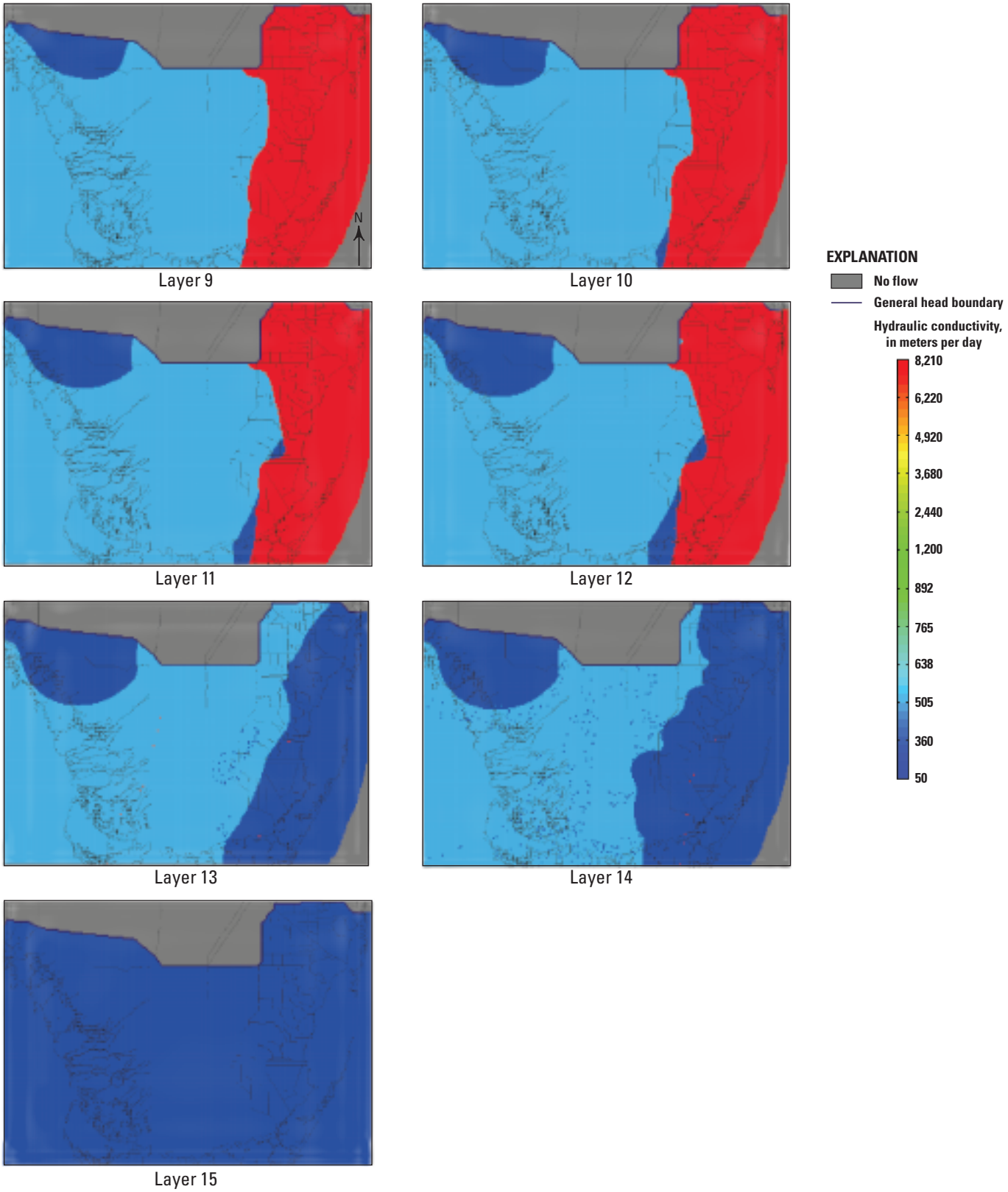

Figure 2-1. Aquifer layer hydraulic conductivities for the Biscayne and Southern Everglades Coastal Transport (BISECT) model application for south Florida.—Continued

Appendix 3. Field Stations Used in the Biscayne and Southern Everglades Coastal Transport (BISECT) Model Simulations

Appendix 3. Field stations used in the Biscayne and Southern Everglades Coastal Transport (BISECT) model simulations.

[dd mm ss, degree minute second; NOAA, National Oceanic and Atmospheric Administration; SFWMD, South Florida Water Management District; DBHYDRO, corporate environmental database of the SFWMD; ENP, Everglades National Park; USGS, U.S. Geological Survey; SOFIA, South Florida Information Access database; FIU, Florida International University; DERM, Department of Environmental Regulation Management; NWIS, National Water Information System]

Field station name (this report)	Map (site) identifier	Latitude (dd mm ss)	Longitude (dd mm ss)	Usage in model	Temporal frequency	Agency	Website or data source
Rainfall (station locations shown in fig. 1–8 in app. 1)							
081306-2	081306-2	25 40 19	80 09 24	boundary	daily	NOAA	SFWMD DBHYDRO
083909-1	083909-1	25 50 00	80 17 00	boundary	daily	NOAA	SFWMD DBHYDRO
084095-1	084095-1	25 30 00	80 33 00	boundary	daily	NOAA	SFWMD DBHYDRO
085663-4	085663-4	25 47 00	80 17 00	boundary	daily	NOAA	SFWMD DBHYDRO
085667-2	085667-2	25 45 19	80 23 01	boundary	daily	NOAA	SFWMD DBHYDRO
086315-2	086315-2	25 57 00	80 12 57	boundary	daily	NOAA	SFWMD DBHYDRO
3AS3WX	3AS3WX	25 51 11	80 46 08	boundary	daily	SFWMD	SFWMD DBHYDRO
Blackwater Sound	BS	25 10 42	80 26 18	boundary	daily	ENP	SFWMD DBHYDRO
Buoy Key	BK	25 07 15	80 50 02	boundary	daily	ENP	SFWMD DBHYDRO
Broad River	BR	25 28 40	80 59 23	boundary	daily	ENP	SFWMD DBHYDRO
Broad River Lower	BD	25 29 11	81 06 40	boundary	daily	ENP	SFWMD DBHYDRO
Butternut Key	BN	25 05 17	80 31 08	boundary	daily	ENP	SFWMD DBHYDRO
Cane Patch	CN	25 25 17	80 56 32	boundary	daily	ENP	SFWMD DBHYDRO
Clearwater Pass	CW	25 17 46	81 00 47	boundary	daily	ENP	SFWMD DBHYDRO
Craighead Pond	CP	25 13 45	80 42 14	boundary	daily	ENP	SFWMD DBHYDRO
Duck Key	DK	25 10 52	80 29 23	boundary	daily	ENP	SFWMD DBHYDRO
EPGW/SW	EPGW/SW	25 16 10	80 30 16	boundary	daily	ENP	SFWMD DBHYDRO
Everglades 8	NP-EV8, EVER8	25 20 47	80 28 43	boundary	daily	ENP	SFWMD DBHYDRO
Everglades City	EVCITY	25 51 11	81 22 50	boundary	daily	ENP	SFWMD DBHYDRO
Everglades IFAS	NP-IFS, IFS	25 30 35	80 29 59	boundary	daily	ENP	SFWMD DBHYDRO
Everglades Robblee	NP-ROB, Robblee	25 26 27	80 33 07	boundary	daily	ENP	SFWMD DBHYDRO
Flamingo	FLAM	25 08 29	80 54 53	boundary	daily	ENP	SFWMD DBHYDRO
Fortymile Bend	NP-FMB, FMB	25 45 30	80 49 42	boundary	daily	SFWMD	SFWMD DBHYDRO
G3353	G3353	25 17 18	80 34 14	boundary	daily	SFWMD	SFWMD DBHYDRO
Garfield Bight	GB	25 10 18	80 47 48	boundary	daily	ENP	SFWMD DBHYDRO
Gunboat Island	GI	25 22 40	81 01 46	boundary	daily	ENP	SFWMD DBHYDRO
Harney River	HR	25 25 26	81 03 36	boundary	daily	ENP	SFWMD DBHYDRO
Hialeah	HIALEAH_R	25 49 39	80 17 09	boundary	daily	NOAA	SFWMD DBHYDRO
Hialeah_W	HIALEAH_W	25 52 01	80 28 59	boundary	daily	SFWMD	SFWMD DBHYDRO
Highway Creek	HC	25 15 20	80 26 40	boundary	daily	ENP	SFWMD DBHYDRO
Homestead Air Reserve Base	HOMES.AFB	25 29 01	80 23 00	boundary	daily	SFWMD	SFWMD DBHYDRO
Homestead Field Station	HOMES.FS_R	25 28 39	80 26 54	boundary	daily	SFWMD	SFWMD DBHYDRO
Joe Bay	JB	25 13 27	80 32 25	boundary	daily	ENP	SFWMD DBHYDRO

Appendix 3. Field stations used in the Biscayne and Southern Everglades Coastal Transport (BISECT) model simulations.—Continued

[dd mm ss, degree minute second; NOAA, National Oceanic and Atmospheric Administration; SFWMD, South Florida Water Management District; DBHYDRO, corporate environmental database of the SFWMD; ENP, Everglades National Park; USGS, U.S. Geological Survey; SOFIA, South Florida Information Access database; FIU, Florida International University; DERM, Department of Environmental Regulation Management; NWIS, National Water Information System]

Field station name (this report)	Map (site) identifier	Latitude (dd mm ss)	Longitude (dd mm ss)	Usage in model	Temporal frequency	Agency	Website or data source
Rainfall (station locations shown in fig. 1–8 in app. 1)—Continued							
Lane River	LN	25 17 03	80 53 38	boundary	daily	ENP	SFWMD DBHYDRO
Little Madeira	LM	25 10 31	80 37 56	boundary	daily	ENP	SFWMD DBHYDRO
Long Sound	LS	25 14 05	80 27 27	boundary	daily	ENP	SFWMD DBHYDRO
Lostmans River	LO	25 33 21	81 10 07	boundary	daily	ENP	SFWMD DBHYDRO
Manatee Bay	MBTS	25 15 26	80 25 20	boundary	daily	SFWMD	SFWMD DBHYDRO
Miami Airport	MIAMI.AP_R	25 49 01	80 16 59	boundary	daily	NOAA	SFWMD DBHYDRO
Miami Field Station	MIAMI.FS_R	25 49 37	80 20 39	boundary	daily	SFWMD	SFWMD DBHYDRO
Middle Key	MDTS	25 16 43	80 23 42	boundary	daily	SFWMD	SFWMD DBHYDRO
North Dade	N DADE_R	25 48 00	80 14 25	boundary	daily	SFWMD	SFWMD DBHYDRO
North River	NR	25 20 23	80 54 41	boundary	daily	ENP	SFWMD DBHYDRO
NP-127	R127	25 21 15	80 36 23	boundary	daily	SFWMD	SFWMD DBHYDRO
NP-201	NP201	25 43 05	80 43 33	boundary	daily	SFWMD	SFWMD DBHYDRO
NP-202	NP202	25 39 40	80 42 45	boundary	daily	SFWMD	SFWMD DBHYDRO
NP-203	NP203	25 37 25	80 44 22	boundary	daily	SFWMD	SFWMD DBHYDRO
NP-205	NP205	25 41 20	80 50 57	boundary	daily	SFWMD	SFWMD DBHYDRO
NP-206	NP206	25 32 42	80 40 22	boundary	daily	SFWMD	SFWMD DBHYDRO
NP-311	R3110	25 26 50	80 37 34	boundary	daily	SFWMD	SFWMD DBHYDRO
NP-A13	A13	25 29 54	80 42 46	boundary	daily	SFWMD	SFWMD DBHYDRO
NP-CR2, Context Road 2	CR2	25 29 59	80 37 19	boundary	daily	SFWMD	SFWMD DBHYDRO
NP-CY3	CY3	25 19 39	80 45 03	boundary	daily	SFWMD	SFWMD DBHYDRO
NP-NE1, North East Shark River Slough	NE1	25 41 29	80 38 06	boundary	daily	SFWMD	SFWMD DBHYDRO
NP-OT, Ornithology Transect	OT	25 34 47	80 57 54	boundary	daily	ENP	SFWMD DBHYDRO
NP-P33	P33	25 36 30	80 41 30	boundary	daily	SFWMD	SFWMD DBHYDRO
NP-P34	P34	25 36 31	80 56 27	boundary	daily	ENP	SFWMD DBHYDRO
NP-P35	P35	25 27 39	80 51 53	boundary	daily	SFWMD	SFWMD DBHYDRO
NP-P36	P36	25 31 42	80 47 45	boundary	daily	SFWMD	SFWMD DBHYDRO
NP-P37	P37	25 17 09	80 41 18	boundary	daily	ENP	SFWMD DBHYDRO
NP-P38	P38	25 22 14	80 50 00	boundary	daily	SFWMD	SFWMD DBHYDRO
NP-RCR, Research Center	RCR	25 23 23	80 40 51	boundary	daily	SFWMD	SFWMD DBHYDRO
NP-RG1, Rocky Glades 1	RG1	25 34 57	80 36 29	boundary	daily	SFWMD	SFWMD DBHYDRO
NP-RPL, Royal Palm	RPALM	25 23 09	80 35 38	boundary	daily	SFWMD	SFWMD DBHYDRO
Oasis Ranger Station	OASIS	25 51 25	81 02 05	boundary	daily	ENP	SFWMD DBHYDRO

Appendix 3. Field stations used in the Biscayne and Southern Everglades Coastal Transport (BISECT) model simulations.—Continued

[dd mm ss, degree minute second; NOAA, National Oceanic and Atmospheric Administration; SFWMD, South Florida Water Management District; DBHYDRO, corporate environmental database of the SFWMD; ENP, Everglades National Park; USGS, U.S. Geological Survey; SOFIA, South Florida Information Access database; FIU, Florida International University; DERM, Department of Environmental Regulation Management; NWIS, National Water Information System]

Field station name (this report)	Map (site) identifier	Latitude (dd mm ss)	Longitude (dd mm ss)	Usage in model	Temporal frequency	Agency	Website or data source
Rainfall (station locations shown in fig. 1–8 in app. 1)—Continued							
Old Ingraham Highway	OIH	25 21 11	80 38 02	boundary	15 minute	USGS	USGS SOFIA website
PERRINE	PERRINE_R	25 36 01	80 20 59	boundary	daily	ENP	SFWMD DBHYDRO
PERRINE_4W	PERRINE_4W	25 35 01	80 25 59	boundary	daily	NOAA	SFWMD DBHYDRO
S123	S123	25 36 37	80 18 28	boundary	daily	SFWMD	SFWMD DBHYDRO
S12D_R	S12D	25 45 43	80 40 54	boundary	daily	SFWMD	SFWMD DBHYDRO
S165_R	S165_R	25 32 33	80 24 34	boundary	daily	SFWMD	SFWMD DBHYDRO
S167_R	S167	25 30 09	80 27 48	boundary	daily	SFWMD	SFWMD DBHYDRO
S174_R	S174	25 29 01	80 33 48	boundary	daily	SFWMD	SFWMD DBHYDRO
S177_R	S177	25 24 10	80 33 30	boundary	daily	SFWMD	SFWMD DBHYDRO
S179	S179_R	25 28 25	80 24 52	boundary	daily	SFWMD	SFWMD DBHYDRO
S18C	S18C	25 19 50	80 31 30	boundary	daily	SFWMD	SFWMD DBHYDRO
S20	S20_R	25 22 01	80 22 35	boundary	daily	SFWMD	SFWMD DBHYDRO
S20F	S20F_R	25 27 46	80 20 51	boundary	daily	SFWMD	SFWMD DBHYDRO
S20G	S20G_R	25 29 21	80 20 50	boundary	daily	SFWMD	SFWMD DBHYDRO
S21	S21_R	25 32 35	80 19 51	boundary	daily	SFWMD	SFWMD DBHYDRO
S21A	S21A_R	25 31 09	80 20 46	boundary	daily	SFWMD	SFWMD DBHYDRO
S26	S26_R	25 48 29	80 15 39	boundary	daily	SFWMD	SFWMD DBHYDRO
S27	S27_R	25 50 55	80 11 20	boundary	daily	SFWMD	SFWMD DBHYDRO
S28Z	S28Z_R	25 54 48	80 17 35	boundary	daily	SFWMD	SFWMD DBHYDRO
S29	S29_R	25 55 42	80 09 03	boundary	daily	SFWMD	SFWMD DBHYDRO
S29Z	S29Z_R	25 57 43	80 15 52	boundary	daily	SFWMD	SFWMD DBHYDRO
S30	S30_R	25 57 24	80 25 53	boundary	daily	SFWMD	SFWMD DBHYDRO
S331	S331_R	25 36 39	80 30 35	boundary	daily	SFWMD	SFWMD DBHYDRO
S332_R	S332	25 25 17	80 35 24	boundary	daily	SFWMD	SFWMD DBHYDRO
S334	S334_R	25 45 42	80 30 08	boundary	daily	SFWMD	SFWMD DBHYDRO
S335	S335_R	25 46 34	80 28 58	boundary	daily	SFWMD	SFWMD DBHYDRO
S336	S336_R	25 45 41	80 29 48	boundary	daily	SFWMD	SFWMD DBHYDRO
S338	S338_R	25 39 38	80 28 49	boundary	daily	SFWMD	SFWMD DBHYDRO
Shark River	SR	25 21 11	81 05 58	boundary	daily	ENP	SFWMD DBHYDRO
Sylvania Heights	SYLVA_G	25 46 01	80 16 59	boundary	daily	SFWMD	SFWMD DBHYDRO
Tamiami Airport	TAMI AIR_R	25 38 28	80 25 36	boundary	daily	SFWMD	SFWMD DBHYDRO
Tarpon Bay East	TE	25 24 34	80 57 51	boundary	daily	ENP	SFWMD DBHYDRO
Taylor River	TR	25 13 28	80 39 11	boundary	daily	ENP	SFWMD DBHYDRO
Taylor Slough 2	NP-TS2, TS2	25 23 59	80 36 25	boundary	daily	SFWMD	SFWMD DBHYDRO
Terrapin Bay	TB	25 09 24	80 43 30	boundary	daily	ENP	SFWMD DBHYDRO
Thursday Point	TPTS	25 12 23	80 22 29	boundary	daily	SFWMD	SFWMD DBHYDRO
Trout Cove	TC	25 12 39	80 31 60	boundary	daily	ENP	SFWMD DBHYDRO

Appendix 3. Field stations used in the Biscayne and Southern Everglades Coastal Transport (BISECT) model simulations.—Continued

[dd mm ss, degree minute second; NOAA, National Oceanic and Atmospheric Administration; SFWMD, South Florida Water Management District; DBHYDRO, corporate environmental database of the SFWMD; ENP, Everglades National Park; USGS, U.S. Geological Survey; SOFIA, South Florida Information Access database; FIU, Florida International University; DERM, Department of Environmental Regulation Management; NWIS, National Water Information System]

Field station name (this report)	Map (site) identifier	Latitude (dd mm ss)	Longitude (dd mm ss)	Usage in model	Temporal frequency	Agency	Website or data source
Rainfall (station locations shown in fig. 1–8 in app. 1)—Continued							
The Watson Place	WP	25 42 34	81 14 53	boundary	daily	ENP	SFWMD DBHYDRO
Whipray Basin	WB	25 04 41	80 43 39	boundary	daily	ENP	SFWMD DBHYDRO
Whitewater Bay	WE	25 13 52	80 56 19	boundary	daily	ENP	SFWMD DBHYDRO
Willy Willy	WW	25 35 11	81 02 38	boundary	daily	ENP	SFWMD DBHYDRO
Surface-water discharge (station locations shown in fig. 4)							
Chatham River	Chatham River	25 42 33	81 14 59	comparison	15 minute	USGS	http://sofia.usgs.gov/exchange/sfl_hydro_data/
Lostmans River	Lostmans River	25 33 20	81 09 53	comparison	15 minute	USGS	http://sofia.usgs.gov/exchange/sfl_hydro_data/
Broad River	Broad River	25 30 05	81 04 37	comparison	15 minute	USGS	http://sofia.usgs.gov/exchange/sfl_hydro_data/
Harney River	Harney River	25 25 50	81 05 09.5	comparison	15 minute	USGS	http://sofia.usgs.gov/exchange/sfl_hydro_data/
Shark River	Shark River	25 22 29	81 02 12.1	comparison	15 minute	USGS	http://sofia.usgs.gov/exchange/sfl_hydro_data/
North River	North River	25 20 19	80 54 48	comparison	15 minute	USGS	http://sofia.usgs.gov/exchange/sfl_hydro_data/
McCormick Creek	McCormick Creek	20 10 05.5	80 44 01	comparison	15 minute	USGS	http://sofia.usgs.gov/exchange/sfl_hydro_data/
Taylor River	Taylor River	25 11 26	80 38 20.6	comparison	15 minute	USGS	http://sofia.usgs.gov/exchange/sfl_hydro_data/
Mud Creek	Mud Creek	25 12 11.9	80 35 02.8	comparison	15 minute	USGS	http://sofia.usgs.gov/exchange/sfl_hydro_data/
Trout Creek	Trout Creek	25 12 53.6	80 32 00.6	comparison	15 minute	USGS	http://sofia.usgs.gov/exchange/sfl_hydro_data/
West Highway Creek	Long Sound	25 14 31.6	80 26 51.3	comparison	15 minute	USGS	http://sofia.usgs.gov/exchange/sfl_hydro_data/
Surface-water stage (station locations shown in fig. 3)							
Angels	Angels	25 37 22.9	80 32 32.5	comparison	daily	ENP	SFWMD DBHYDRO
BARRON	BARRON	25 57 34.6	81 21 18.2	comparison	daily	ENP	SFWMD DBHYDRO
BICYA10	BICYA10	25 53 32.6	81 16 11.2	comparison	daily	SFWMD	SFWMD DBHYDRO
BICYA11	BICYA11	25 46 49.6	80 54 42.2	comparison	daily	SFWMD	SFWMD DBHYDRO
BICYA8	BICYA8	25 42 56.6	81 01 17.2	comparison	daily	SFWMD	SFWMD DBHYDRO

Appendix 3. Field stations used in the Biscayne and Southern Everglades Coastal Transport (BISECT) model simulations.—Continued

[dd mm ss, degree minute second; NOAA, National Oceanic and Atmospheric Administration; SFWMD, South Florida Water Management District; DBHYDRO, corporate environmental database of the SFWMD; ENP, Everglades National Park; USGS, U.S. Geological Survey; SOFIA, South Florida Information Access database; FIU, Florida International University; DERM, Department of Environmental Regulation Management; NWIS, National Water Information System]

Field station name (this report)	Map (site) identifier	Latitude (dd mm ss)	Longitude (dd mm ss)	Usage in model	Temporal frequency	Agency	Website or data source
Surface-water stage (station locations shown in fig. 3)—Continued							
BICYA9	BICYA9	25 47 28.6	81 05 58.2	comparison	daily	SFWMD	SFWMD DBHYDRO
Blackwater Sound	BS	25 10 42	80 26 18	comparison	daily	ENP	SFWMD DBHYDRO
Buoy Key	BK	25 07 15	80 50 02	comparison	daily	ENP	SFWMD DBHYDRO
Broad River	BR	25 28 40	80 59 23	comparison	daily	ENP	SFWMD DBHYDRO
Broad River Lower	BD	25 29 11	81 06 40	comparison	daily	ENP	SFWMD DBHYDRO
Butternut Key	BN	25 05 17	80 31 08	comparison	daily	ENP	SFWMD DBHYDRO
Cane Patch	CN	25 25 17	80 56 32	comparison	daily	ENP	SFWMD DBHYDRO
Clearwater Pass	CW	25 17 46.2	81 00 47.2	comparison	daily	ENP	SFWMD DBHYDRO
Craighead Pond	CP	25 13 45	80 42 14	comparison	daily	ENP	SFWMD DBHYDRO
Duck Key	DK	25 10 52	80 29 23	comparison	daily	ENP	SFWMD DBHYDRO
EPGW/SW	EPGW/SW	25 16 10	80 30 16	comparison	daily	ENP	SFWMD DBHYDRO
EVER3	EVER3	25 20 37.2	80 30 52.3	comparison	daily	ENP	SFWMD DBHYDRO
EVER4	EVER4	25 20 42.7	80 32 43.4	comparison	daily	ENP	SFWMD DBHYDRO
EVER5A	EVER5A	25 17 16	80 34 20.9	comparison	daily	ENP	SFWMD DBHYDRO
EVER6	EVER6	25 17 53.4	80 30 43.4	comparison	daily	ENP	SFWMD DBHYDRO
EVER7	EVER7	25 18 34.9	80 32 34.4	comparison	daily	ENP	SFWMD DBHYDRO
Everglades Robblee	NP-ROB, Robblee	25 26 27	80 33 07	comparison	daily	SFWMD	SFWMD DBHYDRO
Frog Pond	FROGP	25 26 38.4	80 34 28.3	comparison	daily	SFWMD	SFWMD DBHYDRO
G1074B	G1074B	25 42 14.9	80 20 15	comparison	daily	SFWMD	SFWMD DBHYDRO
G1251	G1251	25 19 21.9	80 34 07	comparison	daily	SFWMD	SFWMD DBHYDRO
G1487	G1487	25 41 17.6	80 29 46.8	comparison	daily	SFWMD	SFWMD DBHYDRO
G1502	G1502	25 36 54.5	80 34 59.9	comparison	daily	SFWMD	SFWMD DBHYDRO
G211	G211	25 39 37.6	80 29 51.2	comparison	daily	SFWMD	SFWMD DBHYDRO
G3272	G3272	25 39 59.5	80 32 13.2	comparison	daily	SFWMD	SFWMD DBHYDRO
G3273	G3273	25 37 40.9	80 34 33	comparison	daily	SFWMD	SFWMD DBHYDRO
G3353	G3353	25 17 23.9	80 34 14	comparison	daily	SFWMD	SFWMD DBHYDRO
G3354	G3354	25 19 06.6	80 28 40.6	comparison	daily	SFWMD	SFWMD DBHYDRO
G3437	G3437	25 33 59.9	80 34 04	comparison	daily	SFWMD	SFWMD DBHYDRO
G3576	G3576	25 44 48.5	80 30 51.2	comparison	daily	SFWMD	SFWMD DBHYDRO
G3577	G3577	25 42 13.6	80 30 01.2	comparison	daily	SFWMD	SFWMD DBHYDRO
G3578	G3578	25 42 16.6	80 30 47.2	comparison	daily	SFWMD	SFWMD DBHYDRO
G3619	G3619	25 22 49.6	80 33 54.2	comparison	daily	SFWMD	SFWMD DBHYDRO
G3620	G3620	25 23 18.6	80 32 02.2	comparison	daily	SFWMD	SFWMD DBHYDRO
G3622	G3622	25 30 01.5	80 34 06.2	comparison	daily	SFWMD	SFWMD DBHYDRO
G3626	G3626	25 37 14.6	80 30 41.2	comparison	daily	SFWMD	SFWMD DBHYDRO

Appendix 3. Field stations used in the Biscayne and Southern Everglades Coastal Transport (BISECT) model simulations.—Continued

[dd mm ss, degree minute second; NOAA, National Oceanic and Atmospheric Administration; SFWMD, South Florida Water Management District; DBHYDRO, corporate environmental database of the SFWMD; ENP, Everglades National Park; USGS, U.S. Geological Survey; SOFIA, South Florida Information Access database; FIU, Florida International University; DERM, Department of Environmental Regulation Management; NWIS, National Water Information System]

Field station name (this report)	Map (site) identifier	Latitude (dd mm ss)	Longitude (dd mm ss)	Usage in model	Temporal frequency	Agency	Website or data source
Surface-water stage (station locations shown in fig. 3)—Continued							
G3627	G3627	25 36 38.6	80 32 10.2	comparison	daily	SFWMD	SFWMD DBHYDRO
G3628	G3628	25 35 45.6	80 32 04.2	comparison	daily	SFWMD	SFWMD DBHYDRO
G596	G596	25 38 15.9	80 30 43	comparison	daily	SFWMD	SFWMD DBHYDRO
G613	G613	25 24 24.9	80 32 00	comparison	daily	SFWMD	SFWMD DBHYDRO
G618	G618	25 45 39.9	80 36 00	comparison	daily	SFWMD	SFWMD DBHYDRO
G620	G620	25 39 59.9	80 46 00	comparison	daily	SFWMD	SFWMD DBHYDRO
G69	G69	25 45 47.6	80 33 40.2	comparison	daily	SFWMD	SFWMD DBHYDRO
G789	G789	25 29 27.9	80 33 24	comparison	daily	SFWMD	SFWMD DBHYDRO
Garfield Bight	GB	25 10 18	80 47 48	comparison	daily	ENP	SFWMD DBHYDRO
Gunboat Island	GI	25 22 40	81 01 46	comparison	daily	ENP	SFWMD DBHYDRO
Harney River	HR	25 25 26	81 03 36	comparison	daily	ENP	SFWMD DBHYDRO
Highway Creek	HC	25 15 20	80 26 40	comparison	daily	ENP	SFWMD DBHYDRO
Humble	Humble	25 33 59.9	80 32 00	comparison	daily	SFWMD	SFWMD DBHYDRO
L31NMILE1	L31NMILE1	25 44 59.6	80 29 52.1	comparison	daily	SFWMD	SFWMD DBHYDRO
L31NMILE3	L31NMILE3	25 43 08.6	80 29 49.2	comparison	daily	SFWMD	SFWMD DBHYDRO
L31NMILE4	L31NMILE4	25 42 12.6	80 29 45.2	comparison	daily	SFWMD	SFWMD DBHYDRO
L31NMILE5	L31NMILE5	25 41 15.6	80 29 49.2	comparison	daily	SFWMD	SFWMD DBHYDRO
L31NMILE7	L31NMILE7	25 39 53.6	80 29 53.2	comparison	daily	SFWMD	SFWMD DBHYDRO
L31W	L31W	25 26 17.5	80 35 23.9	comparison	daily	SFWMD	SFWMD DBHYDRO
L67XW	L67XW	25 40 59.9	80 40 24	comparison	daily	SFWMD	SFWMD DBHYDRO
Lane River	LN	25 17 03	80 53 38	comparison	daily	ENP	SFWMD DBHYDRO
Little Blackwater Sound	LB	25 12 47.9	80 26 00	comparison	daily	ENP	SFWMD DBHYDRO
Little Madeira	LM	25 10 31	80 37 56	comparison	daily	ENP	SFWMD DBHYDRO
Long Sound	LS	25 14 05	80 27 27	comparison	daily	ENP	SFWMD DBHYDRO
LOOP1	LOOP1	25 45 46.6	80 54 27.2	comparison	daily	SFWMD	SFWMD DBHYDRO
LOOP2	LOOP2	25 44 53.6	80 57 13.2	comparison	daily	SFWMD	SFWMD DBHYDRO
Lostmans River	LO	25 33 21	81 10 07	comparison	daily	ENP	SFWMD DBHYDRO
Murray Key	MK	25 06 20.4	80 56 32	comparison	daily	ENP	SFWMD DBHYDRO
North River	NR	25 20 23	80 54 41	comparison	daily	ENP	SFWMD DBHYDRO
NP-127	R127	25 21 15	80 36 23	comparison	daily	ENP	SFWMD DBHYDRO
NP-158	R158	25 23 45.6	80 34 41.3	comparison	daily	ENP	SFWMD DBHYDRO
NP-201	NP201	25 43 05	80 43 33	comparison	daily	ENP	SFWMD DBHYDRO
NP-202	NP202	25 39 40	80 42 45	comparison	daily	ENP	SFWMD DBHYDRO
NP-203	NP203	25 37 25	80 44 22	comparison	daily	ENP	SFWMD DBHYDRO
NP-205	NP205	25 41 20	80 50 57	comparison	daily	ENP	SFWMD DBHYDRO

Appendix 3. Field stations used in the Biscayne and Southern Everglades Coastal Transport (BISECT) model simulations.—Continued

[dd mm ss, degree minute second; NOAA, National Oceanic and Atmospheric Administration; SFWMD, South Florida Water Management District; DBHYDRO, corporate environmental database of the SFWMD; ENP, Everglades National Park; USGS, U.S. Geological Survey; SOFIA, South Florida Information Access database; FIU, Florida International University; DERM, Department of Environmental Regulation Management; NWIS, National Water Information System]

Field station name (this report)	Map (site) identifier	Latitude (dd mm ss)	Longitude (dd mm ss)	Usage in model	Temporal frequency	Agency	Website or data source
Surface-water stage (station locations shown in fig. 3)—Continued							
NP-206	NP206	25 32 42	80 40 22	comparison	daily	ENP	SFWMD DBHYDRO
NP-311	R3110	25 26 50	80 37 34	comparison	daily	ENP	SFWMD DBHYDRO
NP-44	NP44	25 26 03.9	80 43 14	comparison	daily	ENP	SFWMD DBHYDRO
NP-46	NP46	25 19 09.9	80 47 46	comparison	daily	ENP	SFWMD DBHYDRO
NP-62	NP62	25 26 21.9	80 46 59	comparison	daily	ENP	SFWMD DBHYDRO
NP-67	NP67	25 19 50	80 39 02	comparison	daily	ENP	SFWMD DBHYDRO
NP-72	NP72	25 23 44.9	80 42 11.9	comparison	daily	ENP	SFWMD DBHYDRO
NP-A13	A13	25 29 54	80 42 46	comparison	daily	ENP	SFWMD DBHYDRO
NP-CR2, Context Road 2	CR2	25 29 59	80 37 19	comparison	daily	ENP	SFWMD DBHYDRO
NP-CR3, Context Road 3	CR3	25 29 52.7	80 39 47.4	comparison	daily	ENP	SFWMD DBHYDRO
NP-CT27R	CT27R	25 18 07.6	80 29 19.9	comparison	daily	ENP	SFWMD DBHYDRO
NP-CT50R	CT50R	25 18 49.4	80 31 16.5	comparison	daily	ENP	SFWMD DBHYDRO
NP-CV1NR	CV1NR	25 17 30.3	80 27 14.8	comparison	daily	ENP	SFWMD DBHYDRO
NP-CV5S	CV5S	25 18 11.2	80 29 14.8	comparison	daily	ENP	SFWMD DBHYDRO
NP-CY2	CY2	25 19 43.9	80 40 59	comparison	daily	ENP	SFWMD DBHYDRO
NP-CY3	CY3	25 19 39	80 45 03	comparison	daily	ENP	SFWMD DBHYDRO
NP-DO1	DO1	25 22 23.5	80 41 28	comparison	daily	ENP	SFWMD DBHYDRO
NP-DO2	DO2	25 23 22.6	80 44 40.6	comparison	daily	ENP	SFWMD DBHYDRO
NP-E112	E112	25 25 22.7	80 35 55.2	comparison	daily	ENP	SFWMD DBHYDRO
NP-E146	E146	25 15 18	80 40 00.9	comparison	daily	ENP	SFWMD DBHYDRO
NP-EP1R	EP1R	25 17 15.1	80 27 11.3	comparison	daily	ENP	SFWMD DBHYDRO
NP-EP9R	EP9R	25 16 19.7	80 33 16.5	comparison	daily	ENP	SFWMD DBHYDRO
NP-NCL	NCL	25 14 37.2	80 44 41.5	comparison	daily	ENP	SFWMD DBHYDRO
NP-NE1, North East Shark River Slough	NE1	25 41 29	80 38 06	comparison	daily	ENP	SFWMD DBHYDRO
NP-NE2, North East Shark River Slough	NE2	25 43 14.9	80 33 15	comparison	daily	ENP	SFWMD DBHYDRO
NP-NE3, North East Shark River Slough	NE3	25 44 55	80 30 07.5	comparison	daily	ENP	SFWMD DBHYDRO
NP-NE4, North East Shark River Slough	NE4	25 38 27.9	80 39 11	comparison	daily	ENP	SFWMD DBHYDRO
NP-NE5, North East Shark River Slough	NE5	25 37 52.9	80 39 36	comparison	daily	ENP	SFWMD DBHYDRO

Appendix 3. Field stations used in the Biscayne and Southern Everglades Coastal Transport (BISECT) model simulations.—Continued

[dd mm ss, degree minute second; NOAA, National Oceanic and Atmospheric Administration; SFWMD, South Florida Water Management District; DBHYDRO, corporate environmental database of the SFWMD; ENP, Everglades National Park; USGS, U.S. Geological Survey; SOFIA, South Florida Information Access database; FIU, Florida International University; DERM, Department of Environmental Regulation Management; NWIS, National Water Information System]

Field station name (this report)	Map (site) identifier	Latitude (dd mm ss)	Longitude (dd mm ss)	Usage in model	Temporal frequency	Agency	Website or data source
Surface-water stage (station locations shown in fig. 3)—Continued							
NP-NMP, Ninemile Pond	NMP	25 15 13.5	80 47 55.1	comparison	daily	ENP	SFWMD DBHYDRO
NP-OT, Ornithology Transect	OT	25 34 47	80 57 54	comparison	daily	ENP	SFWMD DBHYDRO
NP-P33	P33	25 36 30	80 41 30	comparison	daily	ENP	SFWMD DBHYDRO
NP-P34	P34	25 36 31	80 56 27	comparison	daily	ENP	SFWMD DBHYDRO
NP-P35	P35	25 27 39	80 51 53	comparison	daily	ENP	SFWMD DBHYDRO
NP-P36	P36	25 31 42	80 47 45	comparison	daily	ENP	SFWMD DBHYDRO
NP-P37	P37	25 17 09	80 41 18	comparison	daily	ENP	SFWMD DBHYDRO
NP-P38	P38	25 22 14	80 50 00	comparison	daily	ENP	SFWMD DBHYDRO
NP-RG1, Rocky Glades 1	RG1	25 34 57	80 36 29	comparison	daily	ENP	SFWMD DBHYDRO
NP-RG2, Rocky Glades 2	RG2	25 32 37.8	80 36 22.4	comparison	daily	ENP	SFWMD DBHYDRO
NTS1	NTS1	25 26 17.1	80 35 35.3	comparison	daily	ENP	SFWMD DBHYDRO
NTS10	NTS10	25 27 42	80 36 19	comparison	daily	ENP	SFWMD DBHYDRO
NTS14	NTS14	25 25 02.9	80 38 21	comparison	daily	ENP	SFWMD DBHYDRO
OL1	OL1	25 15 54	80 36 48.1	comparison	daily	ENP	SFWMD DBHYDRO
Rutzke	Rutzke	25 31 09.9	80 34 30	comparison	daily	SFWMD	SFWMD DBHYDRO
S12A	S12A	25 45 48.6	80 49 16.2	comparison	daily	SFWMD	SFWMD DBHYDRO
S12B	S12B	25 45 48.6	80 46 10.2	comparison	daily	SFWMD	SFWMD DBHYDRO
S12C	S12C	25 45 51.6	80 43 37.2	comparison	daily	SFWMD	SFWMD DBHYDRO
S12D	S12D	25 45 50.5	80 40 52.2	comparison	daily	SFWMD	SFWMD DBHYDRO
S175	S175	25 25 10.6	80 34 24.2	comparison	daily	SFWMD	SFWMD DBHYDRO
S176	S176	25 29 07.5	80 33 44.2	comparison	daily	SFWMD	SFWMD DBHYDRO
S177	S177	25 24 10	80 33 30	comparison	daily	SFWMD	SFWMD DBHYDRO
S178	S178	25 24 35.5	80 31 25.2	comparison	daily	SFWMD	SFWMD DBHYDRO
S18C	S18C	25 19 50	80 31 30	comparison	daily	SFWMD	SFWMD DBHYDRO
S197	S197	25 17 20.5	80 26 28.2	comparison	daily	SFWMD	SFWMD DBHYDRO
S331	S331	25 36 39	80 30 35	comparison	daily	SFWMD	SFWMD DBHYDRO
S332	S332	25 25 17	80 35 24	comparison	daily	SFWMD	SFWMD DBHYDRO
S333	S333	25 45 49.9	80 40 26.4	comparison	daily	SFWMD	SFWMD DBHYDRO
S334	S334	25 45 42	80 30 08	comparison	daily	SFWMD	SFWMD DBHYDRO
S336	S336	25 45 41	80 29 48	comparison	daily	SFWMD	SFWMD DBHYDRO
S338	S338	25 39 38	80 28 49	comparison	daily	SFWMD	SFWMD DBHYDRO
S343A	S343A	25 47 26.6	80 51 18.2	comparison	daily	SFWMD	SFWMD DBHYDRO
S343B	S343B	25 46 47.6	80 50 38.2	comparison	daily	SFWMD	SFWMD DBHYDRO

Appendix 3. Field stations used in the Biscayne and Southern Everglades Coastal Transport (BISECT) model simulations.—Continued

[dd mm ss, degree minute second; NOAA, National Oceanic and Atmospheric Administration; SFWMD, South Florida Water Management District; DBHYDRO, corporate environmental database of the SFWMD; ENP, Everglades National Park; USGS, U.S. Geological Survey; SOFIA, South Florida Information Access database; FIU, Florida International University; DERM, Department of Environmental Regulation Management; NWIS, National Water Information System]

Field station name (this report)	Map (site) identifier	Latitude (dd mm ss)	Longitude (dd mm ss)	Usage in model	Temporal frequency	Agency	Website or data source
Surface-water stage (station locations shown in fig. 3)—Continued							
Shark River	SR	25 21 11	81 05 58	comparison	daily	ENP	SFWMD DBHYDRO
Sisal Pond 1, NP-SP1	SP	25 23 23.9	80 47 51.6	comparison	daily	ENP	SFWMD DBHYDRO
Tarpon Bay East	TE	25 24 34	80 57 51	comparison	daily	ENP	SFWMD DBHYDRO
Taylor River	TR	25 13 28	80 39 11	comparison	daily	ENP	SFWMD DBHYDRO
Taylor Slough 2	TSH	25 18 43.7	80 37 51.5	comparison	daily	ENP	SFWMD DBHYDRO
Taylor Slough Bridge	TSB	25 24 05	80 36 25	comparison	daily	ENP	SFWMD DBHYDRO
Tenmile Corner, NP-TMC	TMC	25 36 54.7	80 52 21	comparison	daily	ENP	SFWMD DBHYDRO
Terrapin Bay	TB	25 09 24	80 43 30	comparison	daily	ENP	SFWMD DBHYDRO
Trout Cove	TC	25 12 39	80 31 60	comparison	daily	ENP	SFWMD DBHYDRO
The Watson Place	WP	25 42 34	81 14 53	comparison	daily	ENP	SFWMD DBHYDRO
Whipray Basin	WB	25 04 41	80 43 39	comparison	daily	ENP	SFWMD DBHYDRO
Whitewater Bay	WE	25 13 52	80 56 19	comparison	daily	ENP	SFWMD DBHYDRO
Willy Willy	WW	25 35 11	81 02 38	comparison	daily	ENP	SFWMD DBHYDRO
Wind (station locations shown in fig. 1–8 in app. 1)							
Virginia Key	Virginia Key	25 43 48	80 09 42	boundary	hourly	NOAA	tidesandcurrents.noaa.gov
Old Ingraham Highway	OIH	25 21 11	80 38 02	boundary	15 minute	USGS	USGS SOFIA website
Solar radiation, air temperature, and humidity (station locations shown in fig. 1–8 in app. 1)							
Old Ingraham Highway	OIH	25 21 11	80 38 02	boundary	15 minute	USGS	USGS SOFIA website
3AS3WX	3AS3WX	25 51 06	80 45 58	boundary	15 minute	SFWMD	SFWMD DBHYDRO
S331W	S331	25 36 39	80 30 35	boundary	15 minute	SFWMD	SFWMD DBHYDRO
Site 7 (P-33)	P-33	25 36 59	80 42 08	boundary	15 minute	USGS	USGS SOFIA website
Salinity and temperature (station locations shown in fig. 1–26 in app. 1)							
BB50	BB50	25 13 47.6	80 22 36.4	comparison	monthly	DERM	DBHYDRO
BB51	BB51	25 15 05.4	80 24 50.7	comparison	monthly	DERM	DBHYDRO
BNP Marker B	BNPMB	25 40 16.6	80 12 18.8	comparison	monthly	FIU	serc.fiu.edu/wqmnetwork
Broad River Lower	BD	25 29 11	81 06 40	comparison	random interval	ENP	DBHYDRO
Blackwater Sound	BS	25 10 42	80 26 18	comparison	random interval	ENP	DBHYDRO
Card Sound North	CSN	25 21 16.5	80 17 30.8	comparison	monthly	FIU	serc.fiu.edu/wqmnetwork
Cane Patch	CN	25 25 17	80 56 32	comparison	random interval	ENP	DBHYDRO
Convoy Point	CP	25 28 40.5	80 19 15.7	comparison	monthly	FIU	serc.fiu.edu/wqmnetwork

Appendix 3. Field stations used in the Biscayne and Southern Everglades Coastal Transport (BISECT) model simulations.—Continued

[dd mm ss, degree minute second; NOAA, National Oceanic and Atmospheric Administration; SFWMD, South Florida Water Management District; DBHYDRO, corporate environmental database of the SFWMD; ENP, Everglades National Park; USGS, U.S. Geological Survey; SOFIA, South Florida Information Access database; FIU, Florida International University; DERM, Department of Environmental Regulation Management; NWIS, National Water Information System]

Field station name (this report)	Map (site) identifier	Latitude (dd mm ss)	Longitude (dd mm ss)	Usage in model	Temporal frequency	Agency	Website or data source
Salinity and temperature (station locations shown in fig. 1–26 in app. 1)—Continued							
Duck Key	DK	25 10 52	80 29 23	comparison	random interval	ENP	DBHYDRO
Garfield Bight	GB	25 10 18	80 47 48	comparison	random interval	ENP	DBHYDRO
Harney River	Harney River	25 25 50	81 05 09.5	comparison	15 minute	USGS	http://sofia.usgs.gov/exchange/sfl_hydro_data/
Little Madeira	LM	25 10 31	80 37 56	comparison	random interval	ENP	DBHYDRO
Marker G-71	MG71	25 44 10.6	80 11 06.8	comparison	monthly	FIU	serc.fiu.edu/wqmnetwork
Near Black Ledge	NBL	25 34 22.6	80 17 12.8	comparison	monthly	FIU	serc.fiu.edu/wqmnetwork
North I-195 Basin	NIB	25 48 58.6	80 10 00.8	comparison	monthly	FIU	serc.fiu.edu/wqmnetwork
North Normandy Isle	NNI	25 52 00	80 08 60	comparison	monthly	FIU	serc.fiu.edu/wqmnetwork
NP-P33	P33, P-33	25 36 30	80 41 30	comparison	random interval	ENP	DBHYDRO
Sands Cut	SC	25 29 18	80 11 18	comparison	monthly	FIU	serc.fiu.edu/wqmnetwork
Shark River	SR	25 21 11	81 05 58	comparison	random interval	ENP	DBHYDRO
West Arsenicker	WA	25 25 11.2	80 18 39.7	comparison	monthly	FIU	serc.fiu.edu/wqmnetwork
Whitewater Bay	WE	25 13 52	80 56 19	comparison	random interval	ENP	DBHYDRO
The Watson Place	WP	25 42 34	81 14 53	comparison	random interval	ENP	DBHYDRO
Willy Willy	WW	25 35 11	81 02 38	comparison	random interval	ENP	DBHYDRO
Groundwater levels (station locations shown in fig. 1–19 in app. 1)							
Duclos	Duclos	25 33 38	80 30 17	comparison	daily	SFWMD	DBHYDRO
F-179	F-179	25 44 44	80 14 48	comparison	daily	USGS	NWIS
F-239	F-239	25 50 08	80 16 18	comparison	daily	USGS	NWIS
F-319	F-319	25 42 17	80 17 18	comparison	daily	USGS	NWIS
F-45	F-45	25 49 43	80 12 15	comparison	daily	USGS	NWIS
Frog Pond	FROGP	25 26 38.4	80 34 28.3	comparison	daily	SFWMD	DBHYDRO
G-1166	G-1166	25 53 42	80 19 55	comparison	daily	USGS	NWIS
G-1183	G-1183	25 29 18	80 23 42	comparison	daily	USGS	NWIS
G-1251	G-1251	25 19 23	80 34 06	comparison	daily	SFWMD	DBHYDRO
G-1362	G-1362	25 36 37	80 26 47	comparison	daily	USGS	NWIS
G-1488	G-1488	25 49 05	80 28 55	comparison	daily	USGS	NWIS
G-1637	G-1637	25 57 07	80 25 50	comparison	daily	USGS	NWIS
G-3074	G-3074	25 41 57	80 21 40	comparison	daily	USGS	NWIS

Appendix 3. Field stations used in the Biscayne and Southern Everglades Coastal Transport (BISECT) model simulations.—Continued

[dd mm ss, degree minute second; NOAA, National Oceanic and Atmospheric Administration; SFWMD, South Florida Water Management District; DBHYDRO, corporate environmental database of the SFWMD; ENP, Everglades National Park; USGS, U.S. Geological Survey; SOFIA, South Florida Information Access database; FIU, Florida International University; DERM, Department of Environmental Regulation Management; NWIS, National Water Information System]

Field station name (this report)	Map (site) identifier	Latitude (dd mm ss)	Longitude (dd mm ss)	Usage in model	Temporal frequency	Agency	Website or data source
Groundwater levels (station locations shown in fig. 1–19 in app. 1)—Continue							
G-3253	G-3253	25 50 27	80 24 55	comparison	daily	USGS	NWIS
G-3272	G-3272	25 39 53	80 32 14	comparison	daily	SFWMD	DBHYDRO
G-3273	G-3273	25 37 50	80 34 32	comparison	daily	SFWMD	DBHYDRO
G-3328	G-3328	25 47 41	80 16 21	comparison	daily	USGS	NWIS
G-3329	G-3329	25 47 52	80 18 15	comparison	daily	USGS	NWIS
G-3338	G-3338	25 20 16	80 31 27	comparison	daily	SFWMD	DBHYDRO
G-3353	G-3353	25 17 25	80 34 13	comparison	daily	SFWMD	DBHYDRO
G-3354	G-3354	25 18 55	80 28 34	comparison	daily	USGS	NWIS
G-3355	G-3355	25 23 32	80 30 05	comparison	daily	USGS	NWIS
G-3356	G-3356	25 25 06	80 25 41	comparison	daily	USGS	NWIS
G-3437	G-3437	25 34 01	80 34 03	comparison	daily	SFWMD	DBHYDRO
G-3556	G-3556	25 42 14	80 28 14	comparison	daily	SFWMD	DBHYDRO
G-3576	G-3576	25 44 43	80 30 51	comparison	daily	SFWMD	DBHYDRO
G-3578	G-3578	25 42 11	80 30 47	comparison	daily	SFWMD	DBHYDRO
G-3619	G-3619	25 22 44	80 33 54	comparison	daily	SFWMD	DBHYDRO
G-3626	G-3626	25 37 09	80 30 41	comparison	daily	SFWMD	DBHYDRO
G-3763	G-3763	25 12 42	80 38 52	comparison	daily	SFWMD	DBHYDRO
G-3777	G-3777	25 14 58	80 39 57	comparison	daily	SFWMD	DBHYDRO
G-551	G-551	25 41 30	80 23 45	comparison	daily	USGS	NWIS
G-580A	G-580A	25 40 00	80 18 10	comparison	daily	USGS	NWIS
G-618	G-618	25 45 01	80 35 59	comparison	daily	SFWMD	DBHYDRO
G-620	G-620	25 40 01	80 45 59	comparison	daily	SFWMD	DBHYDRO
G-789	G-789	25 29 28	80 33 24	comparison	daily	USGS	NWIS
G-852	G-852	25 54 37	80 10 32	comparison	daily	USGS	NWIS
G-855	G-855	25 40 38	80 28 02	comparison	daily	USGS	NWIS
G-860	G-860	25 37 18	80 19 23	comparison	daily	USGS	NWIS
G-970	G-970	25 57 09	80 22 37	comparison	daily	USGS	NWIS
G-973	G-973	25 52 09	80 21 28	comparison	daily	USGS	NWIS
G-975	G-975	25 52 08	80 27 40	comparison	daily	USGS	NWIS
Krome	Krome	25 45 13	80 29 19	comparison	daily	SFWMD	DBHYDRO
MO-199	MO-199	25 28 05	80 51 15	comparison	daily	SFWMD	DBHYDRO
NP-127	R-127	25 21 15	80 36 23	comparison	daily	SFWMD	DBHYDRO
NP-158	R-158	25 23 45.6	80 34 41.3	comparison	daily	SFWMD	DBHYDRO
Rutzke	Rutzke	25 31 09.9	80 34 30	comparison	daily	SFWMD	DBHYDRO
S-18	S-18	25 55 26	80 14 30	comparison	daily	USGS	NWIS
S-182A	S-182A	25 35 49	80 21 41	comparison	daily	USGS	NWIS

Appendix 3. Field stations used in the Biscayne and Southern Everglades Coastal Transport (BISECT) model simulations.—Continued

[dd mm ss, degree minute second; NOAA, National Oceanic and Atmospheric Administration; SFWMD, South Florida Water Management District; DBHYDRO, corporate environmental database of the SFWMD; ENP, Everglades National Park; USGS, U.S. Geological Survey; SOFIA, South Florida Information Access database; FIU, Florida International University; DERM, Department of Environmental Regulation Management; NWIS, National Water Information System]

Field station name (this report)	Map (site) identifier	Latitude (dd mm ss)	Longitude (dd mm ss)	Usage in model	Temporal frequency	Agency	Website or data source
Water levels at canal structures used for River Package							
G-119	G119_H,G119_T	25 38 33	80 20 18	boundary	daily	SFWMD	SFWMD DBHYDRO
G-211	G211_H,G211_T	25 39 31	80 29 52	boundary	daily	SFWMD	SFWMD DBHYDRO
G-58	G58_H,G58_T	25 54 00	80 09 43	boundary	daily	SFWMD	SFWMD DBHYDRO
G-72	G72_H,G72_T	25 52 09	80 20 21	boundary	daily	SFWMD	SFWMD DBHYDRO
G-93	G93_H,G93_T	25 44 18	80 17 12	boundary	daily	SFWMD	SFWMD DBHYDRO
S-118	S118_H,S118_T	25 37 22	80 20 30	boundary	daily	SFWMD	SFWMD DBHYDRO
S-119	S119_H,S119_T	25 38 33	80 20 18	boundary	daily	SFWMD	SFWMD DBHYDRO
S-12A	S-12A_H,S-12A_T	25 45 42	80 49 17	boundary	daily	SFWMD	SFWMD DBHYDRO
S-12B	S-12B_H,S-12B_T	25 45 42	80 46 11	boundary	daily	SFWMD	SFWMD DBHYDRO
S-12C	S-12C_H,S-12C_T	25 45 43	80 43 37	boundary	daily	SFWMD	SFWMD DBHYDRO
S-12D	S-12D_H,S-12D_T	25 45 44	80 40 55	boundary	daily	SFWMD	SFWMD DBHYDRO
S-120	S120_T	25 40 15	80 19 17	boundary	daily	SFWMD	SFWMD DBHYDRO
S-121	S121_H,S121_T	25 41 13	80 21 39	boundary	daily	SFWMD	SFWMD DBHYDRO
S-122	S122_H,S122_T	25 35 39	80 20 53	boundary	daily	SFWMD	SFWMD DBHYDRO
S-123	S123_H,S123_T	25 36 37	80 18 28	boundary	daily	SFWMD	SFWMD DBHYDRO
S-148	S148_H,S148_T	25 34 12	80 22 58	boundary	daily	SFWMD	SFWMD DBHYDRO
S-149	S149_H	25 35 31	80 21 40	boundary	daily	SFWMD	SFWMD DBHYDRO
S-165	S165_H,S165_T	25 32 33	80 24 34	boundary	daily	SFWMD	SFWMD DBHYDRO
S-166	S166_H,S166_T	25 31 06	80 25 56	boundary	daily	SFWMD	SFWMD DBHYDRO
S-167	S167_H,S167_T	25 30 09	80 27 48	boundary	daily	SFWMD	SFWMD DBHYDRO
S-175	S175_H,S175_T	25 25 04	80 34 25	boundary	daily	SFWMD	SFWMD DBHYDRO
S-176	S176_H,S176_T	25 28 58	80 33 46	boundary	daily	SFWMD	SFWMD DBHYDRO
S-177	S177_H,S177_T	25 24 10	80 33 30	boundary	daily	SFWMD	SFWMD DBHYDRO
S-178	S178_T	25 24 29	80 31 26	boundary	daily	SFWMD	SFWMD DBHYDRO
S-179	S179_H,S179_T	25 28 25	80 24 52	boundary	daily	SFWMD	SFWMD DBHYDRO
S-18C	S18C_H,S18C_T	25 19 50	80 31 30	boundary	daily	SFWMD	SFWMD DBHYDRO
S-194	S194_H,S194_T	25 34 59	80 28 42	boundary	daily	SFWMD	SFWMD DBHYDRO
S-195	S195_H,S195_T	25 33 04	80 23 46	boundary	daily	SFWMD	SFWMD DBHYDRO
S-196	S196_H,S196_T	25 31 01	80 30 41	boundary	daily	SFWMD	SFWMD DBHYDRO
S-197	S197_H,S197_T	25 17 13	80 26 29	boundary	daily	SFWMD	SFWMD DBHYDRO
S-20	S20_H,S20_T	25 22 01	80 22 35	boundary	daily	SFWMD	SFWMD DBHYDRO
S-20F	S20F_H,S20F_T	25 27 46	80 20 51	boundary	daily	SFWMD	SFWMD DBHYDRO
S-20G	S20G_H,S20G_T	25 29 21	80 20 50	boundary	daily	SFWMD	SFWMD DBHYDRO
S-21	S21_H,S21_T	25 32 35	80 19 51	boundary	daily	SFWMD	SFWMD DBHYDRO
S-21A	S21A_H,S21A_T	25 31 09	80 20 46	boundary	daily	SFWMD	SFWMD DBHYDRO
S-22	S22_H,S22_T	25 40 12	80 17 02	boundary	daily	SFWMD	SFWMD DBHYDRO
S-25	S25_H,S25_T	25 47 52	80 14 44	boundary	daily	SFWMD	SFWMD DBHYDRO
S-25B	S25B_H,S25B_T	25 47 38	80 15 45	boundary	daily	SFWMD	SFWMD DBHYDRO

Appendix 3. Field stations used in the Biscayne and Southern Everglades Coastal Transport (BISECT) model simulations.—Continued

[dd mm ss, degree minute second; NOAA, National Oceanic and Atmospheric Administration; SFWMD, South Florida Water Management District; DBHYDRO, corporate environmental database of the SFWMD; ENP, Everglades National Park; USGS, U.S. Geological Survey; SOFIA, South Florida Information Access database; FIU, Florida International University; DERM, Department of Environmental Regulation Management; NWIS, National Water Information System]

Field station name (this report)	Map (site) identifier	Latitude (dd mm ss)	Longitude (dd mm ss)	Usage in model	Temporal frequency	Agency	Website or data source
Water levels at canal structures used for River Package—Continued							
S-26	S26_H,S26_T	25 48 29	80 15 39	boundary	daily	SFWMD	SFWMD DBHYDRO
S-27	S27_H,S27_T	25 50 55	80 11 20	boundary	daily	SFWMD	SFWMD DBHYDRO
S-28	S28_H,S28_T	25 52 15	80 10 42	boundary	daily	SFWMD	SFWMD DBHYDRO
S-29	S29_H,S29_T	25 55 42	80 09 03	boundary	daily	SFWMD	SFWMD DBHYDRO
S-30	S30_H,S30_T	25 57 24	80 25 53	boundary	daily	SFWMD	SFWMD DBHYDRO
S-31	S31_T	25 56 34	80 26 25	boundary	daily	SFWMD	SFWMD DBHYDRO
S-32	S32_H	25 56 33	80 26 22	boundary	daily	SFWMD	SFWMD DBHYDRO
S-331	S331_H,S331_T	25 36 39	80 30 35	boundary	daily	SFWMD	SFWMD DBHYDRO
S-332	S332_H,S332_T	25 25 18	80 35 23	boundary	daily	SFWMD	SFWMD DBHYDRO
S-332D	S-332D	25 28 58	80 33 49	boundary	daily	SFWMD	SFWMD DBHYDRO
S-332B2	S-332B2	25 32 58	80 33 38	boundary	daily	SFWMD	SFWMD DBHYDRO
S-334	S334_T	25 45 42	80 30 08	boundary	daily	SFWMD	SFWMD DBHYDRO
S-335	S335_H,S335_T	25 46 34	80 28 58	boundary	daily	SFWMD	SFWMD DBHYDRO
S-336	S336_H,S336_T	25 45 41	80 29 48	boundary	daily	SFWMD	SFWMD DBHYDRO
S-337	S337_T	25 56 32	80 26 27	boundary	daily	SFWMD	SFWMD DBHYDRO
S-338	S338_H,S338_T	25 39 38	80 28 49	boundary	daily	SFWMD	SFWMD DBHYDRO
Water levels at multiple culverts used for River Package							
L-30 to L-67A, L302L67	2289060	various	various	boundary	daily	USGS	NWIS
Monroe to Carnestown, Mon2Car	2288800	various	various	boundary	daily	USGS	NWIS
Fortymile Bend to Monroe, 40MI2Mon	2288900	various	various	boundary	daily	USGS	NWIS

Appendix 4. Development of Heat Transport and Evapotranspiration Representations

The precursor Tides and Inflows to the Mangrove Everglades (TIME) (Wang and others, 2007) and Biscayne models (Lohmann and others, 2012) have used different numerical methods for applying the evapotranspiration (ET) boundary condition. The TIME model originally computed ET from a user-defined potential evapotranspiration rate (PET) (Wang and others, 2007). Heat transport capabilities were subsequently added to investigate the effects of planned restoration activities in refuges for the large population of endangered West Indian manatee (*Trichechus manatus*) that inhabit the southwestern Florida coast (Swain and Decker, 2009). The latent heat flux is computed as part of this heat budget, so ET is then directly calculated from latent heat flux. The Biscayne model was also constructed with the heat transport computations and the accompanying ET representation (Lohmann and others, 2012) and the same method is used in the Biscayne and Southern Everglades Coastal Transport (BISECT) model.

The precalculated PET method used in the TIME model (Wang and others, 2007) was initially tested as a method to determine computed water temperature characteristics. The method produced acceptable overall ET values, but many shallow sections of the modeled area had excessive heat gain or loss due to high or low latent heat flux values derived from precalculated PET values. This result led to unacceptable areal variations in average water temperatures and, also, contributed to unacceptably large day-to-night water temperature variations.

To eliminate the need for precalculated PET values, two heat transfer concepts were tested by modifying the Simulation of Surface-Water Integrated Flow and Transport in Two Dimensions (SWIFT2D) part of the Flow and Transport in a Linked Overland/Aquifer Density-Dependent System (FTLOADDS) code to apply both a Dalton formulation (Brutsaert, 1982) and a Penman-Monteith formulation (Eagleson, 1970) to the TIME study area at every time step. Details and (or) descriptions of these calculations are available in Decker and Swain (2008), Swain and Decker (2009), and Lohmann and others (2012). Both methods worked well (Swain and Decker, 2009) by eliminating regions of excessive heat gain and other regions of excessive heat loss and by reducing, but not eliminating, unreasonably large day-to-night water temperature variations. Neither computation method was able to produce day-to-night water temperature variations that consistently equaled field measurements. Some model-simulated day-to-night temperature variations were too high and others too low (Swain and Decker, 2009), which could indicate insufficient or incomplete numerical representation of more than one heat-related process within the SWIFT2D part of FTLOADDS.

The two least well-defined heat-related processes were determined to be (1) the daily heat storage to and subsequent heat release from a depth of soil at the bottom of every inundated model cell and (2) the incoming solar radiation reflected back into the atmosphere from the Earth's surface (albedo). The albedo, which was assumed to be a constant 16.9 percent for all inundated, vegetated and nonvegetated parts of the study area, can be variable (Swain and others, 2012). A decision was made to retain the Dalton representation of sensible heat flux and focus refinement efforts on the Penman-Monteith latent heat flux representation because it is more firmly rooted in the physics that control ET processes and is affected by albedo.

The amount of heat that soil actively exchanges with the overlying water column in the Everglades region was investigated for the purposes of this study. Extensive experimental work using large, well-insulated tanks was completed to define precisely the one-dimensional, vertical distribution and movement of heat in carefully prepared layers of soil, water, and artificial plants exposed at the surface to the weather conditions in south Florida from early to mid-July in 2009. Results indicated that 5.1 centimeters of soil were required to add enough heat storage, in addition to the heat stored in the water column itself, to explain the daily change in water temperature (Swain and others, 2012).

The initial heat transport formulation in FTLOADDS used a single spatially uniform albedo value that was determined from wetland energy budget measurements to be about 16.9 percent (Swain and Decker, 2010). For the Biscayne and Southern Everglades Coastal Transport (BISECT) model application, a new modification to the code was made to allow a spatially variable grid of albedo values to be input as a boundary condition. Visual inspection of aerial photographs indicates substantially higher reflectivity and albedo in shallow offshore waters. A higher albedo value of 28 percent was found to work well in the model in shallow offshore areas 0.5 meter (m) below sea level referenced to North American Vertical Datum of 1988 (NAVD 88), where vegetation is sparse and reflection from the lightly colored sand bottom is predominant. Deeper open water, where the bottom is not visible, has a much lower albedo, and 8 percent is a commonly accepted value (Brutsaert, 1982). This low value is used for deeper water areas of BISECT, those that are more than 3 m below sea level, and the transition to the 28 percent albedo values in shallow offshore areas occurs linearly between bottom elevations of 3 and 0.5 m below sea level. Above an elevation of 0.5 m below sea level, the previously calibrated albedo value of 16.9 percent is used uniformly. The albedo distribution used in BISECT (fig. 4–1) substantially improves simulated temperature and ET computations compared to the two precursor models.

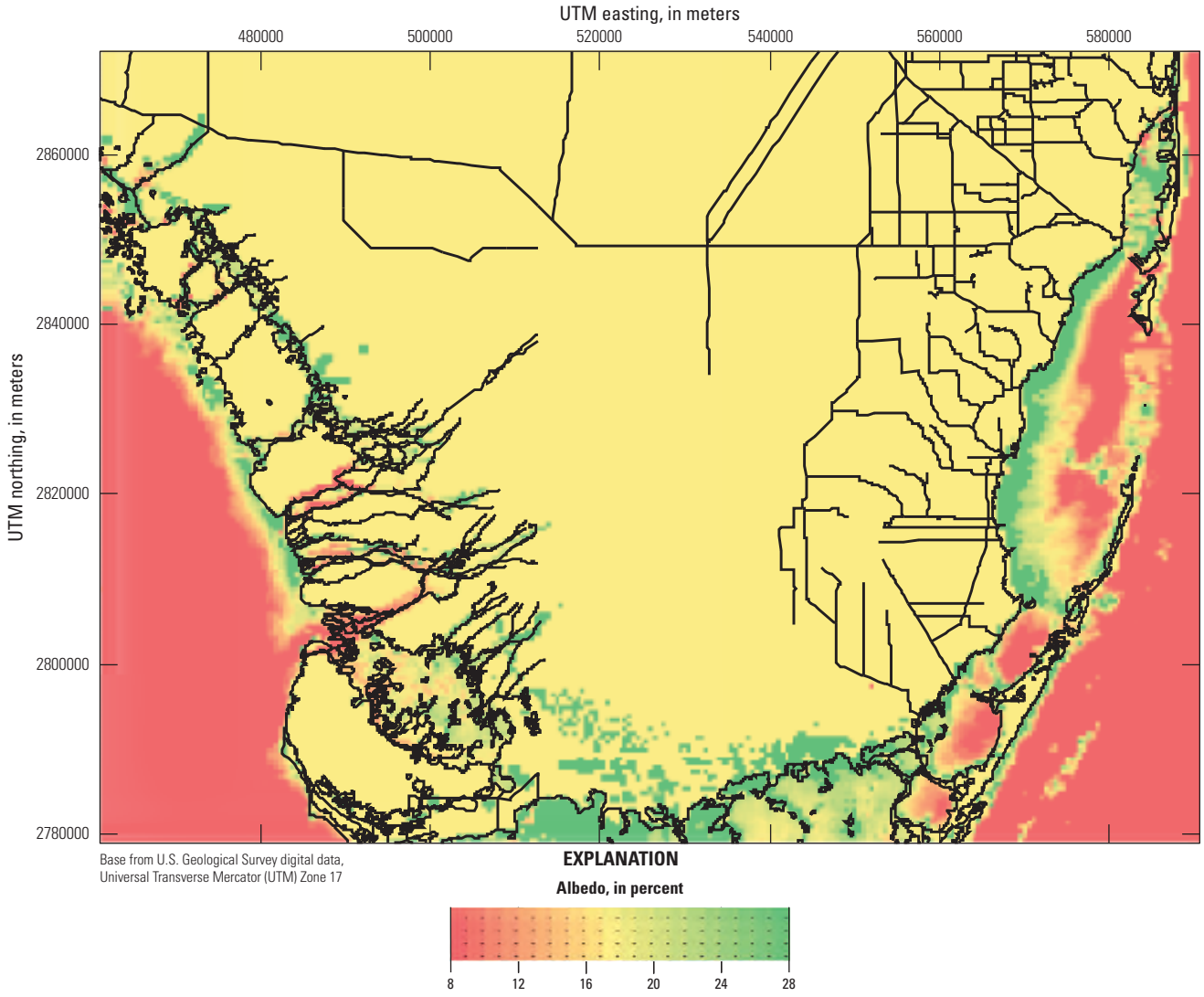

Figure 4-1. Spatially variable albedo distribution used in the Biscayne and Southern Everglades Coastal Transport (BISECT) model for the south Florida peninsula.

References Cited

Brutsaert, W., 1982, Evaporation into the atmosphere: The Netherlands, Kluwer Academic Publishers, 299 p.

Decker, Jeremy, and Swain, Eric, 2008, Hydrologic modeling of south Florida environmental parameters and application to ecology, salinity, and heat transport: 2008 Greater Everglades Ecosystem Restoration Conference, Naples, Fla., July 28–August 1, 2008, p. 81.

Eagleson, P.S., 1970, Dynamic hydrology: McGraw-Hill, New York.

Lohmann, M.A., Swain, E.D., Wang, J.D., and Dixon, Joann, 2012, Evaluation of effects of changes in canal management and precipitation patterns on salinity in Biscayne Bay, Florida, using an integrated surface-water/groundwater model: U.S. Geological Survey Scientific Investigations Report 2012–5099, 94 p.

Swain, E.D., and Decker, J.D., 2009, Development, testing, and application of a coupled hydrodynamic surface-water/groundwater model (FTLOADDS) with heat and salinity transport in the Ten Thousand Islands/Picayune Strand Restoration Project Area, Florida: U.S. Geological Survey Scientific Investigations Report 2009–5146, 42 p.

Swain, E.D., and Decker, J.D., 2010, A measurement-derived heat-budget approach for simulating coastal wetland temperature with a hydrodynamic model: Wetlands, v. 30, no. 3, p. 635–648.

Swain, Michael, Swain, Matthew, Lohmann, Melinda, and Swain, E.D., 2012, Experimental determination of soil heat storage for the simulation of heat transport in a coastal wetland: Journal of Hydrology, v. 422–423, p. 53–62.

Wang, J.D., Swain, E.D., Wolfert, M.A., Langevin, C.D., James, D.E., and Telis, P.A., 2007, Applications of Flow and Transport in a Linked Overland/Aquifer Density Dependent System (FTLOADDS) to simulate flow, salinity, and surface-water stage in the southern Everglades, Florida: U.S. Geological Survey Scientific Investigations Report 2007–5010, 112 p.

Appendix 5. Comparisons of Coastal Discharges Simulated by the TIME Model and BISECT Model

For the western part of the Biscayne and Southern Everglades Coastal Transport (BISECT) model area in the south Florida peninsula, the precursor Tides and Inflows to the Mangrove Everglades (TIME) model has had some post-TIME, pre-BISECT applications, such as Swain and Decker (2009) and Green and others (2014), wherein opportunities for calibration adjustments have been taken. The TIME model was also the subject of an in-depth evaluation (Bahm and Fennema, 2013) by the National Park Service (NPS) that was nearly concurrent with the creation of BISECT. The more recent Biscayne model has not had the same benefit. Nevertheless, considerable effort has been made to (1) improve the calibration of both parts of BISECT, (2) provide a more statistically sound basis for choosing sites at which to compare field and simulated data, and (3) better characterize the ability of model results to simulate measured data.

Sufficient measured data are available to compare with BISECT-simulated mean streamflow in the study area and evaluate the focused streamflow calibration efforts relative to TIME model results. The key to this comparison is that both model simulations had similar boundary conditions for similar time periods that include periods of concurrent measured streamflow data ranging from 15 to 84 months, depending on when individual streamflow gages were established.

Streamflow errors were computed by using measured flows and both TIME- and BISECT-simulated flows for each stream in the study area where these data were concurrent. The data-availability conditions are met for all sites except Harney River. Data-availability periods range from 15 to 84 months. The generally better agreement between measured and BISECT-simulated mean streamflow rates is a direct result of the three previously described calibration efforts to improve computed streamflow rates in BISECT:

- adjusting grid cell elevations,
- adjusting Manning's *n* in selected rectangular marshy areas, and
- adjusting Manning's *n* in stream cells only in the direction of flow.

Compared to TIME, BISECT improves the accuracy of simulated mean discharge for each coastal station with coincident measured data (table 5–1). The reduction in error at each station, compared to the TIME model results, ranges from less than 1 percent to about 13 percent of the sum of all participating BISECT mean discharges for all stations for the coincident time period of each station (table 5–1). The Harney River station is not included because its measured and simulated data have no concurrent time period for the two models. The greatest decrease in error between BISECT-simulated discharge and measured discharge is at Shark River (13.34 percent); in contrast, BISECT-simulated discharge has a higher error with measured discharge at Taylor River (1.54 percent) when compared to TIME-simulated discharge (table 5–1). Assuming that the mean discharge comparison for each station is representative of the entire simulation period (84 months), the error between simulated and measured streamflow, except for Harney River, has decreased about 38 percent.

The lower errors between BISECT-simulated mean streamflow and measured values, compared to TIME, are a substantial modeling objective, but different comparisons are needed to evaluate the ability of BISECT to simulate measured seasonal and daily flow dynamics that respond to the many time-dependent stresses imposed by tides, water deliveries, precipitation, evapotranspiration, and groundwater interactions. Analysis of the adequacy of the BISECT time-dependent streamflow computations can best be accomplished by direct graphical comparison and statistical analysis of concurrent simulated and measured average daily streamflow, where it exists, for the "base case" calibration period of 1996 through 2004 inclusive.

References Cited

Bahm, K.E., and Fennema, R.J., 2013, Evaluation and application of the TIME model v2.0—Restoration alternatives and sea level rise in Everglades National Park: Hydrologic Model Report SFNRC Technical Series 2013.1, 92 p.

Green, T.W., Slone, D.H., Swain, E.D., Cherkiss, M.S., Lohmann, M., Mazzotti, F.J., and Rice, K.G., 2014, Evaluating effects of Everglades restoration on American crocodile populations in south Florida using a spatially-explicit, stage-based population model: Wetlands, v. 34, no. 1, Supplement, p. 213–224.

Swain, E.D., and Decker, J.D., 2009, Development, testing, and application of a coupled hydrodynamic surface-water/groundwater model (FTLOADDS) with heat and salinity transport in the Ten Thousand Islands/Picayune Strand Restoration Project Area, Florida: U.S. Geological Survey Scientific Investigations Report 2009–5146, 42 p.

Table 5–1. Comparison of average streamflow rates simulated by the Tides and Inflows to the Mangrove Everglades (TIME) model, simulated by the Biscayne and Southern Everglades Coastal Transport (BISECT) model, and measured in the study area in the south Florida peninsula, 1996–2004.

[mm/dd/yyyy, month/day/year; TIME, Tides Inflows in the Mangrove Everglades; m^3/s, cubic meter per second; BISECT, Biscayne and Southern Everglades Coastal Transport; --, none. See app. 3 for station details]

River	Coincident time period (mm/dd/yyyy)	TIME mean flow (m^3/s)	BISECT mean flow (m^3/s)	BISECT mean flow as percentage of total
Broad River	02/24/2001–12/31/2004	2.92	13.65	14.1
Chatham River	04/22/2001–12/31/2004	4.07	13.45	13.9
Harney River	10/03/2003–12/31/2004	-8.28	8.65	8.9
Long Sound	02/17/1996–12/31/2004	-0.64	0.73	0.8
Lostmans River	03/27/2001–12/31/2004	5.25	34.99	36.2
McCormick Creek	01/01/1996–12/31/2004	-0.02	0.51	0.5
Mud Creek	01/01/1996–12/31/2004	0.35	1.25	1.3
North River	10/01/2001–12/31/2004	0.85	2.19	2.3
Shark River	03/18/2001–12/31/2004	0.15	11.77	12.2
Taylor River	01/01/1996–12/31/2004	1.50	2.66	2.8
Trout Creek	02/01/1996–12/31/2004	1.10	6.89	7.1

During coincident time periods for TIME, BISECT, and the measured data						
River	Coincident time period (mm/dd/yyyy)	TIME mean error (m^3/s)	BISECT mean error (m^3/s)	Mean discharge improvement (m^3/s)	BISECT mean discharge during time period for all rivers (m^3/s)	Improvement as percentage of BISECT mean discharge for all rivers
Broad River	02/24/2001–12/31/2002	8.07	3.48	4.59	99.77	4.60
Chatham River	04/22/2001–12/31/2002	6.96	5.83	1.13	105.62	1.07
Harney River	--	--	--	--	--	--
Long Sound	02/17/1996–12/31/2002	-1.29	-0.70	0.60	100.16	0.59
Lostmans River	03/27/2001–12/31/2002	16.85	4.95	11.91	102.76	11.59
McCormick Creek	01/01/1996–12/31/2002	0.25	0.07	0.17	99.48	0.17
Mud Creek	01/01/1996–12/31/2002	0.39	0.42	-0.03	99.48	-0.03
North River	10/01/2001–12/31/2002	10.29	0.97	9.32	107.33	8.68
Shark River	03/18/2001–12/31/2002	15.22	-1.63	13.59	101.87	13.34
Taylor River	01/01/1996–12/31/2002	-0.10	1.62	-1.53	99.48	-1.54
Trout Creek	02/01/1996–12/31/2002	-0.37	0.95	-0.58	99.83	-0.58

For more information about this publication, contact

Director, Caribbean-Florida Water Science Center
U.S. Geological Survey
4446 Pet Lane, Suite 108
Lutz, FL 33559
(813) 498-5000

For additional information visit
https://www2.usgs.gov/water/caribbeanflorida/index.html

Publishing support provided by
Lafayette Publishing Service Center

ISSN 2328-0328 (online)
https://doi.org/10.3133/sir20195045